COPY NO._____

ULTRASONIC MEASUREMENT OF WELD FLAW SIZE, PHASE 2
Part 1: Studies of the use of the tandem technique and analysis of echodynamic responses for flaw evaluation

Final Report
Prepared for

National Co-operative Highway Research Program
Transportation Research Board
National Research Council

TRANSPORTATION RESEARCH BOARD

NAS-NRC
Privileged Document
This report, not released for publication,
is furnished only for review to members
of or participants in the work of the
National Co-operative Highway Research Program.
It is to be regarded as fully privileged,
and dissemination of the information included
herein must be approved by the NCHRP.

P.J. Mudge

Welding Institute Project No.3769
Report No.3769/15, Part 1
October 1988

THE WELDING INSTITUTE

Research Laboratory Abington Hall Abington
Cambridge CB1 6AL United Kingdom
Telephone Cambridge 0223 891162
Telefax 0223 892588
Telegrams WELDASERCH CAMBRIDGE
Telex 81183

ACKNOWLEDGEMENTS

This work was sponsored by the American Association of State Highway and Transportation Officials, in co-operation with the Federal Highway Administration, and was conducted in the National Co-operative Highway Research Program which is administered by the Transportation Research Board of the National Research Council.

TABLE OF CONTENTS

LIST OF FIGURES

LIST OF TABLES

ACKNOWLEDGEMENTS

This work was performed by The Welding Institute, Cambridge, England under contract to NCHRP; Project No. 10-13/1.

Peter J. Mudge, Head of the NDT Research Department, was the Principal Investigator under the general guidance of Dr J.D. Harrison, Head of the Engineering and Materials Research Group. The experimental work was conducted by Messrs P.H. Smith (the Laboratory Supervisor), N.J. Farrant, K.S. Hayward and A.M. Lank. Mr S.T. Brown and Miss A.C. Duncumb provided additional assistance with the echodynamic tests.

ABSTRACT

This report describes an investigation into the suitability of using additional ultrasonic techniques to supplement the pulse-echo tests specified in AWS D1.1 for evaluation of vertical planar flaws. Tests were carried out on artificial machined discontinuities and real weld defects to establish the influence of flaw size and orientation on the reliability of rejection of vertical planar defects using the tandem technique. Additional tests were carried out to evaluate the feasibility of using the echodynamic response characteristics of flaws to predict their general shape.

SUMMARY

This work was carried out under Task 2 of NCHRP Project 10-13/1. The aim was to establish whether application of the tandem ultrasonic technique could improve the reliability of rejection of vertical planar flaws using AWS D1.1 procedures, and whether flaw echodynamic responses could be used to discriminate between flaw types. Tests carried out on an array of 92 machined reflectors and on 9 real weld flaws using the tandem technique indicated that reliable rejection of such flaws could be attained provided they were oriented within around 5° of vertical. Defects at greater angles were reliably rejected by pulse-echo tests to D1.1 requirements.

It was established that miniature ultrasonic search units operating at 2MHz provided optimum performance for tandem testing. However, defects in some locations cannot be examined due to access problems.

Comparison of echodynamic responses from drilled holes and cracks indicated that the width of the response is not a reliable discriminator between planar and non-planar flaws. However, echo pattern appearance does differ markedly between different types of flaw and this may be used to predict flaw type. In order to to do this, it is necessary to examine the flaw from a number of orientations with more than one ultrasonic beam angle.

CHAPTER ONE
INTRODUCTION AND RESEARCH APPROACH

PROBLEM STATEMENT

There is an urgent need for ultrasonic testing procedures that can be used to measure the dimensions of weld discontinuities (flaws) with sufficient accuracy to permit evaluation using a fracture mechanics approach. Most state transportation agencies use the provisions of the American Welding Society Structural Welding Code AWS D1.1 (1) to determine the acceptability of structural welds. These provisions are based on an assumed relationship between the ultrasonic "Indication Rating" and flaw size. The results of the first phase of research (2), as well as other experience, indicate that this relationship is not valid. Research is needed to develop improved ultrasonic testing procedures, using equipment presently available, that will permit accurate measurement of the dimensions of flaws common to weldments. These procedures are needed for use in both shop and field inspection of weldments to determine acceptance during construction and for in-service evaluation. Reliable procedures for ultrasonic testing will obviate the costs and delays of unnecessary repairs while reducing the probability that defects, which may lead to structural failures, will be improperly evaluated.

RESEARCH OBJECTIVE

The aim of the program as a whole was to derive and to evaluate ultrasonic techniques which would allow accurate measurements of weld flaw size to be made, thereby permitting fracture mechanics analyses to be used to determine the structural integrity of steel bridges. The previous work (2) demonstrated that the most promising technique for accurate measurements of weld flaws utilised the measurement of flight time of ultrasound diffracted from defect edges. Consequently, the major part of the program was devoted to a study of the capabilities of the time-of-flight diffraction technique. That study constituted the second part of this project and is reported in an accompanying document (3).

However, before advanced accurate flaw sizing methods can be applied, assurance of the detection of potentially significant flaws by ultrasonic testing is essential, if structural integrity is to be maintained. The tendency of the AWS D1.1 procedures not to reject vertical planar flaws by the usual method of determining an indication rating, reported by the previous study (2), suggested that there was scope for augmentation of the D1.1 procedures to ensure the reliable identification of such flaws. Consequently, the aim of this first part of the program was to establish the performance of techniques which would be generally compatible with existing D1.1 requirements and which would reduce inconsistencies of evaluation of vertical planar flaws.

The objectives were:

- to determine the capabilities of both the tandem probe technique and analysis of the features of echodynamic responses from flaws in relation to the existing requirements of AWS D1.1, in particular those of Table 9.25.3
- to comment on how either or both of these techniques could be incorporated into the general requirements of the code.

RESEARCH APPROACH

The findings of the first phase of this project (2) indicated two problems with the AWS D1.1 procedures as far as detection and evaluation of vertical planar flaws were concerned. First, response amplitudes tended to be low owing to the poor orientation of the principal plane of the flaw to the ultrasonic beam, particularly for smooth flaws. This resulted in some indication ratings being such that these flaws were not designated as being rejectable major class A flaws. Second, there was no requirement to perform a diagnosis of flaw type, in order to identify a major flaw. The ultrasonic response pattern can provide more information about the flaw, for example whether or not it is a large extended discontinuity.

To provide information about these problems, so that suitable modifications could be made to the AWS D1.1 procedure, the research approach adopted was to examine a number of artificial flaws and natural weld flaws using both D1.1 and tandem techniques and to compare the defect ratings obtained. Response (echodynamic) envelopes were also recorded and examined in order to provide a basis for diagnosis of vertical flaws.

TANDEM TESTING

It is evident that when ultrasonic waves are incident on a smooth planar flaw at an oblique angle, most of the sound energy will be reflected away from the transmitting transducer. Thus an ultrasonic pulse-echo technique of the type specified in AWS D1.1, which uses a single transducer both to transmit ultrasonic waves and to receive responses from discontinuities, will be relatively insensitive to this type of flaw. The effects of discontinuity size, orientation and roughness on ultrasonic response have been examined in the literature (4,5) and this aspect is discussed further in Chapter 2.

The tandem technique overcomes this by seeking to detect the reflected signal, which would otherwise be lost; the test configuration being such that the ability to capture the reflected signal from the face of a vertical crack is maximised. This utilises two transducers, the first transmitting a sound beam obliquely on to a vertical planar flaw and the second receiving the sound reflected in a mirror-like fashion from the flaw surface. When testing on a parallel sided component, such as a plate, the two transducers are normally placed one behind the other

on the same surface as shown in Fig.1. This test configuration was used for all tandem testing carried out during this program.

The tandem technique is specified in D1.1 for the examination of fusion boundaries in electroslag and electrogas welds where fusion defects would be predominantly perpendicular to the plate surface. It is not required to be used for other types of joint. Nevertheless, this does indicate that its use is compatible with application of D1.1 procedures. Further, no special flaw detection equipment, other than a second transducer, is required to implement tandem testing.

The following parameters were examined using both tandem and pulse-echo ultrasonic procedures to determine their influence on flaw detection:

1. Flaw size.
2. Flaw position in the sample thickness.
3. Plate thickness.
4. Angle of flaw to the vertical.
5. Ultrasonic transducer size and frequency.

Further, the results were examined to determine whether the indication ratings and acceptance/rejection decisions arising from them were compatible with AWS D1.1 requirements.

In order to examine these factors systematically a number of specimens were produced containing artificial flaws in the form of milled notches. The results obtained from pitch-catch and pulse-echo tests on the notches were corroborated by further tests on a smaller number of real weld flaws and by comparison with the large amount of information obtained from real flaws during Phase 1 of Project 10-13 (2).

Specimens

Research specimens were prepared in three thicknesses of steel plate, 3.75in (95mm), 1.5in (38mm), 0.4in (10mm), conforming to the ASTM A36 specification for structural steel. Four samples were produced in each thickness containing machined notches at 0, 2.5, 5.0 and 10° to the vertical respectively. For the larger two thicknesses, ten notches were milled into each plate, three each of approximately 2, 4 and 8% of the plate thickness in height at three positions in the through-thickness. In the 0.4in (10mm) plates three notches only were included, of 5, 15 and 50% of the plate thickness, all positioned at mid-thickness. The end of each notch was flat, in order to represent a vertical or near vertical flaw. An example is shown in Fig.2.

In addition a welded sample was produced in each plate thickness which contained both angled and vertical planar real welding flaws. A total of 92 milled notches and nine weld defects were examined. Details of all specimens are given in Appendix A.

Ultrasonic Tests

Although the principal objective was to examine the performance of the tandem tests, it was also necessary to conduct pulse-echo tests in order to compare the results from the revised procedures with those obtained from "standard" D1.1 type tests on the same defects. Three types of ultrasonic transducer were used for both test modes:

i. 2MHz transducers with an element size of 0.8 x 0.9in (20 x 22mm), which complied with the requirements of Section 6.16 of D1.1,
ii. 2MHz transducers with an element size of 0.31 x 0.35in (8 x 9mm),
iii. 4MHz transducers with an element size of 0.31 x 0.35in (8 x 9mm).

Whilst transducer types (ii) and (iii) do not strictly comply with code requirements they have been used because the large type (i) transducers have certain disadvantages when used for tandem testing. Consequently, it was necessary to investigate the performance of the smaller transducers. The main disadvantage of large transducers for tandem testing is one of access; The two transducers have to be positioned close together to test flaws near the far side of thicker specimens or to examine thinner material. The larger transducer housings can prevent full coverage. Also on rougher surfaces the necessity to couple two transducers with large contact areas may pose additional problems. Smaller transducers are generally less affected. 4MHz transducers were also used, so that the effect of frequency could be assessed. Details of the transducers and flaw detectors used are given in Appendix A.

Pulse-echo tests were carried out according to the appropriate D1.1 requirements for each of the three plate thicknesses, using all three transducer types. Tandem tests were carried out in the manner shown in Fig.1. A jig, described in Appendix A, was used to keep the transducers aligned with each other. This was of considerable assistance in maintaining reproducible test conditions for this investigation; (A straight edge, such as a steel rule, held to the workpiece with small magnets is equally useful when testing welds in the field.) All three transducer types were again used, mainly with 45° beams (to keep the sound path length to a minimum) but for some cases on the 1.5in (38mm) samples and for all the 0.4in (10mm) samples 70° beams had to be used in order to gain access to the flaws. More details of the tests performed and of the results obtained are given in Appendix B.

ECHODYNAMIC RESPONSES

The echodynamic response of a flaw is the shape traced out by the signal on the flaw detector screen when an ultrasonic beam of finite width is scanned across it, in either the vertical or horizontal plane. This is produced by the interaction of the distribution of ultrasonic energy in the beam with the reflecting and diffracting features of the flaw, so that it may be considered as a characteristic of any ultrasonic beam/flaw combination. In practice the flaws vary much more than the ultrasonic beams and therefore an examination of the echodynamic response

may be used to characterise flaws into rudimentary categories; i.e. point reflector (e.g. porosity), thread-like (e.g. slag), planar and smooth (e.g. lack of fusion or smooth cracks) or planar and rough (e.g. rough cracks).

A vertical crack, of the type which tended to give low response amplitudes in previous work (2), can be diagnosed as such by the fact that the location of the echo moves along the flaw detector screen time-base as the ultrasonic transducer is scanned transverse to the flaw, hence the alternative term "walking echo". If the crack is rough then the amplitude of the signal will vary as the transducer is moved and will exhibit several maxima and minima.

This short piece of work involved comparing echodynamic responses from cracks with those from cylindrical holes at different depths in steel blocks to establish whether the echo types from the two kinds of reflector were sufficiently characteristic of flaw type to warrant further consideration as a means of flaw diagnosis.

Specimens

Two specimens were used for these tests. A 3.75in (95mm) thick steel block containing seven 3/16in (4.75mm) diameter cylindrical drilled holes spaced equally at different depths throughout the block thickness was used as a calibration sample. Results from this were compared with responses from flaws in the 3.75in (95mm) welded sample, J301.

Ultrasonic Tests

The holes in the calibration block and the flaws in sample J301 were scanned using a motorised scanning device to produce a number of line scans. This device was controlled by The Welding Institute's Micropulse computer controlled ultrasonic testing system, which allowed the ultrasonic signal to be continuously recorded along each scan line so that the echodynamic response could be displayed.

It should be emphasised that it is not essential to use computer controlled ultrasonic testing equipment in order to detect and evaluate echodynamic responses from flaws. In this case such a device was used to provide a means of recording the shape of the echodynamic envelope for reporting purposes; It is perfectly possible for the pattern to be observed on a conventional flaw detector screen and for the technician to diagnose the flaw type on the basis of the features seen. Indeed, it is a requirement that this be done in the current British Standard for manual ultrasonic weld examination (6).

To collect the echodynamic information 45, 60 and 70° transducers were used in the pulse-echo mode. Both 2MHz transducers conforming to AWS D1.1 and 4MHz miniature transducers (i.e. types (i) and (iii) above) were used. Further details are given in Appendix C.

CHAPTER TWO
FINDINGS

GENERAL

The findings are presented in 3 parts, those from tests on artificial notches, those from tests on weld flaws and finally the results from examination of echodynamic responses. The results are summarised in Tables 1-4 and Fig.4-8. Full details of all results are given in Appendices B and C.

TESTS ON ARTIFICIAL NOTCHES

A large amount of information was collected from both pulse-echo and tandem tests on the 92 artificial notches studied. The three plate thicknesses studied are considered separately, as not only do the test angle, and scanning and acceptance requirements in D1.1 depend heavily on material thickness, but the practicalities of performing tandem ultrasonic tests differ markedly between the heavy section 3.75in (95mm) plates and the 0.4in (10mm) plates.

The results are considered chiefly in terms of whether or not an 'A' rated flaw was predicted in each case, according to the criteria of Table 9.25.3 of AWS D1.1, as such notches represent smooth vertical planar flaws which should be rejectable to the code. The findings are presented in terms of the effect of transducer characteristics, effect of flaw angle, and effect of flaw size and position on flaw acceptance/rejection, for both pulse-echo and tandem tests.

3.75in (95mm) Thick Samples

The results from all tests carried out on the four specimens in this thickness are summarised in Table 1. Individual test results are given in Tables B3-B12 in Appendix B.

Pulse-Echo Tests (see also Tables B3-B9)

Effect of transducer characteristics. The requirement for scanning using D1.1 procedure 6 is:

- 70° PE2 (i) - top quarter and middle half of the thickness,
- 60° PE2 (i) - bottom quarter of thickness plus further coverage if fusion boundary reflectors found,
- 45° PE2 (i) - only for investigation of fusion boundary reflectors found.

It can be seen from Table 1 that all the vertical (0°) notches were classed as rejectable by the 70° D1.1 scan, two were not rejected on the grounds of amplitude by the 60° scan (although neither of these was in the bottom quarter of the plate thickness) and three were not rejected by the 45° scan. This indicates a relatively small dependence of response amplitude on angle of incidence, the average 'd' rating for all vertical

flaws being -4dB for 70° scans, +2.5dB for 60° and +5dB for 45°. This range was smaller than expected compared with previously reported data for smooth flaws (4), in which a change of orientation of 25° should give a change in amplitude of between 15 and 40dB, depending on the flaw size. This is considered further below.

The tests on the vertical notches using miniature 4MHz (type iii) transducers were uniformly poor at all three beam angles, with not one notch being diagnosed as an unacceptable major class A flaw. This result was not unexpected for the large angles of misorientation of the incident beam for these transducers, which have a smaller, much narrower ultrasonic beam than the larger 2MHz, type (i). The differences between the two sets of results can be explained to some extent by the effect of frequency on the interaction of the ultrasonic beam with a flaws. The ultrasonic pulse re-radiated from the flaw will have an angular spread of intensity which is related mainly to the ultrasonic wavelength and the size of the flaw. To gain an idea of the magnitude of the effect of these parameters the flaw can be considered to act as a piston re radiating energy, on which the semi angle of the spread of energy, β, is given by:

$$\beta = \sin^{-1} K\lambda/d \qquad \ldots[1]$$

where λ is the ultrasonic wavelength and d is the height of the flaw. For 20dB beam edges K can be considered to be 1.

Figure 3 shows this relationship plotted for 2 and 4MHz. It can be seen that as flaws become smaller they behave less directionally and more like point sources. As most of the flaws of interest lie in the range 0-10mm, it can be seen that for a given flaw size a large amplitude signal is much more likely to be seen at 2MHz than at 4MHz, irrespective of the actual misorientation angle of the incident beam to the plane of the flaw.

This, however, does not satisfactorily explain the better than expected results with the type (i) 2MHz transducers because:

- even at 2MHz only a poor response would be expected from the large, 50%t flaw which was 47.5mm high,
- 45° PE2 tests carried out with a miniature 2MHz transducer yielded results which were as poor as for the 4MHz tests.

The explanation would appear to be that the large beam area produced by the type (i) transducers tended to impinge not only on the notch faces, but also on the top side of the recess where they were machined into the end of the test samples. Thus the responses were the sum of individual reflectors from the notch face, which would be expected to be very weak for smooth vertical notches, the top corner of the notch, the face of the recess and the corner where the recess met the edge of the sample. The relatively poor resolution of these beams from the larger 22mm crystals (as opposed to 9mm crystals for 4MHz type (i) and the 2MHz type (ii) transducers) did not allow the technician to discriminate between these effects and consequently larger amplitudes were recorded.

Effect of flaw angle. For the D1.1 tests using type (i) transducers there was little effect of angle of the notches to the vertical. This is probably also a result of the beam width encompassing other geometrical reflectors, as discussed above, although it is worthy of note that flaws not designated as class A tended to be those closest to the top surface from which scanning took place.

The 4MHz tests did show some slight improvement for higher beam angles as the plane of the notches was angled towards the beam at 10°, the average d rating changing from +7.0 to +4.5dB for 70° scans, +12.5 to +10.0dB for 60° scans and +17.0 to +17.5dB for 45° scans. However, this did not significantly change the number of flaws reported as class A. The 45° 2MHz type (ii) tests were only carried out at two angles but these remained poor.

Effect of flaw size and position. For type (i) tests at all beam angles and at all notch angles there seemed to be no clear trend of variation in signal amplitude, either with size or position in the plate thickness. Again this may have been a result of the dominant effect of geometrical reflectors on the observed signals. The 4MHz type (iii) results at 45° showed a clear increase in d rating (i.e. a reduction in response amplitude) with flaws positioned deeper into the plate for all flaw orientations, but showed no such trend with flaw size. No discernible trends with either flaw size or location were observed from the 4MHz 60 and 70° tests.

Tandem Tests (see also Tables B10-B12)

Effect of transducer characteristics. The tandem tests were only carried out at 45° for this plate thickness, but all three transducer types were used. The results from the large 2MHz type (i) probes were emphatic in that all the 'd' ratings were large and negative indicating large response amplitudes for all flaw angles up to 10° to the vertical. However, one problem with these transducers was that the size of the casings prevented flaws in the lower part of the plate thickness being detected. It can be seen from Fig.1 that in order to satisfy the geometry of the test the transducers have to be moved closer together to detect signals from flaws near the lower surface of the plate. For these particular transducers the depth limit was around 65mm. This was true for all angles of the notches except 10° to the vertical. Angulation of the notches has the effect of widening the optimum transducer spacing for any given depth, thus enabling the lower flaws to be detected.

Type (ii) transducers operating at 2MHz overcame the problems of the large transducer housing and allowed the flaws at 3/4t to be detected. Again, there were some problems with the 10° angled notches, and these are discussed below. Similar behaviour was observed from the 4MHz tests with notches at 0, 2.5 and 5° to the vertical giving large responses, but those at 10° were not all classified as major class A flaws.

Effect of flaw angle. It can be appreciated from Fig.1 that the effect of tilting the flaw is to alter the direction of the reflected part of the ultrasonic beam by twice the angle of tilt. In this case the notches were tilted towards the direction of the incident ultrasonic beam which tended to increase the optimum transducer spacing. The transducers can, of course, be repositioned in order to obtain a maximum signal, but the beam arriving at the receiver transducer is no longer at an optimum angle for maximum sensitivity. If this variation in angle is too large than the ability to detect the reflected signal will be significantly reduced. This was the case for the 10° angled notches, where the beam was misoriented by 20° to the receiver. As expected, this effect was largest for the 4MHz transducers, which have a relatively poor tolerance of misorientation and was least pronounced for the small 2MHz type (ii) transducers, which have the widest beam divergence. Nevertheless for the 4MHz tests the larger, 8.4%t and 50.5%t flaws were all classified as major rejectable flaws.

Effect of flaw size and position. At 2MHz there was no general trend for amplitude to be related to size or position of flaws, except that the smallest flaws at 0° for type (i) tests gave lower than average amplitudes. On the other hand at 4MHz there was a consistent trend for amplitudes to increase with flaw height for 0 and 2.5° notches. This was, however, not evident at the higher angles of tilt where the geometrical factors, discussed above, also influenced the response.

1.5in (38mm) Thick Samples

Fewer tests were carried out on this plate thickness than on the 95mm samples so that there are fewer data to review. Further, the factors which are believed to affect the results are similar, so that less detail is included concerning the causes of the observations presented. The results are summarised in Table 2. More details are given in Appendix B, Tables B13-B17.

Pulse-Echo Tests (see also Tables B13 and B14)

Effect of transducer characteristics. Only 70° PE2 type (i) tests are specified for this material thickness by D1.1. Table 2 shows that none of the notch reflectors was classified as acceptable by this test. When this was repeated using a 70° type (iii) 4MHz transducers, 5 out of 10 notches at an orientation of 0° were deemed to be acceptable. The same result was obtained at 2.5° and 5°, and one notch was acceptable at 10°. This result showed the same trend as that for the 95mm thick samples, although the difference between 2MHz type (i) and 4MHz type (iii) transducers was not as marked. This probably arose from the fact that the accept/reject levels specified by D1.1 for 38mm thick plate are more stringent than for 95mm plate, causing more reflectors to be considered to be rejectable major flaws despite the poorer performance of the 4MHz type (iii) transducers.

Effect of flaw angle. Angling the flaws towards the incident ultrasonic beam increased the response amplitudes for the type (i) tests from an average of +2.6dB at 0° to -7.7dB at 10°. These were above the level of classification of the notches as major class A flaws at all angles. The type (iii) 4MHz test produced similar responses up to 5°, the average d rating being the same at 0° and 5°, with a value of +9.2dB. However at 10° the average d rating dropped to +3.1dB and all but one of the notches was classed as an unacceptable class A flaw.

Effect of flaw size and position. The results from this plate thickness showed the same general trend as for the 95mm plate, in that the type (i) transducer was relatively insensitive to the position of the flaw, whereas the type (iii) transducer gave generally lower responses the deeper the reflectors were in the plate thickness. However, it should be noted that this effect was not seen with 70° beams when the 95mm plate was examined.

Tandem Tests (see also Tables B15-B17)

Effect of transducer characteristics. On this thickness there would have been considerable problems with detection of most of the flaws with the large type (i) transducers, so that only the miniature types were used. The results from 45° tests at both 2 and 4MHz rejected all reflectors as large unacceptable class A flaws at all notch angles. The principal difference between this and the set of results on the 95mm samples, where some flaws were not rejected at the 10° angle, is thought to be the more stringent acceptance criteria for class A flaws.

Despite the miniature transducers being used, there was some difficulty in placing the transducers close enough together to allow detection of all notches when using the 45° beams. To alleviate this, 70° beams were also used, the results being shown in Tables 2 and B17. Again, all notches were rejected as being class A flaws, but in order to satisfy the geometry of the test, a 60° transmitter was used when examining the 10° angled notches. The necessity to do this shows that the limit of usefulness of the tandem test has been reached when reflectors are angled at around 10° to the vertical. However, at this angle the reflectors are much more likely to be detected by pulse-echo tests, so this is not considered to be a problem.

Effect of flaw angle. The 45° tests were highly tolerant of changes in notch angle, largely due to the wide beam spread of the type (ii) transducers. Despite the effect of flaw angle being such that it was necessary to change the ultrasonic beam angle of the transmitting transducer for the 70° tests, none of the tests failed to diagnose all the notches as major rejectable flaws.

Effect of flaw size and position. The 45° tests showed no consistent trend of sensitivity variation with position in the sample thickness. There was a weak trend, most marked for the vertical notches, for the response amplitude to increase with flaw size, but in general the

responses were all very large. For the 70° tests, both at 2.5 and 4MHz, there was little variation in amplitude with either flaw size or position for a given angle to the vertical. The amplitudes were large for the 70° tests but were significantly lower for the asymmetric 60° transmitter, 70° receiver combinations.

0.4in (10mm) Thick Samples

Plate which is only 0.4in (10mm) thick is nearing the lower limit of that which can be tested by ultrasonics without resorting to special techniques. The range of tests which it is possible to apply to this is therefore restricted; Indeed only limited testing is called for by AWS D1.1. In spite of this the signal amplitude levels for rejection of discontinuities as unacceptable major flaws are more stringent than for the other thicknesses studied. The results are summarised in Table 3.

Pulse-Echo Tests (see also Tables B18-B19)

Effect of transducer characteristics. Only 70° PE2 type (i) tests are specified for this thickness of material. In fact it was impossible to examine the notches in these small samples adequately using the large type (i) transducers so that miniature type (ii) transducers were used for 2.5MHz tests and type (iii) for 4MHz tests. At both frequencies all the notches at all angles were rejected as unacceptable major flaws. However, the response amplitudes were much lower at 4MHz, the average d rating being +5dB compared to -13dB for 2.5MHz.

Effect of flaw angle. There was little effect of notch angle on the response amplitude at either 2.5 or 4MHz. This was expected, because the small size of the flaws tends to make them behave like point reflectors giving omnidirectional responses.

Effect of flaw size and position. Flaw position could only be examined to a limited extent as all the notches were placed at mid thickness. At 2.5MHz there was a tendency for responses to be larger for the bigger flaws, but response amplitude was virtually independent of size at 4MHz.

Tandem Tests (see also Tables B20 and B21)

Effect of transducer characteristics. Only 70° tests could be carried out on this relatively thin material. Again all the notches at all angles were found to be class A flaws. Some very large amplitudes were recorded for the 15 and 50% notches at 2.5MHz. Whilst the amplitudes were somewhat lower for the 4MHz tests, they all comfortably exceeded the limiting value for class A flaws.

Effect of flaw size. For each flaw size at both frequencies there was some tendency for a reduction in amplitude with increasing angle of the notches to the vertical. However, this was not consistent and, as with the pulse-echo tests in this thickness of material, the flaws behaved more like omnidirectional reflectors.

Effect of flaw size and position. At both frequencies the 50% t notch gave the largest responses of the three at all beam angles although there was less consistency about the sizes of responses from the smaller two notches. Again, this is in line with these small notches behaving more like point reflectors.

TESTS ON WELD FLAWS

In some respects the real weld flaws represented a less severe challenge to the capabilities of the ultrasonic detection techniques (both pulse-echo and tandem) than the notches. The roughness and irregularity of real flaws, even those designed to be vertical cracks, increase the chances of detection by a misoriented ultrasonic beam. By and large the flaws were classified as unacceptable category A defects by all beam angles used for all plate thicknesses. Results are summarised in Table 4, and further details are given in Tables B22-B24.

It is noteworthy that the one non- class A result for the 95mm thick sample was obtained using a 45° beam, which is not part of the D1.1 procedure. Further, the same flaw, flaw 2, gave a tandem response d rating of - 36dB, indicating that this flaw was smoother and oriented nearer to the vertical than the others.

Flaw number 3 in the 38mm thick specimen J302 was classified as a class D minor flaw by both 70° and 60° tests to AWS D1.1 requirements. However, it should be noted that the 70° test did classify it as a class A flaw when the block was re-tested after the weld crown had been removed. It can be seen from Fig.A4 of Appendix A that this flaw lay near the top surface of the specimen, such that detection would only have been possible on the 2nd leg of the beam path with the weld crown in place. Removal of the weld crown allowed a direct scan over the flaw location and hence a greater response amplitude. Again, the tandem test gave a very large response for this flaw, demonstrating the value of this means of detection for flaws which give weak responses in pulse-echo tests.

Flaw number 2 in the same specimen was not detected by the tandem test because the transducers could not be placed sufficiently close together to obtain an adequate response from it. Reference to Fig.A4 shows that this flaw lay in the bottom quarter of the plate thickness, a location which is difficult to test using the tandem configuration.

All the flaws in the 10mm thick sample were reported as major class A flaws by all tests.

ECHODYNAMIC CURVES

The echodynamic curve is the locus of the peak of the instantaneous ultrasonic response as a transducer is scanned across a flaw. By scanning across a calibration reflector, usually a cylindrical drilled hole, the

ultrasonic beam profile can be determined. This was carried out for a number of transducers at 2 and 4MHz and at 45°, 60° and 70°. The results showed the expected increase in beam diameter with increasing range; These are presented in Appendix C.

Of interest was whether the echodynamic response from an unknown flaw could be used to determine if it were a large extended discontinuity, and hence substantiate an accept/reject decision made on the basis of response amplitude. Figure 4 shows the echodynamic response from flaw number 1 in specimen J301 taken using a 45° ultrasonic beam. Two peaks are clearly seen, one originating from the top of the crack and the other from the bottom. These are in fact diffracted signals from the crack tips, the same responses which are used for flaw sizing by the time-of-flight diffraction technique (3). The diffracted responses observed here can also be used to measure the height of the crack, but they do not provide any information about whether the two responses are from the edges of a continuous major flaw or arise from two separate minor flaws. However, by changing the ultrasonic beam angle, such additional information can be obtained. Figure 5 shows the echodynamic response from a 70° test on the same crack. Here, instead of two separate responses, each exhibiting a single peak, a continuous response with many maxima and minima was observed as the transducer was scanned across the flaw. In this case the response consists of very little diffracted energy, being mostly ultrasound reflected from different facets on the crack surface. Thus it is evident that a large extended flaw is present. This type of analysis of flaw type, based on the use of a variety of different beam angles, is now an essential part of the British Standard specification for ultrasonic testing (6).

Such analyses are subjective. At the outset of this program it was suggested that one means of making the use of the echodynamic curve more rigorous was to examine whether the width of the response from cracks exceeded that from the calibration holes. Figures 6-8 show the results from 4MHz 45°, 2MHz 45° and 2MHz 70° tests respectively on the same crack, as discussed above. It can be seen that in no case does the width of a single response exceed the response width from the calibration holes, as defined by the least squares fit straight line through the results from the holes at different ranges. Where the widths of the responses from the top and bottom of the crack in Fig.6 were added, the total exceeded the beam width defined by the holes, but it would be difficult to justify doing this in many instances.

These results show that, whilst it is possible to determine that a continuous flaw exists, and even to determine its height, by using the echodynamic responses, it is not possible to use a simple measurement of response width to predict a large continuous reflector, using the transducer types and frequencies studied in this program.

CHAPTER THREE
INTERPRETATION, APPRAISAL, APPLICATIONS

GENERAL CONSIDERATIONS

The principal factors examined in this part of the project were:

- whether the tendency of the D1.1 pulse-echo tests to fail to diagnose vertical planar flaws as unacceptable major defects, as reported previously (2), was again observed,
- whether the ultrasonic tandem test configuration enabled such a shortcoming of the specified ultrasonic test procedures to be overcome,
- the influence of test parameters, such as beam angle, ultrasonic frequency and transducer size, and also prevailing conditions including plate thickness, flaw size, location and orientation, on the ability of tandem tests to diagnose vertical planar flaws,
- the possibility of using the interpretation of the echodynamic response from flaws to reveal more about their nature.

Much of the following discussion depends upon the definition of the boundary between acceptable discontinuities and unacceptable flaws according to the D1.1 code. The requirements for evaluation have been set out in a nomogram, from Ref.(2), which is shown in Fig.9. This indicates a relationship between acceptability of discontinuities and their percentage through wall height. It is known that these criteria are empirical (8) and are not based on a consideration of fitness for service of the weld. Moreover, it is uncertain whether the relationship between rejection of a flaw and its through wall height is maintained in practice because it is not usual for the height of a flaw to be measured according to D1.1 procedures.

Nevertheless, if the true rather than percentage intended limiting rejectable flaw height from Fig.9 is plotted against plate thickness, it can be seen that the absolute flaw size intended to be rejected for most commonly used plate thicknesses is very small, Fig.10. Thus it is evident that in normal operation the D1.1 acceptance criteria are generally very stringent, the stringency becoming considerably greater for thinner plates. With this in mind, all the flaws examined in all plate thicknesses should have been rejectable to the code.

As discussed previously (2), the almost sole reliance of the D1.1 procedures on the assessment of response amplitude from a flaw to determine whether or not it is acceptable makes them prone to failure when a flaw responds only weakly to ultrasound. In such instances there is no provision in the D1.1 procedure for evaluation of a poorly reflecting, but extensive, flaw. Other studies (4,5) have indicated that smooth, misoriented flaws can produce responses more than 20dB lower than favourably oriented ones, suggesting that problems could occur with reliable rejection of such flaws. As vertical planar flaws, the most detrimental from a fitness for service point of view, tend to fall into

this category, this potential shortcoming of the D1.1 procedures should be recognised. Indeed, tandem testing, which is widely used for testing very high quality thick section welds for nuclear power plant (9), is already specified for testing electroslag and electrogas welds where vertical flaws are known to be likely. It was thus considered to be worthwhile exploring whether or not wider application of tandem testing would significantly enhance the reliability of D1.1 procedures for detection and rejection of vertical planar flaws.

PERFORMANCE OF TANDEM TESTING

The tandem tests performed very well on both artificial notches and real weld flaws, when conditions were favourable for using the tandem configuration, with very large response amplitudes being obtained. However, it became evident that there were 3 main limiting factors to application of tandem testing. These were:

i. The physical size of the transducer housings, especially at 2MHz. This limited how close the ultrasonic beam emission points of the two transducers could approach each other thereby limiting coverage and created a practical difficulty of maintaining ultrasonic coupling between two large transducers and the workpiece. To overcome this miniature transducers were successfully used, both at 2.5 and 4MHz, although these did not strictly comply with the requirements of D1.1 with regard to transducer element size.

ii. The extent of coverage of the plate thickness. Figure 1 shows that to examine the far side of the plate the transducers have to be in the same place. Obviously tandem testing becomes impossible before that point is reached, so that even under the most favourable conditions using miniature transducers the lower 25% of the wall could not easily be examined in this way. Further, to examine flaws near the top surface of the plate the weld crown would have to be removed, although this would be carried out anyway for critical welds.

iii. Flaw angle. The smooth artificial notches would be expected to give the most directional responses, the rougher real flaws producing more scattered ultrasound, which can be detected over a wider angular range. Problems were experienced with the notches angled at 10° to the vertical because they deflected the incident sound energy through 20° by a similar effect to an optical lever. Consequently response amplitudes were considerably diminished and some of these flaws were accepted. It was attempted to counter this by using a different angle transmitter transducer for the 1.5in (38mm) and 0.4in (10mm) plates, but as the flaws set at the 10° angle were reliably detected by the pulse-echo tests in accordance with the D1.1 requirements, the failure of the tandem tests to reject them is probably not important.

The practicalities of carrying out the tandem test were straightforward. A simple jig was used to align the two transducers. This could be as basic as a magnetic rule. The tandem test can be carried out using a conventional flaw detector, calibrated in the usual manner.

TANDEM TESTS AND D1.1 REQUIREMENTS

Although the original aim was to demonstrate the use of tandem testing to augment the normal D1.1 procedures, the above discussion and the results summarised in Tables 1-4 indicate that:

i. despite the high certainty of rejection of planar flaws there are several reasonably severe constraints on the general use of tandem testing.
ii. the tests carried out according to the appropriate D1.1 procedures for the difference plate thicknesses performed extremely well in rejecting planar flaws, even on the vertical smooth notches.

The latter finding was surprising in that the performance of pulse-echo tests on the notches, particularly those oriented vertically, would have been expected to be poorer, both from theoretical considerations and from other work (4,5). It is suspected that the reason for this is the inability of the large ultrasonic beams from standard-sized 2MHz transducers to resolve the responses from the face of the notch from other geometrical reflectors, leading to an optimistic result. In retrospect the design of the test specimens should have been modified to reduce such effects.

Nevertheless, another contributory factor is the stringency of the flaw acceptance criteria, especially for the 1.5in (38mm) and the 0.4in (10mm) plate. Figure 10 shows that the target limiting flaw sizes for these plate thicknesses are 1.2 and 0.4mm respectively, which means that even relatively weak reflectors of ultrasound are likely to be rejected as class A flaws.

To summarize, tandem tests perform best where plate thicknesses are larger and manipulation and coverage are not a problem. The use of miniature 2 or 2.5MHz transducers seemed to offer the best performance for coverage and detection of flaws. It would appear that tandem tests would only be of real benefit for testing thicknesses of around 3-4 inches (75-100mm) upwards, as in addition to the greater ease of coverage, the propensity for large planar flaws to occur will increase with thickness and the less severe acceptance criteria may cause pulse-echo inspection to fail to reject unfavourably oriented flaws.

ECHODYNAMIC RESPONSES

Echodynamic pattern type has been shown to be related to the overall form of flaws (4). The 3 basic types of pattern are shown in Fig.11. It can be seen that pattern 1 represents the response from a smooth reflector of smaller size than the ultrasonic beam; The responses from cylindrical holes shown in Appendix C are of this type. Pattern 2 arises from a smooth extended reflector and pattern 3 from an extended rough or multiple reflector.

The echodynamic curves may be obtained by scanning the transducer transversly across a flaw or parallel to it. In the case of a point reflector, such as an isolated pore, a pattern 1 response will be obtained when scanning in both directions. Most other types of weld flaw are elongated along the weld owing to the nature of the welding process. Hence the pattern usually observed when scanning parallel to the flaw will be type 2 or 3. Typically the following combinations of scanning patterns will be observed:

- Point reflector, such as an isolated pore - Transverse, pattern 1, parallel, pattern 1.
- Thread-like flaw, such as a small slag line - Transverse, pattern 1, parallel, pattern 2.
- Extended smooth flaw, such as a lack of fusion - Transverse, pattern 2, parallel, pattern 2 or 3.
- Extended rough flaw, such as a crack - Transverse, pattern 3, parallel, pattern 3.

It should be noted that cluster flaws, such as porosity, will tend to give pattern 3 type responses but are notoriously difficult to evaluate using ultrasonics. Also, it is important to note that it is only attempted to categorise flaws by reference to their general shape, not by their precise type. In most cases an ultrasonic test does not provide sufficient information for an unequivocal diagnosis of flaw type to be made, although other details about metallurgical or welding process conditions may suggest that a particular flaw is likely.

With reference to the echodynamic curves presented in this document, Fig.5 shows pattern 3 behaviour consistent with an extended rough flaw being present. It should be noted that flaws are deemed to be rough when the RMS surface roughness exceeds 1/5 of the wavelength of the ultrasound. This is 0.32mm (0.013in) for 2MHz and 0.16mm (0.007in) for 4MHz, so that flaws do not need to be excessively jagged to behave in a rough manner. Figure 4 requires more explanation, as each of the two peaks is from a diffraction source, a crack tip, and consequently gives a pattern 1 response when considered in isolation. If the two peaks are considered together the behaviour is more akin to pattern 3, but even so it is not clear from this alone that a large flaw is present. This highlights the need to use several ultrasonic beam angles to gather different information about a flaw in order that a correct diagnosis of its type can be made.

In summary, the use of the echodynamic behaviour of ultrasonic signals as a pulse-echo transducer is scanned across a flaw can provide significant additional information about flaw type and even size. The interpretation should be based on an assessment of the echodynamic pattern, as described in a British Standard (6) and International Institute of Welding recommendations (4) because measurements of envelope width do not provide a reliable means of determining whether an indication represents a large extended flaw.

CHAPTER FOUR
CONCLUSIONS AND RECOMMENDATIONS

CONCLUSIONS

1. A tandem ultrasonic test technique proved to be highly effective for rejecting planar flaws, where they could be detected.

2. Coverage of the volume to be inspected was limited by the need to place the transducers in close proximity to each other, especially on the thinner 1.5in (38mm) and 0.4in (10mm) plates.

3. Good coverage was considerably easier to obtain on the thicker 3.75in (95mm) plates.

4. The effectiveness of the tandem technique was severely impaired when flaws were angled at more than 5° to the vertical, but at greater angles this was compensated for by better performance of pulse-echo tests.

5. Echodynamic responses from flaws provide a means of gaining considerable additional information about the type and size of flaws detected by the amplitude based D1.1 techniques.

RECOMMENDATIONS

1. Notwithstanding the good results obtained from pulse-echo tests on both notches and weld defects, it is considered that a requirement to perform an additional tandem test when examining welds greater than 3in (75mm) thick would considerably enhance the confidence which could be placed on ultrasonic inspection to D1.1. This could be confined to particularly important welds such as those in fracture critical tension members.

2. The major shortcoming of the D1.1 procedures is that flaw rejection is almost entirely based on signal amplitude. If evaluation of a flaw's echodynamic response characteristics were incorporated into the accept/reject criteria, then weakly reflecting but extensive flaws would be recognised and rejected.

REFERENCES

1. Structural Welding Code - Steel, AWS D1.1-88 American Welding Society 1988.

2. Jessop, T.J., Mudge, P.J. and Harrison, J.D. "Ultrasonic measurement of weld flaw size". National Cooperative Highway Research Program Report No.242, Transportation Research Board, Washington DC, 1981.

3. Duncumb, A.C. and Mudge, P.J. "Ultrasonic measurement of weld flaw size - phase 2: Studies of the time-of-flight diffraction technique for flaw evaluation". Welding Institute Report No. 3769/15 Part 2, 1987, for NCHRP.

4. Meyer, H-J. "The international state-of-the-art in non-destructive inspection of welds, with special emphasis on flaw characterisation". Materials Evaluation, Vol.42, (May 1984), pp.793-802.

5 Coffey, J.M. "Quantitative assessment of the relability of ultrasonics for detecting and measuring defects in thick section welds". Proc. Conf. "Tolerance of flaws in pressurised components". IMech E, London, May 1978.

6. British Standard 3923. "Ultrasonic examination of welds: Part 1, Methods for manual examination of fusion welds in ferritic steels". British Standards Institution, London 1986.

7. "Boiler and Pressure Vessel Code, Section V Non-Destructive Testing". American Society of Mechanical Engineers, New York, 1986.

8. Shenefelt, G.A. "Ultrasonic testing - requirements of the AWS 1969 Building Code and Bridge Specifications". Welding Journal (May 1971), pp.342-349.

9. Kolb, K. and Wolfel, M. "The ultrasonic testing of nuclear reactor pressure vessels". Materialprufung, Vol.17, No.10, 1975, pp.352-358.

Table 1 Results from 95mm specimens with notches - Summary: Number of Non-A* results

Test**	Angle of notches to the vertical			
	0°	2.5°	5°	10°
45° PE, 2 (i)	3 (2B,1C)*	1 (1B)	0	2 (1C,1D)
45° PE, 2 (ii)	10 (10D)	-	10 (10D)	-
45° PE, 4 (iii)	10 (10D)	10 (10D)	10 (10D)	10 (10D)
60° PE, 2 (i)	2 (2B)	1 (1B)	2 (1B,1C)	0
60° PE, 4 (iii)	10 (10D)	10 (10D)	7 (4D,2C,1B)	9 (8D,1B)
70° PE, 2 (i)	0	0	0	0
70° PE, 4 (iii)	10 (6D,3C,1B)	10 (8D,2C)	10 (4D,4C,2B)	7 (5D,2B)
45° T,2, (i)	0	0	0	0
45° T,2, (ii)	0	0	0	1 (1D)
45° T,4, (iii)	0	0	0	4 (1B,3D)

* Flaw classification, as defined by Table 9.25.3 of AWS D1.1

** Test type:
45° = Ultrasonic beam angle
PE = Test configuration pulse-echo or tandem
2 = Ultrasonic frequency, MHz
(i) = Transducer type - see Chapter 1

P.J. Mudge

Table 2 Results from 38mm specimens with notches - Summary: Number of Non-A* results

	Angle of notches to the vertical			
Test**	0°	2.5°	5°	10°
70° PE, 2 (i)	0	0	0	0
70° PE, 4 (iii)	5 (2B,1C,2D)	5 (2C,3D)	5 (1B,2C,2D)	1 (1B)
70° T,2.5 (ii)	0	0	0	0
70° T,4 (iii)	0	0	0	0
45° T,2 (ii)	0	0	0	0

* Flaw classification, as defined by Table 9.25.3 of AWS D1.1
** Test type:
45° = Ultrasonic beam angle
PE = Test configuration pulse-echo or tandem
2 = Ultrasonic frequency, MHz
(i) = Transducer type - see Chapter 1

P.J. Mudge

Table 3 Results from 10mm specimens with notches - Summary: Number of Non-A* results

Test**	Angle of notches to the vertical			
	0°	2.5°	5°	10°
70° PE, 2.5 (ii)	0	0	0	0
70° PE, 4 (iii)	0	0	0	0
70° T,2.5 (ii)	0	0	0	0
70° T,4 (iii)	0	0	0	0

* Flaw classification, as defined by Table 9.25.3 of AWS D1.1

** Test type:

45°	=	Ultrasonic beam angle
PE	=	Test configuration pulse-echo or tandem
2	=	Ultrasonic frequency, MHz
(i)	=	Transducer type - see Chapter 1

P.J. Mudge

Table 4 Results from weld flaws - Summary: Number of Non-A* results

Test**	Plate thickness, in (mm)		
	3.75 (95)	1.5 (38)	0.4 (10)
70° PE, 2 (i)	0	1 (D)+ 0	-
70° PE, 2.5 (ii)	-	-	0
70° PE, 4 (iii)	-	-	0
60° PE, 2 (i)	0	1 (D)+	-
45° PE, 2 (i)	1 (B)	-	-
70° T, 2.5 (ii)	-	-	0
70° T, 4 (iii)	-	-	0
45° T, 2 (i)	0	-	-
45° T, 2 (ii)	-	1 (not detected)	-

* Flaw classification, as defined by Table 9.25.3 of AWS D1.1
\+ As-welded surface, otherwise all ground finish
** Test type:
45° = Ultrasonic beam angle
PE = Test configuration pulse-echo or tandem
2 = Ultrasonic frequency, MHz
(i) = Transducer type - see Chapter 1

P.J. Mudge

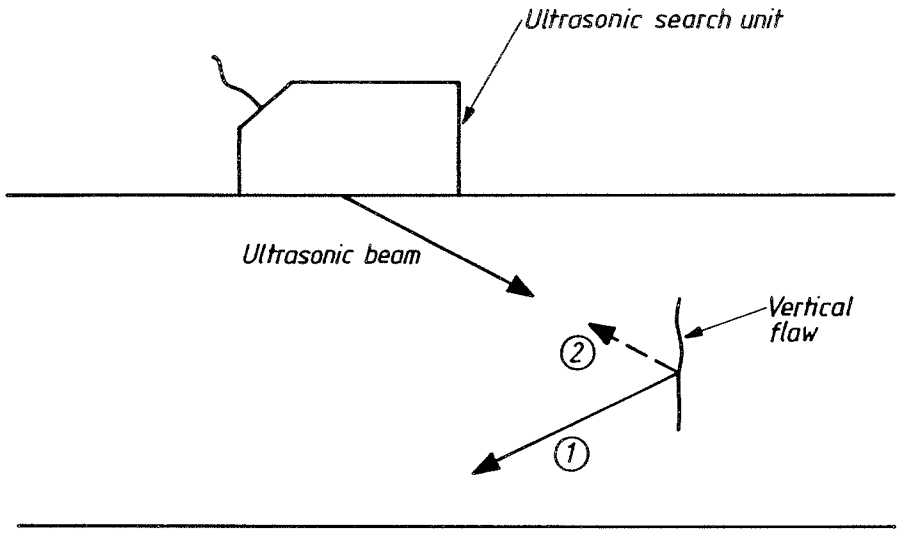

Single search unit
(1) Most incident sound energy reflected away
(2) Only a small amount of sound scattered back towards search unit
Result: Only very low amplitude signals observed

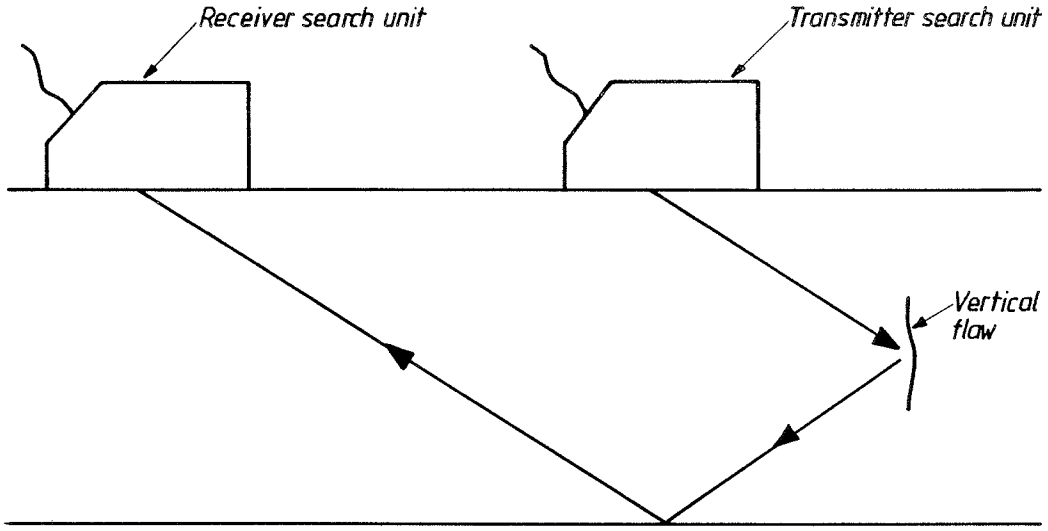

Tandem search units
The reflected sound energy is collected by a second receiver probe to give a high amplitude signal. Amplitude will be related to the flaw's size and roughness.

Fig. 1. Principle of tandem tests.

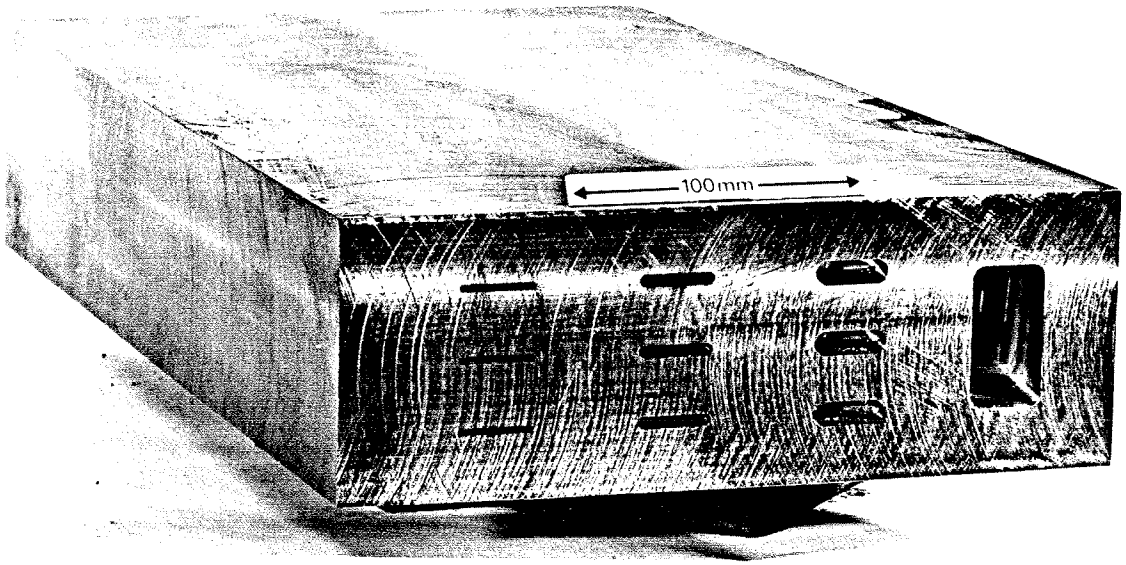

Fig.2 A 3.75in (95mm) specimen containing machined notches. Note the angled end face, which can be seen on the 50%t notch.

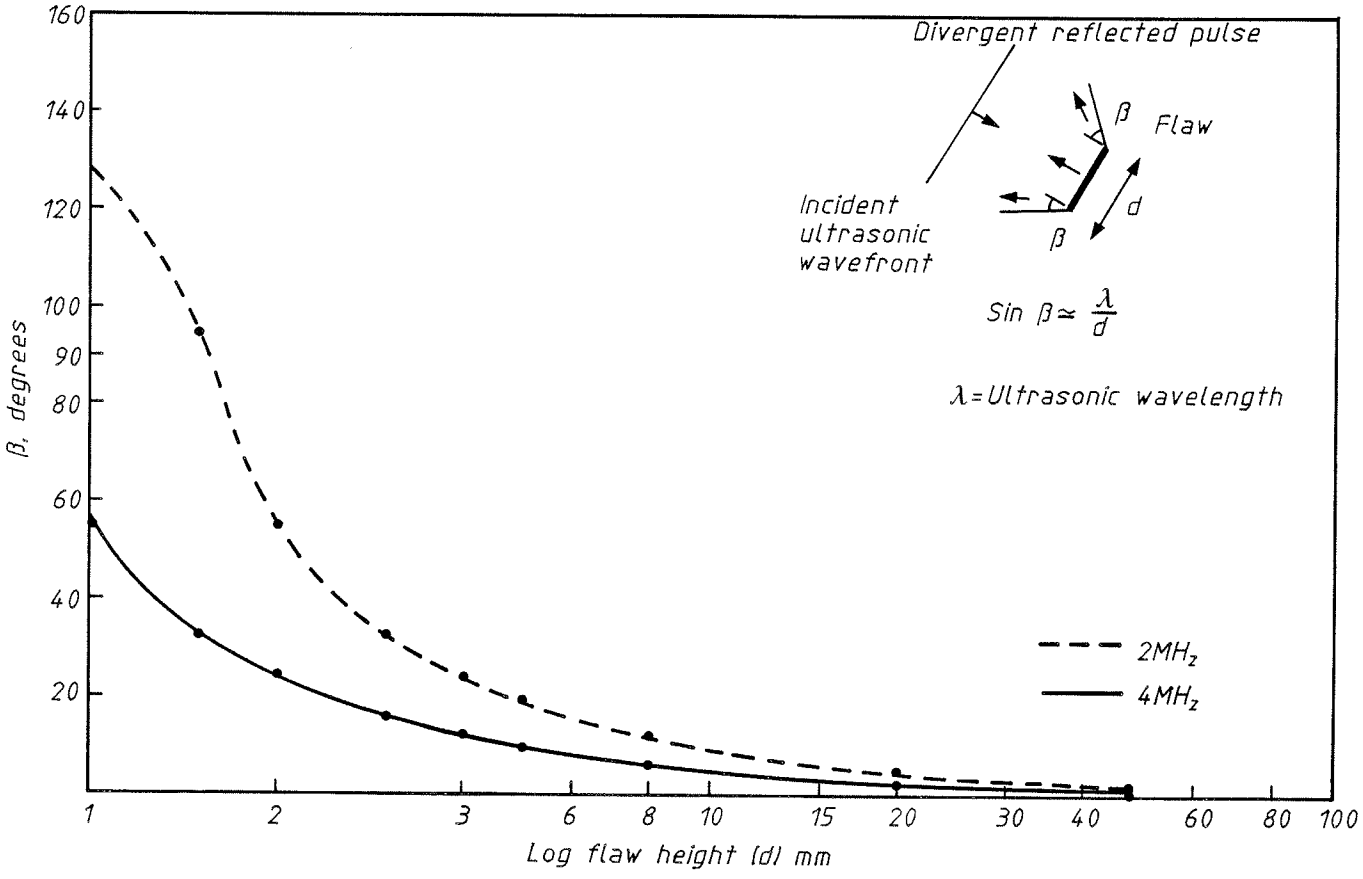

Fig.3 Angular spread of reflected signals, B, versus flaw height, d.

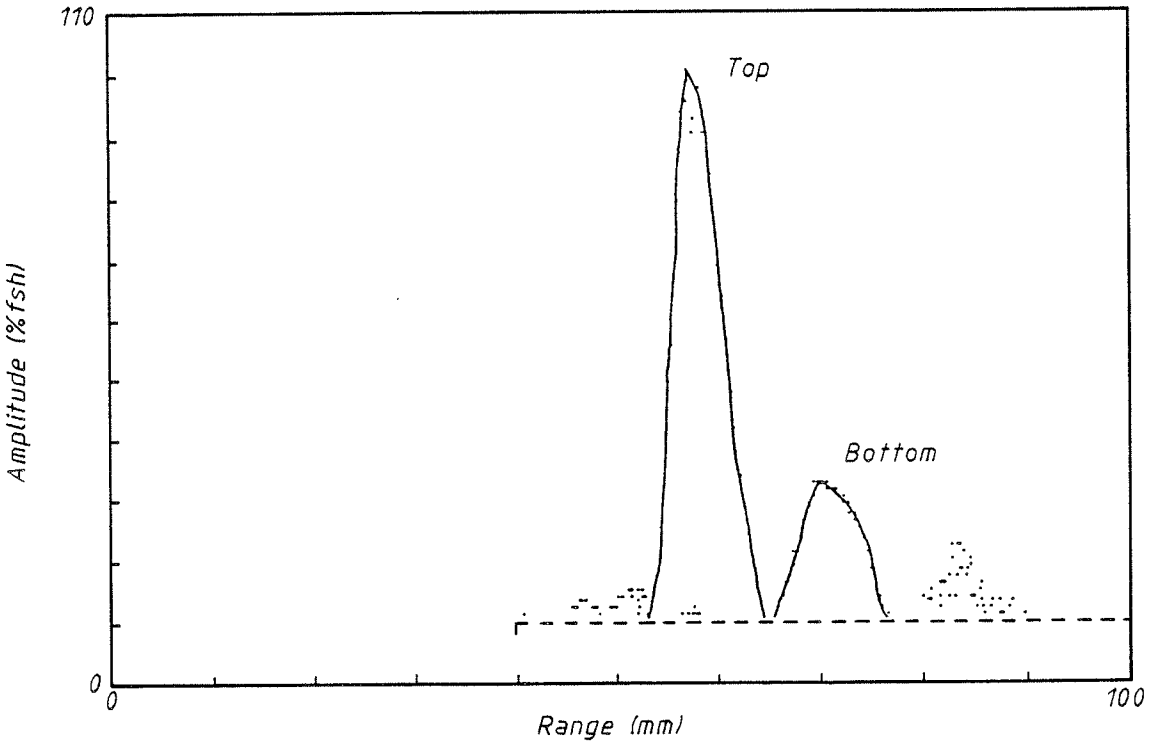

Fig.4 Echodynamic curve from a crack in specimen J301 using a 4MHz 45° miniature transducer.

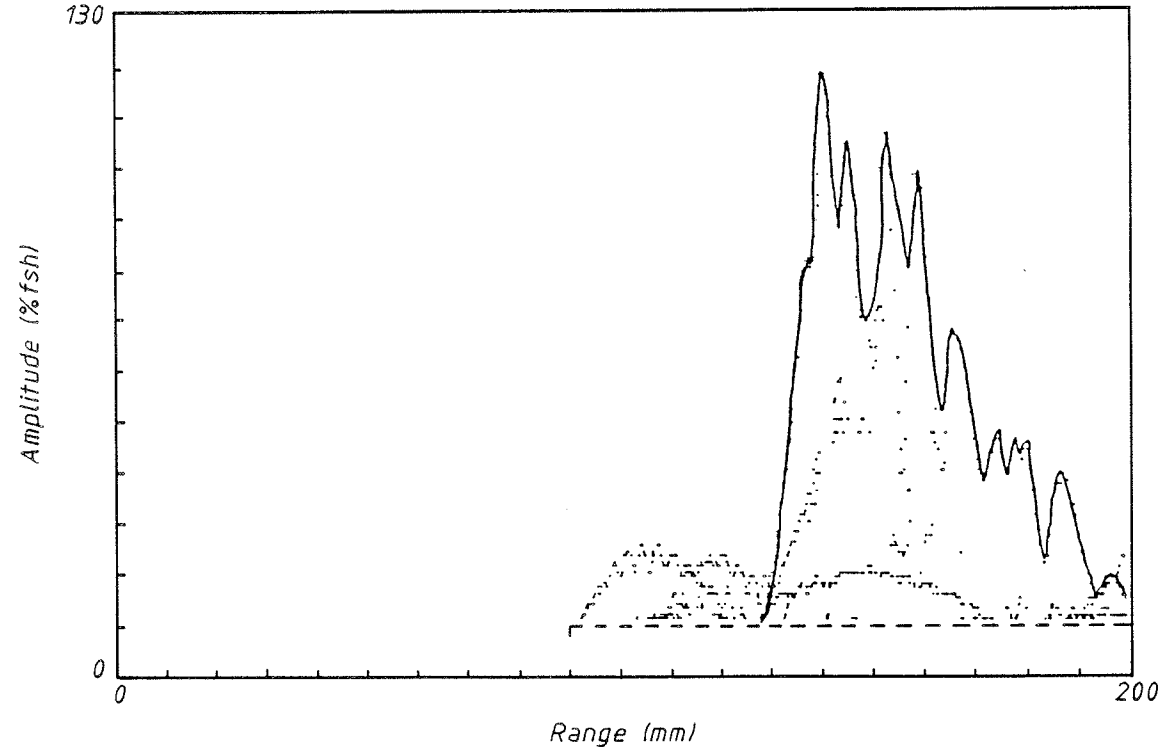

Fig.5 Echodynamic curve from a crack in specimen J301 using a 2MHz 70° transducer.

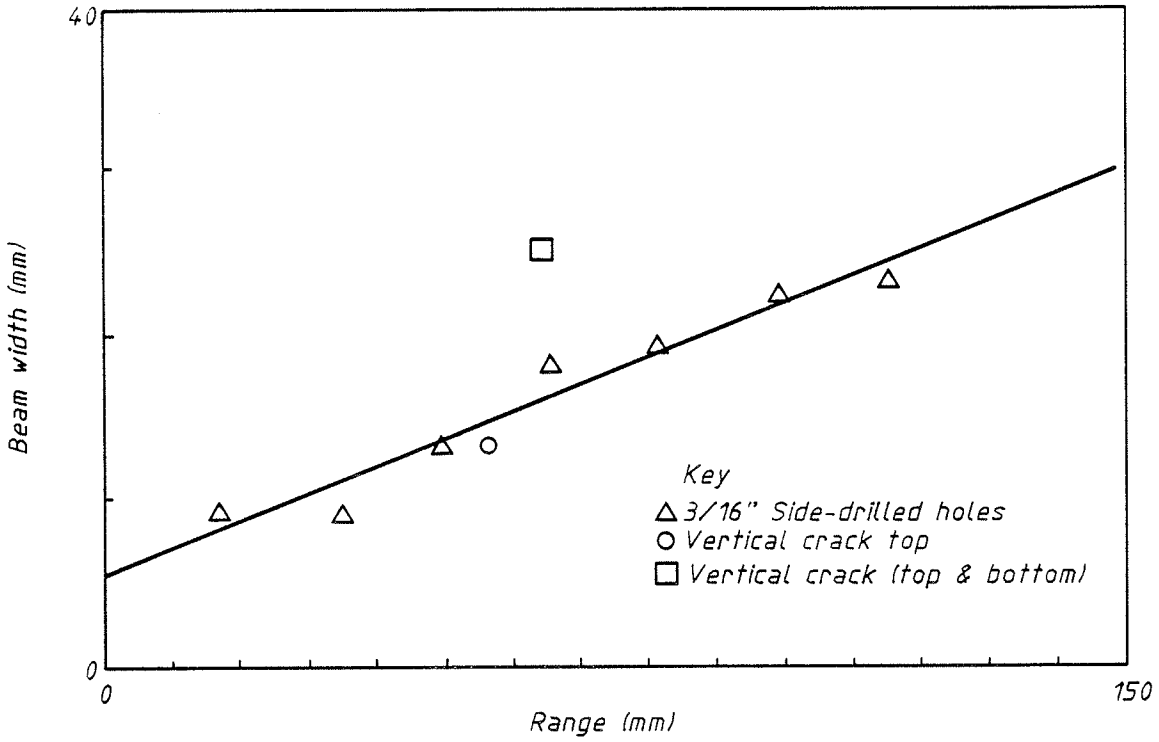

Fig.6 Beam width determined from drilled holes and crack response width using a 4MHz 45° transducer.

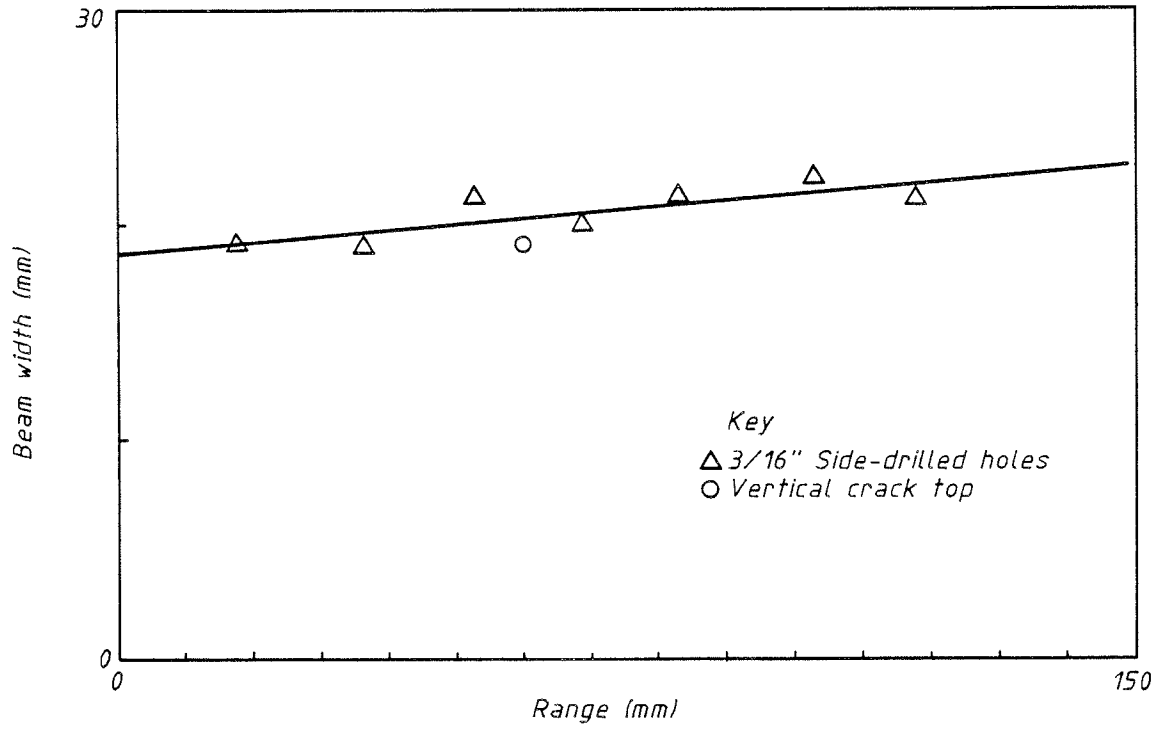

Fig.7 Beam width determined from drilled holes and crack response width using a 2MHz 45° transducer.

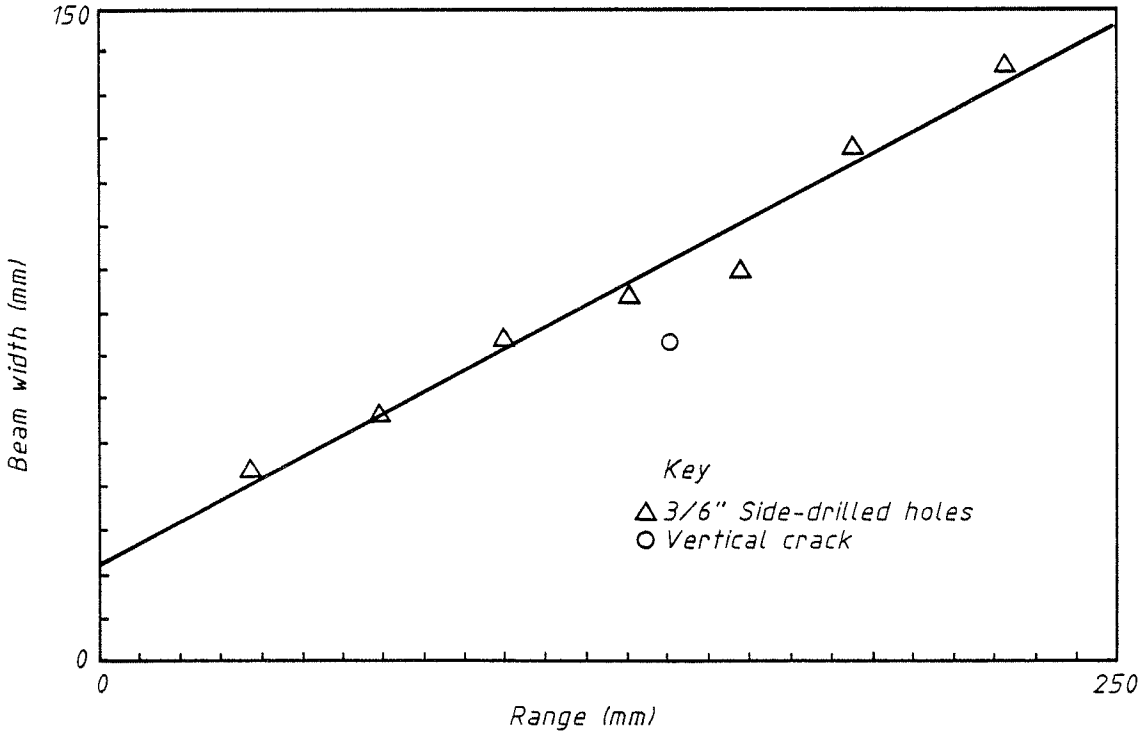

Fig.8 Beam width determined from drilled holes and crack response width using a 2MHz 70° transducer.

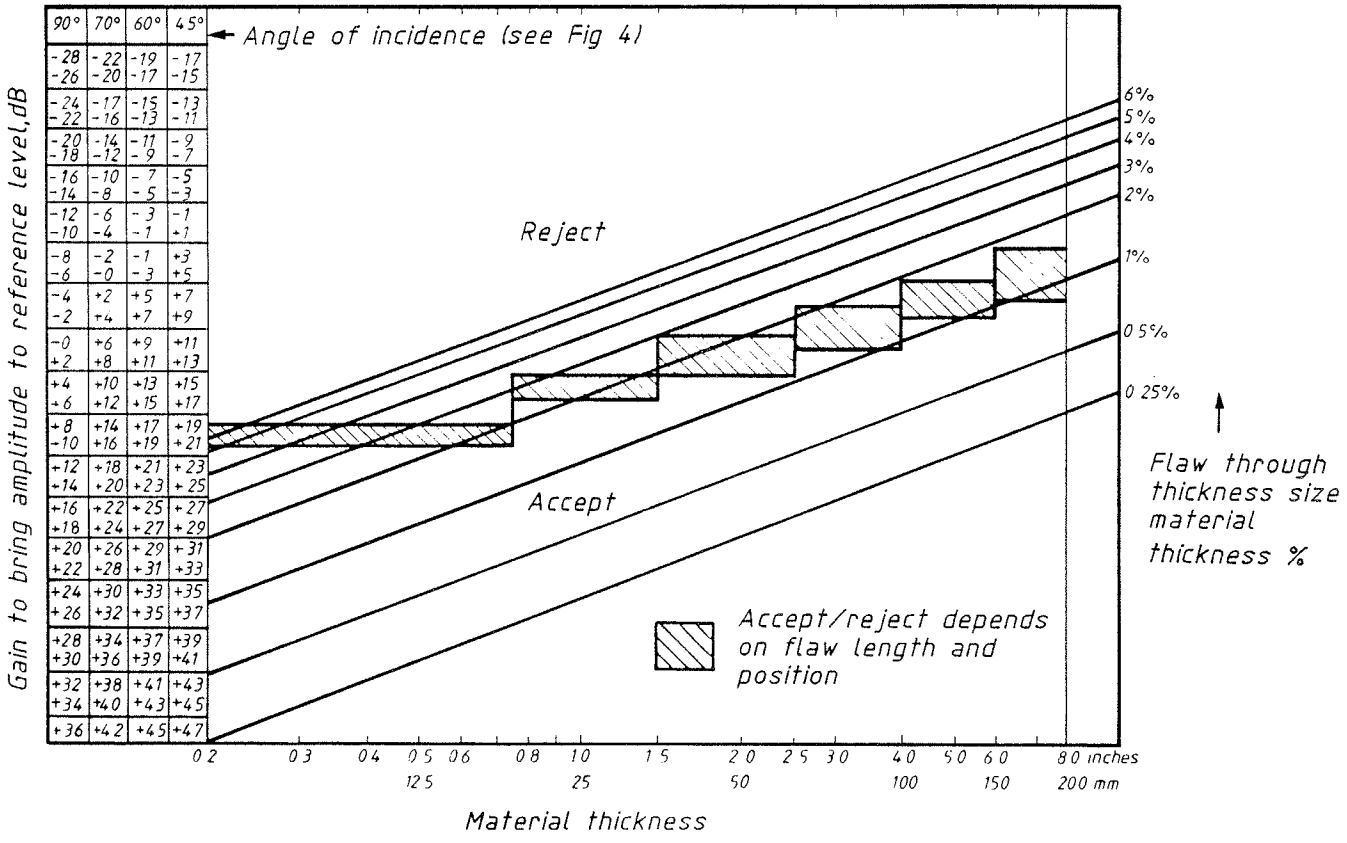

90°	70°	60°	45°
-28 -26	-22 -20	-19 -17	-17 -15
-24 -22	-17 -16	-15 -13	-13 -11
-20 -18	-14 -12	-11 -9	-9 -7
-16 -14	-10 -8	-7 -5	-5 -3
-12 -10	-6 -4	-3 -1	-1 +1
-8 -6	-2 -0	-1 -3	+3 +5
-4 -2	+2 +4	+5 +7	+7 +9
-0 +2	+6 +8	+9 +11	+11 +13
+4 +6	+10 +12	+13 +15	+15 +17
+8 -10	+14 +16	+17 +19	+19 +21
+12 +14	+18 +20	+21 +23	+23 +25
+16 +18	+22 +24	+25 +27	+27 +29
+20 +22	+26 +28	+29 +31	+31 +33
+24 +26	+30 +32	+33 +35	+35 +37
+28 +30	+34 +36	+37 +39	+39 +41
+32 +34	+38 +40	+41 +43	+43 +45
+36	+42	+45	+47

Fig.9 Relationship between material thickness, flaw size and predicted amplitude of response for AWS D1.1 procedures.

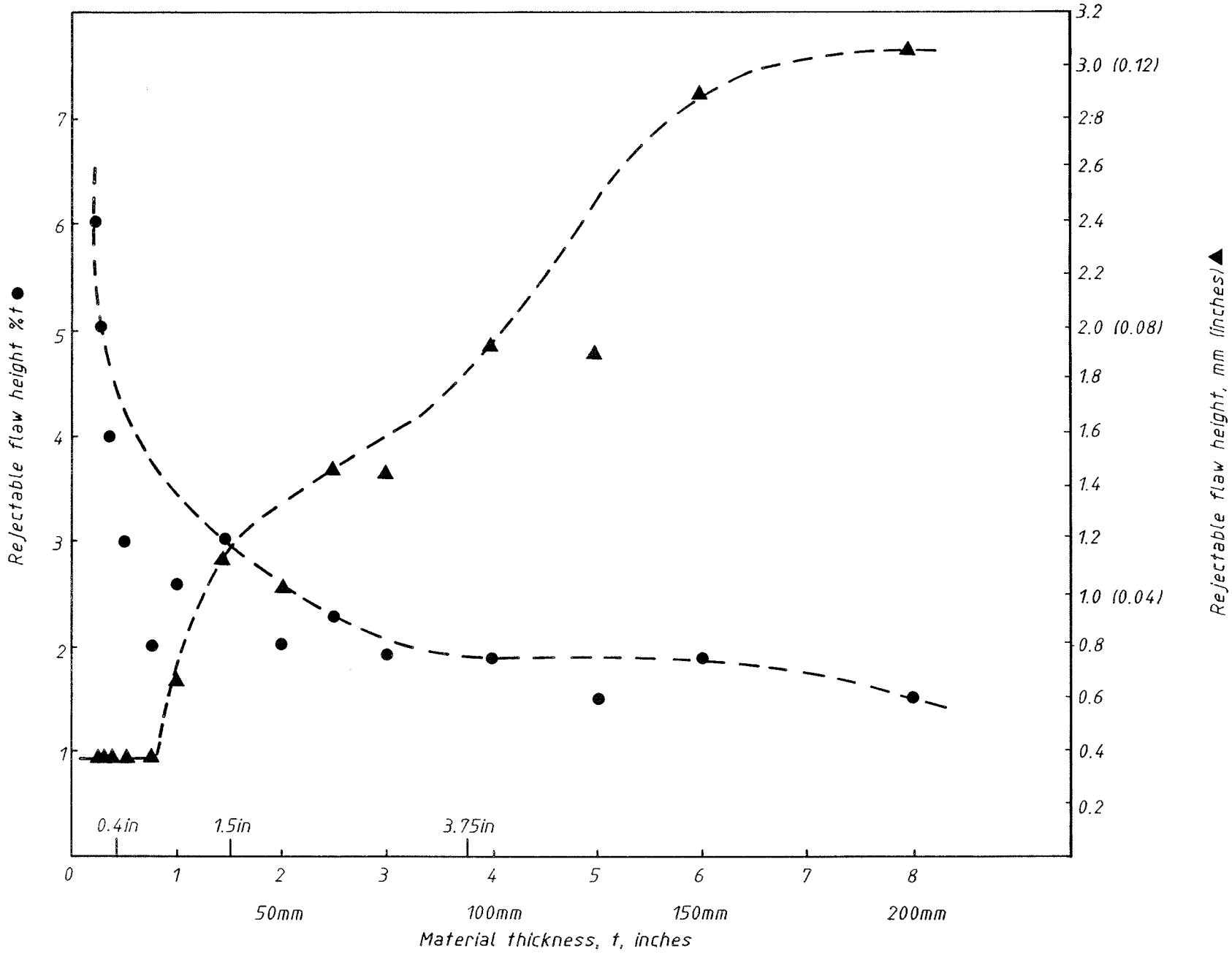

Fig.10 Relationship between limiting acceptable flaw size — in terms of both %t and absolute size — from D1.1 and material thickness.

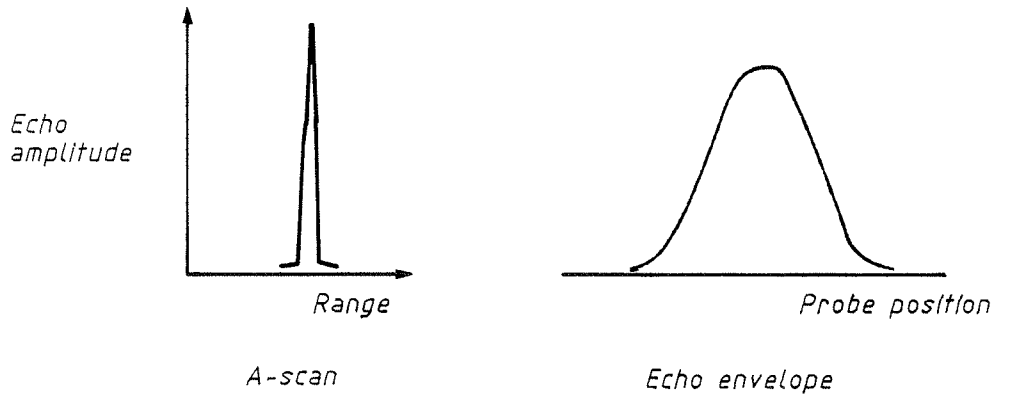

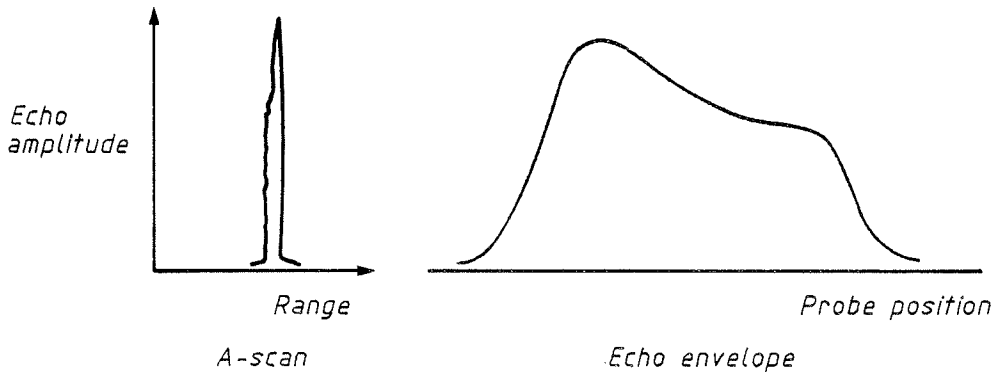

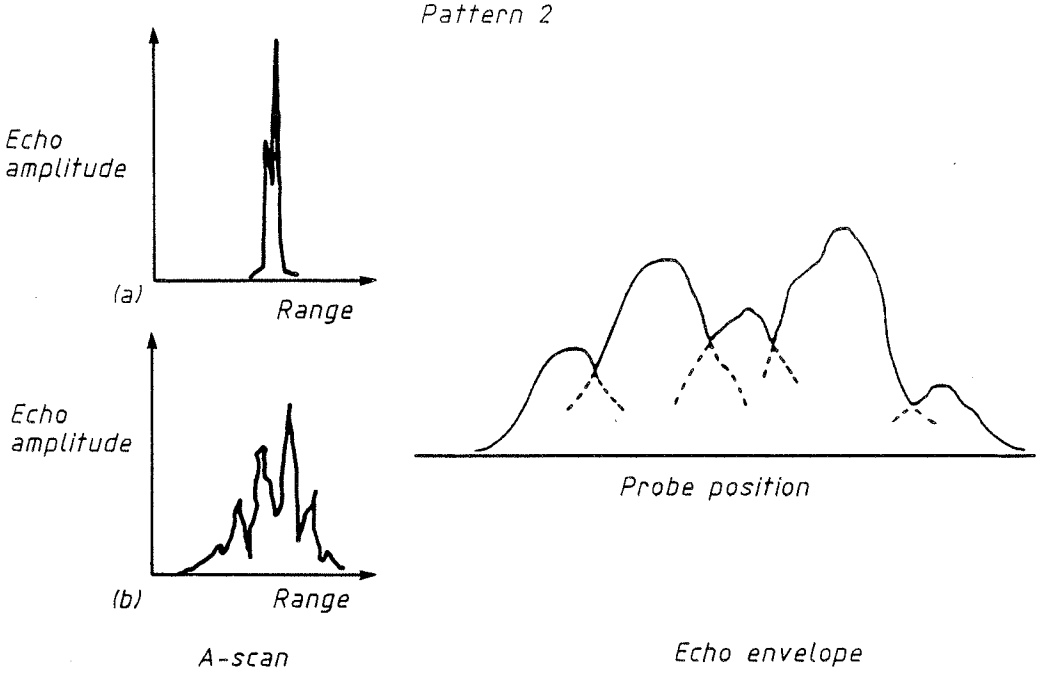

Fig.11 Echodynamic pattern types.

APPENDIX A
SPECIMENS AND EQUIPMENT

SPECIMENS

General

In order to study the capabilities of the tandem technique systematically it was necessary to produce a large number of similar flaws whose size, position and orientation conformed to a controlled pattern. It would not be possible to achieve this with real weld flaws, so that the approach adopted was to manufacture a set of artificial flaws by milling notches into plate material and to corroborate the results obtained by examining a small number of real welding flaws.

To assess the echodynamic responses from flaws, some of the real weld flaws manufactured for evaluation of tandem testing were again examined. The responses from these real flaws were compared with those from reference reflectors, which were cylindrical holes drilled into the opposite end of one of the blocks containing milled slots, 3769/1.

For both plate and welded samples three thicknesses of plate were used; 3.75in (95mm), 1.5in (38mm) and 0.4in (10mm). The chemical compositions of these all conformed to ASTM A36 requirements. Compositions are given in Table A1.

Machined Notches

To simulate vertical planar flaws, notches were machined into the end of rectangular plate samples. Plate sizes are given in Table A2. These flaws took the form of flat-ended slots, the ends of which were used as targets for the ultrasonic tests. The general appearance of the notches can be seen in Fig.A1. For the 95 and 38mm samples a matrix of flaws was machined 2, 4 and 8% of the sample thickness (t) in height, at three positions in the through-wall direction at (1/4, 1/2, and 3/4t) with a further notch, 50%t in height, positioned at ½t. This resulted in 10 notches being machined into each sample, each slot being 25mm long, as shown in Fig.A1. Four samples were produced in each thickness with the slot end faces at 0, 2.5, 5.0 and 10.0° to the vertical respectively. Owing to the small notch sizes required for the 0.4in (10mm) plates, the notch heights were restricted to 5, 15 and 50%t. Furthermore difficulties of producing angled notches in the 0.4in (10mm) plate led to all the notches being positioned at ½t. A total of 92 notches were therefore produced, all by mechanical milling except the 5% notches in the 0.4in (10mm) plate, which had to be electro-discharge machined owing to their small size. Notch details are summarised in Table A3.

All test specimen surfaces were machine ground. Face markings and the positional co-ordinate system according to D1.1 requirements are shown in Fig.A1. It should be noted that angled notches faced towards face "A". A photograph of one of the samples containing machined defects is shown in Fig.A2.

Drilled Holes

Seven 3/16in (4.5mm) holes were drilled into sample 3769/1, which also contained milled notches for evaluation of tandem testing. These holes were drilled parallel to the upper and lower machined surfaces of the sample and extended 3in (75mm) into the steel. The hole centres were at equally spaced depths below the top surface at 1/8, 1/4, 3/8, 1/2, 5/8, 3/4 and 7/8t, where t was the sample thickness.

Weld Samples

One welded sample was produced in each plate thickness, each containing real welding flaws. Specimen J301 was 3.75in (95mm) thick and was welded using submerged arc welding (SAW) with a shielded metal arc (SMA) root. The weld preparation is shown in Fig.A3, as are the locations of the four defects deliberately introduced. Defect type and longitudinal position were determined from radiography and through-wall position from subsequent ultrasonics.

Specimen J302 was 1.5in (38mm) thick and was welded by SMA with a GMA root run. Again, four defects were introduced and these can be seen schematically in Fig.A4.

The 0.4in (10mm) sample, J320, was more difficult to produce owing to its small size. It was welded by SMA and only one defect was introduced, which can be seen in Fig.A5.

EQUIPMENT

Tandem Tests

Flaw Detectors. The equipment used for these tests conformed, as far as was possible, to the requirements of AWS D1.1, Section 6.17. Two Krautkramer USM2M flaw detectors (Serial No.BO 79 and KO 83) were employed, which were checked at the stipulated frequencies in accordance with the requirements of D1.1 Sections 6.16 and 6.22. Both instruments were found to conform to D1.1 in all respects. In particular, the vertical linearity (dB accuracy) was checked in accordance with Section 6.22.2 of the code and Fig.A6 and A7 show the accuracy curves taken from form E10 for BO 79 and KO 83 respectively. Usable range was greater than 72dB for flaw detector BO 79 and greater than 63dB for KO 83.

Scanning Device. To maintain reproducible test conditions and yet retain flexibility of scanning for these trials, a scanning jig was constructed which allowed free movement of each of the tandem probes, but kept them in line. In this way the target reflectors could be thoroughly investigated, while maintaining the optimum test configuration. A view of this device is shown in Fig.A8.

Echodynamic Responses

Ultrasonic Equipment. The Welding Institute's MatEval Micropulse computer controlled flaw detector was used for these tests to facilitate capture of successive ultrasonic responses as the transducers were scanned across the target flaws and to display the echodynamic envelopes of the responses.

The Micropulse system consists of a flaw detector which is set up by commands given to the host computer. A general view of the equipment can be seen in Fig.A9. A large number of independent transducers can be used, although only one was used at any time for this study. The responses obtained from the test at each measurement point are transmitted to the computer for storage, and thus can be then manipulated in the computer and displayed. In this instance the software allowed the loci of the peaks of the signal as the transducer was moved across a flaw, the echodynamic response, to be displayed on the computer terminal screen. In addition paper copies of the screen display could be produced.

The transducers were driven along a number of scan lines by a motorised scanner, which was also controlled by the computer.

Ultrasonic Transducers

Ultrasonic transducers fell into three categories:

i. Krautkramer type WB 2MHz, element size 0.8 x 0.9in (20 x 22mm),
ii. Krautkramer type MAP 2MHz, element size 0.31 x 0.35in (8 x 9mm),
iii. Krautkramer type MWB 4MHz, element size 0.31 x 0.35in (8 x 9mm).

Details of ultrasonic beam angles and The Welding Institute serial numbers are given in Table A4. All transducers are fully characterised on delivery and the performance checked against the appropriate British Standards.

Table A1 Plate chemical composition

Plate thickness	Element, wt%*				
	C	Mn	P	S	Si
0.4in (10mm)	0.045	0.28	<0.005	0.025	<0.01
1.5in (39mm)	0.17	1.37	<0.005	<0.005	0.44
3.75in (95mm)	0.18	1.42	0.020	0.026	0.23

* Elements shown are those quoted in the chemical composition requirements of ASTM Grade A36

Table A2 Specimen sizes for plates containing notches

Imperial (L x W x D) inches	Metric (L x W x D)mm
21.26 x 10.36 x 3.75	540 x 270 x 95
14.17 x 10.63 x 1.50	360 x 270 x 38
7.87 x 5.91 x 0.40	200 x 150 x 10

P.J. Mudge

Table A3 Artificial defects (milled slots)

Defect size (length x depth)	Depth as % of wall thickness	Position
3.75in (95mm) thick samples		
1in (25mm) x 0.08in (2mm)	2.1	1/4t, 1/2t, 3/4t
1in (25mm) x 0.16in (4mm)	4.2	1/4t, 1/2t, 3/4t
1in (25mm) x 0.31in (8mm)	8.4	1/4t, 1/2t, 3/4t
1in (25mm) x 1.9in (48mm)	50.5	1/2t
1.5in (38mm) thick samples		
1in (25mm) x 0.06in (1.5mm)	3.9	1/4t, 1/2t, 3/4t
1in (25mm) x 0.08in (2mm)	5.3	1/4t, 1/2t, 3/4t
1in (25mm) x 0.12in (3mm)	7.9	1/4t, 1/2t, 3/4t
1in (25mm) x 0.75in (19mm)	50.0	1/2t
0.4in (10mm) thick samples		
1in (25mm) x 0.02in (0.5mm)	5.0	1/2t
1in (25mm) x 0.06in (1.5mm)	15.0	1/2t
1in (25mm) x 0.20in (5mm)	50.0	1/2t

Angles (to vertical): 0, 2.5, 5, 10°
Total number of slots = 92

P.J. Mudge

Table A4 Ultrasonic transducers

Type	Frequency, MHz	Angle, degrees	Serial number	Type (see text)
Krautkramer WB	2	45	T62	(i)
Krautkramer WB	2	45	T70	(i)
Krautkramer WB	2	60	T71	(i)
Krautkramer WB	2	70	T68	(i)
Krautkramer WB	2	70	T72	(i)
Krautkramer MAP	2	45	T21	(ii)
Krautkramer MAP	2	45	T77	(ii)
Krautkramer MAP	2	60	T23	(ii)
Krautkramer MAP	2.5	70	T49	(ii)
Krautkramer MAP	2.5	70	T50	(ii)
Krautkramer MWB	4	45	T74	(iii)
Krautkramer MWB	4	45	T65	(iii)
Krautkramer MWB	4	60	T75	(iii)
Krautkramer MWB	4	70	T73	(iii)
Krautkramer MWB	4	70	T67	(iii)
Krautkramer CD/10	5	0	L23	-

Note: L23 used for plate lamination checks only

P.J. Mudge

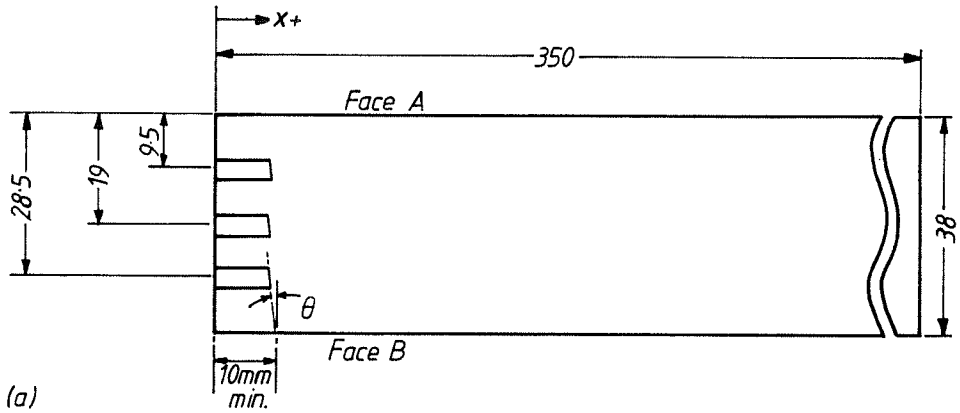

(a)

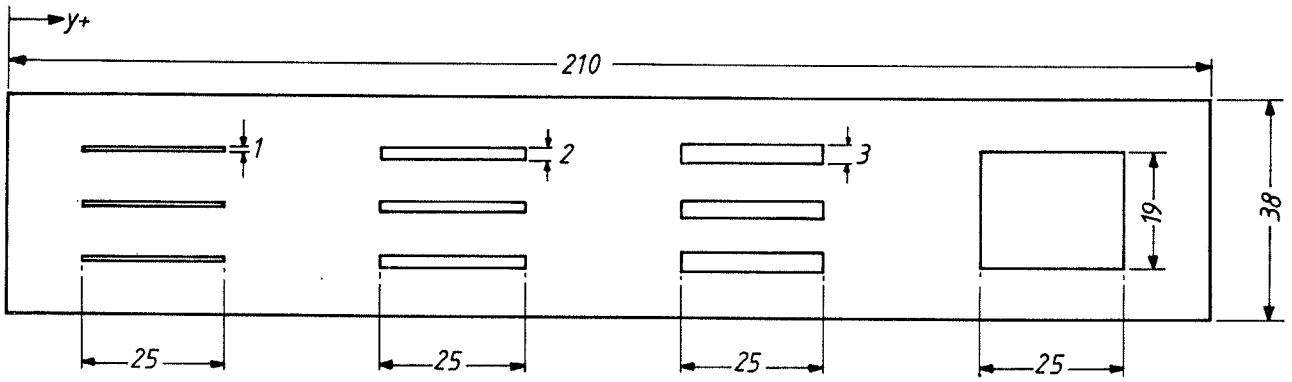

(b)

Dimensions in mm

Fig.A1 Specimen details:

a) side view, and
b) end view of 1.5in. (38mm) sample containing rectangular milled slots at an angle θ to the vertical

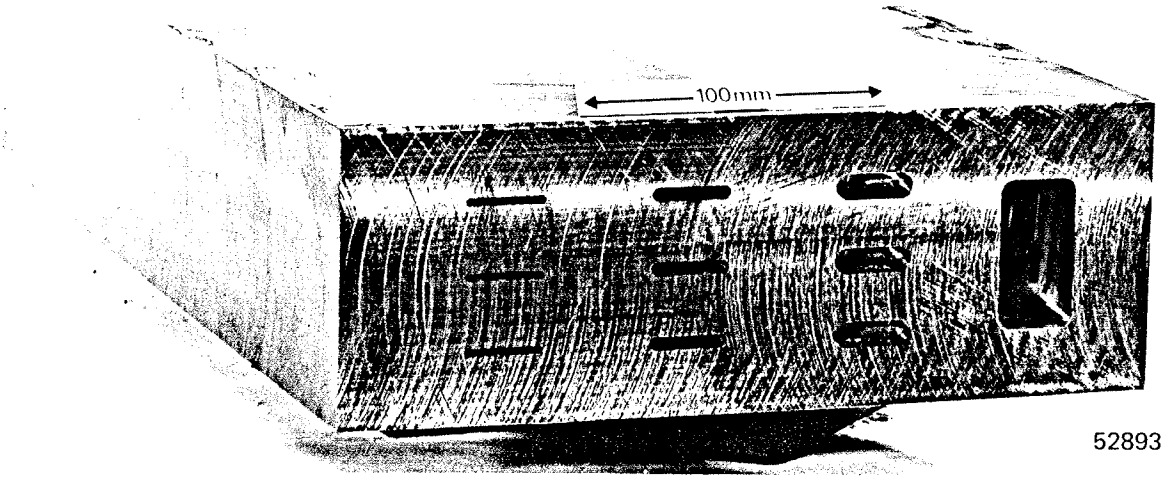

Fig.A2 A 3.75in. (95mm) specimen containing machined notches. Note the angled end face which can be seen on the 50%t notch.

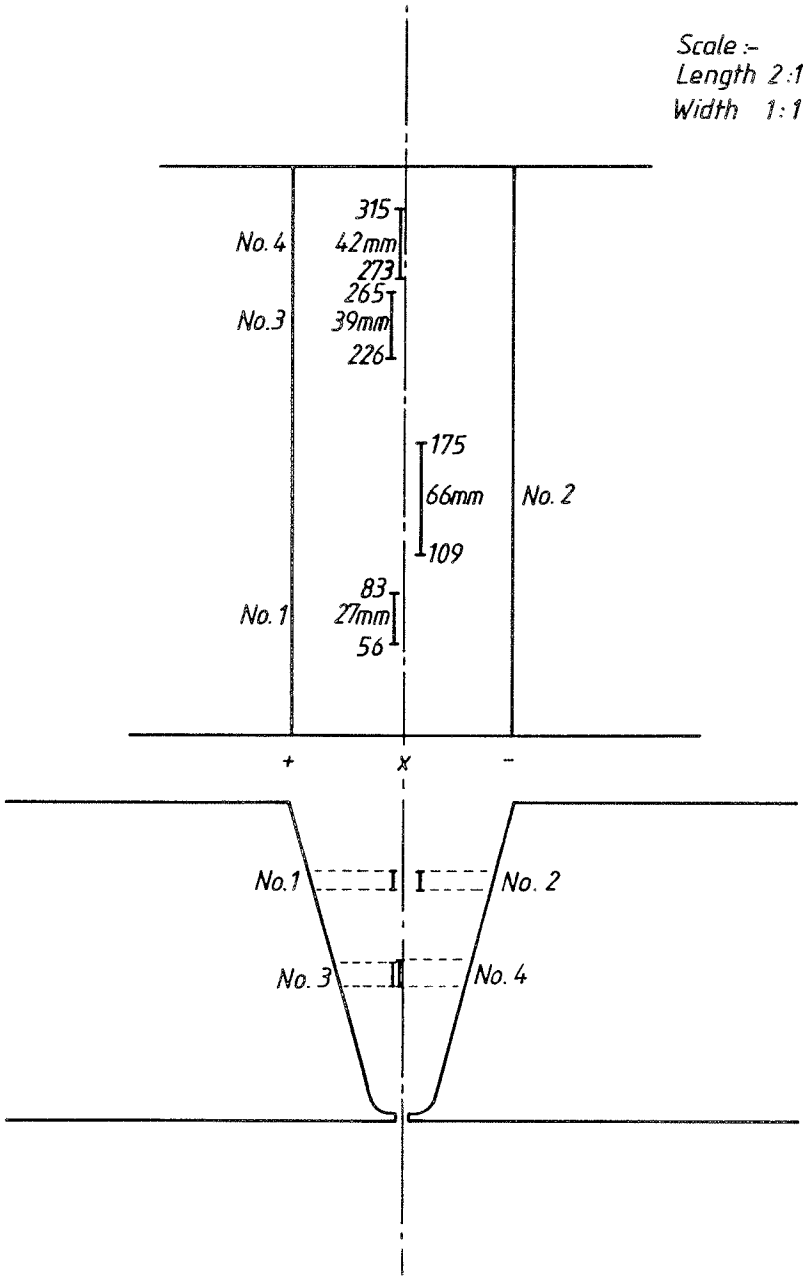

Fig. A3 3.75in (95mm) welded specimen J301.

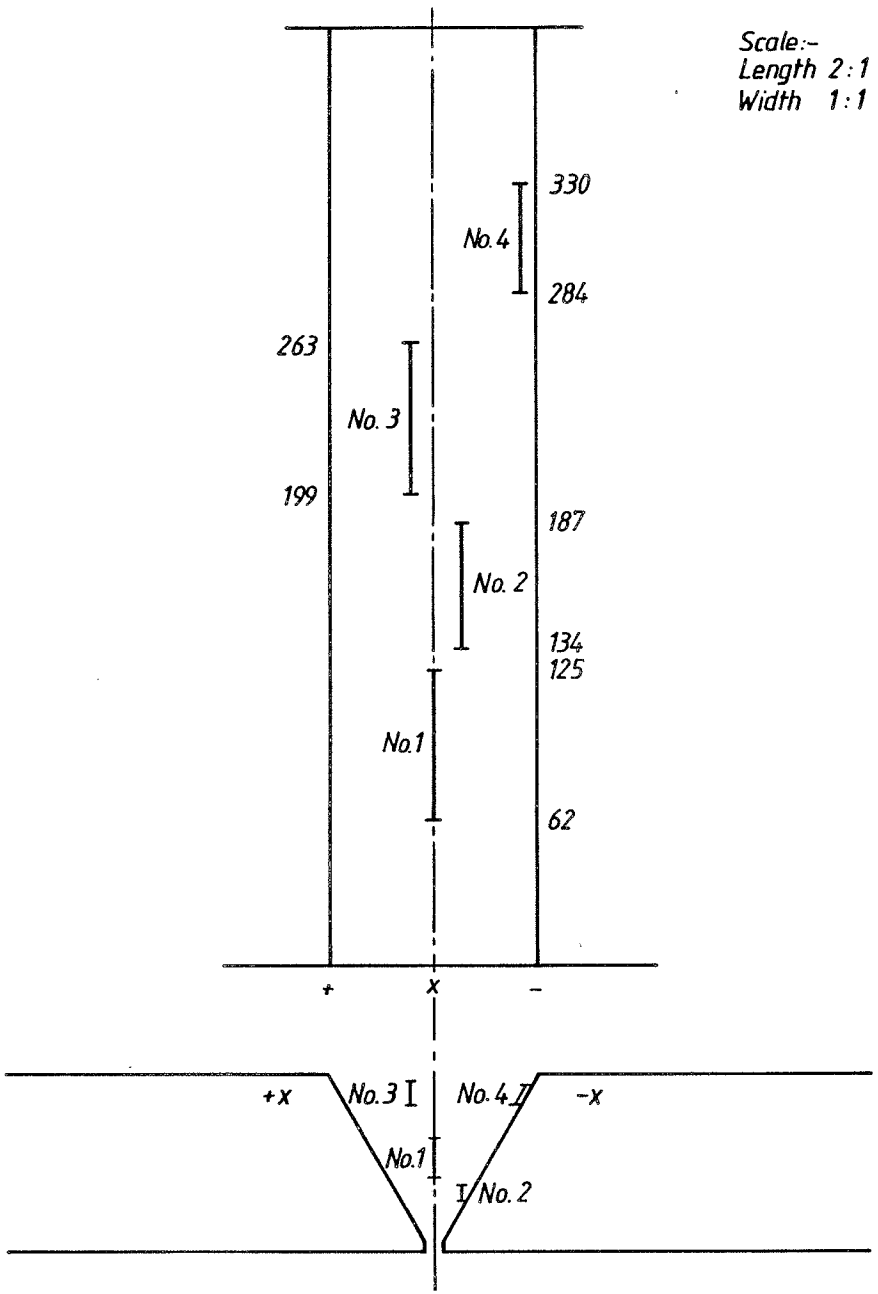

Fig. A4 1.5in (38mm) welded specimen, J302.

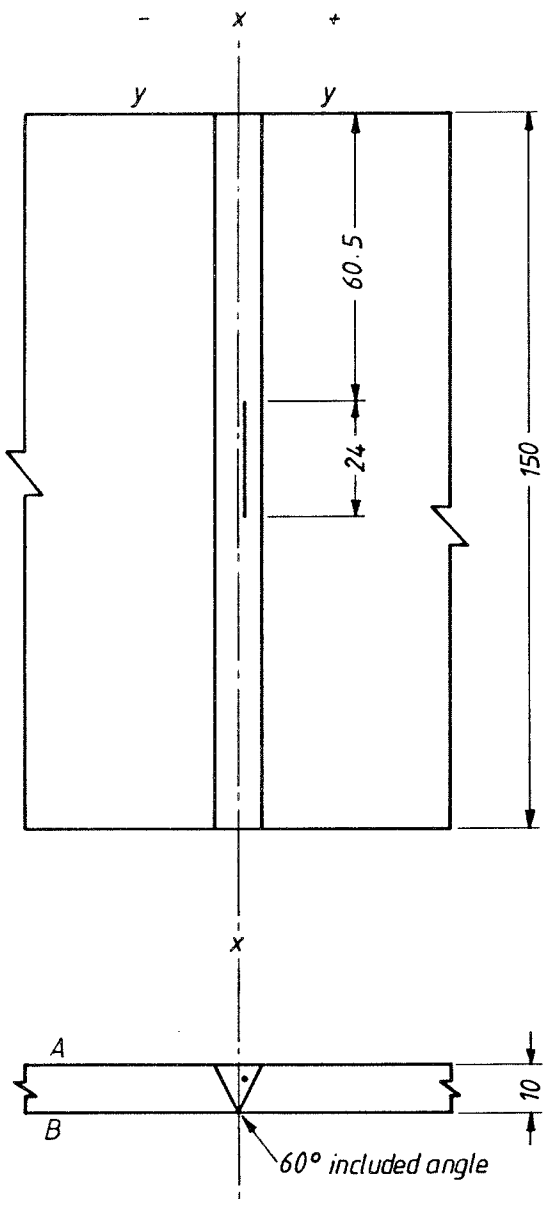

Fig. A5 0.4in (10mm) welded specimen J320.

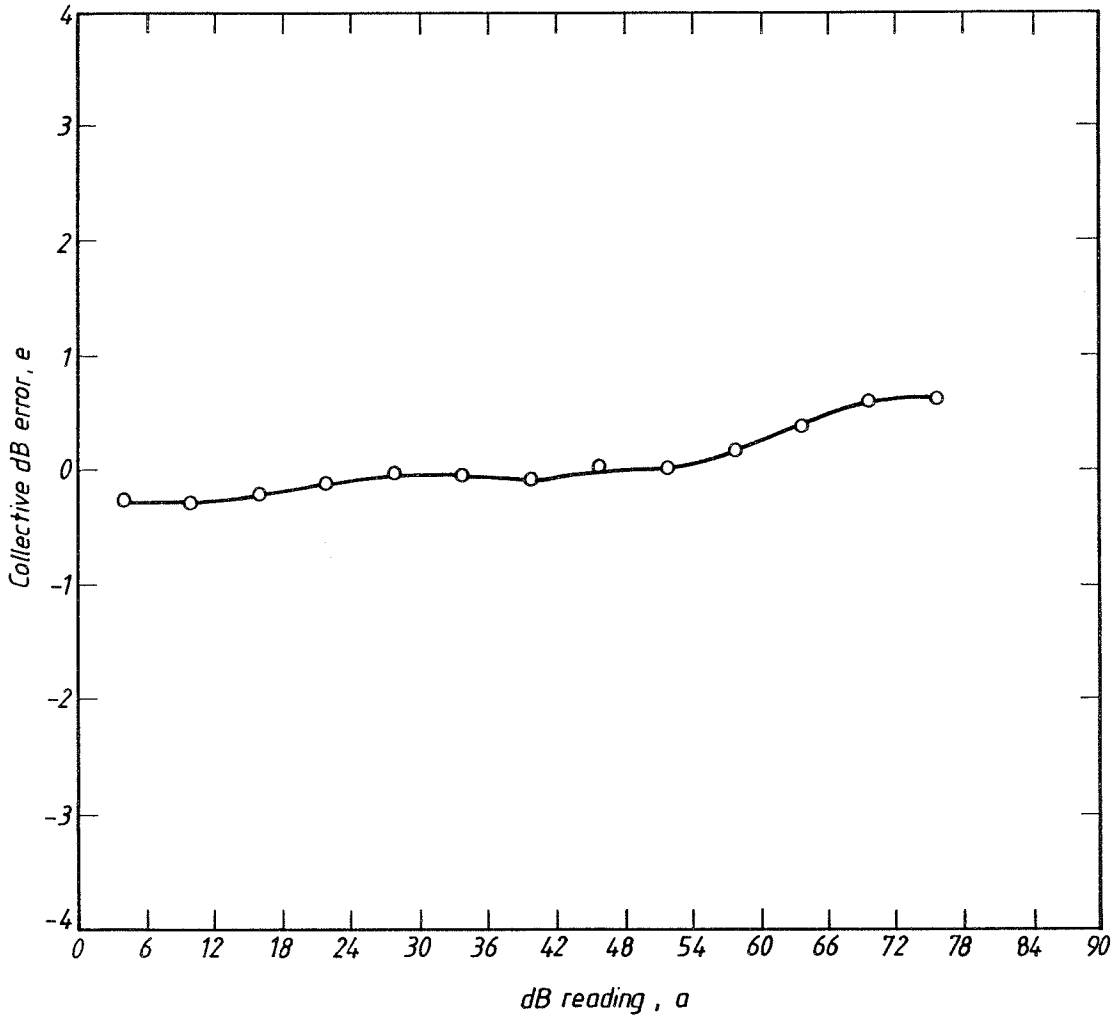

Fig. A6 Vertical linearity (dB accuracy) curve for USM2, B079. 14-4-83.

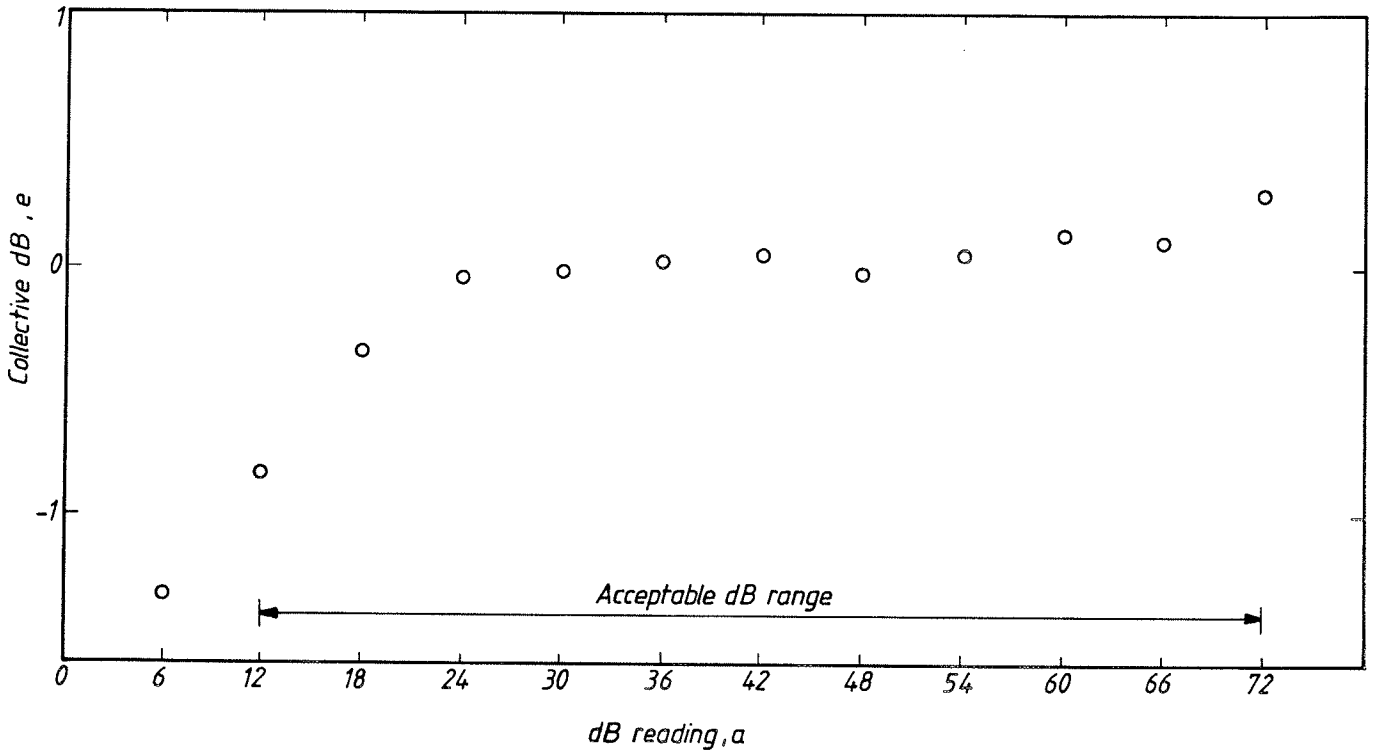

Fig.A7 Vertical linearity (dB accuracy) curve for USM2, KO83.

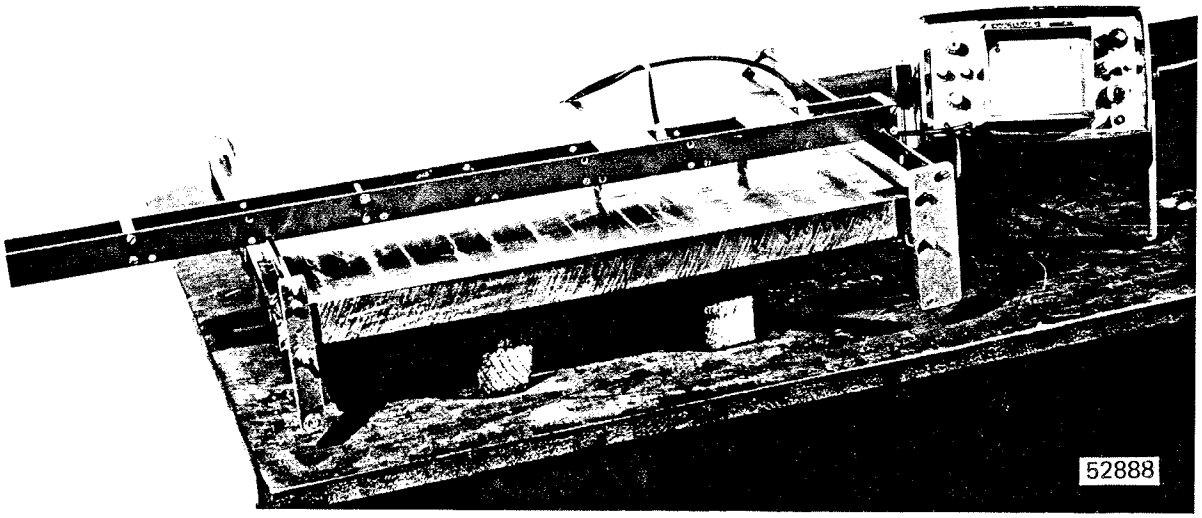

Fig.A8 Tandem scanning device, positioned on welded specimen WO2. The two tandem probes can be clearly seen.

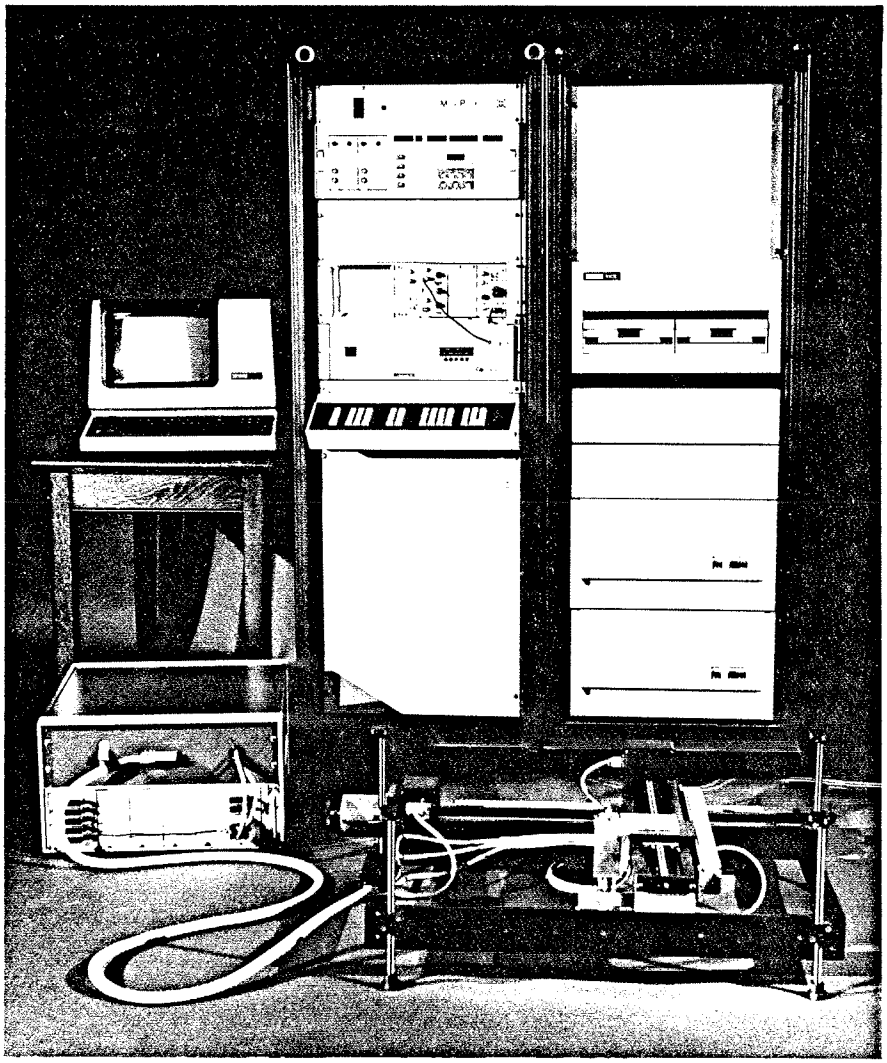

Fig.A9 Micropulse computer controlled ultrasonic testing system.

APPENDIX B
RESULTS OF PULSE-ECHO AND TANDEM TESTS

INTRODUCTION

The aim of these tests was to establish the flaw classification for each discontinuity from tests carried out to normal AWS D1.1 procedures and to compare them with the results of tandem tests. All the flaws were either real weld cracks or vertical planar discontinuities, so that all should be classed as rejectable large flaws (class A) in Table 9.25.3 of D1.1. Thus, each non-class A result suggests a failure of the procedure applied to detect a flaw or to evaluate it adequately.

All 92 machined flaws plus all nine weld defects were examined initially in accordance with the D1.1 requirements using suitable transducers (type (i) in Appendix A), and then examined using the tandem technique with both the large type (i) transducers and the miniature types (ii) and (iii). Further pulse-echo tests using the miniature transducers were also carried out.

All tandem tests were carried out using the scanning jig shown in Fig.A8 to ensure reproducibility of results.

SENSITIVITY AND FLAW EVALUATION

The reference sensitivity for tests conducted in accordance with D1.1 procedures was set on the 0.06in (1.6mm) diameter hole in the IIW V1/5 test block, as stipulated in Section 6.18 of the code. To maintain comparability, the sensitivities for other pulse-echo tests were set in the same way. However, when setting the sensitivity for tandem tests a correction factor had to be applied. Initially the front (transmitter) probe was connected in the pulse-echo mode and the signal from the 0.06in (1.6mm) hole set to the reference level. The flaw detector was then set for two probe operation and the rear (receiver) probe connected. The tandem response from the hole was between 2 and 3dB lower than that obtained in pulse-echo, so that this amount of gain was added to bring the signal back to the required level. The tandem tests were thus calibrated using the same reflector as specified in the code for pulse-echo tests to a comparable sensitivity level.

Similarly, in all cases Table 9.25.3 from the D1.1 code was used as the basis for flaw evaluation, this representing the flaw acceptance/rejection criterion for tension members in steel bridges. This is reproduced as Table B1. It should be noted that the criteria appropriate for 5/16in to 3/4in (8-19mm) thick material were used for the 0.4in (10mm) samples, the criteria for 3/4 to 1½in (19-38mm) thick material for the 1.5in (38mm) samples, and the criteria for 2½ to 4in (64-102mm) thick material for the 3.75in (95mm) samples.

TESTING AND REPORTING

All tests were carried out from face A of the samples unless otherwise stated. On the specimens containing angled machined notches, the notches faced towards the A side (see Fig.A1 Appendix A), thus as the angle to the vertical was increased, the misorientation to the ultrasonic beam was decreased. Scanning procedure 1 from Table 6.19.5.2 of the code was used for pulse-echo tests to D1.1 for the 0.4in (10mm) and 1.5in (38mm) samples. This specified 70° ultrasonic beams, although some 45° tandem tests were carried out. Procedure 6 plus F was used for the 3.75in (95mm) plates. This could require 45° scans as well as 70 and 60° tests - if fusion boundary reflectors are present, so all three angles were used. The tests carried out on each sample are given in Table B2. Frequencies of 2, 2.5 and 4MHz were used with both standard and minaiture transducers.

Defect ratings ("d" ratings) were calculated using the standard "c" factor and the formula: a-b-c = d specified in Section 6.19 of the code, as the ultrasonic instruments were calibrated in terms of gain. The "d" ratings were then used to obtain the flaw classification from Table 9.25.3 of the code (Table B1).

It should be noted that for pulse-echo tests, the range of signals displayed on the time base of the flaw detector screen is one half the actual path length travelled by the ultrasound, as the waves have to travel from the transducer to the flaw and back. This is taken into account when calculating the "c" factor, so that for the tandem tests, where the range observed on the flaw detector screen is the total path length, the value was divided by two to maintain consistency when determining the c factor.

RESULTS

Results are given in terms of the "d" rating and flaw classification for each discontinuity, as described in Appendix A, and for each test in Table A2.

- Tables B3-B12 show the results from the 3.75in (95mm) samples containing notches.
- Tables B13-B17 show the results from the 1.5in (38mm) samples containing notches.
- Tables B18-B21 show the results from the 0.4in (10mm) samples containing notches.
- Tables B22-B24 show the results from welded specimens containing real weld flaws.

The following should be noted from the tables:

- Where no result was recorded for a particular flaw, as in Tables B3 and B11, a flaw classification of D was assumed because any flaw remaining undetected would remain unrepaired, as would an acceptable minor flaw.

- For the 45° PE 2 (ii) tests on 89mm thick samples, Table B6, only notches at 0 and 5° to the vertical were examined.
- Tandem tests using large type (i) transducers could not be used to detect flaws at a depth of 3/4t because they could not be positioned sufficiently close together to satisfy the test geometry, owing to the size of the search unit casings, Table B10.
- For 70° tandem tests on machined notches at 5 and 10° to the vertical in the thinner two plate thicknesses a steeper, 60° transmitter beam was necessary in order to detect the reflected signal, Tables B5, B17 and B20. The effect of flaw angle on test geometry is discussed in Chapter 3.

Table B1 AWS D1.1 ultrasonic acceptance/rejection criteria (Table 9.25.3)

	Weld thickness (inches) and search unit angle										
Flaw severity class	5/16 to 3/4	>3/4 to 1-1/2	>1-1/2 to 2-1/2			>2-1/2 to 4			>4 to 8		
	70°	70°	70°	60°	45°	70°	60°	45°	70°	60°	45°
Class A	+10 & lower	+8 & lower	+4 & lower	+7 & lower	+9 & lower	+1 & lower	+4 & lower	+6 & lower	-2 & lower	+1 & lower	+3 & lower
Class B	+11	+9	+5 +6	+8 +9	+10 +11	+2 +3	+5 +6	+7 +8	-1 0	+2 +3	+4 +5
Class C	+12	+10	+7 +8	+10 +11	+12 +13	+4 +5	+7 +8	+9 +10	+1 +2	+4 +5	+6 +7
Class D	+13 & up	+11 & up	+9 & up	+12 & up	+14 & up	+6 & up	+9 & up	+11 & up	+3 & up	+6 & up	+8 & up

P.J. Mudge

Table B2 Ultrasonic tests

Test	Probe type*	Plate samples 10mm	38mm	95mm	Welded samples 10mm	38mm	95mm
45° PE, 2	(i)			✓			✓
60° PE, 2	(i)			✓		✓	✓
70° PE, 2	(i)		✓	✓		✓	✓
45° PE, 2	(ii)			✓			
70° PE, 2.5	(ii)	✓			✓**		
45° PE, 4	(iii)			✓			
60° PE, 4	(iii)			✓			
70° PE, 4	(iii)	✓	✓	✓	✓**		
45° T, 2	(i)			✓			✓
70° T, 2.5	(ii)	✓	✓		✓**		
45° T, 2	(ii)		✓	✓			
45° T, 4	(iii)			✓		✓	
70° T, 4	(iii)	✓	✓		✓**		

Test Mode

PE = Pulse-echo
T = Tandem
2, 4 etc = Frequency (MHz)
60, 70° etc = Test angle (degrees)

* See Appendix A
** From B face only

P.J. Mudge

Table B3 95mm plate - ultrasonic responses for 2MHz 45° (type i) pulse echo tests on notches - d rating, dB (flaw classification) from AWS D1.1

Flaw size, %t	Position	Angle to vertical			
		0°	2.5°	5°	10°
2.1%	1/4t	+6(A)	+5(A)	+5(A)	+6(A)
	1/2t	+3(A)	+5(A)	+1(A)	-1(A)
	3/4t	+2(A)	+4(A)	+1(A)	-4(A)
4.2%	1/4t	+8(B)	+7(B)	+5(A)	+9(C)
	1/2t	+5(A)	+3(A)	+2(A)	+5(A)
	3/4t	+2(A)	+4(A)	+1(A)	+6(A)
8.4%	1/4t	+9(C)	+2(A)	+2(A)	+5(A)
	1/2t	+5(A)	+3(A)	+4(A)	+1(A)
	3/4t	+2(A)	+3(A)	+4(A)	+6(A)
50.5%	1/2t	+7(B)	+2(A)	+5(A)	*(D)

* No result - assume Class D as flaw remained undetected

NB This test would only be required by AWS D1.1 if suspected fusion boundary reflectors had been detected on previous scans.

P.J. Mudge

Table B4 95mm plate - ultrasonic responses for 2MHz 60° (type i) pulse echo tests on notches - d rating, dB (flaw classification) from AWS D1.1

Flaw size, %t	Position	Angle to vertical			
		0°	2.5°	5°	10°
2.1%	1/4t	+4(A)	+6(B)	+7(C)	-4(A)
	1/2t	+2(A)	+1(A)	+5(B)	-5(A)
	3/4t*	+1(A)	0(A)	+3(A)	-3(A)
4.2%	1/4t	+5(B)	+3(A)	+3(A)	-2(A)
	1/2t	+2(A)	+1(A)	+1(A)	-3(A)
	3/4t*	0(A)	0(A)	0(A)	-2(A)
8.4%	1/4t	+6(B)	0(A)	+1(A)	+1(A)
	1/2t	+1(A)	-1(A)	-3(A)	-2(A)
	3/4t*	0(A)	0(A)	-2(A)	-4(A)
50.5%	1/2t	+3(A)	+2(A)	0(A)	+2(A)

* This test is required by D1.1 procedure 6 for the bottom quarter of the plate thickness.
A general 60° scan would only be required if fusion boundary reflectors had been detected on previous scans.

P.J. Mudge

Table B5 95mm plate - ultrasonic responses for 2MHz 70° (type i) pulse echo tests on notches - d rating, dB (flaw classification) from AWS D1.1

Flaw size, %t	Position	Angle to vertical			
		0°	2.5°	5°	10°
2.1%	1/4t*	-6(A)	0(A)	-6(A)	- 9(A)
	1/2t*	-1(A)	-4(A)	-8(A)	- 9(A)
	3/4t	-3(A)	-3(A)	-4(A)	-12(A)
4.2%	1/4t*	-7(A)	-5(A)	-5(A)	- 3(A)
	1/2t*	-2(A)	-1(A)	-6(A)	- 4(A)
	3/4t	-6(A)	-7(A)	-8(A)	- 6(A)
8.4%	1/4t*	-5(A)	-1(A)	-2(A)	- 8(A)
	1/2t*	-3(A)	-4(A)	-1(A)	- 8(A)
	3/4t	-7(A)	-8(A)	-4(A)	- 6(A)
50.5%	1/2t*	-1(A)	-2(A)	+2(A)	- 4(A)

* This scan is required by AWS D1.1 procedure 6 for the top quarter and middle half of the plate thickness.

P.J. Mudge

Table B6 95mm plate - ultrasonic responses for 2MHz 45° (type ii) pulse echo tests on notches - d rating, dB (flaw classification) from AWS D1.1

Flaw size, %t	Position	Angle to vertical			
		0°	2.5°	5°	10°
2.1%	1/4t	+13(D)	-	+12(D)	-
	1/2t	+15(D)	-	+16(D)	-
	3/4t	+18(D)	-	+14(D)	-
4.2%	1/4t	+15(D)	-	+ 8(D)	-
	1/2t	+18(D)	-	+18(D)	-
	3/4t	+18(D)	-	+18(D)	-
8.4%	1/4t	+13(D)	-	+10(D)	-
	1/2t	+17(D)	-	+16(D)	-
	3/4t	+16(D)	-	+15(D)	-
50.5%	1/2t	+22(D)	-	+15(D)	-

P.J. Mudge

Table B7 95mm plate - ultrasonic responses for 4MHz 45° (type iii) pulse echo tests on notches - d rating, dB (flaw classification) from AWS D1.1

Flaw size, %t	Position	Angle to vertical			
		0°	2.5°	5°	10°
2.1%	1/4t	+13(D)	+15(D)	+13(D)	+12(D)
	1/2t	+17(D)	+18(D)	+16(D)	+21(D)
	3/4t	+19(D)	+21(D)	+18(D)	+18(D)
4.2%	1/4t	+15(D)	+15(D)	+13(D)	+10(D)
	1/2t	+16(D)	+18(D)	+19(D)	+15(D)
	3/4t	+21(D)	+21(D)	+20(D)	+21(D)
8.4%	1/4t	+15(D)	+19(D)	+11(D)	+17(D)
	1/2t	+19(D)	+19(D)	+18(D)	+19(D)
	3/4t	+21(D)	+21(D)	+21(D)	+21(D)
50.5%	1/2t	+13(D)	+24(D)	+21(D)	+22(D)

P.J. Mudge

Table B8 95mm plate - ultrasonic responses for 4MHz 60° (type iii) pulse echo tests on notches - d rating, dB (flaw classification) from AWS D1.1

Flaw size, %t	Position	Angle to vertical 0°	2.5°	5°	10°
2.1%	1/4t	+ 9(D)	+13(D)	+5(B)	+ 4(A)
	1/2t	+10(D)	+ 9(D)	+7(C)	+ 5(B)
	3/4t	+12(D)	+14(D)	+10(D)	+10(D)
4.2%	1/4t	+10(D)	+14(D)	+11(D)	+ 9(D)
	1/2t	+16(D)	+15(D)	+ 9(D)	+11(D)
	3/4t	+17(D)	+15(D)	+ 4(A)	+14(D)
8.4%	1/4t	+15(D)	+11(D)	+ 9(D)	+ 9(D)
	1/2t	+13(D)	+ 9(D)	+ 8(C)	+11(D)
	3/4t	+14(D)	+13(D)	+ 3(A)	+14(D)
50.5%	1/2t	+10(D)	+10(D)	+ 4(A)	+13(D)

P.J. Mudge

Table B9 95mm plate - ultrasonic responses for 4MHz 70° (type iii) pulse echo tests on notches - d rating, dB (flaw classification) from AWS D1.1

Flaw size, %t	Position	Angle to vertical			
		0°	2.5°	5°	10°
2.1%	1/4t	+ 6(D)	+ 4(C)	+3(B)	0(A)
	1/2t	+11(D)	+10(D)	+7(D)	+9(D)
	3/4t	+10(D)	+ 8(D)	+6(D)	+9(D)
4.2%	1/4t	+10(D)	+ 8(D)	+4(C)	0(A)
	1/2t	+ 5(C)	+13(D)	+8(D)	+6(D)
	3/4t	+ 5(C)	+ 6(D)	+3(B)	+9(D)
8.4%	1/4t	+10(D)	+ 7(D)	+4(C)	+1(A)
	1/2t	+ 2(B)	+12(D)	+7(D)	+3(B)
	3/4t	+ 4(C)	+ 5(C)	+4(C)	+6(D)
50.5%	1/2t	+ 9(D)	+ 9(D)	+4(C)	+2(B)

P.J. Mudge

Table B10 95mm plate - ultrasonic responses for 2MHz 45° (type i) tandem tests on notches - d rating, dB (flaw classification) from AWS D1.1

Flaw size, %t	Position	Angle to vertical			
		0°	2.5°	5°	10°
2.1%	1/4t	- 7(A)	-23(A)	-15(A)	0(A)
	1/2t	- 9(A)	-23(A)	-19(A)	- 1(A)
	3/4t	*	*	*	- 2(A)
4.2%	1/4t	-21(A)	-25(A)	-20(A)	- 4(A)
	1/2t	-23(A)	-26(A)	-21(A)	- 3(A)
	3/4t	*	*	*	+ 1(A)
8.4%	1/4t	-27(A)	-29(A)	-23(A)	- 8(A)
	1/2t	-29(A)	-31(A)	-26(A)	- 3(A)
	3/4t	*	*	*	- 7(A)
50.5%	1/2t	-35(A)	-29(A)	-27(A)	-17(A)

* Probes could not be positioned close enough together to detect flaws at 3/4t

P.J. Mudge

Table B11 95mm plate - ultrasonic responses for 2MHz 45° (type ii) tandem tests on notches - d rating, dB (flaw classification) from AWS D1.1

Flaw size, %t	Position	Angle to vertical			
		0°	2.5°	5°	10°
2.1%	1/4t	-21(A)	-26(A)	-19(A)	-15(A)
	1/2t	-26(A)	-27(A)	-24(A)	-12(A)
	3/4t	-27(A)	-25(A)	-25(A)	*
4.2%	1/4t	-18(A)	-23(A)	-17(A)	-11(A)
	1/2t	-19(A)	-20(A)	-17(A)	-14(A)
	3/4t	-21(A)	-20(A)	-17(A)	- 9(A)
8.4%	1/4t	-24(A)	-27(A)	-18(A)	- 9(A)
	1/2t	-25(A)	-28(A)	-23(A)	-15(A)
	3/4t	-26(A)	-24(A)	-21(A)	-13(A)
50.5%	1/2t	-35(A)	-31(A)	-28(A)	-13(A)

* Probes could not be positioned to get an adequate response - assume D classification

P.J. Mudge

Table B12 95mm plate - ultrasonic responses for 4MHz 45° (type iii) tandem tests on notches - d rating, dB (flaw classification) from AWS D1.1

Flaw size, %t	Position	Angle to vertical			
		0°	2.5°	5°	10°
2.1%	1/4t	- 6(A)	- 6(A)	- 5(A)	+13(D)
	1/2t	- 4(A)	- 1(A)	- 6(A)	+14(D)
	3/4t	- 5(A)	- 2(A)	- 9(A)	+ 6(A)
4.2%	1/4t	-13(A)	-14(A)	- 1(A)	+ 8(B)
	1/2t	-16(A)	-13(A)	0(A)	+ 6(A)
	3/4t	-14(A)	-13(A)	- 5(A)	+16(D)
8.4%	1/4t	-17(A)	-15(A)	- 5(A)	- 4(A)
	1/2t	-22(A)	-16(A)	- 9(A)	+ 4(A)
	3/4t	-15(A)	-16(A)	- 6(A)	+ 6(A)
50.5%	1/2t	-23(A)	-19(A)	-11(A)	- 1(A)

P.J. Mudge

Table B13 38mm plate - ultrasonic responses for 2MHz 70° (type i) pulse echo tests on notches - d rating, dB (flaw classification) from AWS D1.1

Flaw size, %t	Position	Angle to vertical			
		0°	2.5°	5°	10°
3.9%	1/4t	0(A)	0(A)	-2(A)	-6(A)
	1/2t	+1(A)	+1(A)	-2(A)	-6(A)
	3/4t	0(A)	-2(A)	-3(A)	-7(A)
5.3%	1/4t	+2(A)	-3(A)	-2(A)	-8(A)
	1/2t	+2(A)	-2(A)	-2(A)	-9(A)
	3/4t	+4(A)	-3(A)	-4(A)	-9(A)
7.9%	1/4t	+4(A)	+8(A)	-2(A)	-9(A)
	1/2t	+4(A)	+4(A)	+2(A)	-8(A)
	3/4t	+3(A)	+1(A)	+2(A)	-9(A)
50%	1/2t	+6(A)	+6(A)	+7(A)	-6(A)

P.J. Mudge

Table B14 38mm plate - ultrasonic responses for 4MHz 70° (type iii) pulse echo tests on notches - d rating, dB (flaw classification) from AWS D1.1

Flaw size, %t	Position	Angle to vertical			
		0°	2.5°	5°	10°
3.9%	1/4t	+ 9(B)	+10(C)	+ 7(A)	-1(A)
	1/2t	+ 7(A)	+12(D)	+10(C)	+1(A)
	3/4t	+18(D)	+16(D)	+14(D)	+2(A)
5.3%	1/4t	+ 3(A)	+ 2(A)	+ 8(A)	+1(A)
	1/2t	+ 7(A)	+ 3(A)	+10(C)	+6(A)
	3/4t	+ 8(A)	+ 6(A)	+12(D)	+9(B)
7.9%	1/4t	+ 8(A)	+ 7(A)	+ 8(A)	0(A)
	1/2t	+ 9(B)	+10)C)	+ 6(A)	+5(A)
	3/4t	+13(D)	+13(D)	+ 9(B)	+6(A)
50%	1/2t	+10(C)	+ 5(A)	+ 8(A)	+2(A)

P.J. Mudge

Table B15 38mm plate - ultrasonic responses for 2.5MHz 70° (type ii) tandem tests on notches - d rating, dB (flaw classification) from AWS D1.1

Flaw size, %t	Position	Angle to vertical			
		0°	2.5°	5°*	10°*
3.9%	1/4t	-29(A)	-29(A)	- 4(A)	- 1(A)
	1/2t	-23(A)	-23(A)	- 2(A)	- 3(A)
	3/4t	-21(A)	-23(A)	0(A)	- 1(A)
5.3%	1/4t	-25(A)	-23(A)	- 9(A)	- 9(A)
	1/2t	-28(A)	-26(A)	- 7(A)	- 6(A)
	3/4t	-26(A)	-21(A)	- 4(A)	- 7(A)
7.9%	1/4t	-26(A)	-27(A)	-21(A)	- 8(A)
	1/2t	-25(A)	-21(A)	-15(A)	- 9(A)
	3/4t	-27(A)	-18(A)	-14(A)	-13(A)
50%	1/2t	-34(A)	-33(A)	-19(A)	-13(A)

* For these angles a 60° transmitter was used

P.J. Mudge

Table B16 38mm plate - ultrasonic responses for 2MHz 45° (type ii) tandem tests on notches - d rating, dB (flaw classification) from AWS D1.1

Flaw size, %t	Position	Angle to vertical			
		0°	2.5°	5°	10°
3.9%	1/4t	-14(A)	-16(A)	-13(A)	-13(A)
	1/2t	-16(A)	-17(A)	-17(A)	-14(A)
	3/4t	-22(A)	-19(A)	-19(A)	-22(A)
5.3%	1/4t	-14(A)	-16(A)	-15(A)	-15(A)
	1/2t	-17(A)	-17(A)	-13(A)	-17(A)
	3/4t	-21(A)	-15(A)	-19(A)	-25(A)
7.9%	1/4t	-25(A)	-19(A)	-21(A)	-14(A)
	1/2t	-27(A)	-17(A)	-19(A)	-17(A)
	3/4t	-25(A)	-16(A)	-19(A)	-19(A)
50%	1/2t	-34(A)	-29(A)	-24(A)	- 8(A)

P.J. Mudge

Table B17 38mm plate - ultrasonic responses for 4MHz 70° (type iii) tandem tests on notches - d rating, dB (flaw classification) from AWS D1.1

Flaw size, %t	Position	Angle to vertical			
		0°	2.5°	5°	10°*
3.9%	1/4t	-12(A)	-14(A)	-13(A)	0(A)
	1/2t	-15(A)	-14(A)	-12(A)	-2(A)
	3/4t	-12(A)	-10(A)	- 9(A)	+2(A)
5.3%	1/4t	-15(A)	-13(A)	-14(A)	-4(A)
	1/2t	-15(A)	-15(A)	-15(A)	0(A)
	3/4t	-15(A)	-14(A)	-13(A)	+2(A)
7.9%	1/4t	- 7(A)	-16(A)	-16(A)	-3(A)
	1/2t	-12(A)	-18(A)	-18(A)	-4(A)
	3/4t	-17(A)	-15(A)	-16(A)	+1(A)
50%	1/2t	-26(A)	-23(A)	-15(A)	-2(A)

* For this angle a 60° transmitter was used.

P.J. Mudge

Table B18 10mm plate - ultrasonic responses for 2.5MHz 70° (type ii) pulse echo tests on notches - d rating, dB (flaw classification) from AWS D1.1

Flaw size, %t	Position	Angle to vertical			
		0°	2.5°	5°	10°
5%	1/2t	- 8(A)	-9(A)	-10(A)	-10(A)
15%	1/2t	-10(A)	-12(A)	-12(A)	-21(A)
50%	1/2t	- 9(A)	-21(A)	-17(A)	-21(A)

Table B19 10mm plate - ultrasonic responses for 4MHz 70° (type iii) pulse echo tests on notches - d rating, dB (flaw classification) from AWS D1.1

Flaw size, %t	Position	Angle to vertical			
		0°	2.5°	5°	10°
5%	1/2t	+7(A)	+2(A)	+7(A)	+7(A)
15%	1/2t	+7(A)	+7(A)	+3(A)	+3(A)
50%	1/2t	+7(A)	+1(A)	+3(A)	+5(A)

P.J. Mudge

Table B20 10mm plate - ultrasonic responses for 2.5MHz 70° (type ii) tandem tests on notches - d rating, dB (flaw classification) from AWS D1.1

Flaw size, %t	Position	Angle to vertical			
		0°	2.5°	5°*	10°*
5%	1/2t	-21(A)	-15(A)	-24(A)	-15(A)
15%	1/2t	-31(A)	-26(A)	-21(A)	-14(A)
50%	1/2t	-36(A)	-35(A)	-27(A)	-18(A)

* For these angles a 60° transmitter was used.

Table B21 10mm plate - ultrasonic responses for 4MHz 70° (type iii) tandem tests on notches - d rating, dB (flaw classification) from AWS D1.1

Flaw size, %t	Position	Angle to vertical			
		0°	2.5°	5°	10°
5%	1/2t	-15(A)	0(A)	- 9(A)	-1(A)
15%	1/2t	+ 4(A)	- 5(A)	-11(A)	-1(A)
50%	1/2t	-16(A)	-12(A)	-20(A)	-6(A)

P.J. Mudge

Table B22 95mm plate - results from ultrasonic tests on flaws in welded sample J301 - d rating (flaw classification) from AWS D1.1

	Flaw number			
Test	1	2	3	4
70° PE, 2 (i)	- 6(A)	- 6(A)	- 1(A)	- 4(A)
60° PE, 2 (i)	0(A)	- 1(A)	- 6(A)	- 3(A)
45° PE, 2 (i)	- 7(A)	+ 7(B)	+ 3(A)	- 2(A)
45° T, 2(i)	-36(A)	-36(A)	-18(A)	-36(A)

P.J. Mudge

Table B23 38mm plate - results from ultrasonic tests on flaws in welded sample J302 - d rating (flaw classification) from AWS D1.1

	Flaw number			
Test	1	2	3	4
70° PE, 2 (i) (as-welded)	+ 5(A)	+ 1(A)	+17(D)	+ 4(A)
70° PE, 2 (i) (machined surface)	-10(A)	- 7(A)	0 (A)	- 8(A)
70° PE, 2 (i) (from face B)	+ 5(A)	+ 6(A)	+ 6(A)	- 3(A)
60° PE, 2 (i) (as-welded)	+ 8(A)	+ 4(A)	+11(D)	+ 1(A)
45° T, 2 (ii)	-17(A)	*	-25(A)	- 6(A)

* Probes could not be positioned sufficiently close together to detect this flaw.

P.J. Mudge

Table B24 10mm plate - results from ultrasonic tests on the flaw in welded sample J320

Test	d rating	Flaw classification from AWS D1.1
70° PE, 2.5 (ii)	-10	A
70° PE, 4 (iii)	- 7	A
70° T, 2.5 (ii)	-22	A
70° T, 4 (iii)	-17	A

NB All tests were conducted from face B - the root side of the weld.

P.J. Mudge

APPENDIX C
ECHODYNAMIC CURVES - DATA COLLECTION AND RESULTS

INTRODUCTION

In order to study the echodynamic behaviour of real cracks it was necessary to have a means of recording the echodynamic curve, which is the locus of the peak of the ultrasonic signal. This curve is traced out as the signal rises and falls when the ultrasonic beam is swept across a flaw by moving the transducer. This effect is observable on any ultrasonic flaw detector; The technician builds up a mental picture of the outline of the echodynamic response envelope as he scans his transducer over a flaw. For this program it was necessary to plot the envelope for further scrutiny and to enable results to be reported. The simplest method is to display the ultrasonic signal on a storage oscilloscope, so that the accumulated stored signal can be viewed. Problems can occur in making a permanent record of the screen, so it was decided to use a computer test system - the "micropulse" produced by MatEval, available in The Welding Institute's NDT Research laboratory, in order to record and display the echodynamic curves.

EXPERIMENTAL

Echodynamic curves are used in a comparative manner. It was therefore necessary to establish a suitable reference with which comparisons would be made. It was decided to use cylindrical holes as these were convenient to manufacture and are highly reproducible. Seven holes each 3/16in diameter were drilled into one of the 95mm thick samples, as described in Appendix A. The diameter was that specified in the ASME Boiler and Pressure Vessel Code, Section V (7) for this thickness of material. This diameter was chosen as it is difficult to drill deep holes with diameters as small as 1/16in straight and parallel to the surface of the test block. The difference in signal height between a 1/16in and a 3/16in diameter hole is 5dB.

Echodynamic response curves for the series of holes were produced using 45 and 50°, 4MHz, and 45, 60 and 70°, 2MHz transducers. The 4MHz units were miniature (type iii) while the 2MHz units conformed to AWS D1.1 specification (type i), as stated in Appendix A. A 70° 4MHz scan was attempted, but interpretation of the results proved difficult due to excessive beam spread.

Each transducer in turn was securely held in a spring loaded gimbal holder, attached to a motorised X-Y scanner. Initial scans were made on the calibration block containing the holes. The transducer was driven forwards over the reflectors. Each hole was scanned with different gain settings in order to ensure that the maximum response height was approximately constant - 100% full screen height (FSH) in each case. The lower signal threshold for was 10% FSH, i.e. 20dB down on the maximum amplitude. The response envelopes were recorded on the computer for analysis and displayed as plots of Amplitude (% FSH) versus Range (mm).

Measurements of 20dB drop beam widths were made for each response envelope, and from these results, plots of Beam Width (mm) as a function of Range (mm) were produced. A least squares best fit line was then drawn through the points. These are described in the main text, Chapter 2.

Using each of the five transducers, scans were then made on the 3.75in (95mm) thick welded specimen (J301) containing five vertical planar defects. As with the calibration block, echodynamic response envelopes were obtained and 20dB drop beam width measurements were made for comparison with the calibration holes.

RESULTS

Figures C1 through C5 show echodynamic response curves of the 3/16in drilled holes, taken using each of the five ultrasonic search units. These figures show the broader response envelope obtained from holes at greater range, this being consistent with the divergence of the ultrasonic beam with distance. The side lobe effect seen in the first peak of Fig.C3 occurs because the reflector lay well within the near zone of the transducer. The use of higher angled probes introduced difficulties in interpretation of responses due to echoes within the calibration block, this may be seen especially well in Fig.C5. This fact also made 20dB drop beam width measurement more difficult, indicating the impracticality of determining the response width when the signal to noise level is poor.

Figures C6 and C7 show examples of echodynamic responses obtained from scanning the flaw in the welded specimen. The particular flaw of interest was a 0.37in (9.5mm) through-thickness crack at a depth of approximately 1.9in (48mm) and is described in more detail in Appendix E of Part 2 of this report (3). It was found that with all but the 70°, 2MHz transducer, separate response envelopes were obtained from the top and bottom extremities of the flaw, Fig.C6. The 70° beam produced a much more uneven, continuous response, indicating a greater tendency to scatter the ultrasound.

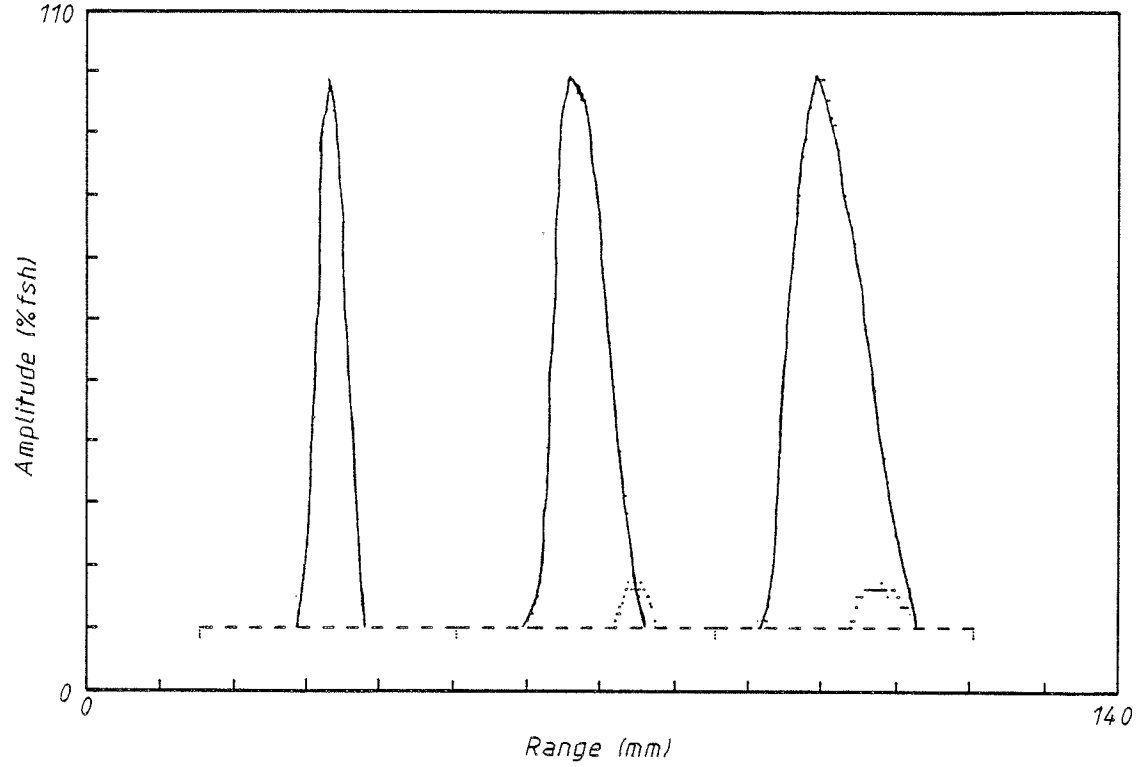

Fig.C1 Echodynamic curve from three drilled holes using a 4MHz 45° miniature transducer.

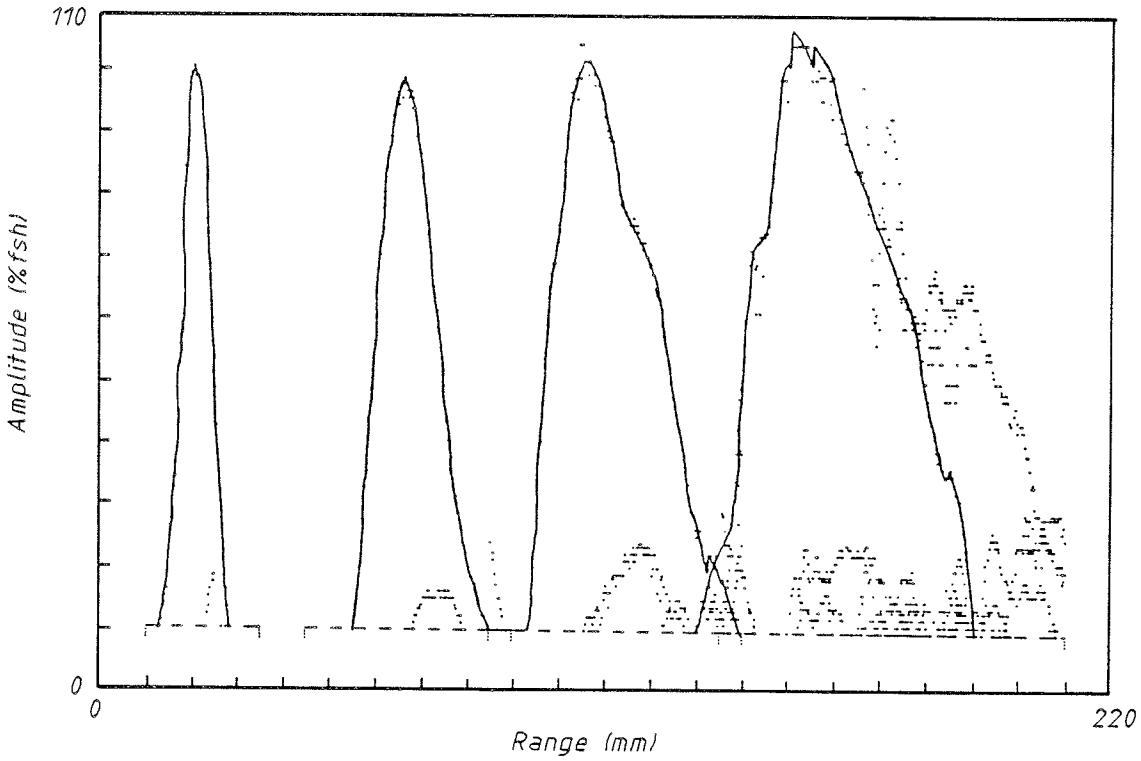

Fig.C2 Echodynamic curve from four drilled holes using a 4MHz 60° miniature transducer.

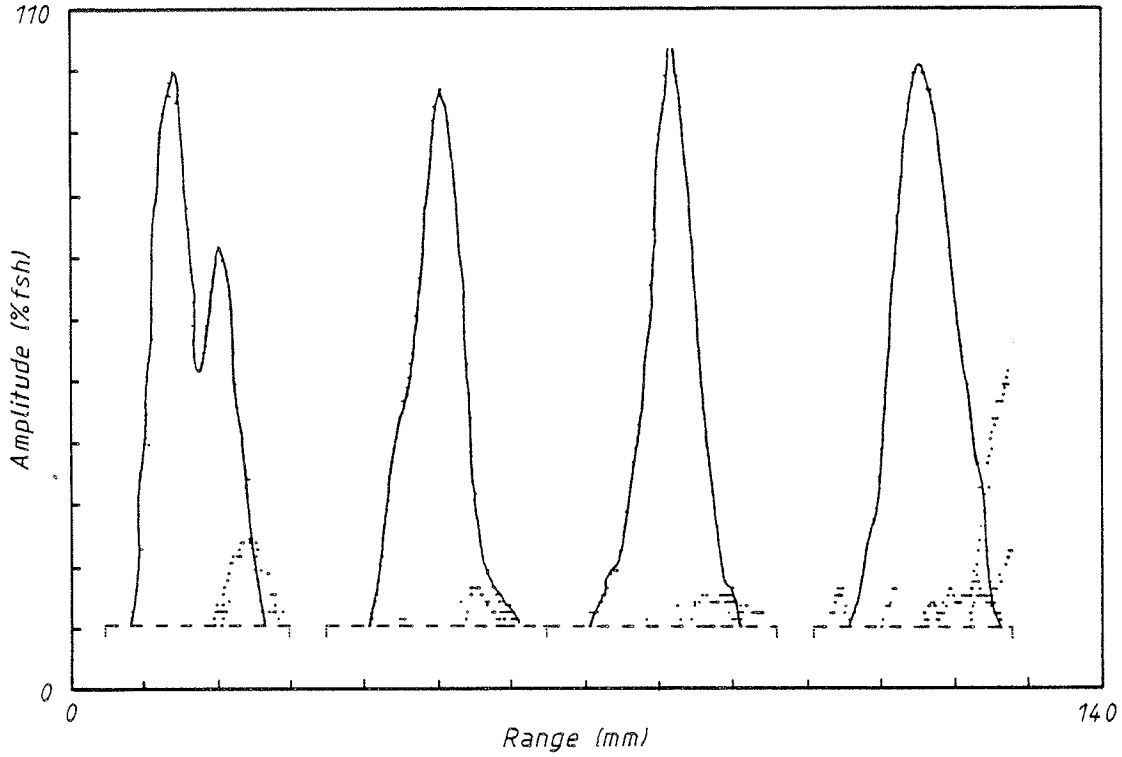

Fig.C3 Echodynamic curve from four drilled holes using a 2MHz 45° transducer.

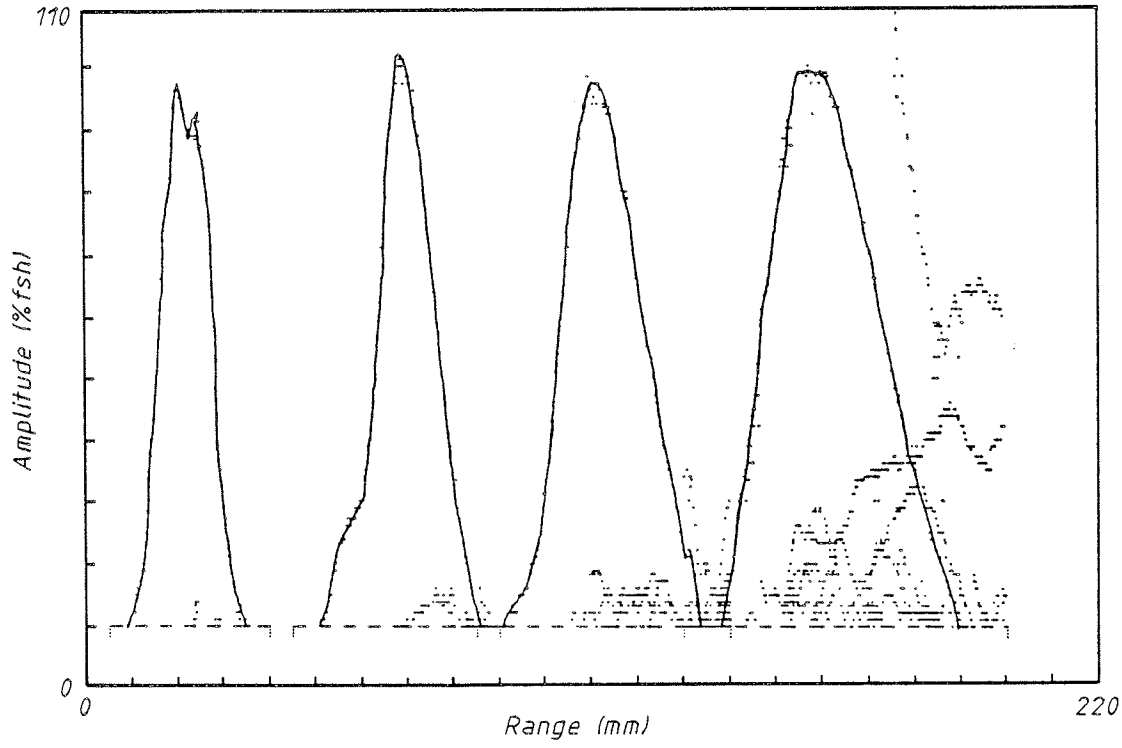

Fig.C4 Echodynamic curve from four drilled holes using a 2MHz 60° transducer.

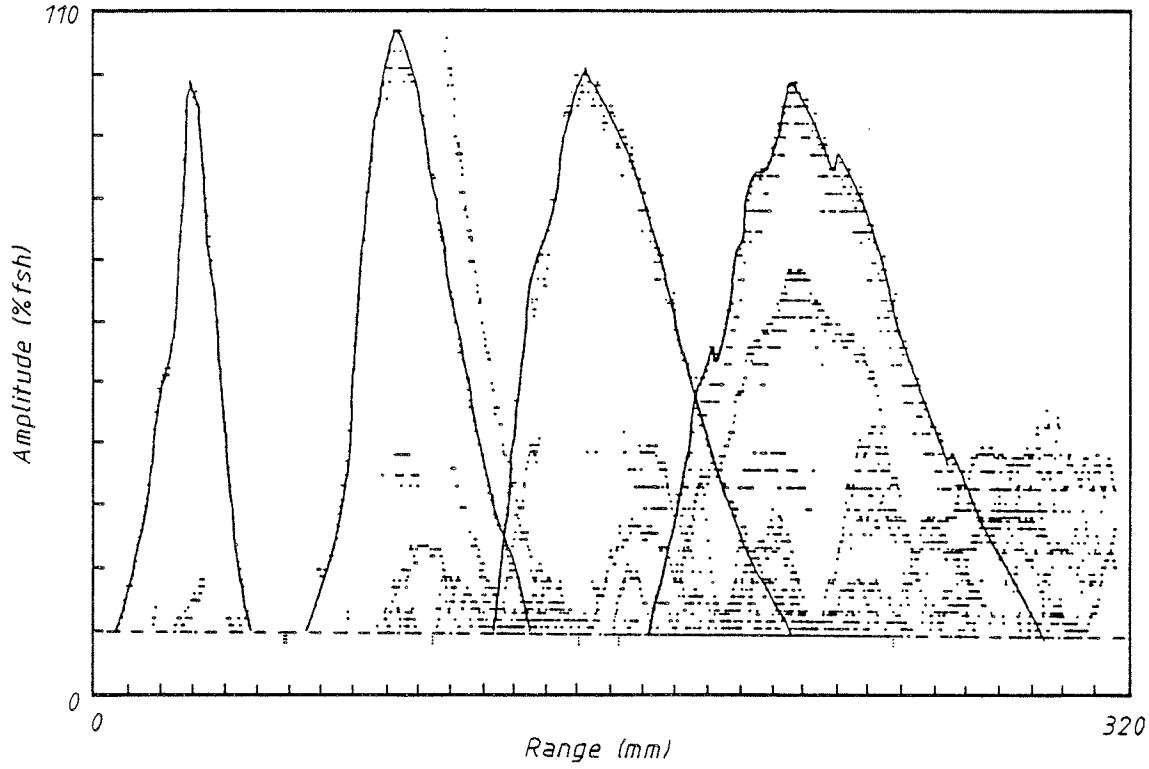

Fig.C5 Echodynamic curve from four drilled holes using a 2MHz 70° transducer.

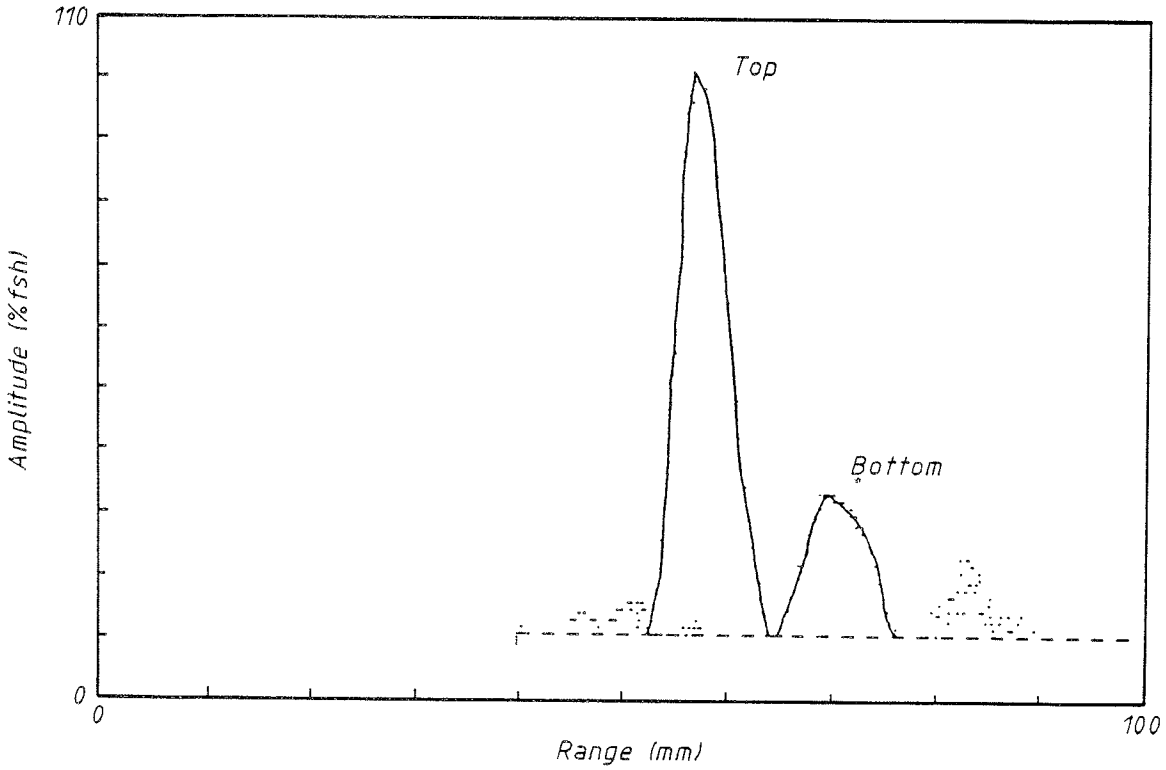

Fig.C6 Echodynamic curve from a crack in specimen J301 using a 4MHz 45° miniature transducer.

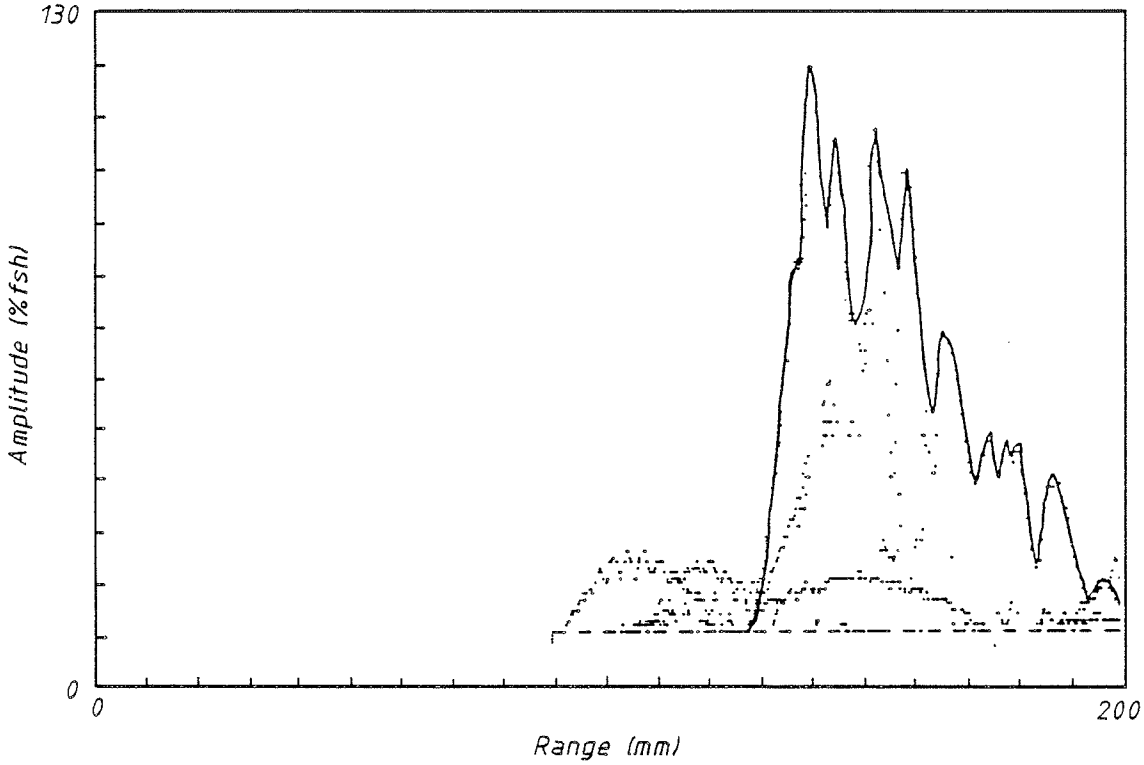

Fig.C7 Echodynamic curve from a crack in specimen J301 using a 2MHz 70° transducer.

ULTRASONIC MEASUREMENT OF WELD FLAW SIZE, PHASE 2
Part 2: Studies of the time-of-flight diffraction technique for flaw evaluation

Final Report
Prepared for

National Co-operative Highway Research Program
Transportation Research Board
National Research Council

TRANSPORTATION RESEARCH BOARD

NAS-NRC
Privileged Document
This report, not released for publication,
is furnished only for review to members
of or participants in the work of the
National Co-operative Highway Research Program.
It is to be regarded as fully privileged,
and dissemination of the information included
herein must be approved by the NCHRP.

A.C. Duncumb and P.J. Mudge

Welding Institute Project No.3769
Report No.3769/15, Part 2
February 1987

THE WELDING INSTITUTE

Research Laboratory Abington Hall Abington
Cambridge CB1 6AL United Kingdom
Telephone Cambridge 0223 891162
Telefax 0223 892588
Telegrams WELDASERCH CAMBRIDGE
Telex 81183

ACKNOWLEDGEMENT

This work was sponsored by the American Association of State Highway and Transportation Officials, in co-operation with the Federal Highway Administration, and was conducted in the National Co-operative Highway Research Program which is administered by the Transportation Research Board of the National Research Council.

Contents **Page No.**

Contents - Continued **Page No.**

Contents - Continued

LIST OF FIGURES

LIST OF TABLES

G2. Statistical data on accuracy of flaw through-wall size measurement for time-of-flight tests.

G3. Results of length measurement from SAFT processed data.

ACKNOWLEDGEMENTS

This work was performed by The Welding Institute, Abington, Cambridge, England under contract to NCHRP; project number 10-13/1.

Alison C. Duncumb, formerly a Senior Physicist with the NDT Research Department, was the researcher responsible for this part of the program in conjunction with Peter J. Mudge, Head of the NDT Research Department and Principal Investigator for this project. The project is conducted under the general guidance of Dr. John D. Harrison, Manager, Engineering and Materials Group (of which the NDT Department is a part). The experimental work was conducted by Messrs Peter H. Smith, the NDT Research Laboratory Supervisor, and Kim S. Hayward, who are both certified under the UK Certification Scheme for Weld Inspection Personnel (CSWIP), for ultrasonics.

Helpful discussions were also held with Peter J. Carter of AERE Harwell and William S. Browne of SGS Sonomatic Ltd., Warrington, UK.

ABSTRACT

This report describes an investigation into the ultrasonic time-of-flight diffraction technique as a means of locating and dimensioning flaws accurately at welds in fracture critical structural steel members. Results of a laboratory study on real weld flaws are presented together with a theoretical appraisal of the technique's limitations and a survey of the potential of the technique for use in the field.

SUMMARY

This report describes work carried out within tasks 3 and 4 of NCHRP Project 10-13/1. The aims were to specify and construct a computer based test instrumentation package for ultrasonic time-of-flight diffraction tests, and to evaluate the technique for sizing weld flaws on real discontinuities in welded research samples. A total of 46 weld flaws on both crack-like and non-crack-like form were examined in three plate thicknesses, 10mm (0.4in), 38mm (1.5mm) and 95mm (3.75in).

Theoretical studies showed that accuracy of flaw height measurement was around $\pm$ 1mm (0.04in) with a similar accuracy of positioning the flaw below the test surface. Sectioning of 21 flaws has confirmed that these theoretical limits are realized in practice.

The flaws studied were generally well detected by the system except when they lay close to the test surface where detection is poor due to the test geometry. Difficulties were also experienced when testing the thinnest, 10mm (0.4in), plate as the zone of poor detection at the test surface extended to half the plate thickness in this case. Flaws near one surface can generally be detected from the opposite face, but nevertheless further investigations are required in this area.

The practicalities of applying the technique on site are also considered. Two factors are required to be considered further,

(a) engineering of the scanner device for robust site operation and,

(b) reduction in size of the system electronics package.

It was considered that there are no insurmountable problems for the application of the technique on-site as far as procedures or personnel are concerned.

CHAPTER ONE

INTRODUCTION AND RESEARCH APPROACH

PROBLEM STATEMENT

There is an urgent need for ultrasonic testing procedures that can be used to measure the dimensions of weld discontinuties (flaws) with sufficient accuracy to permit evaluation using a fracture mechanics approach. Most State transportation agencies use the provisions of the American Welding Society Structural Welding Code, AWS D1.1 (1) to determine the acceptability of structural welds. These provisions are based on an assumed relationship between the ultrasonic "Indication Rating" and flaw size. The results of the first phase of research (2), as well as other experience, indicate that this relationship is not valid. Research is needed to develop improved ultrasonic testing procedures, using equipment presently available, that will permit accurate measurement of the dimensions of flaws common to weldments. These procedures are needed for use in both shop and field inspection of weldments to determine acceptance during construction and for in-service evaluation. Reliable procedures for ultrasonic testing will obviate the costs and delays of unnecessary repairs, whilst reducing the probability that major flaws will be improperly evaluated.

RESEARCH OBJECTIVE

The overall objective of the program was to derive and to validate ultrasonic techniques which would allow weld flaws to be evaluated reliably and their size to be measured with sufficient accuracy to enable fracture mechanics assessments to be applied.

It is highly desirable to apply such analyses to critical welds in steel structures, such as bridges, in order to increase confidence that flaws which may cause failure of welds during service are not present. For the purposes of performing the numerical analysis it is convenient to assume that the flaw is bounded by a rectangle of length l and height h_{max}, as shown in Fig. 1. Considerable emphasis is therefore placed on the accuracy with which these dimensions can be measured non-destructively, the height being particularly important.

The ultrasonic time-of-flight diffraction technique has been shown to be consistently more accurate than other sizing methods for measuring the height (or through wall size) of flaws (2, 5), particularly of highly detrimental vertical planar flaws. However, the technique has not been widely applied outside the laboratory except for highly specific examinations of nuclear power generation plant and, so far, has not had any great impact on the non-destructive testing industry in general. This is partly because the cost and complexity of the equipment presently available does not make the technique attractive for general use for ultrasonic inspection. In addition, most welded fabrications are built to standards which are aimed at generally ensuring an overall good quality of workmanship, and do not require a detailed quantitative assessment of the significance of each flaw by application of fracture mechanics. However in circumstances where fracture mechanics is needed to assess a potentially dangerous or growing flaw, the accuracy provided by the time-of-flight technique is highly desirable.

The aim of this work was to demonstrate that the use of the time-of-flight technique for the evaluation of weld flaws in the fracture critical major tension members in steel bridge structures was feasible

and to provide information from which optimum test procedures of known performance level could be derived. This would enable recommendations for deployment of the technique in the field to be made. Prototype equipment was to be used from which site compatible equipment could be derived.

This work constituted tasks 3 and 4 of NCHRP project 10-13/1 which is in turn Phase 2 of project 10-13.

THE TIME-OF-FLIGHT TECHNIQUE

Principles

Time-of-flight testing was developed to obviate many of the uncertainties normally associated with ultrasonic sizing of weld flaws by utilising a parameter which can be measured very precisely, i.e. time. Two transducers are used, one acting as a transmitter and the other as a receiver. These are placed facing each other, one on each side of the weld, as shown in Fig. 2. The transmitter emits a very broad beam of ultrasound consisting of angled longitudinal waves, in this case at centre frequency of 3MHz.

The principle of the technique is to detect diffracted waves which emanate from the tips of a flaw when the transmitted beam strikes it and to measure their transit times from the transmitter to the receiver via the flaw. From this the distance of the flaw below the test surface and its height in the through thickness direction can be calculated. In order to maximise the resolution between different pulses, transducers which emit very short pulses, of about $1\frac{1}{2}$ cycles, are used. The other parameters that are required to be known are the transducer separation and the ultrasonic velocity; Pythagoras's

theorem can then be used to calculate flaw depth. This is demonstrated in Appendix A. A discussion of the development of time-of-flight testing, as documented in the literature is given in Appendix B.

The depth calculation assumes that the diffraction source lies on the centre line between the transducers. In fact, for any given transit time the source could lie anywhere on an ellipse with the transducers at the focii (Fig. 3). However, physical restrictions imposed by the fact that the transducers have a finite beam spread and that the diffraction source will normally lie within the weld, mean that its actual portion is likely to lie along the horizontal position at the bottom of the ellipse in Fig. 3. Therefore assuming that diffraction source lies on the central plane does not have too significant an effect on the accuracy of the depth measurement. Such errors are discussed further in Appendix C. It should, however, be noted that a single measurement, although giving the depth of a flaw, will not give its transverse location within the weld.

In addition to the diffracted signals from any flaws present a lateral wave is generated which travels at the surface along the line of sight between the two transducers in the absence of a surface breaking flaw, and is thus the first wave to arrive. The back wall wave, which is the directly reflected wave from the opposite surface of the sample, will also be present, see Fig. 2. These signals are useful as timing references, as between them they define the time window of interest corresponding to the top and bottom surfaces of the workpiece respectively. In the absence of any discontinuities, no signals would be expected to arrive between the lateral and back wall waves.

Fig. 4 shows a digital reconstruction of a received unrectified radio frequency waveform. This is conventionally known as A-Scan presentation. The lateral wave, diffracted signals from the top and bottom of a flaw and the back wall wave are identified. Signals arriving later in time than the back wall wave are mode converted signals; i.e. signals that have part of all of their path length in the shear wave mode. These signals may be ignored for the present and can be removed from the final presentation of the ultrasonic test results.

Theory predicts that the diffracted signals from the top and bottom of a flaw should be out of phase by 180° with respect to each other, i.e. one is the mirror image of the other. This is useful for determining whether two signals are from the top and bottom of a single large flaw or from two separate flaws, both of which are too small for the extremities to be resolved. The 180° phase change can quite clearly be seen for the diffracted tip signals in Fig. 4. The arrival times of these signals are measured from some well defined point on the waveform. In this work measurements have been made from the first point where the pulse waveform crosses zero, from negative to positive for the lateral wave, positive to negative for tip signals from the top of flaws and negative to positive again for tip signals from the bottom of flaws - thereby taking phase reversals into account. These time measurements can then be used to calculate the depth of the flaw below the test surface and its through thickness height.

Capabilities

Whether or not a discontinuity can be sized depends on whether the tip signals can be resolved from each other and from the lateral and back wall waves. As a result of the two transducer geometry, depth resolu-

tion increases with depth into the workpiece and increases for decreasing transducer separation (this is discussed further in Appendix C). As a result, the resolution of tip signals depends not only on the height of a flaw but also on its depth below the surface. This is best illustrated by the graph in Fig. 5 which shows the resolution limits for time-of-flight tests carried out with transducers of 3MHz centre frequency. Here the minimum height of flaw measurable has been plotted versus depth below the test surface for a number of transducer separations. In deriving these curves it was assumed that for pulses of $1\frac{1}{2}$ cycles in length to be resolved they must be separated in time by the equivalent of two cycles. In fact in some instances it was possible to achieve better resolution than the 2 cycles assumed but Figure 5 gives typical resolution limits.

It can be seen from Figure 5 that for flaws close to the test surface the smallest flaw that can be sized is somewhat larger than for flaws some distance below the test surface. As the depth increases the minimum size of flaw that may be measured, h, decreases, down to the limiting value of 2mm. For example, for a transducer separation of 70mm and a flaw at a depth of 25mm below the surface, the smallest flaw that may be sized is about 3.3mm in height. This type of presentation is therefore useful for determining the expected resolution limits for any depth as a result of having selected a given transducer separation.

Figure 5 also shows the extent to which the lateral wave obscures a zone close to the test surface because of its finite duration. Although flaws in this near surface zone may be detected by variations in the shape of the lateral wave, accurate measurements of flaw depth cannot generally be made. For example, for a transducer separation of

70mm the lateral wave obscures a depth zone down to 15mm below the surface for the transducers used in this program. Surface breaking flaws, however, may be measured as in such cases there would be no lateral wave to obscure the tip signal.

Display of Results

In general for time-of-flight testing, raster scanning of the transducer pair is not required. It is sufficient to scan the transducers at a fixed spacing in a straight line along the weld (Fig. 6) and to repeat the scans at different transducer separations if adequate coverage of the weld volume cannot be achieved in a single pass.

The instrumentation required to perform a test must also be considered. Whilst single measurements can be taken from an A-Scan trace, as shown in Fig. 4, it is not possible to do so from the large numbers of scans collected when scanning along a weld. For example if a 500mm length of weld is scanned, recording A-Scans every 1mm, the number of A-Scans generated rapidly becomes unmanageable unless they are collected and stored in some way. To do this it is necessary to use a computer to control the test and collect the data. It is then possible to present the data via the B-Scan display format (Fig. 7). This is a time versus distance plot which represents an ultrasonic map of a longitudinal cross section of the weld. It consists of many A-Scans placed side by side. However, instead of displaying them as positive and negative excursions about zero as in Fig. 4, the amplitude of the signal is used to modulate the intensity of a single line on a video display, i.e. the signal amplitude is represented by a grey scale, with white representing the maximum positive excursion and black representing the maximum negative excursion. Signals at each transducer

location may then be displayed alongside each other, building up a side view, as shown in Fig. 7, of diffraction sources within the test-piece.

The A-Scan shown in Fig. 4 represents the responses at 200mm from the datum in Fig. 7. As described above, the lateral wave represents the top surface and the back wall wave the bottom surface. The phase inversion of the flaw tip signals may be recognised on the B-Scan display by a reversal of the black-to-white and white-to-black transitions. The detailed interpretation of time-of-flight displays is covered in Chapter 2.

The vertical axis of the B-Scan display represents time and not depth. The two are not linearly related because of the two transducer geometry shown in Fig. 2, so that measurements of flaw depth and height cannot be made directly from the raw B-Scan image. Either time measurements may be made using a movable cursor on the video TV image and the depth calculated by the computer or the display may be converted to be linear with depth by the computer to give a true picture of the location of the flaws. Fig. 8 shows a linearised B-Scan display. The vertical scale now represents depth, and the depth and height of any flaws can then be measured directly from a correctly scaled paper copy of the display. The non-linear relationship between depth and time is apparent by the fact that the lateral wave appears to be stretched out.

The major advantage of the time-of-flight technique is that flight time and velocity are the only ultrasonic parameters measured. Consequently it is far less sensitive to factors that are difficult or impossible to control, such as flaw type and orientation and ultra-

sonic beam spread characteristics, than conventional ultrasonic methods.

RESEARCH APPROACH

The research approach was, firstly, to specify and procure an equipment which would retain the essential flexibility of a laboratory system, but which could also be used outside the laboratory, and secondly, to establish the size measurement capability of the technique. To this end an equipment was produced which could be used both in and outside the laboratory. A description of this is given in Appendix D. Procedures for its use are given in Appendix F. To investigate the time-of-flight technique 19 welded samples were manufactured in a structural grade steel which were representative of butt welds in the fracture critical major tension flanges in steel bridges. The welds were in thicknesses of 10, 38 and 95mm and contained a total of 46 deliberately introduced flaws, such as lack of sidewall fusion, solidification cracking and slag. Of these 38 were planar flaws, which reflected the importance of the ability to evaluate the type of discontinuity and the fact that the performance of the D1.1 procedures for their evaluation was poorer than for volumetric flaws from previous work (2). The specimens are described in detail in Appendix E. Time-of-flight data were collected from all specimens. Tests carried out are summarized in Table 1. Experimental details are given in Appendix F. After testing, six samples containing a total of 21 embedded flaws were examined destructively to enable the actual dimensions of the flaws present to be compared with the time-of-flight test results. The remaining samples were retained for future investigations as samples containing realistic flaws are costly to produce and the six samples sectioned provided sufficient data from which assess the results from the remaining 13.

In addition to the practical work, the technique was also studied from a theoretical standpoint in order to assess its expected capabilities and limitations. Furthermore, a sound understanding of the technique facilitated a more thorough interpretation of the B-Scan displays.

CHAPTER TWO

FINDINGS

RESULTS OF TIME-OF-FLIGHT TESTS

From the large amounts of information gathered from time-of-flight tests on the flaws studied, the aim was to determine the flaw parameters d_{min}, h_{max} and 1 as defined by Fig. 1 for each flaw. The measurements in the through wall direction, d_{min} and h_{max}, were determined from time-of-flight data, whilst the length, 1, was determined from the B-Scan image by the 6dB drop method. A side view of the weld with rectangles representing each flaw could then be drawn. Details of the results are presented in Appendix G.

In general, where it was possible to determine d_{min} and h_{max} from more than one scan, there was good consistency between measurements. However, results from flaws close to the testing surface tended not to be so consistent, for the reasons given in Chapter 1 and Appendix C. Where signals from flaws were partially covered by the lateral wave, it was not always possible to separate the two signals and hence measurement of the flaw was not feasible.

Where individual flaws gave more complex responses than the simplified top and bottom edge diffracted signals described so far, or where a number of flaws were in close proximity giving multiple signals, a degree of interpretation was required before measurements could be made.

Detection of Flaws

All the intended flaws and some unintended ones in all specimens were detected by the combination of scans carried out (Table 1 and Appendix F). For the 38 and 10mm thick samples scans from one plate surface only were sufficient to detect all the flaws. However, for the 95mm thick samples scans from both plate surfaces had to be considered in combination in order for all flaws to be detected.

The diffracted edge signals from flaws were, in general, of low amplitude. For the thickest samples studied, the combination of the increased transducer separation and the longer ultrasound path lengths needed to cover the full thickness (see Fig. 2) further reduced the diffracted signal amplitudes to the point where those from flaws near the opposite plate surface could not be distinguished from the background noise. This limitation was initially overcome by scanning these test pieces from both surfaces, but later an additional preamplifier providing an extra 64dB of gain was incorporated into the test system which enabled weak signals to be detected and obviated the need to test from both sides.

Flaw Size Measurement - Limitations

Where the tip signals of flaws were resolvable, measurements of the depth of the flaw below the test surface, d_{min}, and its height, h_{max}, could be made. In some instances the tip signals from flaws buried in the lateral wave could be resolved by decreasing the transducer separation but in many cases, a scan from the opposite plate surface was required in order to determine size of the flaw. However, owing to the very short time window between the lateral and backwall waves for scans of 10mm thick samples (as predicted by Fig. 5) no size measure-

ments were possible, although the flaws could be detected. For some of the flaws in this plate thickness it was possible to combine results from scans from both plate surfaces and hence to calculate the height and depth of the flaw.

For 3 out of the 21 flaws in the 95mm thick samples it was not possible to make measurements of height and depth owing to the signal to noise ratio problem described above. This situation was ameliorated when the pre-amplifier was incorporated.

All the intended flaws in the 38mm thick samples could be sized in accordance with the resolution limits defined in Fig. 5.

Flaw Length Measurement

Approximate flaw length was determined from the B-Scan images by a conventional transducer movement technique for all specimen thicknesses. A more rigorous approach to flaw length measurement using the synthetic aperture focusing algorithm (SAFT) (22) can be applied to data already collected. However this has a significant time penalty (approx. 15 minutes per 400 A-Scans collected) and ideally requires a central processor of increased computing power. A preliminary investigation indicated a significant improvement to the ease with which flaw length could be determined (see Appendix G) although insufficient data were available to enable any assessment of the increased accuracy to be made.

CORRELATION OF TIME-OF-FLIGHT RESULTS WITH DESTRUCTIVE DATA

Six specimens, containing a total of 21 flaws were examined destructively. For each flaw the minimum rectangle totally enclosing it was drawn on a scale diagram. The time-of-flight measurements from the

scan yielding the greatest value of h_{max} were superimposed in order to compare measured and actual sizes (Appendix G). The results were more easily assimilated by plotting graphs of measured height v actual height and measured depth of the flaw below the testing surface v actual depth. These graphs are shown in Fig. 9 and 10. Again the time-of-flight measurement that yielded the greatest value of h_{max} has been used as this would be the most likely value to be taken in practice in order that subsequent assessment of the significance of the flaw would remain conservative.

A statistical analysis of these results is given in Table 2, where, for comparison purposes, results of previous work are also given. In the present work the mean error for flaw height measurement was -0.2mm (-0.01 in) showing a tendency for the height to be underestimated, but only by a very small amount. The standard deviation was 1.0mm (0.04 in) and therefore the 95% probability scatter was $\pm$ 2.0mm ($\pm$ 0.08 in). These results show a marked improvement over results reported previously (Tables 2-4).

For measurements of the depth of the top of the flaw below the testing surface, the error was slightly larger, as predicted in Appendix C. The tendency was to overestimate the depth of the diffraction site by + 0.5mm (0.02 in) with a standard deviation of 1.3mm (0.05 in) - a 95% probability scatter of $\pm$ 2.6mm (0.10 in).

In the above analysis it is the time-of-flight measurements that yielded the maximum value of h_{max} that have been used. However a large number of other time-of-flight tests were carried out with various test parameters. For the 21 flaws sectioned a total of 55 measurements of flaw height were made. It is useful to consider all the data in a

statistical analysis in order to give some idea of the sensitivity of the accuracy of the technique to choice of test parameters and more generally to procedural abuse.

If the data from all 55 measurements are considered then the mean error in height measurement is -0.8mm (0.03 in) with a standard deviation of 1.3mm (0.05 in) and the mean error in depth measurement + 1.2mm (0.05 in) with a standard deviation of 1.3mm (0.05 in). The absolute value of both mean errors has increased and arises as a result of some of the small variations in the time-of-flight measurements with the different values of the test parameters used, as discussed in Appendix C. Another contributing factor is the effect of the flaw not being on the centre line between the transducers as is assumed in the depth calculation equation. However, an analysis of the errors caused, given in Appendix C, shows the errors involved to be small for weld inspection.

COMPARISON WITH STANDARD MANUAL ULTRASONIC TESTS

It has been shown that the time-of-flight results compare very favourably with the destructive data available. In an assessment of the flaws to the AWS D1.1 code, all but one of the flaws were deemed to be rejectable flaws. However no quantitative information is made available as to each flaw's actual size or its true severity in terms of fitness for purpose criteria.

Another important comparison is between the time-of-flight results and the results of standard manual ultrasonic tests where decibel drop (transducer movement) methods were used for sizing the flaws. Fig. 11 shows a graph of measured v actual flaw height for the 20dB drop

tests. The widely recognised tendency of the 20dB drop method to underestimate the through thickness height (2, 5) is quite evident. The mean error was -4.8mm (-0.19 in) with 95% confidence limits of $\pm$ 6.2mm ($\pm$ 0.24 in). The mean error here is rather worse than in previous work (see Table 3) although the scatter is of the same order. This is due to the fact that more of the flaws in the present program were vertically orientated and it is known that the 20dB drop technique does not perform reliably on such flaws. It would appear that generally only part of the flaw has been identified and sized. However the results do serve to illustrate the superior capability of the time-of-flight technique for sizing flaws (compare Tables 2 and 3).For the majority of flaws the height as determined from the time-of-flight results, was 3mm to 5mm (0.12 in to 0.20 in) greater than that determined by the 20dB drop method thereby indicating the amelioration of the tendency of the conventional test to undersize flaws.

Another widely used conventional technique for sizing weld flaws is the maximum amplitude technique. Like the time-of-flight technique it relies on the diffracted signal from the tips of a flaw being detected but in this case with a single transducer operating in pulse-echo mode. Although not used during the present studies it is interesting to recall that in results of some previous work (2, 5), see Table 4, the mean error in measurements of flaw height by the maximum amplitude method was comparable with that for the time-of-flight measurements and considerably less than for 20dB drop measurements (Table 2). However the scatter in these results was of the same order as for the 20dB drop measurements. It is thought that the wide scatter band for the maximum amplitude measurements is due partly to the process of maximising the signal by transducer movement and partly due to in-

correct identification of the signals from the top and bottom tips of a flaw. The time-of-flight technique thus has advantages over the maximum amplitude technique in that the signal is not required to be maximised and it is easier to recognise the signals from the tips of a flaw. The scatter in the time-of-flight results is significantly reduced as can be seen by comparing Tables 2 and 4. The results described above together with the demonstrated capability of the time-of-flight technique on 21 flaws examined destructively, demonstrate clearly that the technique can be used effectively to supply accurate measurements of flaw size which can be used an input to fracture mechanics calculations.

CHAPTER THREE

INTERPRETATION APPRAISAL AND APPLICATIONS

A COMPARISON OF TIME-OF-FLIGHT AND MANUAL ULTRASONIC TESTING

In a conventional manual ultrasonic test a hand held transducer is manipulated over the surface of the specimen. In addition to ensuring that adequate coupling is maintained, the operator has to watch the screen of the flaw detector, interpret and record any indications, dimension (if required) any flaws detected and log the position of the transducer. This process relies heavily on the skill and the integrity of the operator as once the transducer is removed indications are lost and the only record is the operator's notes.

A test system incorporating some degree of computer control/automation offers considerable advantages over standard manual ultrasonic testing:-

(i) Test data can be collected more rapidly than by manual scanning.

(ii) More complete data can be collected and transducer position can be logged automatically.

(iii) Data are more consistent and more objective than those collected manually.

(iv) Results can readily be stored on disk or magnetic tape for future reference and for further analysis.

(v) Display and analysis of results are superior to those from manual tests.

(vi) There is potential for advanced signal processing of waveform data which are related to flaw characteristics.

(vii) Test parameters, testing conditions and results can be logged automatically and stored together, thereby providing a degree of quality control over the ultrasonic test process which is not generally possible with manual testing.

(viii) Hard copy output of test results can be produced.

Such attributes would be particularly advantageous for shop floor and site testing where, due to the long lengths of weld to be inspected, large volumes of data can be generated very rapidly. The ability to use mass-storage media is particularly advantageous in that the subsequent analysis can be far more thorough than is possible with manually collected test results. The quality control aspects of an automated data collection and display system also ensure correct treatment of large volumes of data.

If the computer system can collect data from an ultrasonic time-of-flight pair then for complete coverage of the weld volume only a single scan or a small number of uniaxial scans with different transducer separations are required. This represents a considerable saving in time over simply automating a manual test where raster scanning with a number of different transducer angles is required in order to obtain complete coverage of the weld volume. Furthermore the time-of-flight data readily allow accurate measurements of flaw through wall size to be made.

Therefore in comparison with the manual test, the time-of-flight test is relatively easy to apply. The display, however, has been criticised by non-experts in the field as being difficult to interpret. Whilst such displays are undeniably unfamiliar to personnel not engaged in automated testing they are not inherently confusing. First, it must be

remembered that the B-Scan display contains a great deal more information than a single A-Scan trace normally seen on a flaw detector. A B-Scan image, such as Fig. 7, consists of around 256 A-Scans placed side by side; that is 256 traces such as shown in Fig. 4. Interpretation of the latter would be the more onerous and time consuming. Second, every perturbation of the grey level in Fig. 7 is a diffraction site for ultrasound, which must arise from some discontinuity. Clearly, a crucial stage is the interpretation of the signals seen to determine which indicate significant flaws, and this aspect needs to be developed in conjunction with appropriate acceptance standards for ultrasonic inspection in relation to fracture mechanics. It should also be emphasised at this point that a common feature of most NDT methods is that suitable training combined with practical experience and a sound understanding of the underlying physical principles are required for a reliable test. Interpretation of the B-Scan image and operator training are discussed below.

INTERPRETATION OF THE B-SCAN IMAGE

At the present stage in the development of processing routes for the results from time-of-flight tests a certain amount of practical experience is required on the part of the operator in order to interpret the B-Scan images. However the B-Scan presentation does have considerable advantages.

(i) The B-Scan gives a representation of all diffraction sources within the volume inspected by a given transducer configuration.

(ii) These signals occur in a well defined region between the lateral and backwall waves.

(iii) During data collection all signals are recorded. There is no signal rejection by amplitude, implying that even the smallest modulation of the background noise will be recorded as a signal.

(iv) The possibility exists for flaw characterisation if a library of typical responses from different flaw types can be built up.

These factors demonstrate that the test data are presented in a readily assimilated, although novel, format and suggest that it is not unreasonable to anticipate that a trained technician could interpret such test results satisfactorily, i.e. expert interpretors would not generally be required. An example interpretation of a B-Scan image is given below. More are to be found in Appendix G.

INTERPRETATION OF B-SCAN OF SPECIMEN J307

A B-Scan of the entire length of weld sample J307 is shown in Fig. 12 (scan 1, test surface "A", transducer separation = 80mm). The lateral and back wall waves delineating the area of interest and representing the top and bottom surfaces respectively are indicated. Signals occurring later in time than the back wall wave are mode converted signals and may be ignored. The datum end ("Y") is at the right hand end of the picture and distance along the weld from the datum is indicated by markers every 50mm. Five major sources of diffracted waves can be identified on the B-Scan between the lateral and back wall waves or as perturbations to the lateral wave.

Between 50 and 100mm from "Y" there is a very noticeable perturbation to the lateral wave, indicative of a flaw very close to the test surface (Flaw 25). In order to make measurements of this flaw's through thickness extent there are three alternatives (see Appendix C).

(i) Decrease the transducer separation - this may necessitate removal of the weld crown - and may still not be sufficient to enable the tips of the flaw to be resolved either from each other or from the lateral wave.

(ii) Increase the frequency of ultrasound used to increase the resolution and decrease the time occupied by the lateral wave.

(iii) Inspect the sample from the opposite plate surface.

In this instance it was the third alternative that was adopted and this allowed the height and depth of the flaw to be determined.

In addition to the intentional flaw, there is a complex region of indications from unintentional flaws between the start of the scan and Y = 150mm. These indications were difficult to interpret. However, the depth and through thickness height could be determined and the overall profile of the flaws could be found. This can be seen in Fig. 12b. Sectioning revealed four flaws (Fig. E3b) - two small inclusions or lack of inter-run fusion in the mid-wall thickness of the weld and two cracks in the heat affected zone (HAZ) each of 1 to 2mm in through thickness extent). In order to differentiate these from each other on a B-Scan image it would have been necessary to carry out a scan transverse to the longitudinal axis of the weld in order to locate them by means of the minimum points on the hyperbolas of Equation C8 for each flaw. This would have necessitated removal of the weld crown. This example however does serve to illustrate the use of transverse scans to enable the transverse position of the flaw within the weld to be determined.

The indications in the region 175 to 225mm from "Y" are from a single flaws as the phase reversal between the upper and lower signals can be

seen clearly. If the time-to-depth conversion is made for the appropriate points on the top and bottom signals for all scan increments along the flaw, then the flaw profile may be plotted. This is shown in Fig. 12b, where the results of the destructive examination are plotted. There was good correlation between the actual and estimated profile of this flaw, which was number 26, a solidication crack.

Again between 250 and 320mm from "Y" there is evidence of a perturbation to the lateral wave indicative of the presence of a flaw (no. 27). However, this time it is only the top tip of the flaw that is obscured as the diffracted wave from the bottom of the flaw is readily identified by its characteristic phase reversal. In fact it was possible to make measurements of the depth of the top tip of the flaw below the testing surface. However due to the large diffracted angle ϕ (see Appendix C) the error in the measurement could be expected to be greater than 2mm.

The profile of the flaw as determined from the time-of-flight measurements is shown in Fig. 12 with the destructive results superimposed. The flaw, a lack of sidewall fusion flaw (Fig. E3d), did not lie on the central axis between the transducers, as is assumed in calculating the depth (Appendix C). This will have been another contributory factor to the 2mm overestimation of its depth. However, the profile of the flaw and its measured height show a good correlation with the actual values.

The final major flaw occurs between 300-420mm from "Y". The top and bottom signals can be identified easily by their relative phases. However between these two there is a third signal of the same phase as would be expected from the top of a flaw. Sectioning revealed that the

flaw was in fact a slag line with a crack extending for about 3mm vertically upwards out of it (Flaw 28, Fig. E3c). The additional signal would appear to be associated with the top of the slag. It is thought that the presence of the slag may have allowed some of the ultrasound to travel via the top of the slag to the receiving transducer. The correlation between measured and actual height is again shown in Fig. 12.

It is interesting to note that the other 38mm thick sample containing a slag line with associated crack (J309, Flaw 32) gave a similar B-Scan image.

Other sources of diffracted waves in this sample (e.g. those marked "s" on Fig. 12) were from point sources such as pores. Some of these were identified on the sections taken, where they happened to coincide precisely with the edge of the saw cut.

Improvements to the B-Scan Image

A number of possibilities exist, however, for improving the presentation of the B-Scan image from that shown in Fig. 7. These include automatic computer recognition of the lateral and back wall waves and their identification on the B-Scan image. This can be accomplished by simple calculation from some of the test parameters (transducer separation, delay time in the polystyrene shoes etc) followed by identification of the appropriate zero crossing of responses on each A-Scan trace. Signals occuring later in time than the back wall wave may then not be displayed leaving an area of the screen blank for the display of text such as test parameters. Additionally the markers representing distance along the specimen may be numbered to facilitate identification of flaw position. Examples of the B-Scan display before and after improvement are shown in Fig. 7 and 13.

Furthermore, it is also possible to envisage the situation where the computer may assist the operator in the identification and measurement of flaws and the minimum rectangle enclosing the flaws could be superimposed semi-automatically. However, totally automatic identification and evaluation of flaws is thought to be a long way off and would require the use of a very powerful computer. In the short term very substantial benefits may be gained from computer controlled time-of-flight testing by providing the experienced operator with better information on which to base any decision as to the integrity of the weld under test. A further benefit is that it releases the operator from the onerous task of manually manipulating transducers and logging information. If a library of typical B-Scan images of different types of flaw is built up, then the computer may also aid in flaw characterisation.

CAPABILITIES OF THE TIME-OF-FLIGHT TECHNIQUE

A good degree of correspondence between experimental results and theoretical predictions of the capabilities of the time-of-flight technique is demonstrated by the results obtained to date. A rigorous quantitative treatment of the capabilities and limitations of the technique is to be found in Appendix C, a more qualitative approach being adopted here.

Resolution

In order to resolve one received pulse from another, and thus to make measurements of flaw through thickness parameters, the two pulses must be separated in time. In Appendix C it was assumed that the minimum difference in arrival times that allowed two pulses to be resolved was equivalent to the time occupied by one pulse of 2 cycles duration

(i.e. 0.667 μs at 3MHz). In practice the pulses were of approximately 1½ cycles in duration (equivalent to 0.5 μs at 3MHz), and therefore it was possible to achieve better resolution than was predicted in Appendix C.

As two pulses must be resolved from each other in order to measure their arrival times, there is a minimum flaw height that can be measured. However, due to the depth/time non linearity in two transducer time-of-flight testing, this minimum flaw height depends on the depth of the flaw below the surface and on the transducer separation. For a given transducer separation, as the depth d below the surface increases, the height of the smallest flaw that can be measured decreases, tending to a limiting value of 2mm (0.08 in) (Fig. 5).

This dependence of the smallest height of a flaw that can be measured on its depth below the scanning surface and on the transducer separation is exemplified by the results from some of the near surface flaws (e.g. nos. 32, 35 and 37, see Table G1). When inspected from one surface of the plate the diffracted signals from the tips of such flaws near to that surface could not be resolved, whilst from the opposite surface it was possible to make a reliable estimate of flaw height in every case. Flaw 36 (in the 38mm thick plate, J311) could not be sized from either plate surface with the transducer separations used, which were limited by the presence of the weld crown. Destructive data would indicate whether the height of this flaw is less than 3.5mm (0.4 in) which is the resolution limit derived from Fig. 5 for the transducer separation of 72mm and flaw depth (d_{min}) of 23mm. However, this sample has not been sectioned.

Near Surface Depth Zone Obscured by the Lateral Wave

Despite being useful as a timing reference, the lateral wave effectively renders a region close to the surface uninspectable. This is due to the finite duration of the lateral wave and the requirements for resolving pulses defined above. Furthermore, as the lateral wave pulse travels via the shortest route between the transducers, which generally lies at the edge of the ultrasonic beam, its frequency content is inherently lower than that of a wave which has followed a path along the beam axes and it therefore occupies more time. In Appendix C, the pulse length of the lateral wave was found to be 1 μs from observation of typical lateral waves over a number of scan lines for a single specimen. It was assumed that its duration was independent of transducer separation and the condition of the weld crown. This may have resulted in a slightly pessimistic view of the capabilities for near surface flaw detection and sizing, as is exemplified by the results from the 10mm (0.4 in) thick specimens. (These results are discussed further below). In practice it was possible to recognise the presence of a shallower flaw than was predicted in Appendix C by an abnormal appearance of the lateral wave (e.g. Flaw 25, Fig. 12) and even to make an estimate of flaw depth and through thickness height in some cases.

The lateral wave is also slightly affected by the presence of the weld crown. Thus changes in the appearance of the lateral wave due to variations in the weld crown profile must be distinguished from those due to the presence of a flaw. To improve test performance in the near surface region it may be necessary to remove the weld crown. From the limited information available, in the absence of the weld crown the lateral wave remains constant, assuming no variations in coupling and

no weld discontinuities. Such consistency was observed on samples J301 and J302. It is thought that, in this case, the use of signal correlation techniques could offer substantial improvements for the detection and sizing of near surface flaws.

The lateral wave is attenuated at a rate which depends on the square of the distance between the transducers. Its amplitude observed on scans of 10mm (0.4 in) thick samples, where the transducer separation was less than 40mm (1.59 in), was considerably larger than for the scans of thicker specimens where the transducer separations were generally in excess of 70mm (2.76 in). Consequently, although the depth zone obscured by the lateral wave is smaller in thinner materials, it is more difficult to detect signals from flaws which lie in this zone. Additionally for the 10mm specimens the pulse length of the lateral wave was significantly shorter (almost a factor of two) than for thicker plates, indicating a higher frequency content. This factor and test geometry combine to produce a dead zone depth of around 5mm. The time window between the lateral wave and backwall waves was thus sufficient to allow not only detection of mid-wall flaws but also positioning of diffraction sources in the lower half of the plate thickness.

For surface breaking flaws the lateral wave is obstructed. The presence of a surface breaking flaw can thus be readily identified. Furthermore the diffracted signal from the bottom tip will be detected even for shallow flaws i.e. ones that if sub surface would otherwise have been buried in the lateral wave.

The Accuracy of Time-of-Flight Measurements

A theoretical study of the errors in depth determination (d_{min}) as a result of measurement errors in flight time and transducer separation (Appendix C) has indicated that for a flaw symmetrically placed between the transducers and not obscured by the lateral wave the error in depth estimation of one tip of a flaw varies between $\pm$ 0.5mm ($\pm$ 0.02 in) for a diffracted angle $\phi < 10°$, to $\pm$ 2.0mm for $\phi < 80°$. That is to say, the accuracy varies with depth and transducer separation. This is shown in Appendix C, Fig. C4 to C6.

The results from experimental observations given in Table G1 and shown graphically in Fig. 10 show good agreement with this value except in the case of some of the flaws displaced from the centre line of the weld by more than about 10mm (0.4 in). In these cases the calculated depth of the flaw will be greater than the measured depth as shown in Appendix C (equation C8). This accounts for the apparent tendency of the technique to overestimate the depth of a flaw as shown by a statistical analysis of the results. The mean error in depth determination was + 0.5mm (0.02 in) with 95% confidence limits of $\pm$ 2.6mm ($\pm$ 0.10 in). However, when a correction for lateral displacement is applied, all errors tend to lie within the theoretical limits.

The error in depth measurement due to a flaw not lying in the central plane between the transducers could be corrected for by combining the results from scans at different transducer separations. The displacement of the flaw X, from the central plane can then be eliminated from equation C5 of Appendix C. Alternatively, in the absence of the weld crown, a scan transverse to the flaw could be carried out. As the transducers approach and pass the flaw a hyperbola is traced out (equation C8) due to the beam spread. The transverse position of the

flaw, X, is then given by the point at which the ultrasonic pulse transit time is a minimum. Both these approaches allow only the transverse position of flaws to be determined but also the orientation of the flaw with respect to the vertical.

It might be expected that the error in flaw height measurement, h_{max}, would be greater than for flaw depth measurement. This is true if the extremities of the flaws are located from separate scans. However, when both top and bottom edges are positioned from the same scan then errors of timing reference and transducer separation measurement tend to cancel out. This is born out in the experimental results with a mean error in height estimation of -0.2mm (0.01) with 95% confidence limits of $\pm$ 2.0mm ($\pm$ 0.08 in), Fig. 9.

It is evident that far superior results are being achieved with the present system than in previous work (2) where only a simple analogue time-of-flight system was available. In that work a mean error of -1.0mm (0.04 in) was reported with 95% confidence limits of $\pm$ 3.3mm ($\pm$ 0.13 in). There are a number of factors contributing to the superior sizing capability of the computer controlled system.

(i) The B-Scan presentation is easier to interpret than the A-Scan presentation alone.

(ii) The use of shorter pulse length transducers improves resolution.

(iii) Data are automatically stored so that when the transducers are removed from the testpiece the information contained in the A-Scan is not lost and can be subsequently analysed.

Extending the Capabilities of the Time-of-Flight Technique

Two possibilities need to be investigated for extending the present capability of time-of-flight diffraction technique thereby improving resolution, the near surface detection capability and accuracy.

The possible use of pulse correlation techniques to improve near surface flaw detection capability has already been discussed. As this is fundamentally a problem of resolution, such techniques might also be employed to improve the time-of-flight technique's capability for the sizing of small flaws (i.e. smaller than the minimum heights measurable as predicted by Fig. 5 for different transducer separations).

The other option is to use higher frequency transducers and to make time measurements more accurately by increasing the digitisation rate.

Increasing the transducer frequency by about a factor of 3, to 10MHz (and correspondingly increasing the digitisation rate to 60MHz), would improve depth resolution by the same amount. The smallest height of flaw measurable would also be reduced by as much as a factor of three for the same transducer separation and depth of flaw below the surface. For 3MHz transducers the limiting value of the minimum height measurable is 2mm (0.08 in). At 10MHz it is 0.6mm (0.02 in).

Although this approach would be suitable for near surface flaws or for thin section material, it is unclear how viable it would be for thicker section samples. This is due to the increased attenuation of ultrasound in steel at higher frequencies. However as accurate size measurement and resolution of very small flaws only tends to be important for thin material and not for thick materials it is not thought to be a problem, transducers of 3MHz centre frequency giving sufficient resolution to meet most requirements.

IMPLEMENTATION OF TIME-OF-FLIGHT TESTING IN THE FIELD

Although the time-of-flight system developed as part of the present program is a prototype with all the flexibility required of such a system, it is sufficiently transportable for limited site trials. Furthermore it is operated in a manner very similar to that envisaged of a portable site instrument. However for extended site use the present equipment is not suitable. Developments are in hand for a more site orientated instrument (see Appendix D) which is packaged in a number of smaller boxes. The overall size of the system is similar to the present system but its capabilities in terms of sophistication of control and display software are significantly enhanced. For general site testing a smaller instrument, dedicated to time-of-flight testing would be desirable. The technology exists for such miniaturisation of the necessary electronic circuitry but development costs would be high. However, the resulting instrument would find far more widespread use on structures and installations where access is difficult than the present systems.

The present equipment has been demonstrated to be operated easily for the inspection of flat butt welds in three plate thicknesses, 10mm, 38mm and 95mm (0.4 in, 1.5 in and 3.75 in). In order to perform a test the only manual tasks required of the operator are to:-

(i) place the scanner centrally over the testpiece,

(ii) select and adjust the transducer separation,

(iii) apply sufficient couplant over the area to be traversed by the transducers.

The test then proceeds under computer control allowing the advantages of a computer controlled set-up to be realised. The above tasks are considerably less onerous than those required by standard manual ultrasonic testing, which is particularly advantageous for site testing. However, a number of points must be considered:

Scanning Device

The scanning device employed to date was designed principally for traversing the flat butt welds in the research samples specially made for this study, see Fig. D4. This was not intended to be generally suitable for site testing, but would be suitable for limited site trials.

The simple linear scanning motion makes the design of more robust or larger scanners relatively simple and the engineering of suitable devices for general site testing is not anticipated to be a problem. Another possibility would be for the operator to move the transducers manually along some sort of rail incorporating a transducer positioning device. This approach could be far more flexible for areas where access is a problem.

Choice of Transducer Separation

To ensure adequate coverage of the weld volume to be inspected it was found to sufficient to overlay a plot of the theoretical 20dB beam edges of the transducers, on a sketch of the weld preparation (see Document F1). Recommended transducer separations for the weld preparations and thicknesses examined in this program are given in Table F1. A single scan from either face "A" or face "B", using a suitable transducer separation is sufficient to detect all potentially severe flaws

in welds in the thickness range 10mm to 38mm (0.4 in to 1.5 in). However if two scans are performed with different transducer separations, it then becomes possible to estimate the transverse position of the flaw, X, as well as the depth of the flaw d, besides confirming that all potentially severe flaws have been detected. For thicker samples e.g. (95mm (3.75 in) thick) two scans with different transducer separations are necessary to cover the whole depth and therefore to detect all the flaws.

In practice the minimum transducer separation will be limited by the weld crown, if present, although this is often removed as a matter of course for fracture critical members. If, on the first scan, the tip signals of a near surface flaw cannot be resolved or are obscured by the lateral wave then two options are available. Either a second scan may be carried out from the opposite surface of the testpiece or the transducer separation reduced and the weld crown removed if necessary. However, a reduction of the transducer separation may still not be sufficient to enable the tips of the flaw to be resolved if the flaw is small or close to the scanning surface. The resolution chart of Fig. 5 can be used to aid this process.

As there is a well defined procedure for determing transducer separations, using the theoretical 20dB beam edges for the transducers in use (see Appendix F), it is possible to envisage that suitable transducer separations might be calculated by a computer program in which the sample thickness and details of the joint preparation are required as input parameters. The operator would be left only with task of setting the transducer separation. Such an approach could be used to eliminate a further source of operator error, and would ensure coverage of the whole weld volume as well as improving quality control aspects.

Surface Finish

The importance of a smooth test surface, free from spatter, for reproducible results from conventional ultrasonic tests has been discussed previously (2). Any effects of surface roughness are more severe when using the time-of-flight technique because of the need to couple two transducers to the test surface simultaneously. Furthermore, diffraction is a less efficient process than reflection and less loss in signal amplitude due to poor coupling can be tolerated. This is particularly the case for thicker section material (e.g. 95mm, 3.75 in) where the amplitude of the received signals is lower than for the thinner materials due to the longer sound path lengths involved.

Uneveness and irregularities in the surface can cause the transducers to move unevenly over the test surface resulting in local variations in transducer separation. For this reason undulations in the testpiece surface, as a result of considerable amounts of hand grinding, could be more detrimental to test performance than a rougher, as-rolled surface.

The effect of surface finish on the time-of-flight test results has not been studied rigourously. However the surface of the two specimens (J301 and J302) from the previous work on tandem testing had been machined as part of that work. In the results from these specimens it was evident that the shape of the lateral wave showed less variation but in general, the amplitude of the received signals was no larger than for the same transducer separations on the un-machined (as-rolled) surfaces of the other specimens.

Couplant

The couplant has a dual role. It allows the ultrasound to be transmitted from the transducer to the testpiece and enables the transducers to be moved easily across the test surface. For this purpose a light machine oil or one of the proprietary coupling gels have been found to be the most satisfactory. Industrial grease or cellulose paste, both often used in ultrasonic testing, can be too viscous to allow free movement of the transducers across the test surface.

Predicted Performance of Time-of-Flight Tests in the Field

Provided that adequate coupling can be maintained and that suitable procedures are used, there is no reason for the accuracy of time-of-flight measurements on flat butt welds in the field to be inferior to the accuracy of measurements on laboratory samples.

Time-of-Flight Testing of Other Weld Geometries

It is recognised that the results of the present work are only directly applicable to flat butt welds, but other weld geometries e.g. T butt welds may be examined. The main requirement for the inspection of other geometries is that using suitable transducer angles one weld volume can be flooded with ultrasound. For T butt welds this neccesitates the placing of one transducer on the flange and the other on the web and thus a more complex transducer joining mechanism is required. Because of the geometry there are more complicated paths for reflected signals and it is important that the expected flight times of these are calculated to aid in interpretation of the B-Scan image. Flaw location is thus more complicated and will necessitate a number of scans. However success has been reported in examining welds of this type (31).

Operator Training

It has already been suggested that the training of operators should not prove too difficult. The main requirements for interpretation of the B-Scan images are:-

(i) a sound understanding of the physical principle of the technique,

(ii) an appreciation of its capabilities and limitations,

(iii) experience in interpretation of the B-Scan images.

A suitable course could be devised covering both theoretical aspects of the time-of-flight technique and "hands on" experience with a suitable system. Like all areas of expertise (including other NDT methods) gaining experience is a continuing process and a student does not become an expert after a short course. However the learning process could be greatly aided by having a library of B-Scan images from different flaw types together with macrographs of the actual flaws.

No major problems are foreseen in training competent manual ultrasonic operators to carry out time-of-flight tests and to interpret the results.

CHAPTER FOUR

CONCLUSIONS AND FURTHER WORK

CONCLUSIONS

A total of 46 embedded weld flaws, including solidication cracks, incomplete fusion and slag lines, were manufactured in C-Mn steel butt welds in thicknesses 10, 38 and 95mm (0.4, 1.50 and 3.75 in). These were all ultrasonically tested using a computer controlled system employing the time-of-flight technique both for flaw detection and measurement of flaw through-wall height. Additionally the flaw sizes were determined using the 20dB drop technique. Twenty-one of the weld flaws were subsequently sectioned so that their true size could be measured and the capabilities of the time-of-flight technique evaluated. The conclusions that can be drawn from this work are as follows:

1. The time-of-flight technique, as applied here, has been shown to be capable of detecting all flaws in butt welds in plate in the thickness range 10mm to 95mm (0.4 in to 3.75 in).
2. The depth of the flaw below the test surface and its through thickness height (where the diffracted signals from the top and bottom could be resolved) could be determined for flaws in 38mm and 95mm (1.5 in and 3.75 in) thick samples given a suitable choice of transducer separation and due consideration of the theoretical capabilities of the technique.
3. A good correlation was observed between actual flaw depth (d_{min}) and through thickness height (h_{max}) and values determined from the time-of-flight B-Scans. The errors were + 0.5 $\pm$ 2.6mm (0.02 $\pm$ 0.10 in) for d_{min} and -0.2 $\pm$ 2.0mm (0.01 $\pm$ 0.08 in) for h_{max}. These

results are in line with the findings of other studies and offer a considerable improvement over results obtained using the 20dB drop method.

4. Further work is required in order to be able to size flaws in thinner material (e.g. the 10mm (0.4 in) specimens of this program) as well as flaws close to the test surface, where access from the opposite surface of the specimen is not possible.
5. The series of tests on flat butt-welded specimens containing real welding flaws has enabled the ease of operation of the demonstrated that time-of-flight testing is straightforward to apply. However, instrumentation, although being developed all the time, still needs considerable miniaturisation for extended site use.
6. At the present stage of development, interpretation of the B-Scan image requires a level of skill from the operator different from that normally expected from ultrasonic technicians. However, considerable expertise can be built up over a relatively short period of time by the use of suitable training samples backed by a sound understanding of the underlying physical principles of the technique. Means of improving the display to make it easier to interpret have, however, been suggested.

POSSIBLE FURTHER RESEARCH

Further Evaluation of the Time-of-Flight Technique

1. The feasibility of the use of higher frequency transducers for the sizing of near surface flaws and for the inspection of thin plate should be investigated.
2. Methods of determining the transverse location of a flaw and its location should be considered, either by combining the results

from two or more scans at different transducer separations or by carrying out transverse scans.

Extension to the Basic Technique

1. In order to improve the accuracy and reduce the variability of flaw length measurement a number of avenues are open for investigation. A more rigorous approach to a decibel drop technique could be applied or synthetic aperture focusing algorithms (SAFT) may be implemented.
2. With a view to aiding interpretation of the B-Scan image, pulse correlation techniques could be investigated for flaw detection and size measurement.
3. A library of typical responses from different types of flaw could be built up both to act as a training aid and to assist in flaw characterisation.

Equipment Developments

Although developments are underway in the United Kingdom to make the instrumentation more compatible with the site environment (Appendix D and Ref. 34) the physical bulk of the equipment will not be much reduced. There is however a need for a smaller, more portable system, possibly dedicated to time-of-flight testing alone, which is no larger in size than one of the larger standard ultrasonic flaw detectors. The technology within the electronics industry is now in existence. Instrumentation developments are now of paramount importance in gaining a recognition of the capabilities of the time-of-flight technique in a site environment.

RECOMMENDATIONS

Provisions should be made in the AWS D1.1 code for the use of accurate non-destructive techniques to evaluate the dimensions of weld flaws thereby permitting fracture mechanics analyses of structure integrity to be carried out. The time-of-flight technique has been shown to be suitable for this role. Other techniques for sizing and flaw type diagnosis however, should be kept under surveillance and evaluated at such a time when they are fully developed.

The development of a suitable system orientated towards site use is feasible within known technology and should be pursued as a matter of some urgency.

REFERENCES

1. Structural Welding Code Steel. AWS D1.1-84. American Welding Society, 1984.

2. JESSOP T.J., MUDGE, P.J. HARRISON J.D. "Ultrasonic Measurement of Weld Flaw Size". National Cooperative Highway Research Program Report, No. 242. Transportation Research Board, Washington DC, 1981.

3. American Society of Mechanical Engineers (ASME) Boiler and Pressure Vessel Code, Section V (1983).

4. Reports of the Plate Inspection Steering Committee (PISC) exercise, Commission of the European Communities. Nuclear Science and Technology Series, Report No. EUR 6371, vol. 1-V Luxembourg (1979).

5. JESSOP, T.J. et al. "Size Measurement and Characterisation of Weld Defects by Ultrasonic Testing, Part 2. Planar Defects in Ferritic Steel". Welding Institute Report 3527/10/80 (1980).

6. SERABIAN, S. "Reliability of Ultrasonic Weld Interrogation Methods". University of Lowell, Mass, Report No. DOT-RC-92014 (June 1980).

7. KATO, et al. "Estimation of Weld Defects Through Ultrasonic Testing". Welding Journal (Nov. 1976) pp. 946-953.

8. MUDGE P.J. WILLIAMS S. "Performance of Ultrasonic Non-Destructive Methods for Defect Assessment in Relation to Fracture Mechanics Requirements". In Fitness for Purpose Validation of Welded Constructions. International Conference, London 17-19 Nov. 1981. Publ: The Welding Institute, Abington, Cambridge, CB1 6AL, England. Session IV. Paper 44 pp. 44-1 to 44-11.

9. SILK, M.G. "Sizing Crack-Like Defects by Ultrasonic Means". In: Research Techniques in NDT, vol. III. Chapter 2. Ed: R.S. Sharpe. Academic Press, 1977.

10. SILK, M.G. "Accurate Crack Depth Measurement in Welded Assemblies". In: Proceedings 8th World Conference on NDT. Cannes 6-11 Sept. 1976, Paper No. 2B16.

11. CURTIS, G.J., HAWKER, B.M. "Automated Time-of-Flight Studies of the Defect Detection Trial Plates 1 and 2". British Journal of NDT, vol. 25, no. 5. Sept. 1983. pp. 240-248.

12. SILK, M.G. "The use of Diffraction Based Time-of Flight Measurements to Locate and Size Defects". British Journal of NDT, vol. 26, No. 3. May 1984.

13. CECCO, V.S. "Ultrasonic Time-of-Flight B-Scan Presentation". Report No. AERE R10887, April 1983.

14. SILK, M.G., LIDINGTON, B.H. "Defect Sizing Using an Ultrasonic Time Delay Approach". British Journal of NDT, vol. 17, no. 2. March 1975, pp. 33-36.

15. BOTTCHER, B., SCHULZ E., WUSTENBERG H. "A New Method of Crack Depth Determination in Ultrasonic Materials Testing". In: Proceedings of 7th International Conference on NDT Warsaw, 1973.

16. LIDINGTON, B.H., SILK, M.G., MONTGOMERY, P., HAMMOND. G. "Ultrasonic Measurement of the Depths of Fatigue Cracks". British Journal of NDT, vol. 18, no. 6. November, 1976, pp. 165-170.

17. MUDGE, P.J. "Ultrasonic Time-of-Flight Measurement of Fatigue Pre-Crack Growth in Fracture Toughness Specimens". In: Measurement of Crack Length and Shape During Fracture and Fatigue. Proc. Conf. Birmingham England. May 1979. (Publ: 1980). pp. 393-399.

18. SIGMOND, R.S., LIEN, E. "Ultrasonic Diffraction Measurements of Fatigue Crack Growth". British Journal of NDT, vol. 22, no. 6. November 1980, pp. 281-283.

19 CHARLESWORTH, J.P., LIDINGTON, B.H., SILK, M.G. "Defect Sizing Using Ultrasonic Flaw Diffraction". In: Proceedings European Conference on NDT, Mainz Germany, 24-26 April 1978.

20. SILK, M.G. "The Fundamental Accuracy of Ultrasonic Time-of-Flight Testing Techniques". In: Periodic Inspection of Pressurised Components. Proceedings I Mech E Conference, London 1982. Paper C149/82. pp. 125-133.

21. SILK, M.G. "Ultrasonic Diffraction as a Tool for Inspection". In: New Trends in NDT. Proceedings International Conference Brussels, 24-26 March 1982. Paper, REF SV-4.

22. CURTIS, G.J., FOSSUM, T., HIGHMORE, P.J. "Ultrasonic Synthetic Aperture Imaging of Defects". In: Inspection of UK Reactors. Proceedings: British Nuclear Energy Society Symposium, 30th Sept. 1980.

23. TEMPLE, J.A.G. "Time-of-Flight Inspection Theory". Nuclear Energy, vol. 22, no. 5. October 1983, pp. 335-348.

24. OGILVY, J.A., TEMPLE, J.A.G. "Diffraction of Elastic Waves by Cracks. Application to Time-of-Flight Inspection". Ultrasonics, vol. 21 no. 6. November 1983.

25. CHAPMAN. R.K. (1981), CEGB Report NW/SSD/RR/145/81, 1981.

26. GOLAN, S., ADLER, L., COOK, K.V., NANSTAD, R.K., BOLLAND, T.K. Journal of Non-Destructive Evalution, vol. 1, no. 1. (1980), pp. 11-19.

27. MAUE, A.W. Zeitschrift für Angewandte Mathematik und Mechanik. vol. 33, no. 1/2 (1953), pp. 1-10.

28. CARTER, P., SLESENGER, T. "Harwell Ultrasonic Flaw Detection and Sizing Equipment with Digital Recording". Report No. AERE R10386, December 1981.

29. QT News (Newsletter of the NDT Centre, AERE Harwell), Issue No.19, November 1983.

30. SILK, M.G. "The Transfer of Ultrasonic Energy in the Diffraction Technique for Crack Sizing". Ultrasonics, vol. 17, no. 3. May 1979.

31. HAWKER, B M. "Sizing Weld Defects in Sub-Sea Structures Using the Harwell Ultrasonic TOFD Technique". Paper presented at 5th Offshore Inspection Repair and Maintenance Conference, Aberdeen, 5-6 November 1984.

32. CARTER, P. "Initial Operational Experience with the Automated Digital Ultrasonic Inspection System - ZIPSCAN". Paper presented at Welding Institute International Conference on: Non-Destructive Testing in the Fitness-for-Purpose Assessment of Welded Constructions. London, 20-22 November 1984.

33. CONSTANTINIS, D.A. "Mechanised Inspection of Nozzle Welds Using ZIP-SCAN Equipment". Ibid.

34. ZIPSCAN Publicity Literature. SGS Sonomatic Ltd.

35. PD6493. "Guidance on some methods for the derivation of acceptance levels for defects in fusion welded joints". B.S.I. London 1980.

TABLE 1. Scans required for each plate thickness and joint preparation.

Specimen thickness mm	(inch)	Joint preparation	angle	Test surface	Transducer angle deg.	Transducer separation 2S mm	(inch)
38	(1.5)	Single "V"	60° included angle	A	60	70	(2.76)
				A	60	100	(3.94)
				B	60	100	(3.94)
				B	60	70	(2.76)
				B	60	40	(1.57)
38	(1.5)	Single "U"	15° semi-angle	A	60	80	(3.15)
				A	60	65	(2.56)
				B	60	100	(3.94)
				B	60	70	(2.76)
				B	60	40	(1.57)
38	(1.5)	Double "V"	60° included angle	A	60	90	(3.54)
				A	60	70	(2.76)
				B	60	70	(2.76)
				B	60	95	(3.74)
95	(3.74)	Single "U"	15° semi angle	A	60	100	(3.94)
				A	45	110	(4.33)
				B	45	100	(3.94)
				B	45	170	(6.70)
				B	60	80	(3.15)
10	(0.39)	-	-	A	70	45	(1.77)
				B	70	38	(1.50)

TABLE 2. Statistical data on accuracy of flaw through-wall size measurements for time-of-flight tests.

Test	Mean error $\bar{x}$ mm	(inches)	Standard deviation σ mm	(inches)	95% probability limits 2σ mm	(inches)
h_{max} (maximum values)	-0.17	(-0.007)	1.00	(0.039)	2.00	(0.079)
d_{min} (from above maxima)	+0.55	(0.022)	1.31	(0.052)	2.62	(0.103)
h_{max} (all data)	-0.79	(-0.031)	1.31	(0.052)	2.62	(0.103)
d_{min} (from above)	+1.22	(0.048)	1.32	(0.052)	2.64	(0.104)
Results from previous Welding Institute program (2) with simple analogue equipment (h_{max})	-1.03	(-0.041)	1.63	(0.064)	3.26	(0.128)
Results from previous Welding Institute program (5) with complex equipment (h_{max})	0.50	(0.020)	1.80	(0.071)	3.60	(0.42)

TABLE 3. Statistical data on accuracy of flaw through-wall size measurements for probe movement (20dB drop) tests from this and previous work.

Test	Mean error $\bar{x}$ mm	(inches)	Standard deviation mm	(inches)	95% probability limits 2 σ mm	(inches)
20dB drop, present program	-4.83	(-0.190)	3.11	(0.122)	6.22	(0.245)
Results from previous Welding Institute program (2)						
20dB drop, 45° and 60°	-2.03	(-0.080)	2.91	(0.115)	5.82	(0.229)
20dB drop, 45 only	-3.10	(-0.122)	2.89	(0.114)	5.78	(0.228)
20dB drop, 60° only	-0.81	(-0.032)	2.45	(0.096)	4.90	(0.193)
Results from previous Welding Institute program (5) (planar defect only)						
20dB drop, 45°	-2.3	(-0.091)	2.6	(0.102)	5.2	(0.205)
20dB drop, 60° and 70°	-2.7	(-0.106)	3.0	(0.118)	6.0	(0.236)

Table 4. Statistical data on accuracy of flaw through wall size measurements for maximum amplitude tests (from previous work)

Test	Mean error $\bar{x}$ mm	(inches)	Standard deviation σ mm	(inches)	95% probability limits 2 σ mm	(inches)
Maximum amplitude, 45° (Ref. 2)	+ 0.20	(0.008)	2.50	(0.098)	5.00	(0.196)
Maximum amplitude, 45° (Ref. 5)	- 1.2	(- 0.047)	3.4	(0.134)	6.8	(2.68)

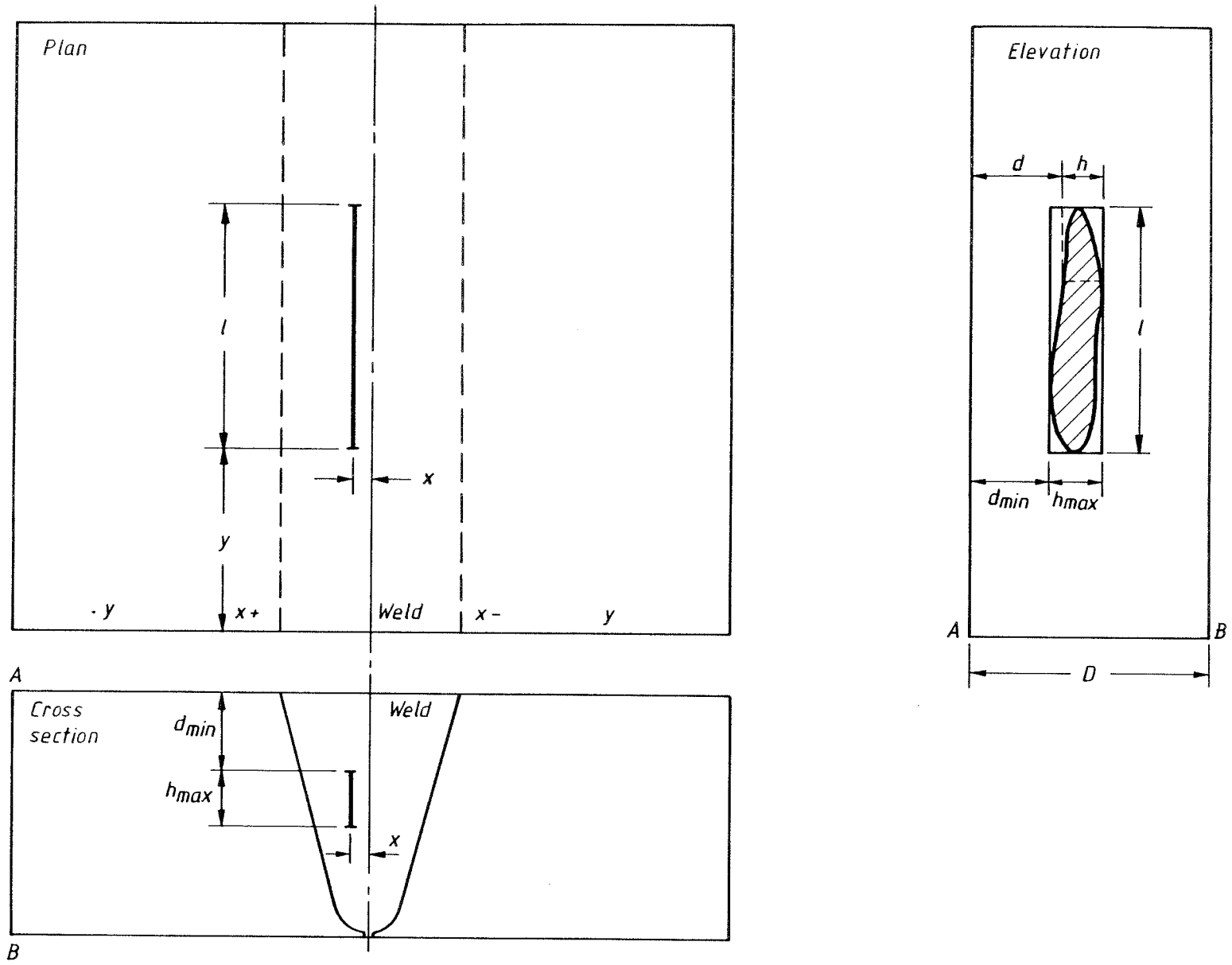

Fig. 1. Dimensions and location of a rectangle circumscribing a vertical planar flaw.

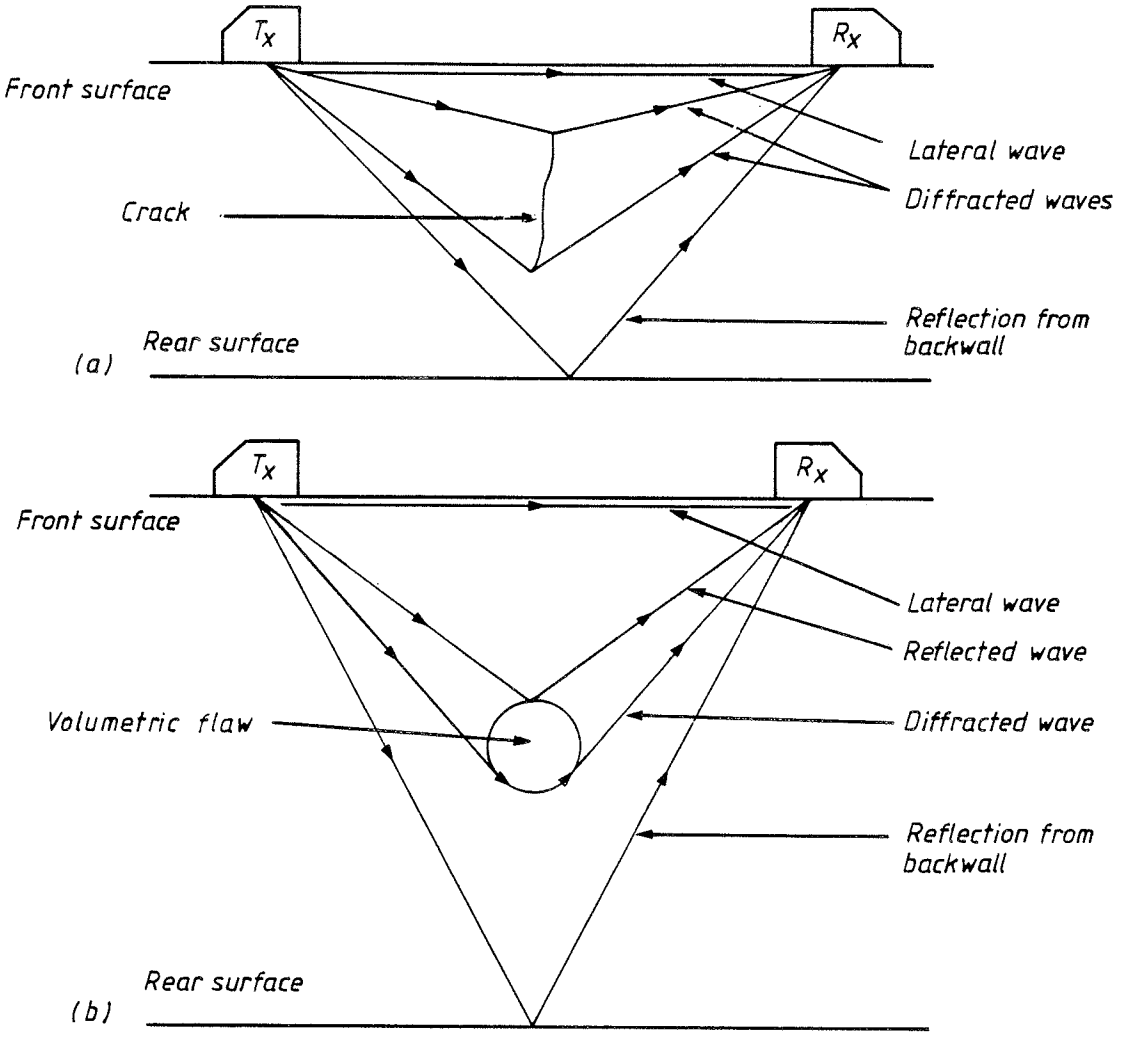

Fig.2. Principle of time-of-flight test:
a) planar flaw b) non-planar flaw

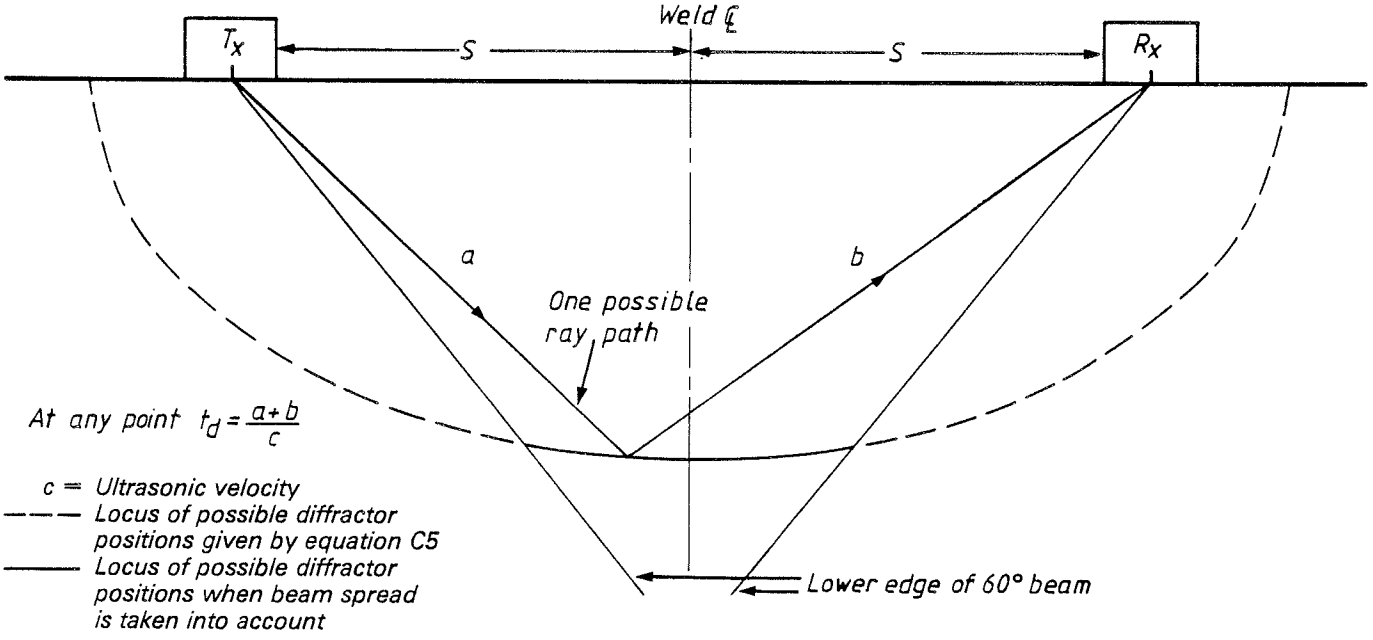

Fig.3. Locus of the position of a diffraction source for a given sound path time-of-flight, t_d.

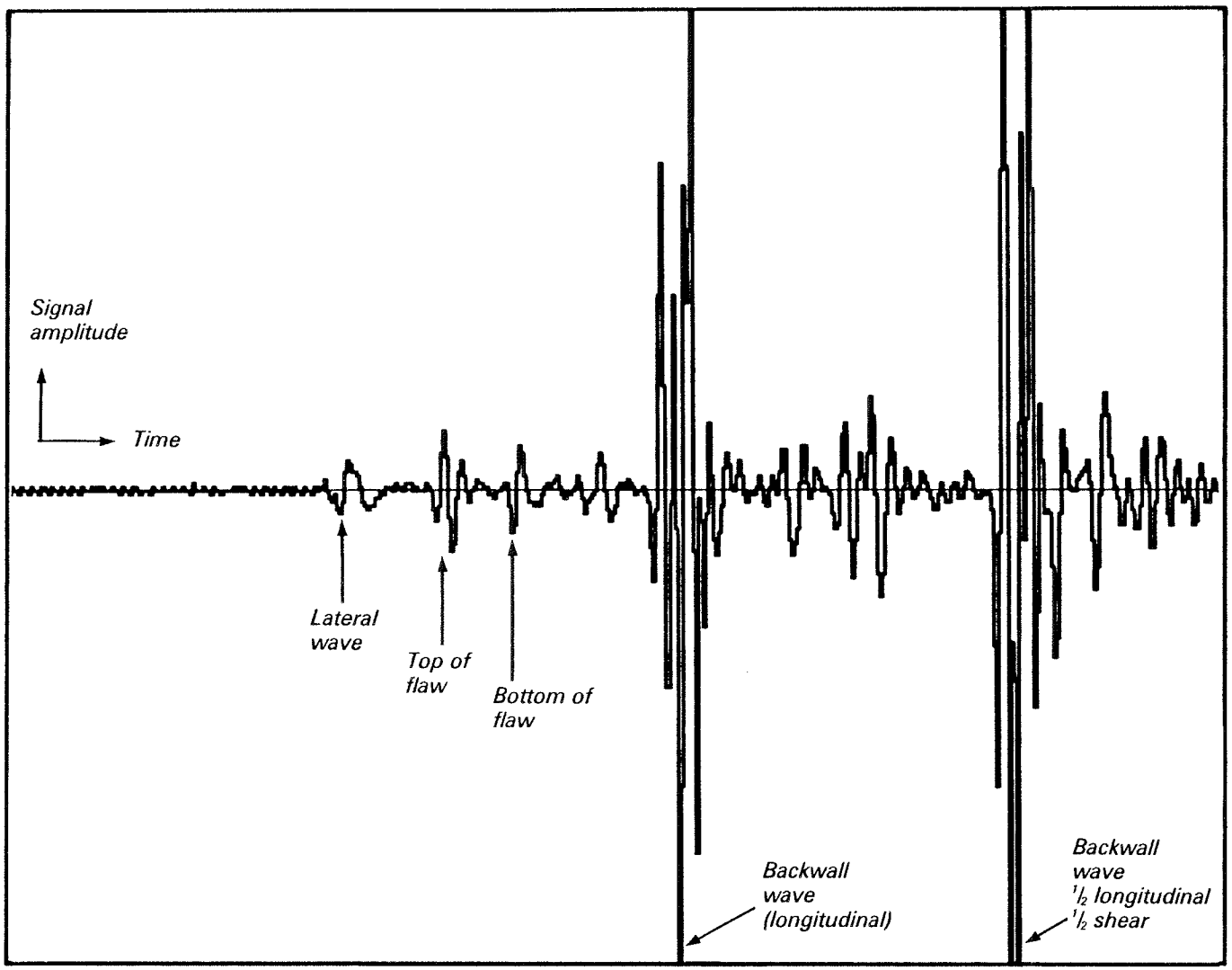

Fig.4. Typical received A-scan waveform (digital reconstruction).

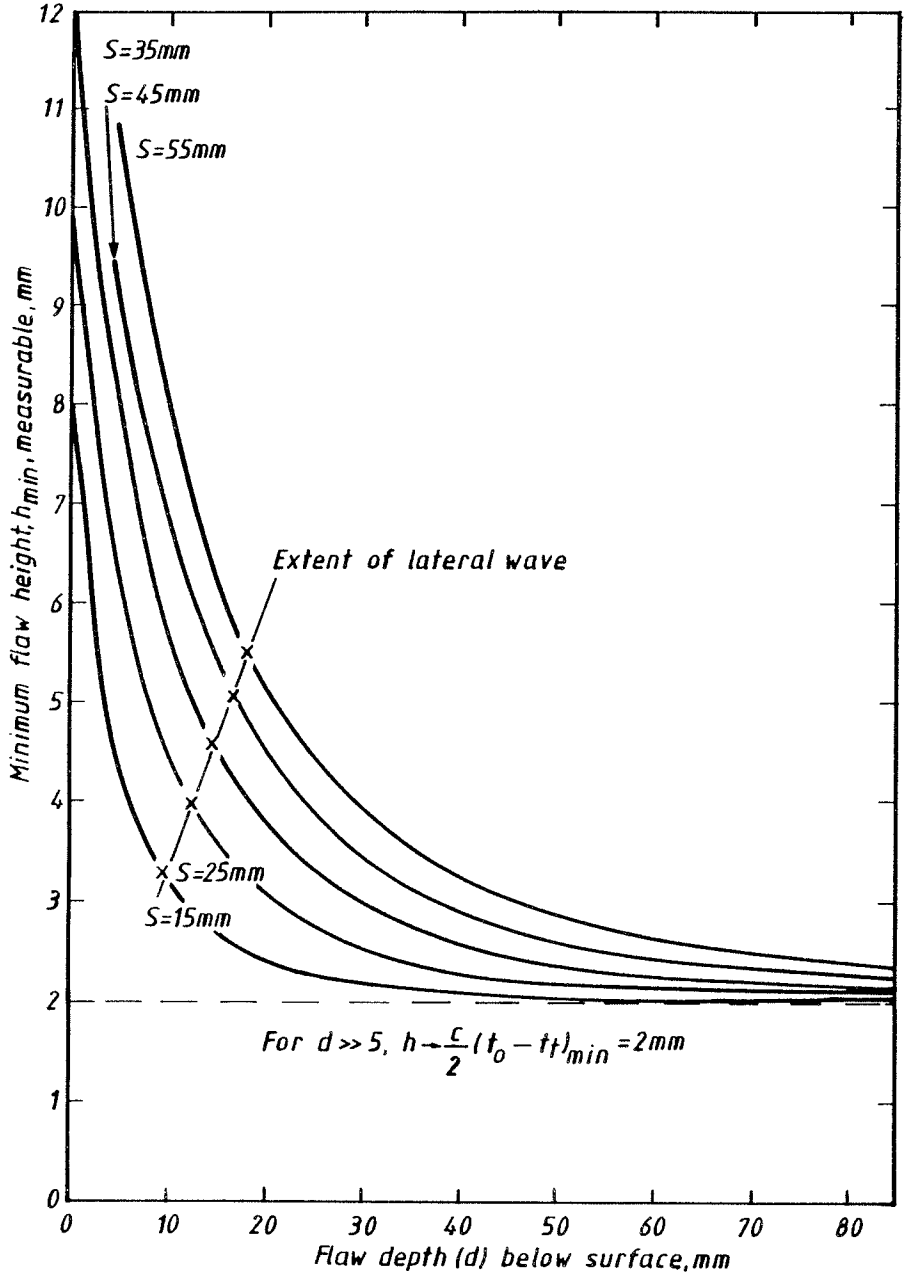

Fig.5. Minimum flaw height measurable v. flaw depth below the surface for different transducer separations at 3MHz, the depth obscured by the lateral wave is superimposed.
Δt_{min} = 2/3μsec f = 3MHz S = half transducer separation

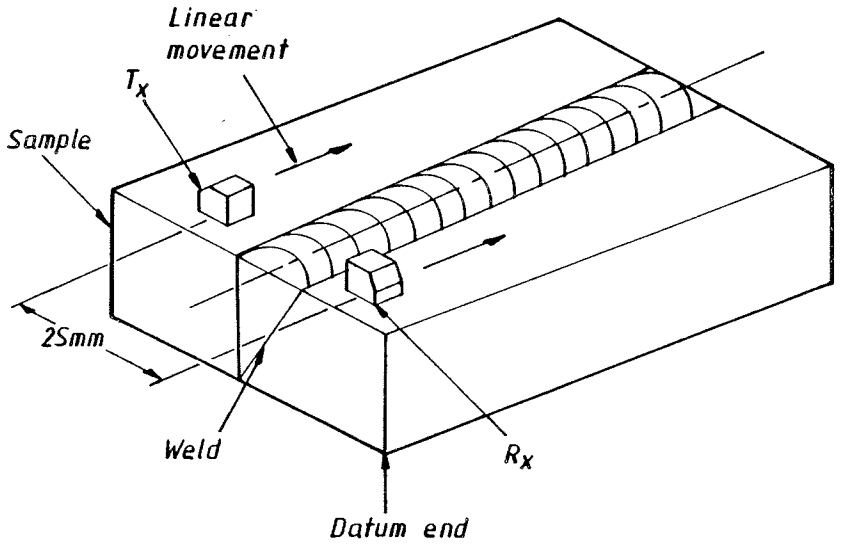

Fig.6. Schematic diagram of scan configuration for time-of-flight tests.

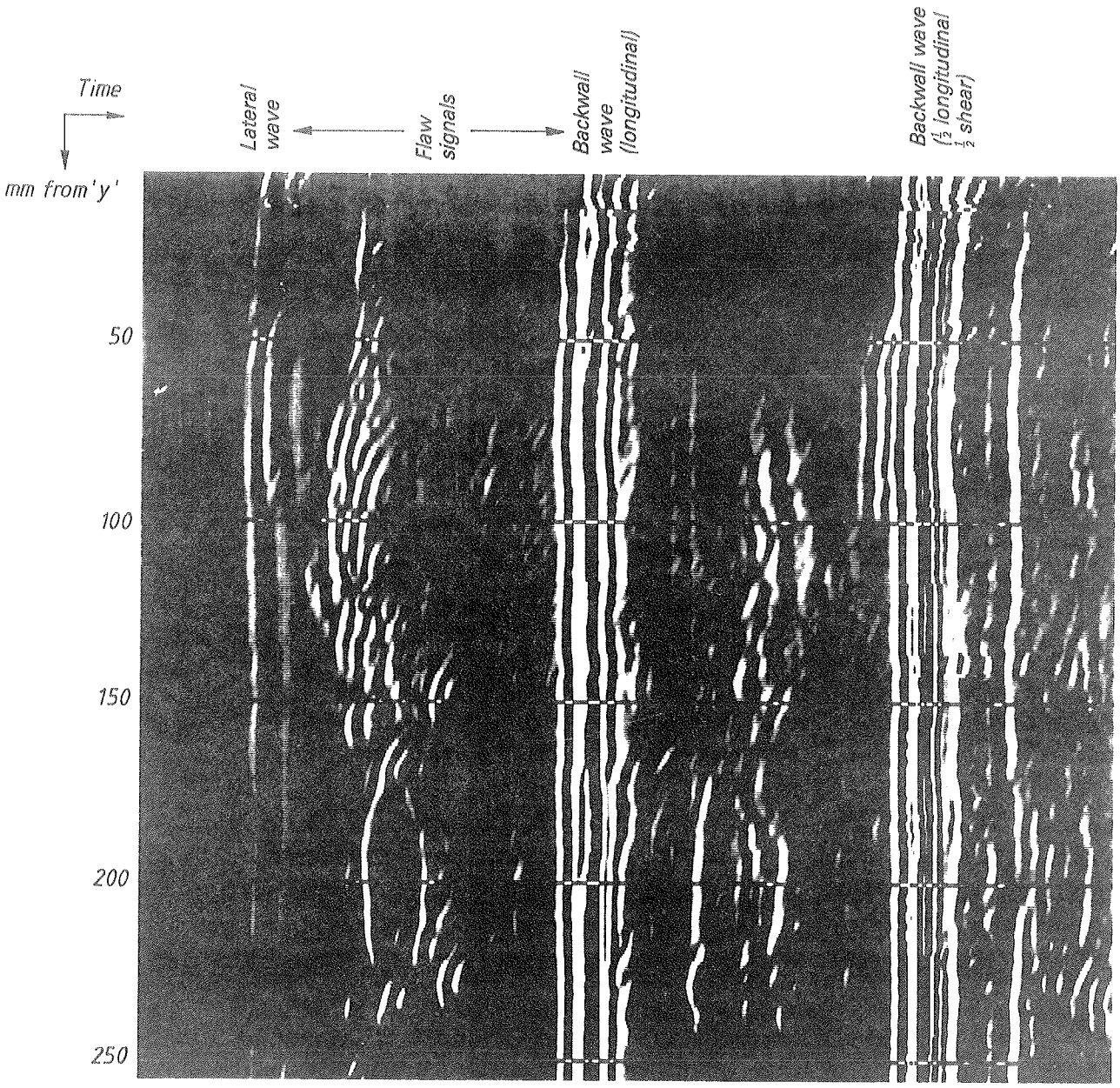

Fig. 7. Example of B-scan presentation, sample J307.

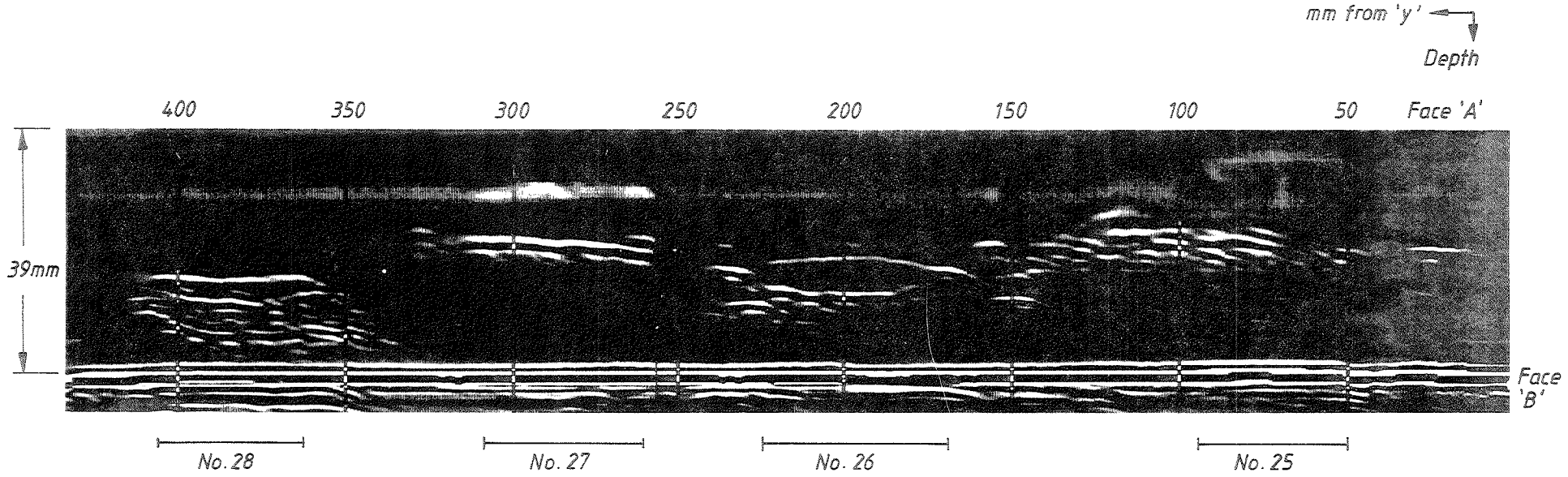

Fig.8. B-scan of J307, scan 1, linearised.

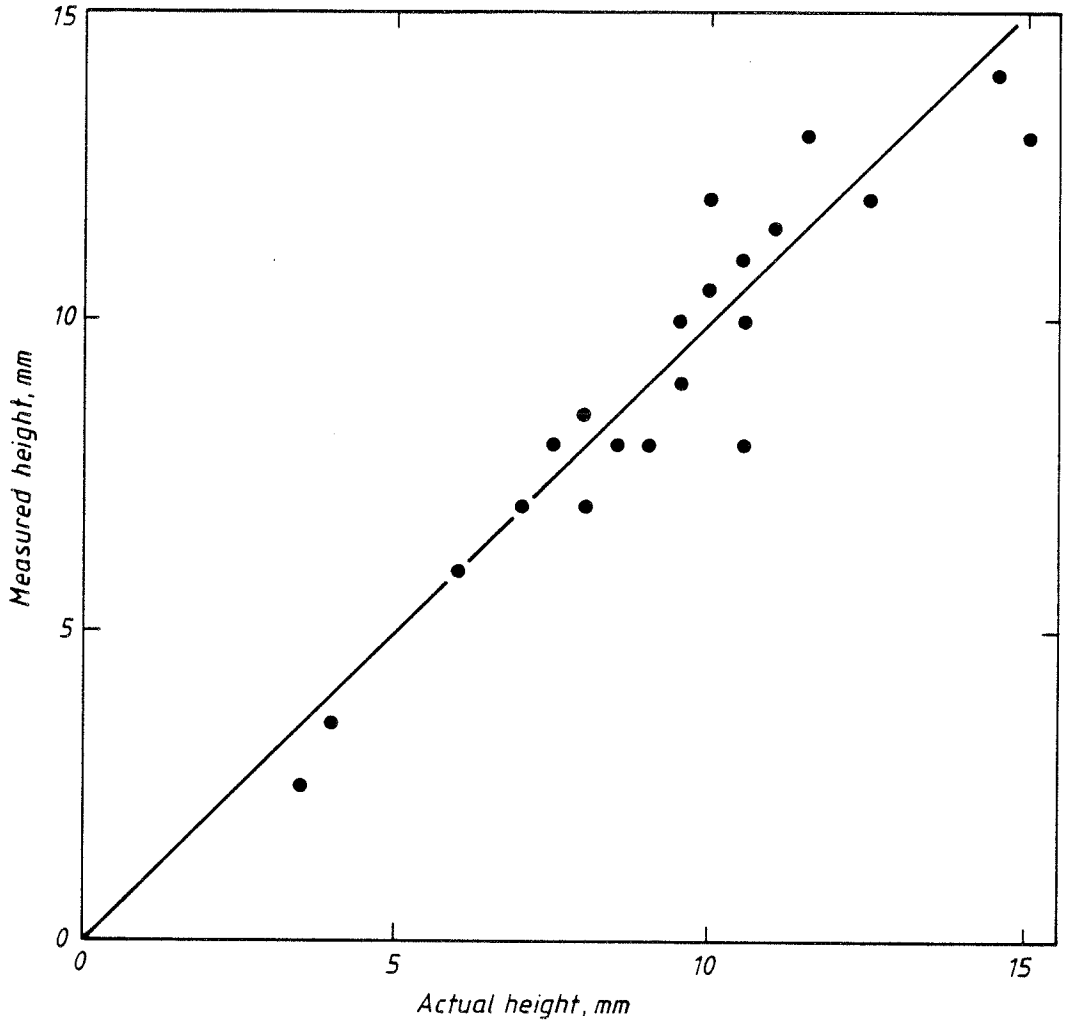

Fig.9. Measured v. actual flaw through-thickness height (h_{max}) for time-of-flight test for each flaw sectioned.

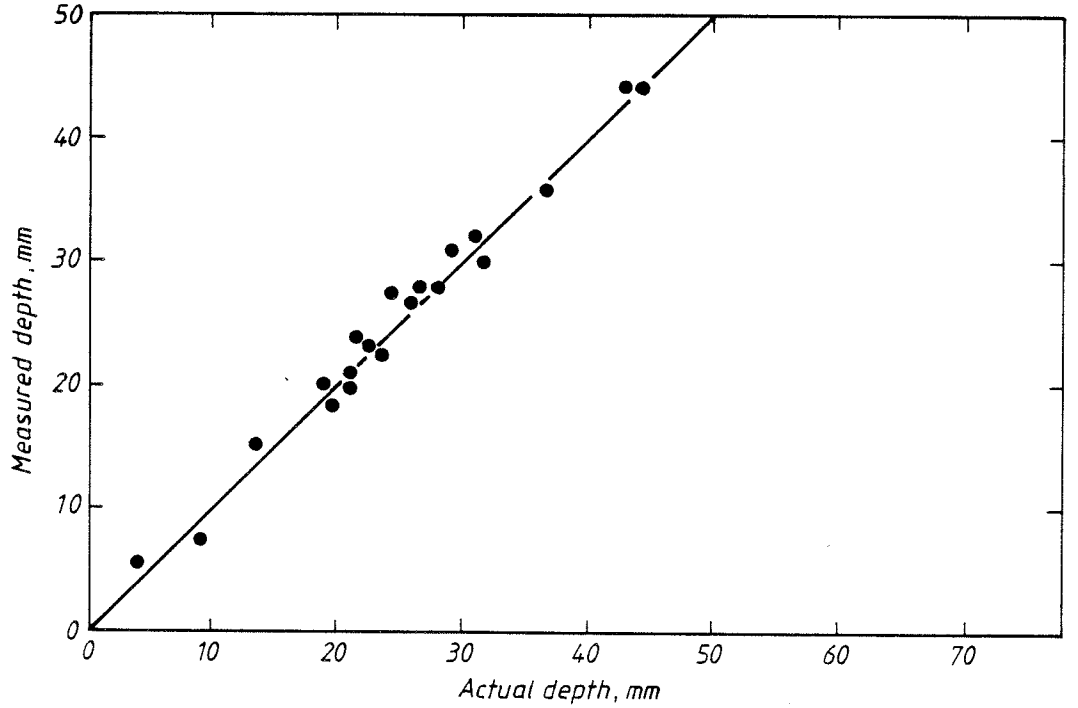

Fig.10. Measured v. actual flaw depth below the testing surface (d_{min}) for time-of-flight tests for each flaw sectioned.

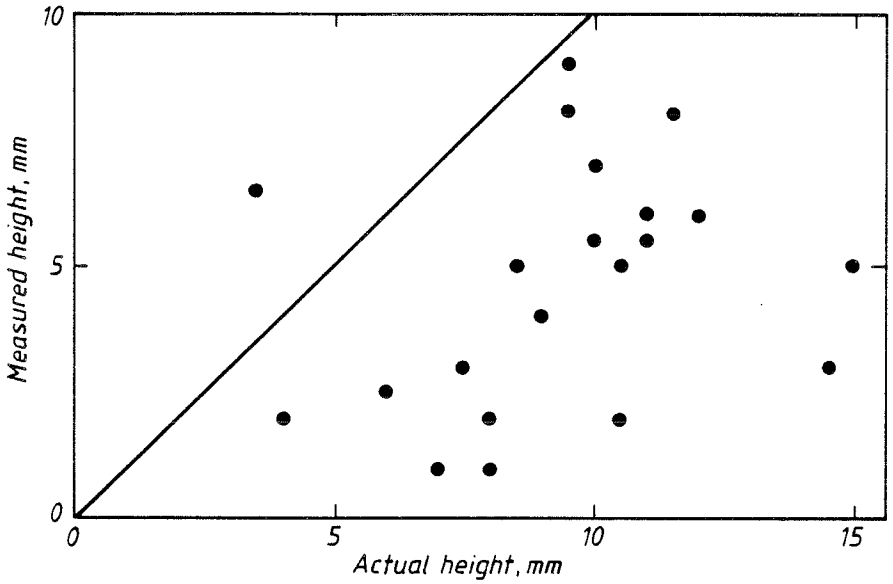

Fig.11. Measured v. actual flaw size from 20dB drop measurements, for each flaw sectioned.

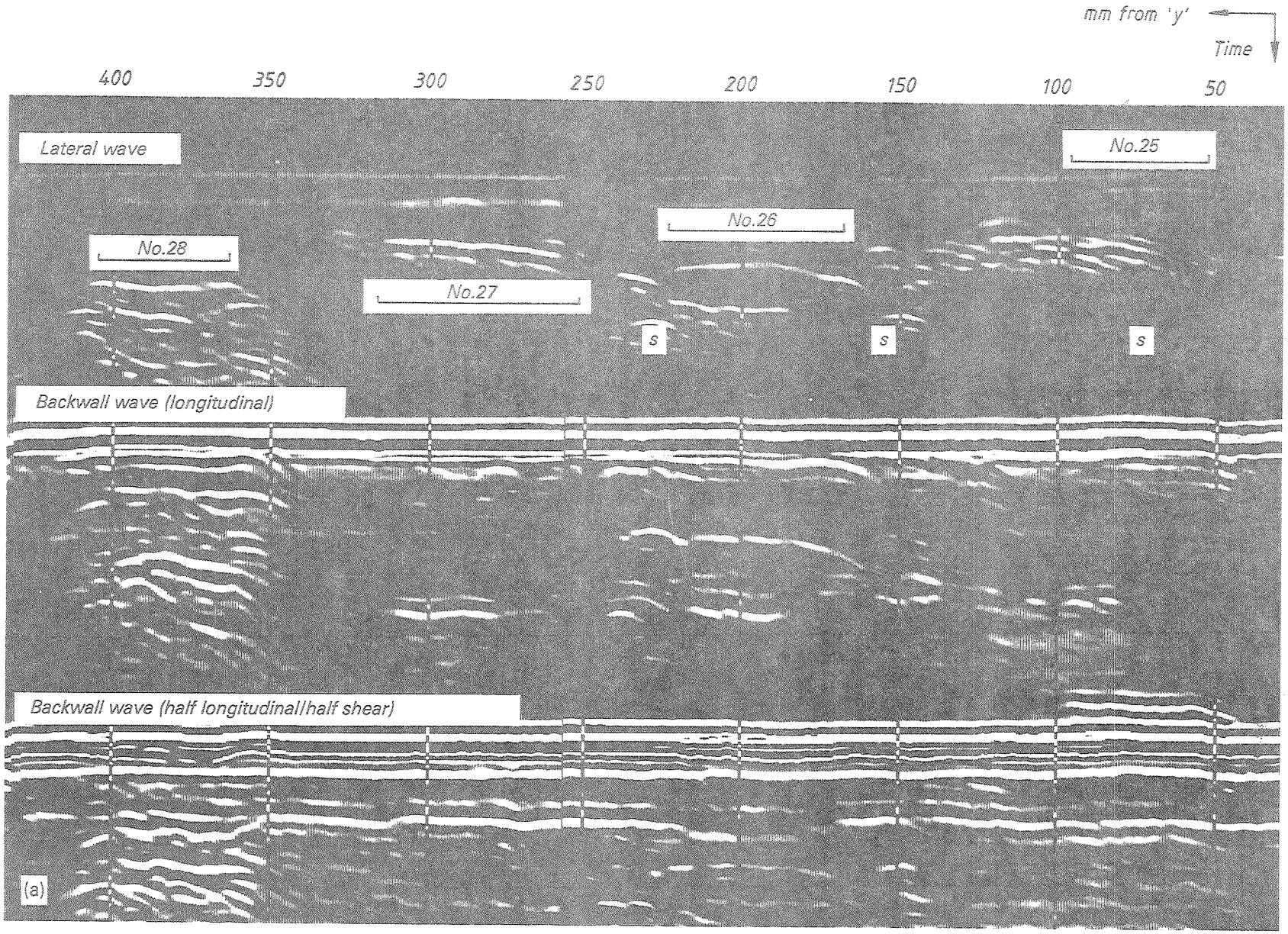

Fig.12:

a) B-scan image (not linearised) J307 scan 1 — entire data set.

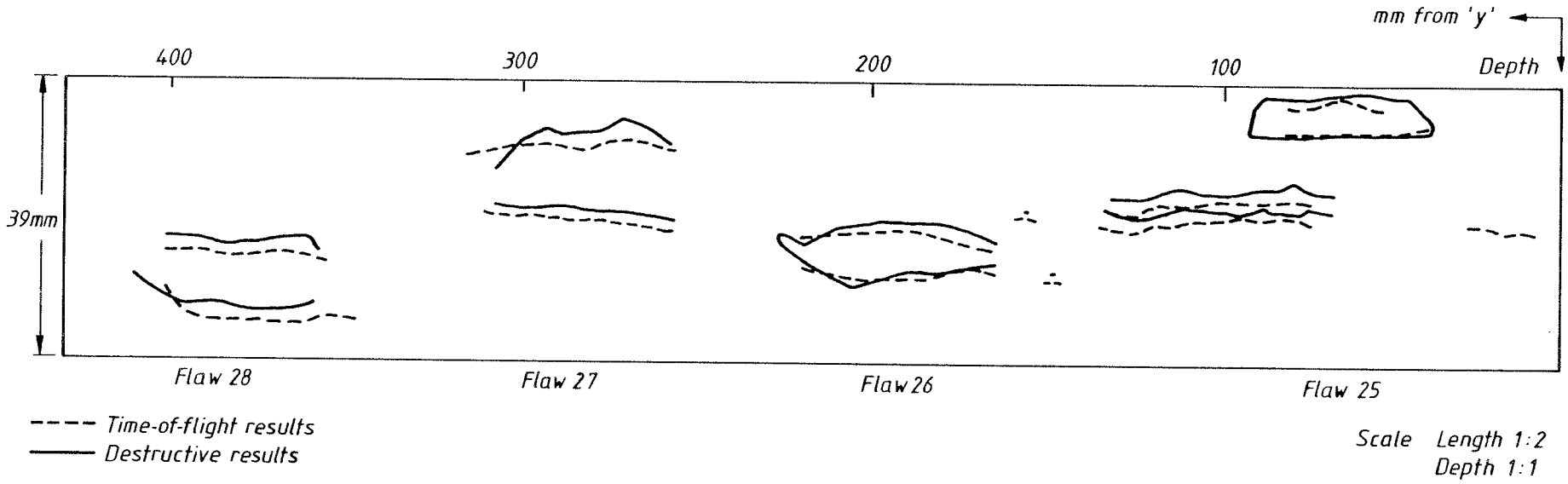

(b)

Fig.12 contd:

b) Flaw profiles determined from time-of-flight results with destructive test results superimposed, J307.

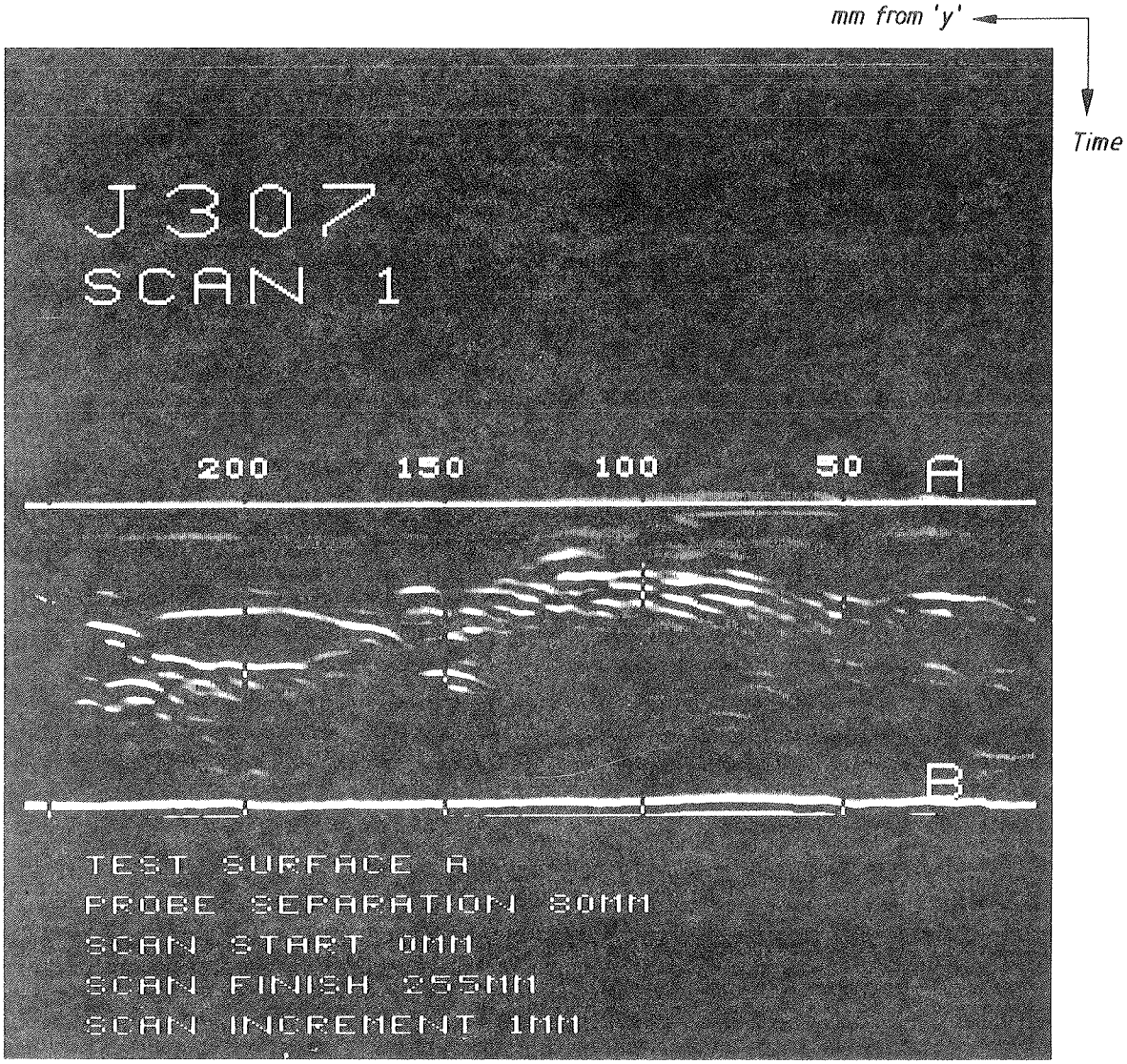

Fig.13. B-scan display showing features to make it more easily understood.

APPENDIX A

INTRODUCTION TO THE TIME-OF-FLIGHT TECHNIQUE

PERSPECTIVE

The amplitude of an ultrasonic signal reflected from a discontinuity is an easily measured parameter which is widely used as a basis for assessing flaw severity; such as in the AWS D1.1 code procedure (1). However, other factors such as the orientation, shape and roughness also of a discontinuity influence the reflected amplitude, which thus may not be directly related to its size or shape. This has been demonstrated in previous work at The Welding Institute (2), in which the procedures of the AWS D1.1 code were evaluated. In particular, the poor reliability of sentencing of vertically oriented planar flaws was shown to be of major concern.

The AWS code is not the only code where problems have been experienced by using response amplitude as the main criterion for assessing the severity of flaws. Perhaps the most notable example was the round robin evaluation of the ASME code procedure (3) for ultrasonic testing conducted under the auspices of the Plate Inspection Steering Committee (PISC) in Europe (4). In some cases very large flaws were reported as being acceptable simply because their orientation was such that only a small amplitude response was obtained.

The poor reliability of using signal amplitude as the main criterion for accepting or rejecting flaws is thus widely recognised. An alternative approach, using the so-called "probe movement" sizing

techniques seek to overcome this difficulty by manipulating the transducer in order to determine the extremities of each flaw. Although amplitude is not used as a basis for the transducer movement technique as such, the way in which a flaw's shape influences the rise and fall of the signal as a transducer is traversed across it, and assumptions made about beam profile, have a significant effect on accuracy. Studies (5-7) have demonstrated that flaw size measurement errors are inherent when using such methods.

The increasing use of fracture mechanics assessments for determining the integrity of a fabrication places more stringent requirements on the capability of the NDE method employed to determine flaw through thickness size accurately (8). Problems of ensuring reproducibility of results with amplitude based methods prompted Silk and his colleagues to investigate time-of-flight methods for flaw assessment, initially for measurement of surface breaking fatigue cracks (9) and subsequently for evaluation of embedded flaws (5). These methods largely overcome the problems associated with amplitude measurements and a high degree of accuracy has been demonstrated (5, 10). Furthermore, the technique, when coupled with computer controlled data aquisition and analysis, may also be used for flaw detection as well as sizing. This is demonstrated in the results achieved in the UK-organised Defect Detection Trials (11).

STATEMENT OF PRINCIPLE - BASIC THEORY

It is well known that when an acoustic wave interacts with a discontinuity, diffracted waves are generated as well as reflected waves. As a result of diffraction a cylindrical wavefront effectively originates at the extremity of the discontinuity. This may be detected and used

to locate the source of the diffracted signal i.e. the edge or edges of the flaw. The strength of the diffracted wave increases the sharper the edge of the discontinuity becomes. Thus a crack is a more efficient diffraction source than a blunt notch. In practice detection of the diffracted wave is achieved by using a second transducer, suitably placed, so that the flight time from the transmitter to the receiver via the flaw can be used to position the depth of the flaw tip accurately. If this is done for both extremities of the flaw, its through-thickness size can be determined. This is shown in Fig. 2 for planar and volumetric flaws. The main advantage of the technique is that, as flight time and velocity are the only ultrasonic parameters measured, the accuracy is much less sensitive to factors which are difficult or impossible to control, such as flaw type, orientation, tightness (particularly of cracks), and ultrasonic beam size, than is the case for conventional sizing methods.

In order to simplify interpretation of the received waveform, transducer angles are chosen to give refracted longitudinal waves in the test material. Although transverse waves have a wavelength of the order of half that of longitudinal waves of the same frequency, thereby offering improvements in resolution, they are not, in general, employed in the time-of-flight diffraction technique. This is because they travel at only half the velocity of their longitudinal wave counterparts, and tend to coincide with multiple reflections of any faster moving longitudinal waves and other mode converted signals. The longitudinal wave signals, being the first to arrive, can in general be studied without the complication of mode converted signals or the shear waves emitted by the transducers themselves at a smaller refracted angle. Maximum resolution between incoming pulses is achieved by the use of very short pulse length transducers - typically $1\frac{1}{2}$ cycles.

A typical example of a received waveform, in the unrectified amplitude v time "A-Scan" format, is shown in Fig. 4. The main components, in order of arrival time are:- the lateral wave, diffracted longitudinal waves from any discontinuities present, the longitudinal wave reflected from the back wall (referred to as the back wall wave), the half longitudinal/half shear reflection from the back wall, followed by any totally shear components.

In calculating sound path lengths from pulse arrival times (and hence the depth of the diffraction site below the test surface) it is simplest to assume that the transducers straddle the flaw symmetrically. In fact the locus of constant flight time is an ellipse with the transducers at the focii (Fig. 3). It can be shown (12) that the error in depth measurement as a result of the transducers not being symmetrically placed about the flaw is small for the lateral displacements commonly encountered given that the degree of offset is generally limited by the width of the weld. The various transit times within the specimen may then be calculated using the following formulae for the test configuration shown in Fig. 2.

$$t_l = \frac{2S}{c} \qquad [A1]$$

$$t_d = \frac{2(S^2 + d^2)^{\frac{1}{2}}}{c} \qquad [A2]$$

$$t_D = \frac{2(S^2+D^2)^{\frac{1}{2}}}{c} \qquad [A3]$$

Where:

S = half transducer centre separation, mm (in)

d = flaw depth below test surface. mm (in)

D = specimen thickness, mm (in)

c = longitudinal wave velocity mm/ μs (in/μs)

t_l = transit time of the lateral wave, μs

t_d = transit time of flaw diffracted wave from a flaw, μs

t_D = transit time of the backwall echo, μs

In a practice there is an additional transit time across transducer wedges and couplant. This can be calculated, if required, from a knowledge of the expected arrival times of the lateral wave (Equation A1) or the back wall echo (Equation A3).

If the transducer delay is known, the flaw's depth of the diffracting source below the test surface, d, may be calculated simply by re-arranging Equation A2.

$$d = \left[\frac{t_d^2 \, c^2}{4} - S^2\right]^{\frac{1}{2}} \qquad [A4]$$

APPENDIX B

LITERATURE REVIEW

An assessment of literature relevant to the program was carried out in order to provide background information on the time-of-flight technique and to allow the present state of the art to be assessed. Four computerised literature data bases were searched for relevant publications:- Weldasearch, Inspec, Metadex and Compendex.

The majority of the papers published are by Silk and his co-workers at AERE Harwell UK, and the basic principles of the technique are described in most of these. Three papers however, emerge as being of general interest by way of introduction. Silk's review chapter "Sizing crack like defects by ultrasonic means" (9) provides a general overview of ultrasonic techniques available for sizing flaws. A more recent paper (12) describes qualitatively the state of the art of the use of diffraction based time-of-flight measurements to locate and size flaws. In the third paper Cecco (13) presents the technique from the standpoint of a user of current equipment with the emphasis on practical considerations.

Silk's ultrasonic time-of-flight diffraction technique emerged in the mid 1970's (14) as a result of the requirements of fracture mechanics fitness for purpose analyses for accurate flaw through-thickness size measurement. Although a similar transducer configuration to that used earlier by Bottcher et al (15) was employed, flaw size was determined solely on the basis of the arrival time of pulses from various well

defined sources of secondary radiation from the flaw, rather than on their amplitude, as in the previous work.

Early work was restricted to the measurement of the depth of surface breaking flaws such as fatigue cracks (16-18). Here, using transducers of $2\frac{1}{2}$MHz centre frequency, crack depths were measured to $\pm$ 0.2mm for a crack approximately 10mm deep. However, the error in depth measurement increases rapidly as the depth of the crack decreases. In order to improve resolution it is necessary to use transducers of higher frequency, smaller transducer separations and to measure time delays more accurately. Charlesworth et al (19) reported experiments using a specially constructed high angle 15MHz transducer pair, with a separation of only 4mm, on simulated cracks consisting of narrow slits in aluminium. An accuracy of $\pm$ 0.05mm was claimed for slits of depth about 1mm.

The capability of the technique to size embedded cracks accurately was soon realised (5, 8). The accuracy with which a flaw may be sized has also been studied. Here errors in the estimation of crack depth owing to measurement of the various parameters from which depth is calculated are taken into account (20, 21). The capabilities and fundamental limitations of the technique are given a more rigourous treatment in Appendix C.

Although the accuracy for depth measurement is high, such accuracy is not maintained for flaw length measurement because the lateral resolution is no better than for conventional ultrasonic techniques owing to the large angular spread of the ultrasonic beam. flaw lengths parallel with the welding direction have traditionally been measured by an amplitude drop transducer movement technique. However considerable

improvement in lateral resolution may be achieved by the use of synthetic aperture focusing techniques (11, 21, 22).

In addition to the largely experimentally oriented work referred to above, considerable effort has been made in gaining a sound understanding of the underlying physical principles. This has been achieved by standard analytic techniques as well as by the use of computer modelling (23-27). The angular dependence of the amplitude of the diffracted signal from the crack tip has been calculated at different angles of the incident wave. These results suggest optimum angles of incidence of 65° for longitudinal waves and 45° for shear waves (23). There is good agreement between theoretical and experimental results. This work also suggests that the diffracted signal from the crack tip is less sensitive to angular variation than the specularly reflected wave which is of particular advantage when setting reporting thresholds. The 180° phase change observed between scattered signals from the top and bottom of a flaw (referred to in Appendix A) is also predicted by theory.

Originally it was not expected that a technique of this type would find application in flaw detection, but rather it would be employed as a means of sizing accurately cracks found by standard NDE techniques. However developments in computing technology and techniques for data acquisition and analysis have lead to the use of the time of flight technique in a dual flaw detection and sizing role. As a result of various round-robin exercises (5, 11), its ability to locate flaws and size them accurately has become well established.

The continued trend towards miniaturisation in the computer industry coupled with requirements to use the technique in the field have prom-

pted further equipment developments (13, 28, 29) with considerable reductions in system size - a trend which continues. These developments have resulted in wider field use of the system (30-33). In particular Hawker (31) has reported application of the technique in the UK offshore industry.

Much of the work reported however has originated from the UK Nuclear Power Program. Round-robin exercises have thus been aimed at welds in thick sections, typically 200-300mm, simulating welds in a nuclear reactor pressure vessel. The added problems of inspecting through a layer of austenitic cladding have thus been encountered. The results of these programs as regards the capability of the time-of-flight diffraction technique in a flaw detection and sizing role (11) are nevertheless encouraging for its application on other welded constructions such as bridges, although more attention is required to the development of techniques for the examination of thinner sections adequately and for easier deployment of the technique in the field.

APPENDIX C

THEORETICAL APPRAISAL OF THE CAPABILITIES OF THE TIME-OF-FLIGHT TECHNIQUE

Although the superior flaw sizing capability of the two transducer ultrasonic time-of-flight technique over standard amplitude based techniques has been demonstrated, it is necessary to consider its fundamental accuracy and limitations for determining flaw depth and through-thickness size. Extensions of the basic technique to improve its capabilities further are also considered in this Appendix.

Basic Accuracy of Time-of-Flight Systems

Any technique employing flight-time measurements is limited by the accuracy with which pulse arrival times may be measured. It is common in text books for the error in recording the arrival time of an incoming wave, Δt, to be quoted as;

$$\Delta t = \frac{1}{f} \qquad [C1]$$

Where f is the frequency of that wave. This results in an inherent uncertainty in range measurents, Δr, of;

$$\Delta r = c\Delta t = \frac{c}{f} = \lambda \qquad [C2]$$

Where λ is the wavelength and c the wave velocity. Assuming that the pulse shape remains relatively constant throughout and by measuring to some well defined point on the pulse, such as the second zero crossing, the error in the measurement may be reduced considerably.

In a digital system the waveform is sampled at discrete points along its length. The maximum uncertainty in time measurement is $\pm$ 1 sample point.To avoid sampling errors it is necessary that the interval between these points is less than Δt. However, there is another factor which must be considered. The sampling rate of the digitiser of the present equipment is 21MHz. Standard sampling theory requires that frequency components exceeding half the sampling rate, in this case 10½MHz, should not be present in order to avoid errors of aliasing. (incorrect reconstruction of the waveform because it is represented by too few sampling points). Transducers of a centre frequency of 5MHz, which will emit some frequency components approaching 10MHz, are therefore about the highest that may be used without necessitating a higher digitisation rate.

A sampling rate of 21MHz corresponds to a Δt of $\pm$ 47.6 ns and an error in range estimation in the region of 0.28mm (0.01 inch) for longitudinal waves in steel.

Two Transducer Techniques

Before proceeding further with the discussion of the capabilities and limitations of the time-of-flight diffraction technique it is necessary to consider the effect of the two transducer geometry.

In equation A4 it has been assumed that the flaw lies on the central plane between two transducers, thereby allowing unambiguous calculation of the flaw depth. This is a simplification of the actual test situation where the flaw may be displaced by an amount X from the centre line (Fig. C1). In this case the transit time, t, via a flaw at depth d may be calculated from;

$$ct = [d^2 + (S-X)^2]^{\frac{1}{2}} + [d^2 + (S+X)^2]^{\frac{1}{2}} \qquad [C3]$$

Where: S is half the transducer centre separation, mm (in)

c is the ultrasonic velocity, mm/μs (in/μs)

d is the depth of the flaw below the surface,mm (in)

X is the lateral displacement of the flaw, (mm or in), from the centre plane between the transducers.

By differentiation it may be shown that t is a minimum when X=0, in which case the flight time is given by;

$$ct = 2\,[d^2 + S^2]^{\frac{1}{2}} \qquad [C4]$$

In practice, whilst t may be measured, X will not be known with any degree of accuracy. Rearranging C3 gives;

$$d^2 = \left[\frac{c^2t^2}{4} - S^2\right]\left[1 - \frac{4X^2}{c^2t^2}\right] \qquad [C5]$$

For a given flight time, the locus of the diffraction source may lie anywhere on an ellipse with the assumed beam entry points at the foci, Fig. 3. The maximum measured depth will occur when X = 0, when equation C5 reduces to equation C4 which is in turn equivalent to equation A4. When X = ct/2, d takes on its minimum value of zero. However, this corresponds to a point beyond one of the two transducers and does not arise in practice. If consideration is given to the finite spead of the ultrasonic beam then the locus of possible sources of the signal may be reduced further, Fig. 3. Silk (21) gives a conservative assumption for the maximum value of X as being no greater than 40% of the value ct/2. Thus;

$$d^2_{max} = \frac{c^2t^2}{4} - s^2 \qquad [C6]$$

$$d^2_{min} = 0.84\left[\frac{c^2t^2}{4} - s^2\right] \qquad [C7]$$

Let the apparent depth of a flaw at a distance X from the centre-line between the transducers, calculated by assuming $X \neq 0$ in equation C5 (or by using equation A4), be denoted as d_x. By substituting this in equation C5 and rearranging, the apparent depth of the flaw, d_x, is given by

$$d_x^2 = d^2\left[\frac{1}{1 - \frac{4X^2}{c^2t^2}}\right] \qquad [C8]$$

This is the equation of a hyperbola and is shown in Fig. C2 for different values of central depth d. A practical application of this is the lateral location of flaws by using scans transverse to the weld, where the distance of the flaw from the weld centreline may be defined by that point at which d_x^2 is a minimum.

From equations C6 and C7 it can be shown that if the transducers are placed symmetrically about the weld centreline, then the error in determining the depth of a diffraction source within the weld, but not necessarily on the centre line, is unlikely to exceed 9%. The technique is therefore relatively insensitive to non-symmetrical placement of the transducers. In the following discussion of sources of error in flaw depth measurement, it will be sufficient to consider the simpler case of X = 0.

Depth Resolution and Choice of Transducer Angle

Consideration has already been given to the range resolution in time-of-flight measurement testing. Unlike the single transducer case, in a two transducer system the flight time is not directly proportional to the depth of the flaw below the surface. The depth v time non-linearity is exemplified by Fig. C3, where the depth of the diffracting source below the test surface has been plotted against flight time for various transducer separations. At small depths there is relatively little increase in flight-time with increasing depth, whilst for $d >> s$ the relationship is more nearly linear.

The error in depth measurement Δd_t due to a timing error Δt may be found by differentiation of equation C6.

$$\Delta d_t = \Delta t \frac{t}{d} \frac{c^2}{4} \qquad [C9a]$$

$$= \frac{c}{2} \frac{(d^2+S^2)^{\frac{1}{2}}}{d} \Delta t \qquad [C9b]$$

As d decreases the error Δd_t for a given error Δt increases rapidly. Thus near surface resolution is poor.

Alternatively the error in d may be expressed as;

$$\Delta d_t = \frac{c}{2} \frac{1}{\cos\theta} \Delta t \qquad [C9c]$$

Where θ is the angle of incidence at the flaw (see inset of Fig. C4). For digitisation at 21MHz (i.e $\Delta t = 0.0476\mu s$ the angular dependence of Δd_t in steel ($c = 5.95$ mm/μs (0.234 inch/ μs)) becomes;

$$\Delta d_t = \frac{0.14\text{mm}}{\cos\theta} \text{ or: } \Delta d_t = \frac{5.5 \times 10^{-3}\text{inch}}{\cos\theta} \qquad [C10]$$

This relationship is shown graphically in Fig. C4 where it can be seen that the resolution increases as the angle of incidence on the flaw decreases. If flaw depth is to be determined to better than $\pm$ 1mm ($\pm$0.04in) then an upper limit of 80° is imposed on θ. In practice, due to the lower frequency content of the lateral wave, to which reference most timing measurements are made (Equation A5), Δt may be greater than $\pm$ 1 digitiser sample interval, resulting in a decrease in the maximum usable angle. Observation of experimental results indicates that Δt may be of the order of $\pm$ 3 samples ($\Delta t = 0.14\mu s$) in which case, if d is is to be determined to better than $\pm$ 1mm, then θ must be less than about 65°. This is also shown in Fig. C4.

The angular dependence of the efficiency of the diffraction process also needs to be considered in the choice of beam angle. Silk has shown experimentally that, for two transducers symmetrically placed about a flaw, the maximum amplitude of the forward scattered signal at the receiving transducer occurs at an angle of incidence of about 60° for longitudinal waves (30). Theory (24) supports these observations, concluding that the optimum angles for the detection of forward scattered signals from the tops and bottoms of flaws are in the range 60° to 65°. This angular dependence has been superimposed on the depth resolution graph of Fig. C4.

The most useful (and commonly used) angle of refraction for the axis of the ultrasonic beam is 60° with a refracted angular range of 45° to 80° in ferritic steel. Transducers with an angle of 45° in steel are used only for the detection and sizing of deeper flaws where the wider transducer separations that would be required for 60° transducers in

this instance result in inordinately long path lengths, which outweigh any advantage gained by use of 60° transducers. The useful depth range for 60° transducers depends on the efficiency of the ultrasonic system and whether the signal to noise ratio can be improved sufficiently for flaw detection by signal averaging. In the present work 45° transducers were used where the beam axes were required to intersect at depths in excess of 50mm.

Other Sources of Error in Flaw Depth Measurement

It can be seen from equations A4 and A5 that uncertainties in the measurement of pulse arrival times are not the only sources of error in flaw depth determination. Another source is due to error in measurement of the transducer centre separation, 2S, or variations in this parameter. Differentiation of the basic equation for flaw depth determination, (A4 or C6) yields.

$$\Delta d_S = - \frac{S\Delta S}{d} \qquad [C11a]$$

$$\Delta d_S = - \tan \theta \, \Delta S \qquad [C11b]$$

Where: ΔS is the error in the measurement of S

Δd_s is the error in d due to Δs

for $\Delta S = \pm$ 1mm ($\pm$0.04in), which is not pessimistic due to uncertainty in the assumed beam entry point,

$$\Delta d_s = \tan\theta \qquad [C12]$$

This source of error becomes dominant for angles of $\theta > 45°$. The effects of errors in the measurement of S may be reduced by using equation A5, where time measurements are made with respect to the lateral wave.

$$\Delta d_S = \frac{(S^2 + d^2)^{\frac{1}{2}}}{d} - \frac{S}{d} \qquad [C13a]$$

$$\text{or } \Delta d_S = \frac{1}{\cos\theta}(1-\sin\theta) \qquad [C13b]$$

Errors in depth determination can also accrue from errors in measurement of the ultrasonic velocity and local variations, albeit small, in the ultrasonic velocity in the weld metal and surrounding material. However, compared with the accuracy with which time, t, and transducer separation, 2S, can currently be measured, the velocity can be determined with sufficient accuracy such that any error in its measurement is, in general, insignificant. It is only where transducers of higher frequency are used, (when the digitisation rate must necessarily be increased, with a resulting increase in the precision with which pulse arrival times may be measured), and if the transducer separation can be measured more accurately, that error in the measurement ultrasonic velocity could be significant.

The error in d arising from errors in measurement of t (Δt = 3 samples) and S (ΔS = 1mm) is plotted versus incident angle ϕ in Fig. C5 (equations C9c and C13b). By plotting Δd v θ, the error for any combination of S and d may be inferred. In general, however, the transducer separation (2S) for a test is fixed and it is more convenient to assimilate the effects of measurement errors on depth from a plot of Δd versus d (Fig. C6, equations C9b and C13a).

The most probable error, $< \Delta d >$ may be expressed as the square root of the sum of the squares of the partial errors:

$$< \Delta d > = (\Delta d_t^2 + \Delta d_s^2)^{\frac{1}{2}} \qquad [C14]$$

This has been superimposed on the graphs of Fig. C5 and C6. It can be seen that the error in depth measurement due to an error in the measurement of the transducer separation 2S does not affect significantly the maximum incident angle (θ = 65 degrees) that may be used for errors in depth measurement to be less than 1mm.

Error in Flaw Height Determination

The height of a flaw is determined by subtracting the depth of the top of the flaw from the depth of the bottom of the flaw. In this instance, because measurements of the extremeties of the flaw are made for the same transducer separations and from the same point on the lateral wave, the errors partially cancel out and the height of the flaw can in general be determined to a greater accuracy than its depth. The result of this is that if errors in depth measurement in excess of 1mm can be tolerated then the useful range of incident angles can be extended to about 70 or 80 degrees for flaw height measurement to remain better than $\pm$ 1mm.

The Effects of Pulse Length on the Smallest Flaw Height Measurable

Having considered the accuracy with which the depth and height of a flaw may be determined, it is necessary also to consider the effect of the finite length of the received pulse on the smallest flaw height measurable. For the diffracted signals from the top and bottom of a flaw to be resolvable, the two pulses must be separated in time. Ass-

uming a transducer centre frequency of 3MHz and a pulse duration of two cycles, then the minimum time delay between pulses that can be measured is approximately 2/3 μs. From equation A4, this time difference may be written as:

$$\frac{c}{2}(t_b - t_t) = [S^2+(d+h)^2]^{\frac{1}{2}} - [S^2+d^2]^{\frac{1}{2}} \qquad [C15]$$

Where: t_b is the arrival time of the diffracted signal from the bottom of the flaw,

t_t is the arrival time of the diffracted signal from the top of the flaw.

h is the height of the flaw

d is its depth below the inspection surface

$(t_b-t_t)_{min}$ is the minimum time delay between pulses that can be measured (= 2/3μs)

The minimum flaw height (h_{min}) for the diffracted pulses to be resolved can be determined by solving this equation for h for a given transducer separation and depth below the surface.

$$h_{min} = [d^2 + c^2 \frac{(t_b-t_t)^2_{min}}{4} + c\,(S^2+d^2)^{\frac{1}{2}}\,(t_b-t_t)_{min}]^{\frac{1}{2}} - d \qquad [C15]$$

This is shown in Fig. C7, where the minimum flaw height measurable, h_{min}, is plotted versus flaw depth, d, for different transducer separations. For shallow flaws h_{min} increases rapidly. In the limit, as S tends to 0 or as >> then h_{min} tends to $c(t_b-t_t)/2$ which for c = 5.95mm/ μs gives h_{min} = 1.98mm (0.08in).

Consideration needs also to be given to the effective depth obscured by the lateral wave. Theory suggests a lower frequency content for the lateral wave due to beam divergence effects. This has been observed in practice by the longer duration of the lateral wave and can be seen on the sample A-Scan trace shown in Fig. 4. From observation of these experimental results the time duration of the lateral wave can be as much as 1 μs. Substituting this value into equation A5 as the value for $t_d - t_1$ then the effective depth obscured by the lateral wave, for a given transducer separation, may be calculated. This has been superimposed on the graph of Fig. C7, from which the result of choosing a particular transducer separation on the minimum flaw height measurable and the effective depth obscured by the lateral wave, may be assessed.

Alternatively Fig. C7 can be used to determine the maximum size a flaw can have at a given depth for its tip signals not to be resolved for a given transducer separation. This allows flaws that are below the resolution limit to be assigned a maximum size. If this is still below the critical flaw size then the flaw can still be acceptable. In practice, as transducer separations greater than 40mm (i.e. S = 20mm) are generally employed, the amplitude of the lateral wave is low and flaw signals occuring within this may be detected although their depth cannot be determined with any degree of accuracy.

The above discussions have implications for the testing of thin plate, for example the 10mm (0.4in) material used in the present work. From the graph of Fig. C7 it can be seen that, even for a transducer centre separation of only 30mm (S = 15mm), the depth effectively obscured by the lateral wave is 10mm and the lateral wave would be barely resolvable from the back wall wave. The response from any flaw present would thus coincide with the lateral wave rendering measurement of depth or height impossible, though a flaw may still be detected.

It is obvious, from the way that the resolution of two pulses has been defined, that an increase in the ultrasonic frequency would improve the resolution for flaw height measurement, solving both the near surface flaw detection problem and the thin section inspection problem. The effect of increasing the transducer centre frequency to 10MHz on the minimum size if flaw whose height may be measured for a given depth below the surface can quite easily be seen in Fig. C8: as a result of increasing the transducer centre frequency from 3MHz to 10MHz the limiting flaw height is reduced from 1.98mm to 0.60mm. An alternative solution might be to look at pulse correlation techniques to identify pulses of a well defined shape coinciding with the lateral wave or other diffracted wave pulses. This assumes that the pulse shape remains invariant through its travel time and it is unclear at present whether this approach could offer significant advantages in this instance.

It should be noted that the limiting effects of pulse length on the minimum height of flaw which can be measured only applies to embedded flaws. The depth of surface breaking flaws can be determined down to probably around $\lambda/2$ owing to the fact that it is merely the shift in arrival time of a single pulse which is measured.

Extensions of the Technique

Although flaw height may be determined more accurately by the time-of-flight technique than by any of the standard amplitude based techniques, as is born out by experimental observations both in the present program of work (see Appendix G) and in other work (5, 10), a number of avenues are open for enhancing the capabilities of the time-of-flight technique still further. Some of these have already been men-

tioned, such as improving depth and higher resolution by the use of higher frequency transducers and a higher digitisation rate, or pulse correlation techniques.

Before increasing the transducer frequency and the digitisation rate, a number of considerations have to be taken into account. At higher frequencies the attenuation of ultrasound in the test-piece increases significantly. The use of higher frequencies would limit the ultrasonic path lengths for flaw detection and their use would thus be restricted to the detection and sizing of near surface flaws or the inspection of welds in thin material. However, as in general it is in thinner materials that small flaws must be measured, restricting the use of higher frequencies to thinner sections is not thought to be a disadvantage. Furthermore, such a restriction is necessary from a practical standpoint, because at a higher digitisation rate more picture memory is required to store information from the same depth zone. Alternatively at a higher digitisation rate, a fixed time-window covers a smaller depth range.

The feasibility of using pulse correlation techniques to improve depth resolution has not been assessed and will be discussed no further at present.

For the determination of the transverse position of a flaw within a weld, combining the results of more than one scan is a possible approach. Alternatively, a single transverse scan (across the weld) would be a more accurate, but would necessitate removal of the weld crown. As the weld crown is nominally removed for the welds in major tension flanges this latter solution would be practical; transverse scans could be carried out only at locations where welding discontinuities had been identified.

The improvement to lateral resolution by the use of one dimensional synthetic aperture focusing algorithms has been mentioned already in Appendix B.

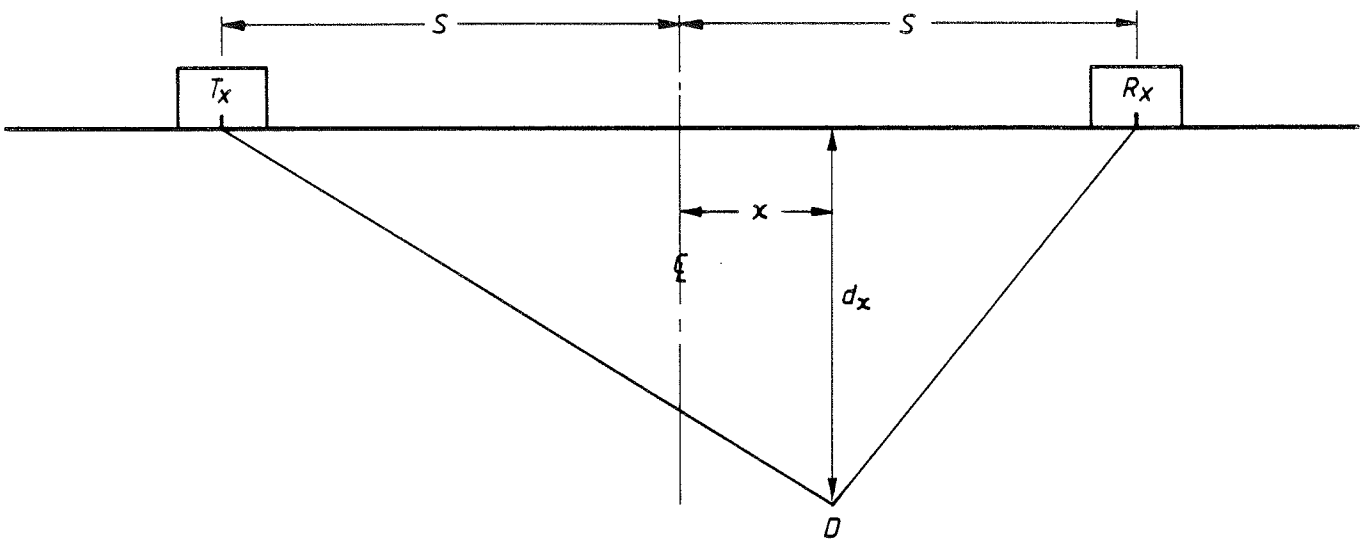

Fig.C1. Generalised two-probe testing geometry for a flaw D displaced an amount x from the centreline between the transducers.

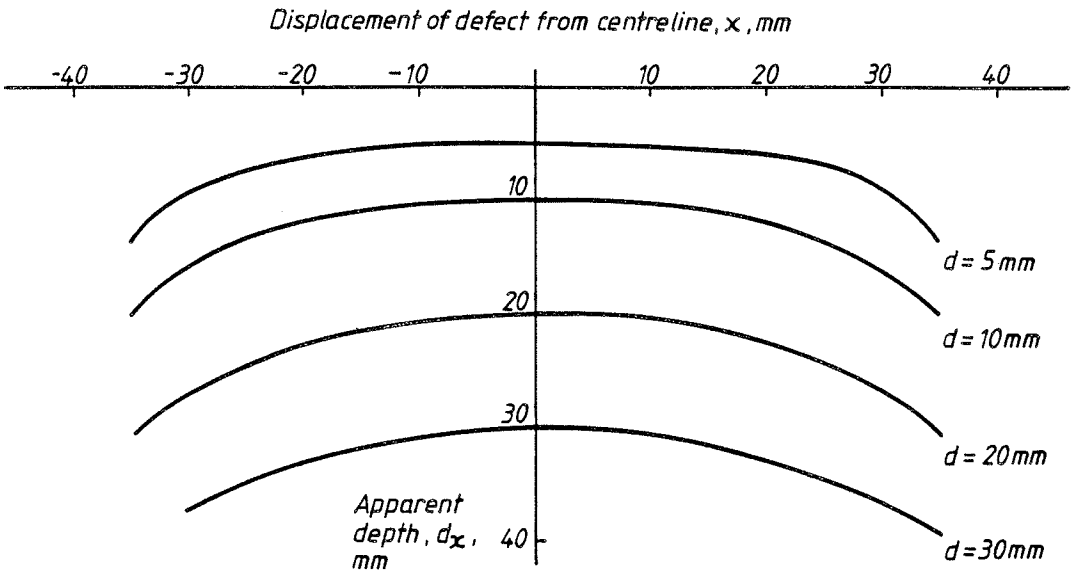

Fig.C2. Apparent depth, d_x of a flaw for various displacements, x, from the centreline. 2S = 70mm.

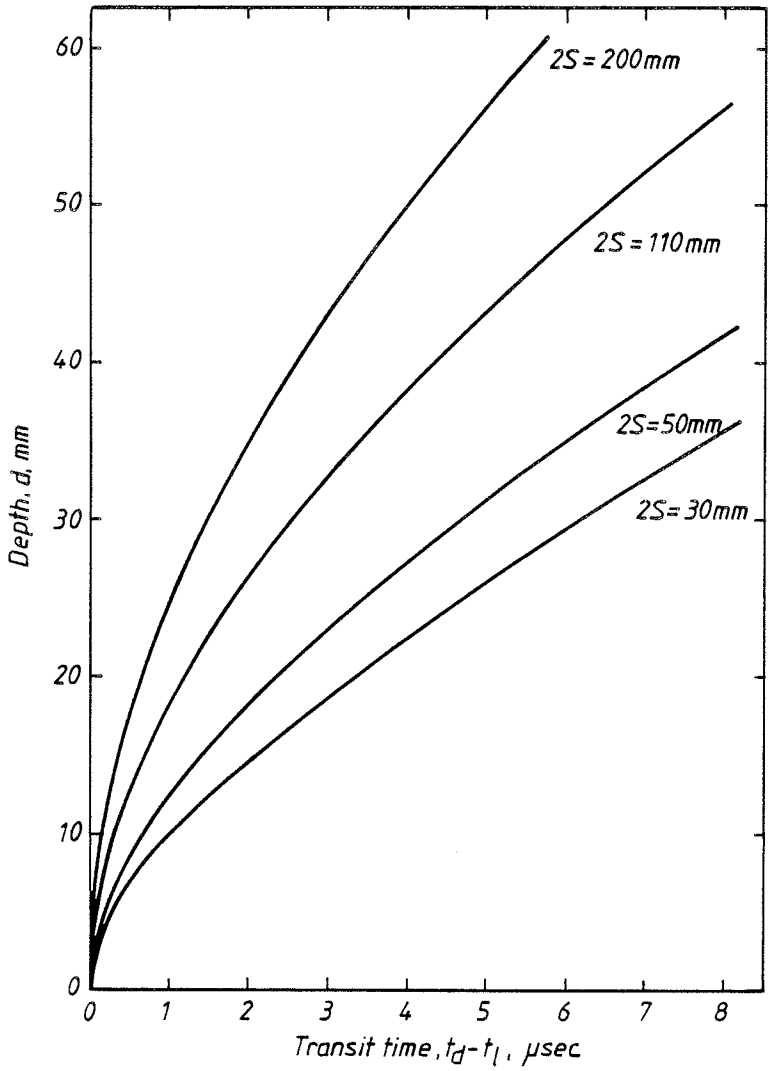

Fig.C3. Depth of diffracting source, v. transit time for different transducer separations, (2S).

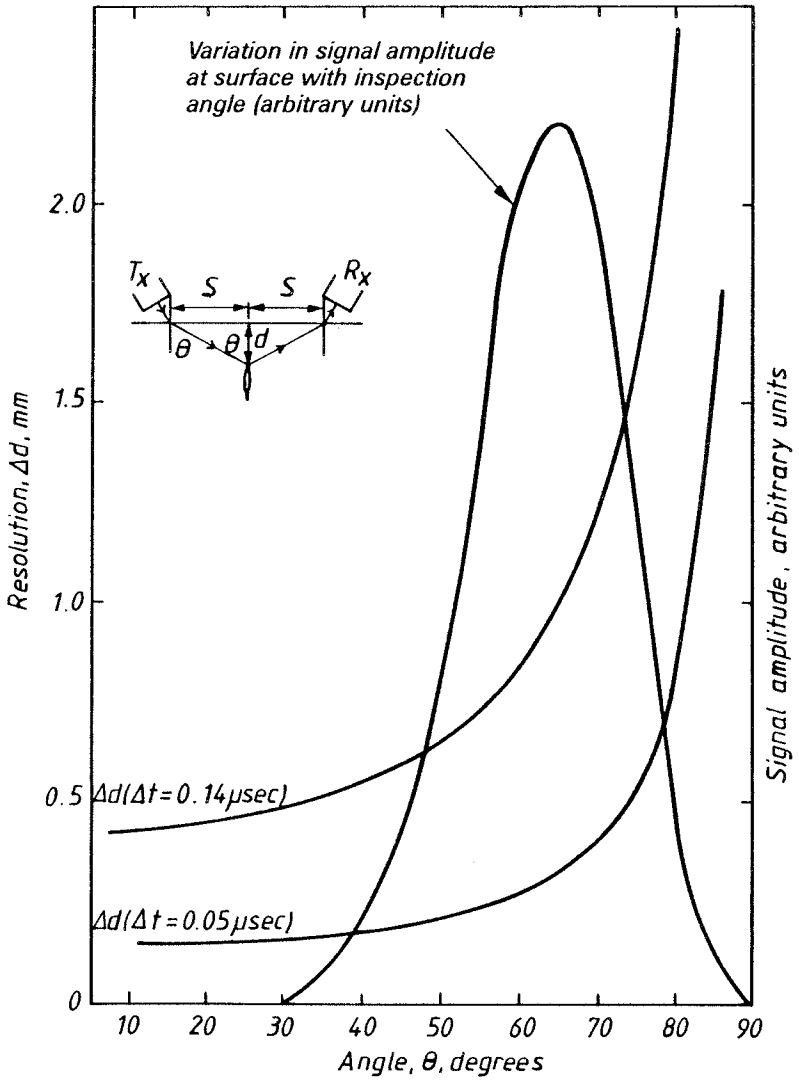

Fig.C4. Variation of depth resolution and diffracted signal amplitude at the surface with inspection angle (after Ref.11).

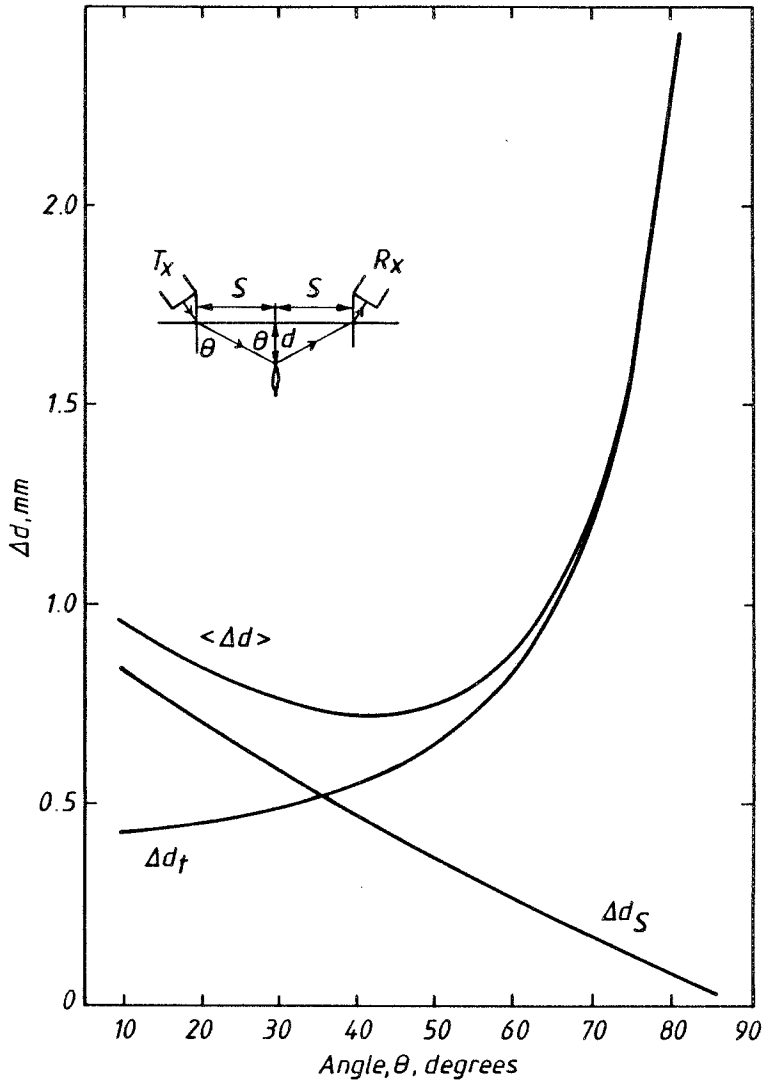

Fig.C5. Variation of depth resolution with inspection angle as a result of errors in the measurement of pulse transit time and transducer separation. $\Delta t = \pm 3$ samples, $\Delta S = \pm 1$mm.

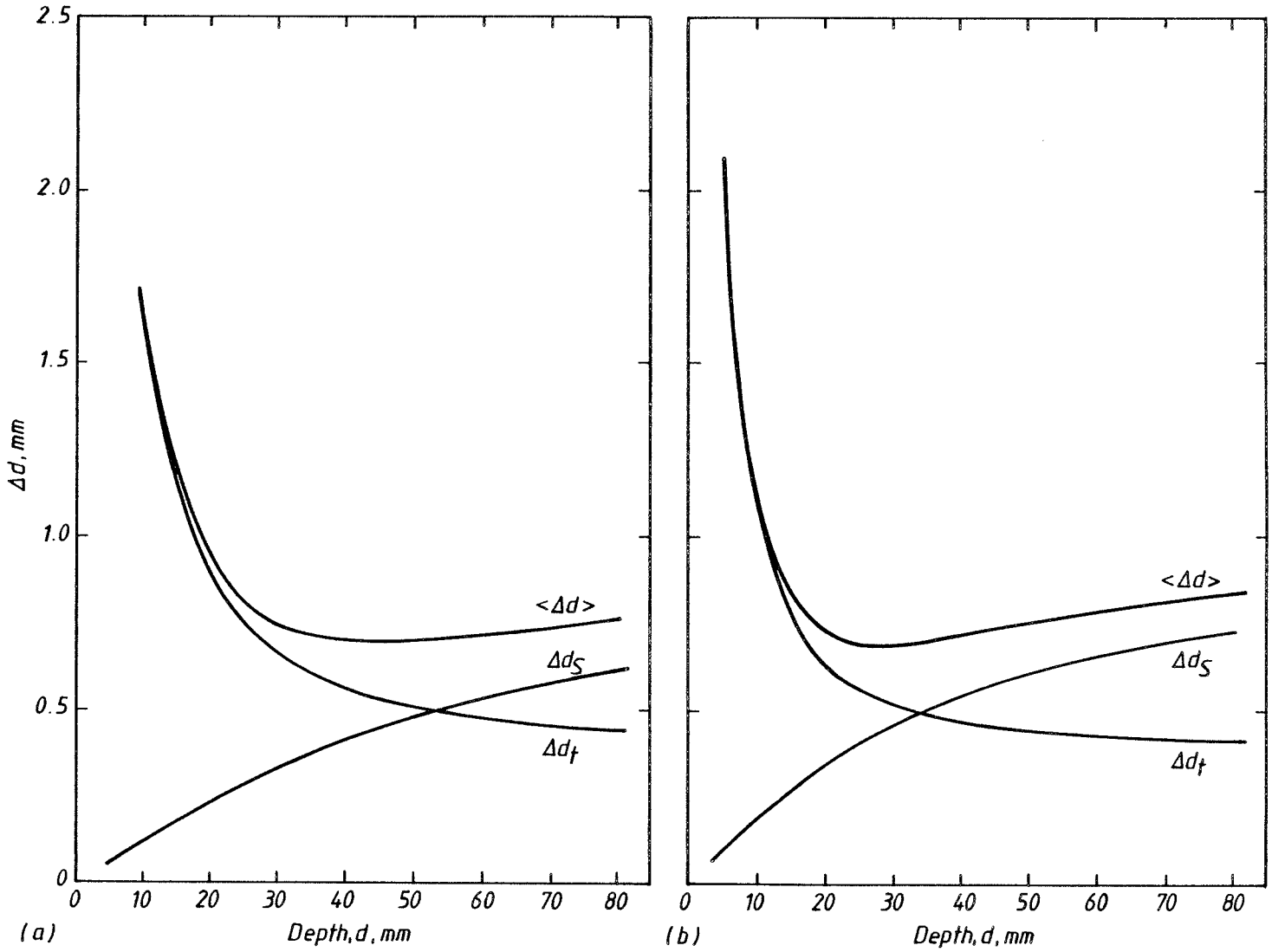

Fig.C6. Variation in depth resolution at different depths, d, as a result of errors in the measurement of pulse transit time and transducer separation:

a) $2S = 80mm$, $\Delta t = \pm 3$ samples, $\Delta S = \pm 1mm$
b) $2S = 50mm$, $\Delta t = \pm 3$ samples, $\Delta S = \pm 1mm$

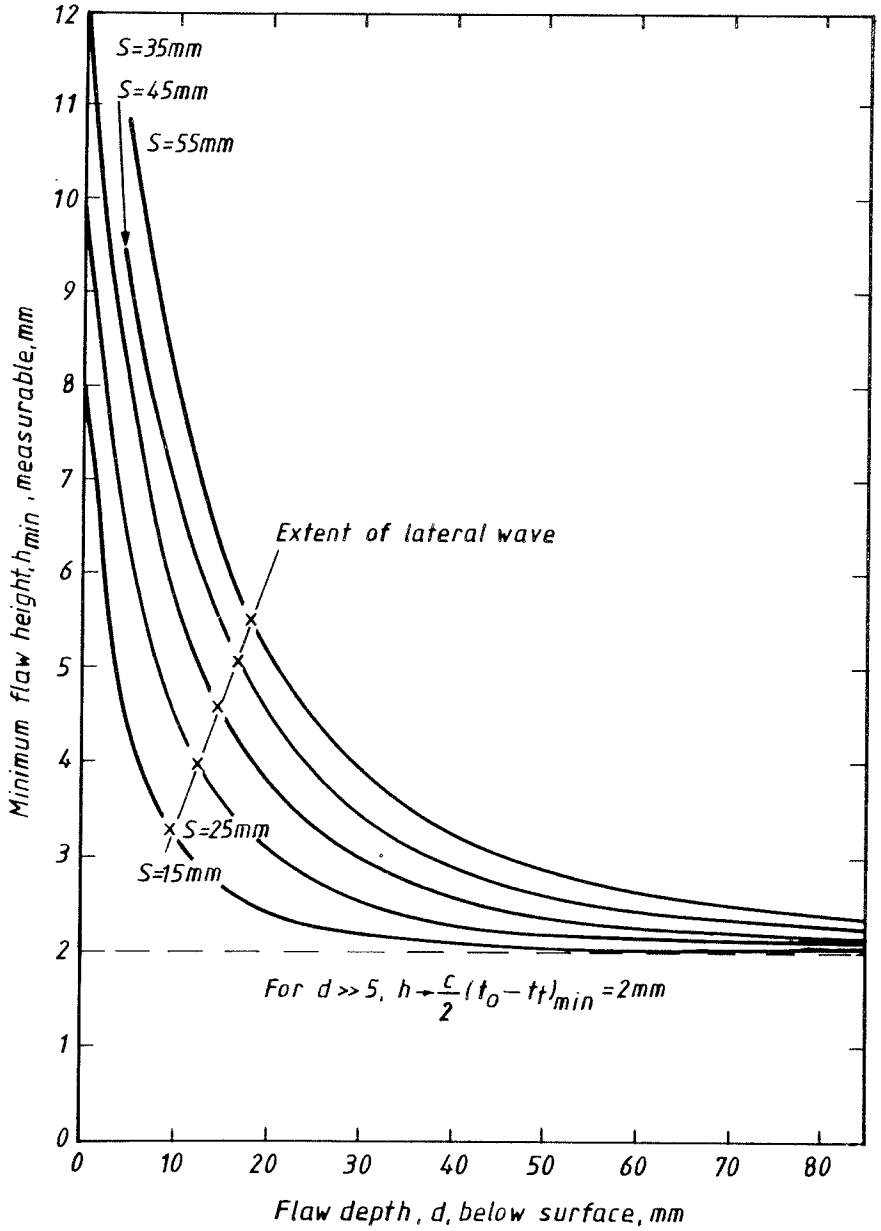

Fig.C7. Minimum flaw height measurable v. flaw depth below the surface for different transducer separations at 3MHz. The depth obscured by the lateral wave is superimposed:

Δt_{min} = 2/3μsec f = 3MHz S = half transducer separation

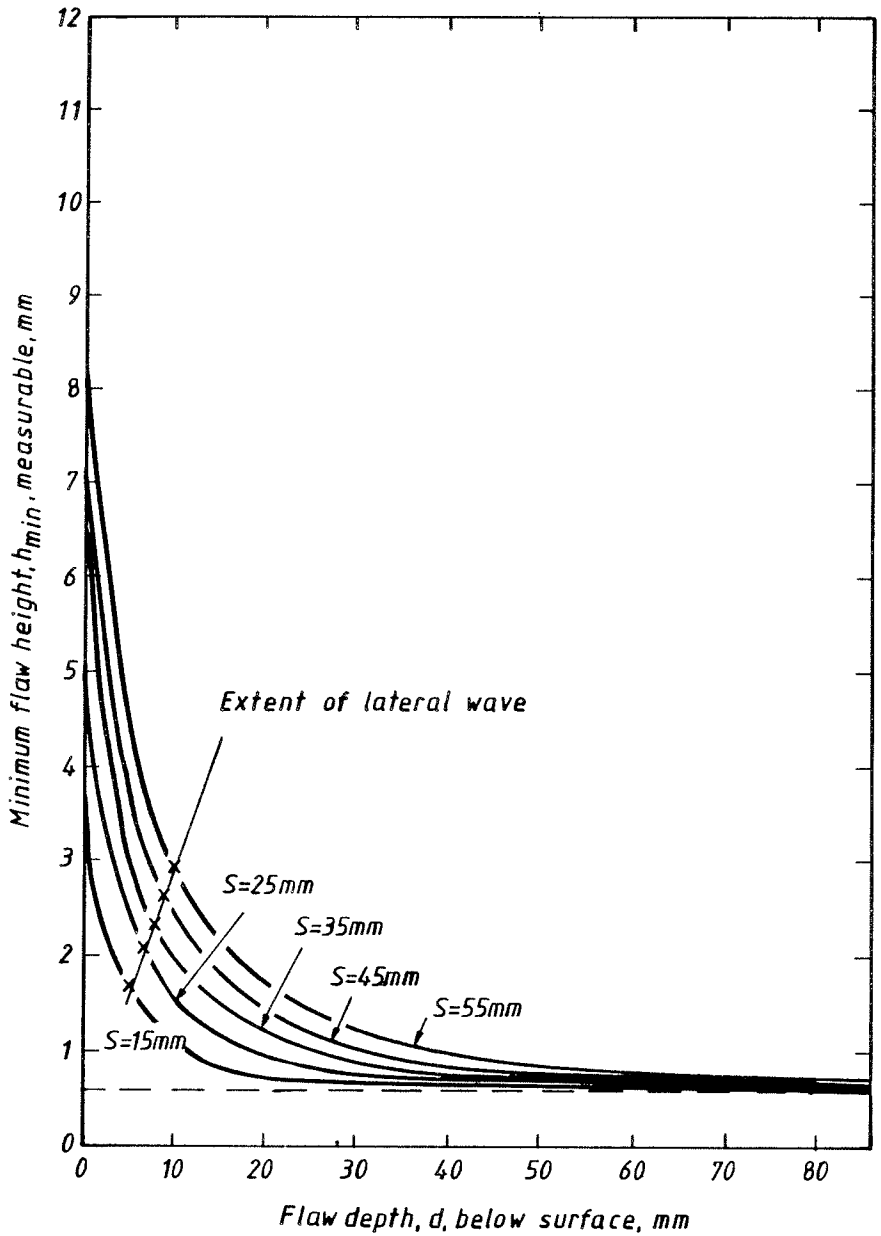

Fig.C8. Minimum flaw height measurable v. flaw depth below the surface for different transducer separations at 10MHz. The depth obscured by the lateral wave is superimposed:

Δt_{min} = 0.2μsec f = 10MHz S = half transducer separation

APPENDIX D.

EQUIPMENT FOR THE GENERATION AND DISPLAY OF TIME-OF-FLIGHT INSPECTION DATA

General Overview

Equipment for the generation and display of time-of-flight inspection data is described below. Both hardware and software are detailed. Two factors had to be taken into consideration when specifying the system:

i) It was a prototype. Although the principle of time-of-flight testing was well established, it was by no means clear at the outset of the program, how equipment employing this principle would best be configured and would operate if used widely in the field.

ii) The system was to be both a research tool for the development of test techniques and a vehicle for demonstrating that the time-of-flight technique can be used in the field. It was therefore required to be powerful and flexible enough for research purposes whilst retaining features such as ruggedness and portability to enable its use in the field.

The system was designed and built by the NDT Systems Development Unit of the NDT Centre at AERE Harwell, to a specification supplied by The Welding Institute. The NDT Systems Development Unit has built up expertise in the design and construction of such systems over recent years. In essence, the present system is similar to the Harwell system known as ZIPSCAN (13, 29). However, some aspects have been enhanced considerably to meet the requirements of the present program.

Conventional analogue pulsers, amplifiers and ultrasonic transducers are used to excite and receive ultrasonic pulses. The unrectified A-Scan data containing the various pulses of interest is digitised and stored. A single A-Scan may be displayed on a video monitor in a similar manner to that on a conventional cathode ray tube. Alternatively, data may be displayed in B-Scan format, i.e. a plot of distance along the specimen against signal flight time, with the intensity of the display representing signal amplitude. Examples of A- and B-Scan displays are shown in Fig. 4 and 7 respectively. The present system is capable of building up three different pictures simultaneously from a combination of two-transducer time-of-flight data and single-transducer pulse-echo data. The pictures may be stored on disk for later computer-assisted visual analysis.

A block diagram of the system is given in Fig. D1 and a photograph of the system is shown in Fig. D2.

The main unit shown in Fig. D2 houses the Digital Equipment Corporation LSI 11/23 computer and standard interfaces, the signal digitising and averaging module, the picture generation unit and the stepping motor driver. It also contains the analogue circuitry:- pulse generators, receivers, multiplexer, programmable attenuator and signal amplifier. The modules are mounted in an 8U (= 14") high 19" wide rack. The rack is enclosed in a "Skypack" carrying case which may be sealed for transit and for operation under site conditions. The efficiency of the fan-cooling is such that no problems are experienced with components overheating even when the system is operated with the lid closed.

The components of the system which are not housed in the main unit are kept to a minimum. These consist of:- Winchester disk drive for data storage, visual display unit (VDU) for computer/operator communication, and a small black and white TV monitor for displaying the collected images. The scanning rig and transducers are necessarily separate from the main unit.

For site work the VDU may be replaced by a small hand-held terminal, with only a subset of system commands available to the operator, and the Winchester disk drive, like the computer, can be mounted in a Skypack carrying case. The storage capacity of the Winchester is sufficiently large that a day's worth of data may be collected before floppy disk back-up is required. Data analysis and archiving may then be carried out away from the test location when the added bulk of a VDU is not a hinderance.

The major elements of the hardware are described in more detail in the section on hardware, below.

Hardware (see Fig. D1).

Transducers

Krautkramer, model G5KB, 5MHz transducers were used in conjunction with the appropriate angle of cross-linked polystyrene wedge to produce the required refracted angle in steel. The wedges attenuate the higher frequencies of the emitted pulse, thus the effective centre frequency is reduced to about 3MHz, as determined from the time between zero crossings of a typical pulse. The G5KB transducers are shock wave transducers, i.e. the crystals are critically damped, so that when excited by a high amplitude voltage spike, the resulting pulse

length is only approximately 1½ to 2 cycles, even with the polystyrene wedges.

Transmitters, Receivers and Amplifiers

Transmit and receive facilities are provided for up to 4 transducers. The selection of the transducer which will act as the transmitter and receiver is made via the computer. Four of the possible eight input channels are connected to the outputs for use in pulse-echo mode whilst the other four are used in time-of-flight mode. The selection of transmit and receive channels determines whether the unit operates as time-of-flight or pulse echo. The attenuater is also controlled by the computer as different gain settings are often required for the two modes.

Averaging Digitiser (SCAMP)

SCAMP consists of an 8 bit resolution transient recorder, adder and memory. The sample rate is 21MHz. In theory such a rate is capable of reproducing frequencies in the ultrasonic signals of up to 10.5MHz. In practice it is more suited for frequencies below 5MHz. An anti-aliasing filter ensures that frequencies exceeding half the sampling frequency do not reach the digitiser. The transient recorder memory enables signals of up to 380 microseconds duration to be collected. The delay of the starting point of the 512 sample long portion of this signal that is to be stored is computer selectable.

The amplitude of diffracted waves is relatively small, and may be hidden in the noise. Thus to obtain a detectable signal, the signals may need to be averaged over several transient acquisitions. The number of averages, 2^N, is computer selectable where the maximum value of

N is 8 (i.e. 256 averages). This necessity for signal averaging can be seen from Fig. D3. Fig. D3a shows the digitised signal without averaging, and Fig. D3b shows the same signal averaged 32 times. The improvement to the signal to noise ratio is quite pronounced. As the averaging process is hard wired, the increase in the time spent at a given location as a result of averaging the signal 256 times is small compared with the time to move between locations, and other necessary computer operations. Thus N = 8 has been selected as standard.

Picture Memories

There are three identical picture memories. Each is capable of holding 512 (horizontal = time) by 256 (vertical = distance along specimen) picture points which together make up the video display, as in Fig. 7. Selection of the picture type collected in each memory and the selection of which memory is displayed is controlled by the computer, which also has access to the picture memories for reading and writing via the interface. Transfer of data is achieved under program control.

PJAZZ

PJAZZ is a unit which has extensive capabilities to modify the visual impact of the picture selected for display. It can transform the linear grey-scale of the picture generated into an arbitrary linear or non-linear continuous function allowing contrast enhancement, thresholding etc. These effects allow the viewer to discern the important features of the image more readily. These functions are computer selectable.

LSI 11/23 Computer

The Digital Equipment Corporation (DEC) LSI 11 computer consists of an 11/23 CPU with memory management unit, 256 Kbytes RAM, serial interfaces for the VDU and line printer (when required) and sufficient parallel interfaces for communication with the data acquisition and image generation system. Communication with the computer is via a video terminal equivalent to a DEC VT 100.

A Data Systems DSD880/30 30 Mbyte Winchester disk drive with floppy disk back up is used for program and data storage.

Scanning Rig

This device transports the selected transducers over the test piece. As the transducers are scanned at a fixed spacing, a simple one-axis movement only is required. The transducer head assembly is driven along the specimen via a lead screw by a five phase 28 volt DC stepping motor. The maximum distance of travel is at present 450mm (18"). Limit switches are incorporated to ensure that this limit will not be exceeded. Switchable magnets in the feet of the scanner allow it to be clamped firmly even to the underside of the testpiece. A photograph of the scanner is included as Fig. D4, and more detail of the transducer head assembly may be seen in the close-up of Fig. D5.

Whilst the present scanner is suitable only for the testing of the flat samples studied, crawlers capable of carrying out scans on more complex joint configurations would be similar in concept.

Software

A standard test facility is provided by a computer program written in FORTRAN. This provides the interface between the computer and the user.

Three modes of operation are possible:-

i) set up for test,

ii) perform a test,

iii) analyse results.

Single characters entered via the VDU keyboard activate the various functions. General functions such as "wipe-screen", "exit", and "display help menu" are active in each mode. The functions relevant to a particular mode of operation are only active when that mode has been selected. This keeps to a minimum problems associated with striking the wrong key. When the help menu is requested, active functions are displayed as highlighted text (Fig. D6). Details of the various functions is given in Table D1, only a summary being given here. The procedure for testing is given in Appendix F.

Equipment Developments

Considerable interest has been shown in transportable instrumentation for computer controlled time-of-flight (and pulse-echo) ultrasonic tests, both within the nuclear power generating industry and outside it, since the system described above was specified and built. As it is outside Harwell's remit to build equipment on a commercial basis a licensing agreement has been entered into with SGS Sonomatic Ltd. (Warrington, UK) to build and develop further ZIPSCAN instrumentation. SGS Sonomatic also offer a service facility and their procedures and ZIPSCAN instrumentation operating in pulse-echo mode have been validated by the Electric Power Research Institute (EPRI) in the USA for the detection of intergranular stress corrosion cracking (IGSCC) in the primary pipework of the Boiling Water Reactor (BWR).

At present the SGS Sonomatic ZIPSCAN system (34) is configured very much along similar lines to the original Harwell models, and our own, but a computer controlled ultrasonic system of the utmost flexibility, ZIPSCAN II is now being produced. For increased portability the system will be housed in separate boxes.

The two basic units are:

i) Flaw detection unit - comprising monochromatic or colour display monitor, processor controlled modular "front end" circuitry and compact, transferable bulk data storage.

ii) Data processing unit - comprising an LSI 11/73 processor, averaging digitiser frame store and other digital circuitry, alphanumeric plasma panel for data display and integral keyboard for data address.

In this form ZIPSCAN II can be used for the collection and display of ultrasonic data generated by normal manual or jig assisted scanning or in conjunction with a separately controlled motorised mechanism. A third unit is available which will enable ZIPSCAN II to be used to collect and process position related inspection data in conjunction with a wide range of manipulators, automatic scanner and robotic devices equipped with positional encoders and tachogenerators for fully programmable "closed loop" remote operation.

iii) Drive Control Unit - which comprises a user programmable microprocessor control network and powerful D.C. linear amplifiers for independent operation of each axis of scan motion.

Table D1. Commands available when operating the time-of-flight system.

Command	Function
GENERAL FUNCTIONS	
E	Exit from program or change to another mode of operation
H	Display help menu
W	Wipe the screen
Space bar	Stop or restart any process
SET-UP FUNCTIONS	
A	Set attenuation [dB]
D	Set initial delay to digitised A-Scan [μsec]
N	Set up or change the number of averages [2^N]
T	Turn present Tx on continuously to allow monitoring of the signal on an oscilloscope.
Z	set transmit and receive channels (pulse-echo or time of flight)
?	Query parameters set
TEST FUNCTIONS	
G	Go. Move the probes over the sample and display a grey-scale image of the received signals
M	Move scanning head to required location or to one of the limit switches
S	Save frame store data to a file
ANALYSIS FUNCTIONS	
A	Write ASCII characters to screen
C	Change the output contrast table (changes appearce of display)
F	Fetch data from a file to frame store
L	Linearise the data
P	Plot one A-Scan from frame store or file on disk
X	Set up X cursor
Y	Set up Y cursor
↓←↑→	Move the cursor (reports cursor position simultaneously)

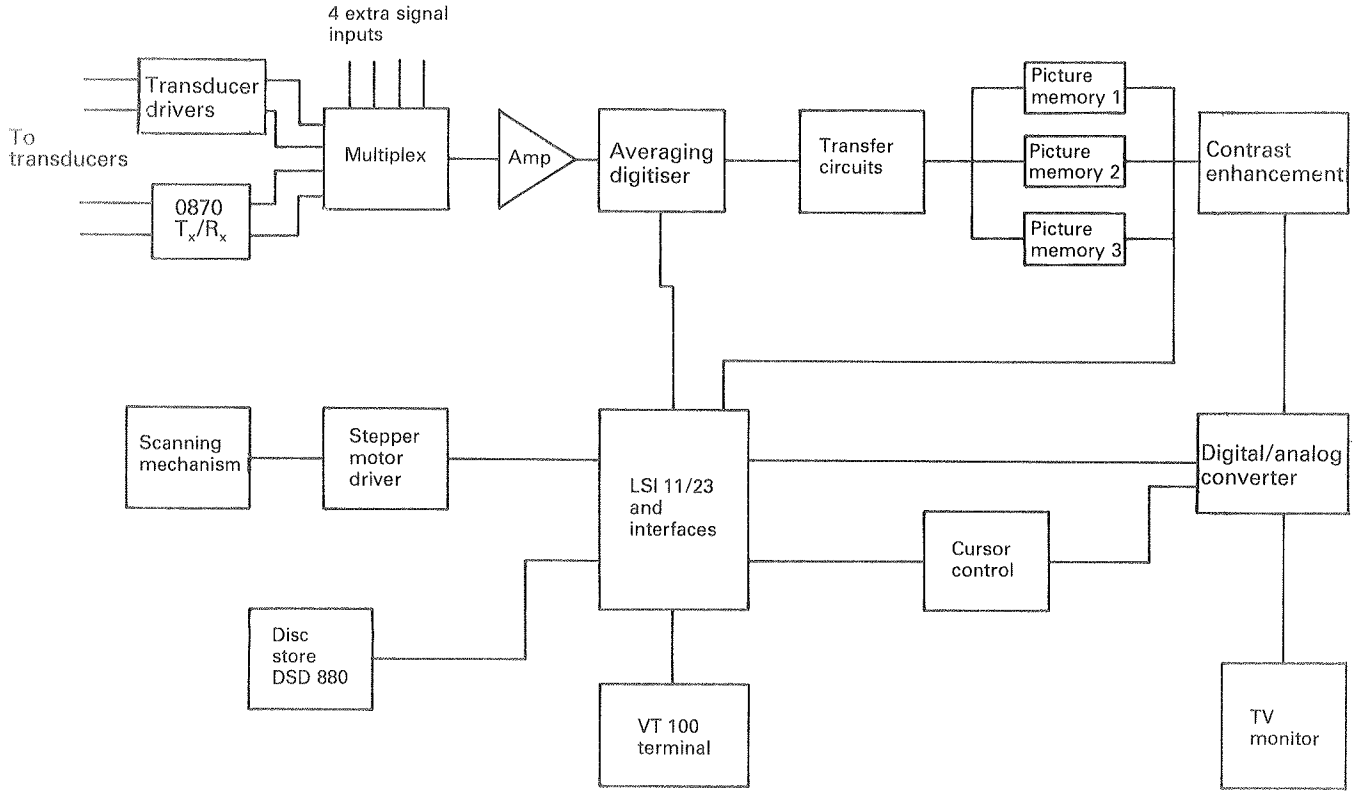

Fig.D1. Block diagram of the time-of-flight imaging system.

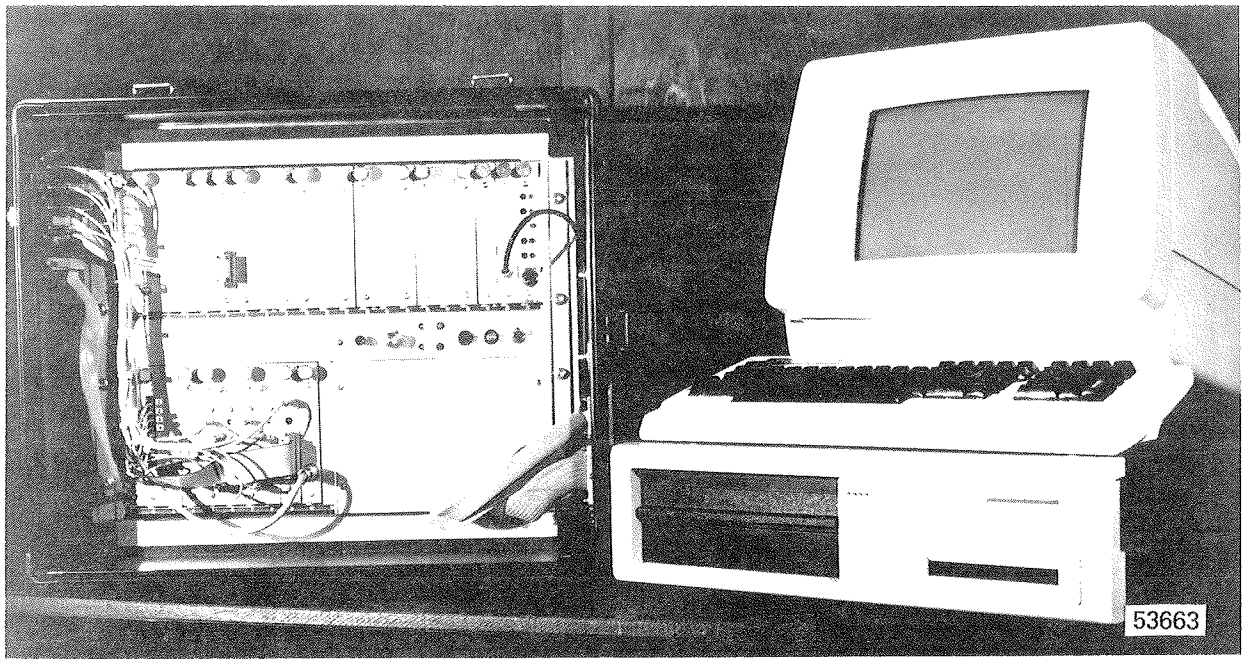

Fig.D2. Time-of-flight ultrasonic system for laboratory investigations: left, time-of-flight electronic package/computer, right, terminal/display and disc store unit.

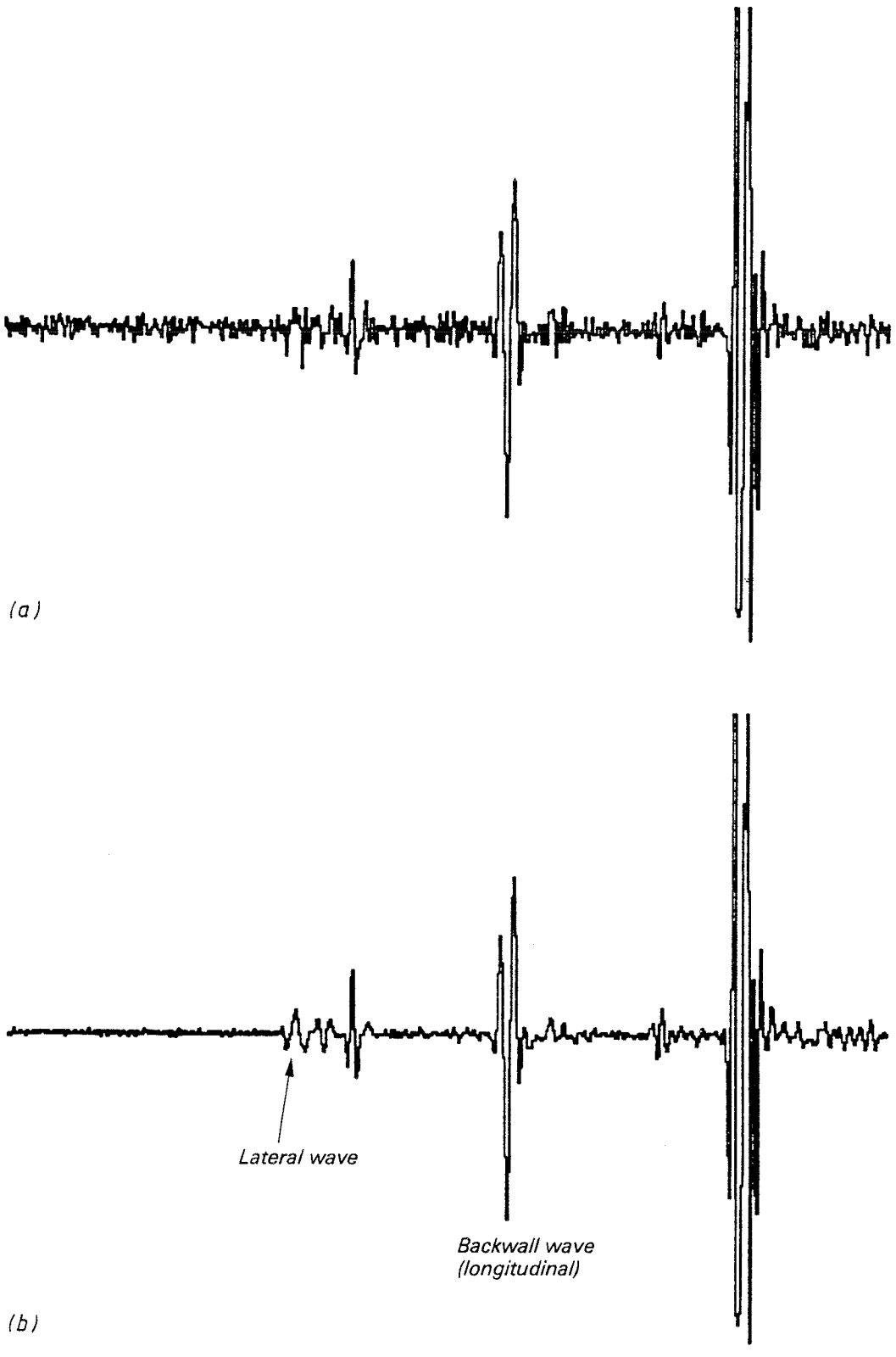

Fig.D3. A-scan reconstruction showing the effect of signal averaging, number of averages = 2^N:

a) N = 0 b) N = 5

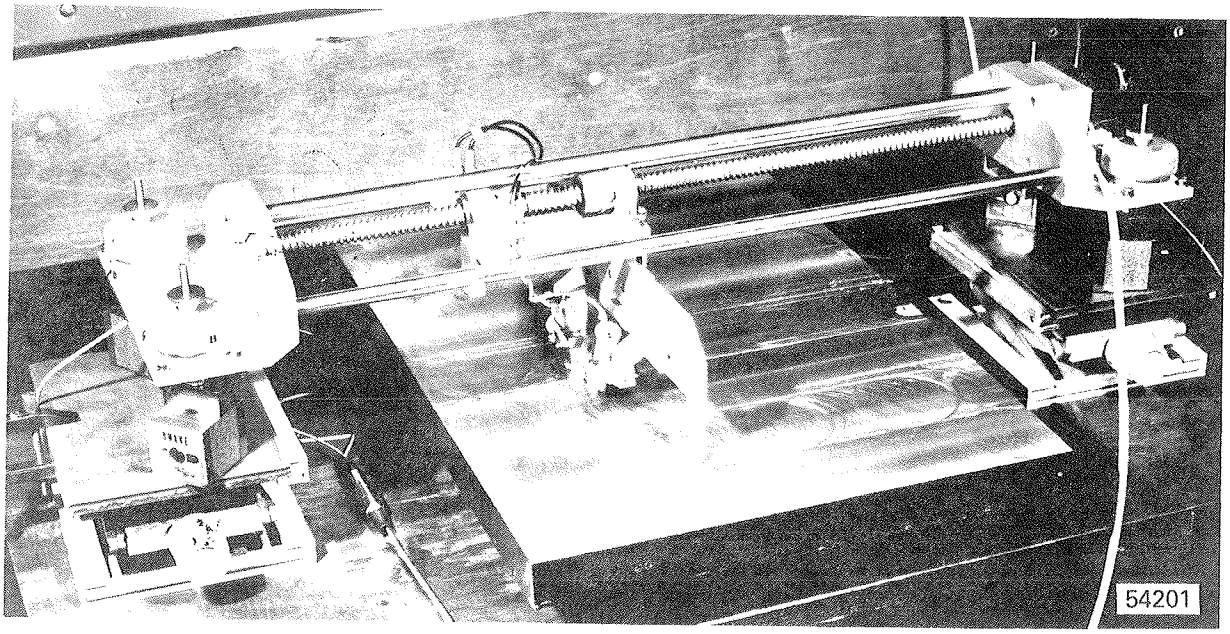

Fig.D4. Scanning rig positioned over specimen J302.

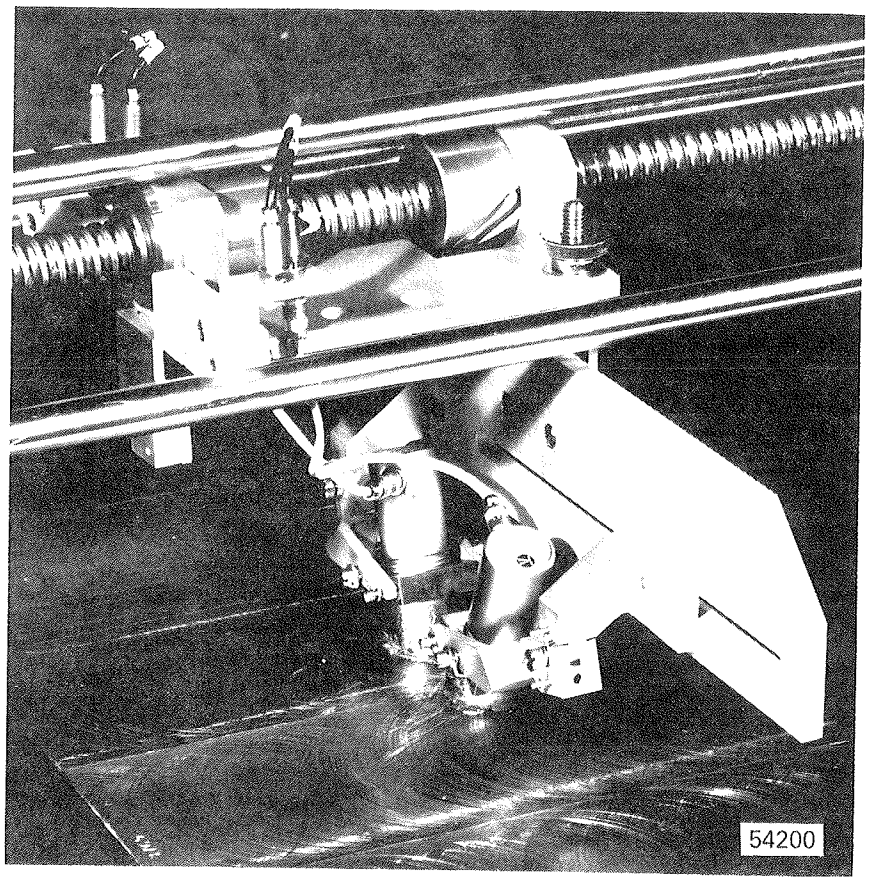

Fig.D5. Close-up of transducer assembly.

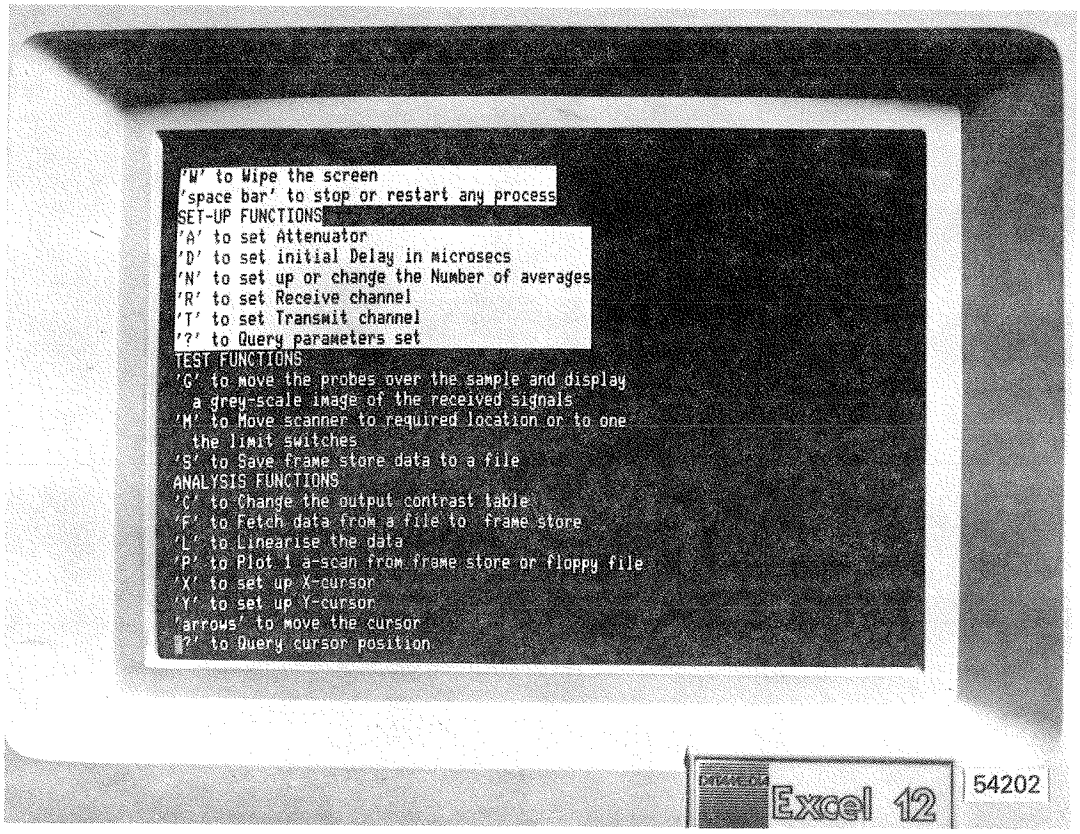

Fig.D6. Part of 'help-menu' displayed on the VDU screen. Active functions are displayed as highlighted text.

APPENDIX E

RESEARCH SPECIMENS

General Description

In a program such as this, where an NDE technique is being studied with respect to a particular type of joint (i.e. structural welds in bridges), it is highly desirable that the specimens used represent as closely as possible the conditions prevailing in such joints. To this end, all welded specimens produced were manufactured from an equivalent grade of steel to the ASTM A36 grade widely used in the United States for structural steelwork. Welding processes were representative of those widely used for welding bridge structures, namely shielded metal arc (SMA) and submerged arc welding (SAW). Surface finish was typical of that found in structural weldments, generally with weld crowns and root beads still present, although some samples were tested with weld crowns removed. Flaws introduced for study were "natural" flaws, and were intended to be representative of fabrication flaws only. Fatigue cracks were not included, one reason being that the capability of the time-of-flight technique for the measurement of surface breaking fatigue cracks has been documented previously (16, 17).

A total of 17 welded specimens were produced in three thicknesses of steel plate, (10mm, 38mm and 95mm (0.4in, 1.5in and 3.75in)). Additionally two specimens, one in each of the 38mm and 95mm plate thicknesses, were available from other work on tandem testing within this project. All nineteen welded specimens containing a total of 46 flaws were examined.

Material

Steels conforming to ASTM Grade A36, a typical structural grade, were used. Table E1 gives the chemical composition of the three plate thicknesses used for this investigation. The elements shown are those quoted in the chemical composition requirements for A36 steels.

Specimen Production

Welding was carried out entirely in a conventional manner using the SMA and SAW processes, except where conditions needed to be modified to introduce the required flaws. Details of the weld preparation and the dimensions of each specimen are given in Table E2. Four types of flaw were included;

i) Slag lines - linear inclusions produced by insufficient inter-run cleaning.

ii) Porosity clusters - spherical pores originating from some physical or chemical reaction releasing gas during welding.

iii) Lack of sidewall fusion - produced by using lower power gas metal arc (GMA) welding - to deposit the required area of the flaw. This method effectively casts metal into the joint with no fusion of the metal below because of insufficient heat input.

iv) Solidification cracking - produced by using a welding condition to give a deep, narrow weld bead, the shrinkage stresses on cooling causing the bead to rupture along the centre line.

All these mechanisms produce entirely natural flaws which are highly desirable for demonstrating the capabilities of NDT techniques. Furthermore, their location and dimensions can be closely controlled

during the welding operation, with the exception of porosity. Details of the population of different types of flaw in each specimen are given in Table E2.

Each specimen was clearly marked with its individual number, and reference points were identified according to the requirements of the AWS D1.1 code, Section 6.19. Surfaces A and B were identified (A being marked with a Y) and on both surfaces a centre line was marked on the weld cap representing X = 0. This enabled distance along the weld to be measured (from end Y) and identification of the surfaces A+,A-, B+,B-, the distance X being measured from the weld centre line.

Preliminary Non-Destructive Testing (NDT)

After welding all specimens were radiographed to establish whether the intended flaws had been produced successfully (Table E3). However, radiographs of the 95mm thick samples were of poor quality due to the lack of a sufficiently high energy X-ray source. All specimens were then subjected to a thorough manual ultrasonic examination in accordance with Welding Institute standard procedure NDT/P/2 (1984), which is based on British Standard 3923 Part 1, in order to confirm the presence of the flaws ultrasonically. From the ultrasonic test results "best" estimate plots of flaw location, and size for each specimen were produced. Table E4 gives a summary of flaw lengths and heights determined from these tests. Additionally 95mm and 35mm thick specimens were inspected following the procedures of the AWS D1.1 code in order to determine flaw severity class, as defined in Table 9.25.3 of the code, for later comparison with the time-of-flight results. Table E4 also gives the most serious severity class and associated accept/reject decision obtained from each test on each flaw.

Sectioning

Two specimens in the 95mm thickness and four in the 38mm thickness (Table E2) were sectioned to reveal the actual dimensions of the flaws present for correlation with the NDT results; a total of 21 flaws out of a possible 46. This sectioning was done in one of two ways. First, a brittle fracture technique was used for flaws of simple shape. This involved determination of a flaw's location from radiographic and ultrasonic data and cutting a full width slice containing it from the specimen. A shallow V notch was then milled in the surface of the slice directly above the position of the flaw to act as an initiator. The block was cooled in liquid nitrogen to promote brittle behaviour, thus ensuring minimal deformation. The sample was then fractured in a three-point bend loading mode, revealing the faces of the flaw for measurement of size and morphology (Fig. E1).

A second technique was employed for more complex flaws and those not suitable for brittle fracture, whereby cross-sections of the flaw were revealed by progressive sectioning. This involved isolating a block containing the flaw and then taking transverse sections (perpendicular to the X = 0 line) every 5mm (0.2in). This enabled the detail of the flaws cross-section to be clearly seen, and morphology along its length could be determined by interpolation of the flaw on each of the slices (Fig. E2). Note that 5mm was the thinnest slice which could be handled conveniently. Measurement of the through thickness dimension of flaws thus revealed was aided by Magnetic Particle Inspection (MPI).

In both cases all parts of the specimen were marked up and reference points for dimensions scribed on before cutting, so that positions of flaws in various sections could be related to the original datum points.

Various etched and freeze-broken sections are shown in Figs. E3 and E4. The types of flaw found and their sizes are given in Table E3.

Table E1. Plate Chemical Composition

Plate Thickness	Element, Wt%*				
	C	Mn	P	S	Si
10mm (0.4in)	0.045	0.28	< 0.005	0.025	< 0.01
38mm (1.5in)	0.17	1.37	< 0.005	< 0.005	0.44
95mm (3.75in)	0.18	1.42	0.020	0.026	0.23

* Elements shown are those quoted in the chemical composition requirements of ASTM Grade A36.

Table E2. Specimen Details

Specimen Number	Dimensions (L x W x D) mm	inches	Weld Preparation	Population of Intended Flaws Solidification Cracks	Lack of Side-Wall Fusion	Slag Line	Porosity
J301*+	340x540x94	(13.4x21.3x3.7)	Single "U"	4		–	–
J302*+	397x591x38	(15.6x23.3x1.5)	Single "V"	3	1	–	–
J303	448x426x93	(17.6x16.8x3.7)	Single "U"	3	–	–	1
J304	450x426x93	(17.7x16.8x3.7)	Single "U"	4	–	–	–
J305+	422x429x93	(16.6x16.9x3.7)	Single "U"	–	3	1	–
J306	400x447x93	(15.7x17.6x3.7)	Single "U"	–	4	–	–
J307+	451x415x39	(17.8x16.3x1.5)	Single "U"	1	2	1	–
J308+	302x297x40	(11.9x11.7x1.6)	Single "U"	1	1	–	–
J309+	298x296x40	(11.7x11.7x1.6)	Single "U"	–	1	1	–
J310	417x411x38	(16.4x16.2x1.5)	Double "V"	3	–	–	–
J311	449x414x38	(17.7x16.3x1.5)	Double "V"	1	–	–	1
J312	220x285x10	(8.7x11.2x0.4)	Single "V"	–	1	–	–
J313	220x289x10	(8.7x11.7x0.4)	Single "V"	–	1	–	–
J314	220x282x10	(8.7x11.1x0.4)	Single "V"	–	–	1	–
J315	143x208x10	(5.6x8.2x0.4)	Single "V"	–	–	–	1
J316	150x218x10	(5.9x8.6x0.4)	Double "U"	1	–	–	–

Table E2. Specimen Details, Continued

Specimen Number	Dimensions (L x W x D) mm	inches	Weld Preparation	Population of Intended Flaws Solidification Cracks	Lack of Side-Wall Fusion	Slag Line	Porosity
J317	152x218x10	(6.0x8.6x0.4)	Single "V"	1	-	-	-
J318	151x425x10	(5.9x16.8x0.4)	Single "V"	1	-	-	-
J319	152x428x10	(6.0x16.8x0.4)	Single "V"	1	-	-	-

* Specimens available from previous work on tandem testing.

+ Specimens sectioned.

Table E3a) Specimen Type and Size of Intended Flaws as Determined by Radiography and Destructive Tests (38mm Specimen).

Spec.	Flaw No.	Flaw Type	Radiographic Interpretation						Results of Destructive Test									
			"X" mm	(inches)	"Y" mm	(inches)	l mm	(inches)	"X" mm	(inches)	"Y" mm	(inches)	l mm	(inches)	d_{min} mm	(inches)	h_{max} mm	(inches)
J302	5	Solidification crack	0	-	62	(2.44)	63	(2.48)	0	-	62.5	(2.46)	60.5	(2.38)	15.0	(0.59)	9.5	(0.37)
	6	Solidification crack	- 4	(-0.16)	134	(5.28)	53	(2.09)	-4.0	(-0.16)	132.0	(5.20)	55.5	(2.19)	25.0	(0.98)	9.0	(0.35)
	7	Solidification crack	+ 5	(0.20)	199	(7.83)	64	(2.52)	5.5	(0.22)	194.5	(7.66)	65.5	(2.58)	3.0	(0.12)	10.0	(0.39)
	8	Lack of sidewall fusion	-17	(-0.67)	284	(11.18)	46	(1.81)	-17.5	(0.69)	278.0	(10.94)	45.5	(1.79)	3.0	(0.12)	8.5	(0.33)
J307	25	Lack of sidewall fusion	+10	(0.39)	47	(1.85)	46	(1.81)	12.0	(0.47)	40.0	(1.57)	52.0	(2.05)	1.5	(0.06)	7.0	(0.28)
	26	Solidification crack	- 3	(-0.12)	168	(6.61)	55	(2.17)	-1.5	(0.06)	169.0	(6.65)	50.0	(1.97)	20.0	(0.79)	8.0	(0.31)
	27	Lack of sidewall fusion	-12	(-0.47)	264	(10.39)	55	(2.17)	-9.0	(0.35)	258.5	(10.18)	49.0	(1.93)	6.0	(0.24)	14.5	(0.57)
	28	Slag	- 3	(-0.12)	363	(14.29)	52	(2.05)	1.0	(0.04)	357.5	(14.07)	52.5	(2.07)	22.5	(0.89)	10.5	(0.41)
J308	29	Lack of sidewall fusion	+12	(0.47)	16	(0.63)	64	(2.52)	11.5	(0.45)	26.5	(1.04)	56	(2.20)	3.0	(0.12)	6.0	(0.24)
	30	Solidification crack	0	-	175	(6.89)	56	(2.20)	-0.5	(0.02)	182.5	(7.19)	56	(2.20)	22.5	(0.89)	4.0	(0.16)
J309	31	Lack of sidewall fusion	-12	(-0.47)	93	(3.66)	55	(2.17)	-11	(0.43)	<98	(3.86)	>42	(1.65)	8.5	(0.33)	8.0	(0.31)
	32	Slag	0	-	203	(7.99)	64	(2.52)	0	-	<07	(8.15)	>60	(2.36)	26.0	(1.02)	7.5	(0.30)
J310	33	Solidification crack	9	(0.35)	83	(3.27)	63	(2.48)	-		-		-		-		-	
	34	Solidification crack	?	-	182?	(7.17)	40?	(1.57)	-		-		-		-		-	
	35	Solidification crack	0	-	302	(11.89)	62	(2.44)	-	-	-	-	-	-	-	-	-	
J311	36	Solidification crack	0	-	62	(2.44)	63	(2.48)	-		-		-		-		-	
	37	Linear porosity	-1	(-0.04)	187	(7.36)	37	(1.46)	-		-		-		-		-	

Table E3b) Specimen Details: Flaw Type and Size as Determined by Radiography and Destructive Tests (95mm Specimens)

Spec.	Flaw No.	Flaw Type	Radiographic Interpretation						Results of Destructive Tests									
			"X" mm	"X" (inches)	"Y" mm	"Y" (inches)	l mm	l (inches)	"X" mm	"X" (inches)	"Y" mm	"Y" (inches)	l mm	l (inches)	d_{min} mm	d_{min} (inches)	h_{max} mm	h_{max} (inches)
J301	1A	lack of sidewall fusion	-	-	16.0	(0.63)	37.0	(1.46)	16.0	(0.63)	23.0	(0.91)	28.0	(1.10)	37.5	(1.48)	12.5	(0.49)
	1	solidification crack	-	-	43.0	(1.69)	40.0	(1.57)	0.0	-	56.0	(2.20)	34.0	(1.34)	21.0	(0.83)	10.0	(0.39)
	2	solidification crack	-	-	130.0	(5.12)	32.0	(1.26)	-19.0	(-0.75)	115.0	(4.53)	65.0	(2.56)	22.5	(0.89)	10.5	(0.41)
	3	solidification crack	-	-	not visible on radiograph				-6.5	(-0.26)	213.0	(8.39)	37.0	(1.46)	47.5	(1.87)	3.5	(0.14)
	4	solidification crack	-	-	273.0	(10.75)	37.0	(1.46)	-4.5	(-0.18)	252.5	(9.94)	63.0	(2.48)	48.0	(1.89)	9.5	(0.37)
J303	9	solidification crack	-	-	45.0	(1.77)	38.0	(1.50)	-	-	-	-	-	-	-	-	-	-
	10	not confirmed radiographically			-	-	-	-	-	-	-	-	-	-	-	-	-	-
	11	solidification crack	-	-	251.0	(9.88)	55.0	(2.17)	-	-	-	-	-	-	-	-	-	-
	12	solidification crack	-	-	363.0	(14.29)	60.0	(2.36)	-	-	-	-	-	-	-	-	-	-
J304	13	not confirmed radiographically			-	-	-	-	-	-	-	-	-	-	-	-	-	-
	14	solidification crack	-	-	148.0	(5.83)	26.0	(1.02)	-	-	-	-	-	-	-	-	-	-
	15	solidification crack	-	-	261.0	(10.28)	18.0	(0.71)	-	-	-	-	-	-	-	-	-	-
	16	solidification crack	-	-	357.0	(14.06)	33.0	(1.30)	-	-	-	-	-	-	-	-	-	-
J305	17	slag line	-	-	25.0	(0.98)	50.0	(1.97)	-3.5	(-0.14)	22.0	(0.87)	51.0	(2.01)	72.5	(2.85)	11.5	(0.45)
	18	lack of sidewall fusion	-	-	148.0	(5.83)	52.0	(2.05)	9.0	(0.35)	145.0	(5.71)	53.5	(2.11)	55.0	(2.17)	10.0	(0.39)
	19	lack of sidewall fusion	-	-	220.0	(8.66)	52.0	(2.05)	-19.0	(-0.75)	220.0	(8.66)	50.0	(1.97)	29.0	(1.14)	11.0	(0.43)
	20	lack of sidewall fusion	-	-	319.0	(12.56)	53.0	(2.09)	-	-	310.0	(12.20)	48.0	(1.89)	21.0	(0.83)	15.0	(0.59)
J306	21	lack of sidewall fusion	-	-	46.0	(1.81)	30.0	(1.18)	-	-	-	-	-	-	-	-	-	-
	22	lack of sidewall fusion	-	-	107.0	(4.21)	40.0	(1.57)	-	-	-	-	-	-	-	-	-	-
	23	lack of sidewall fusion	-	-	273.0	(10.75)	37.0	(1.46)	-	-	-	-	-	-	-	-	-	-
	24	lack of sidewall fusion	-	-	337.0	(13.27)	35.0	(1.38)	-	-	-	-	-	-	-	-	-	-

Table E3c) Specimen Type and Size of Intended Flaws as Determined by Radiography and Destructive Test (10mm Specimens)

Spec.	Flaw No.	Flaw Type	Radiographic Interpretation						Results of Destructive Test									
			"X" mm	(inches)	"Y" mm	(inches)	l mm	(inches)	"X" mm	(inches)	"Y" mm	(inches)	l mm	(inches)	d_{min} mm	(inches)	h_{max} mm	(inch)
J312	38	Lack of sidewall fusion	+2.5	(+0.10)	89	(3.50)	30	(1.18)										
J313	39	Lack of sidewall fusion	-2.5	(-0.10)	116	(4.57)	30	(1.18)										
J314	40	Slag line	0	(0)	65	(2.56)	41	(1.61)										
J315	41	Porosity		-	46	(1.81)	35	(1.38)										
J316	42	Solidification crack	not visible on radiograph															
J317	43	Solidification crack	not visible on radiograph															
J318	44	Solidification crack	not radiographed															
J319	45	Solidification crack	not radiographed															

Table E4a). Summary of results from manual ultrasonic tests (TWI Procedures) and AWS D1.1 tests. 38mm specimens.

Specimen	Flaw No.	Manual Ultrasonic Test Results (TWI Procedures)										AWS D1.1 Tests	
		"X"		"Y"		"l"		d_{min}		h_{max}		Severity Class	Accept/ Reject
		mm	(in)	mm	(in)	mm	(in)	mm	(in)	mm	(in)		
J302	5	0	(0)	55	(2.17)	65	(2.56)	13	(0.51)	9	(0.35)	B	Reject
	6	-6	(0.24)	135	(5.31)	49	(1.93)	24	(0.94)	4	(0.16)	A	Reject
	7	5	(0.20)	190	(7.48)	61	(2.40)	2	(0.08)	5	(0.20)	C	Reject
	8	-19	(-0.75)	284	(10.40)	46	(1.81)	3	(0.08)	5	(0.20)	A	Reject
J307	25	13	(0.51)	38	(1.50)	51	(2.01)	6	(0.24)	1	(0.04)	-	-
	26	-1	(-0.04)	160	(6.30)	65	(2.56)	19	(0.75)	1	(0.04)	A	Reject
	27	-11	(-0.43)	260	(10.24)	52	(2.05)	16	(0.63)	3	(0.12)	A	Reject
	28	-1.5	(-0.06)	358	(14.09)	49	(1.93)	24	(0.94)	2	(0.08)	A	Reject
J308	29	-10.5	(-0.41)	35	(1.38)	43	(1.69)	17.5	(0.69)	2.5	0.10	A	Reject
	30	5	(0.20)	173	(6.81)	97	(3.82)	22	(8.66)	2	(0.08)	A	Reject
J309	31	+11.5	(0.45)	93	(3.66)	63	(2.48)	14	(0.55)	2	(0.08)	D	Accept
	32	+2.5	(0.10)	206	(8.11)	59	(2.32)	24.5	(0.96)	3	(0.12)	A	Reject
J310	33	+3.5	(1.38)	86	(3.39)	43	(1.69)	29.5	(1.16)	3	(0.12)	-	-
	34	-4.5	(-1.77)	206	(8.11)	37	(1.46)	9	(3.54)	2	(0.08)	-	-
	35	0	(0.00)	284	(11.18)	82	(3.23)	10.5	(0.41)	1.5	(0.06)	-	-
J311	36	-1	(-0.04)	55	(2.17)	78	(3.07)	21	(0.83)	3.5	(0.14)	-	-
	37	+6	(0.24)	170	(6.69)	46	(1.81)	18	(0.71)	2	(0.08)	-	-

Table E4b. Summary of results from manual ultrasonic tests (TWI Procedures) and AWS D1.1 Tests 95mm Specimens

Specimen	Flaw No.	Manual Ultrasonic Test Results (TWI Procedures)										AWS D1.1 Tests	
		"X"		"Y"		"l"		d_{min}		h_{max}		Severity Class	Accept/ Reject
		mm	(in)	mm	(in)	mm	(in)	mm	(in)	mm	(in)		
	1A	+19	(0.75)	21	(0.83)	34	(1.34)	38	(1.50)	6	(0.24)	B	Reject
J301	1	+3	(0.12)	56	(2.20)	27	(1.06)	20	(0.79)	5.5	(0.22)	A	"
	2	-5	(-0.20)	109	(4.29)	66	(2.60)	20.5	(0.81)	5.5	(0.22)	A	"
	3	+4	(0.16)	226	(8.90)	39	(1.54)	48	(1.89)	6.5	(0.26)	A	"
	4	+1	(0.04)	273	(10.75)	42	(1.65)	47	(1.85)	8	(0.31)	A	"
J303	9	+6	(0.24)	45	(1.77)	50	(1.97)	69.5	(2.74)	3.5	(0.14)	A	Reject
	10	-8	(-0.31)	123	(4.84)	78	(3.07)	53	(2.09)	8	(0.31)	A	"
	11	+10	(0.39)	240	(9.45)	65	(2.56)	31	(1.22)	8	(0.31)	A	"
	12	+4	(0.16)	352	(13.86)	58	(2.28)	20	(0.79)	0	(0.0)	A	"
J304	13	+7	(0.28)	50	(1.97)	79	(3.11)	67	(2.64)	11	(0.43)	A	Reject
	14	-2	(-0.08)	156	(6.14)	70	(2.76)	59	(2.32)	3.5	(0.14)	A	"
	15	+13	(0.51)	257	(10.12)	41	(1.61)	33.5	(1.32)	3	(0.12)	A	"
	16	-5	(-0.20)	348	(13.70)	44	(1.73)	21.5	(0.85)	3.5	(0.14)	A	"
J305	17	-3	(-0.14)	25	(0.98)	60	(2.36)	72	(2.83)	8	(0.31)	A	"
	18	+7	(0.28)	149	(5.87)	41	(1.61)	51.5	(2.03)	7	(0.28)	A	"
	19	-19	(-0.75)	221	(8.70)	50	(1.97)	35	(1.38)	6	(0.24)	A	"
	20	+14	(0.55)	311	(12.24)	56	(2.20)	26	(1.02)	5	(0.20)	D	Accept
J306	21	-1	(-0.04)	32	(1.26)	44	(1.73)	70.05	(2.78)	5.5	(0.22)	A	Reject
	22	+21	(0.83)	84	(3.31)	17	(0.67)	31	(1.22)	2	(0.08)	A	"
	23	-10	(-0.39)	177	(6.97)	47	(1.85)	55	(2.17)	3	(0.12)	A	"
	24	+23	(0.91)	299	(11.77)	41	(1.61)	19	(0.75)	5	(0.20)	D	Accept

TABLE E4c. Summary of results from manual ultrasonic tests (TWI procedures) 10mm specimens.

Specimen	Flaw No.	Manual Ultrasonic Test-Results (TWI Procedures) "X" mm	(in)	"Y" mm	(in)	l mm	(in)	d_{min} mm	(in)	h_{max} mm	(in)
J312	38	+3	(0.12)	89	(3.50)	30	(1.18)	4	(0.16)	3	(0.12)
J313	39	-2	(-0.08)	116	(4.57)	30	(1.13)	5	(0.20)	25	(0.10)
J314	40	2	(0.08)	72	(2.83)	34	(1.34)	4	(0.16)	1.5	(0.06)
J315	41	*	-	60	(2.36)	22	(0.87)	4	(0.16)	1	(0.04)
J316	42	+2	(+0.08)	61	(2.40)	55	(2.17)	1	(0.04)	2.5	(0.10)
J317	43	0.5	(-0.02)	47	(1.85)	23	(0.91)	3	(0.12)	2	(0.80)
J318	44	1	(0.04)	49	(1.93)	58	(2.28)	7	(0.28)	-	
J319	45	1	(0.04)	63	(2.48)	31	(1.22)	8	(0.31)	-	

* Porosity cluster

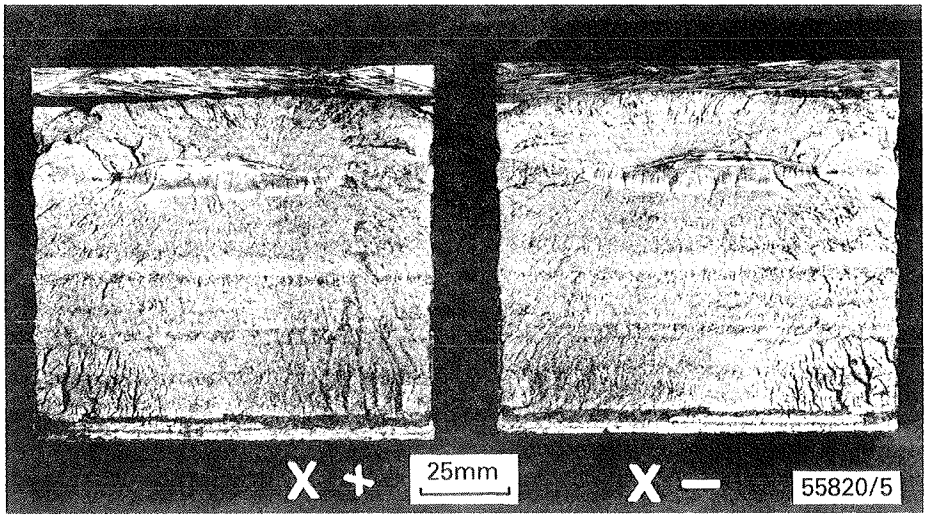

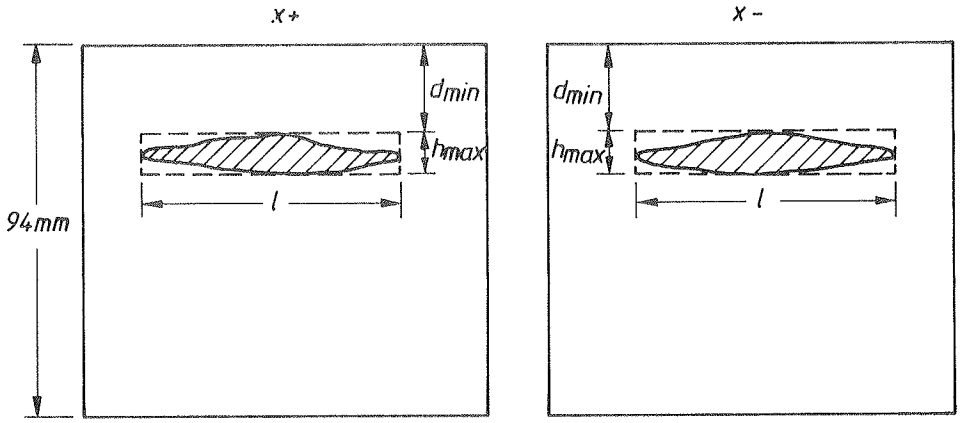

Fig.E1. Flaw profile determined from fracture faces. Flaw 2 (J301), solidification crack.

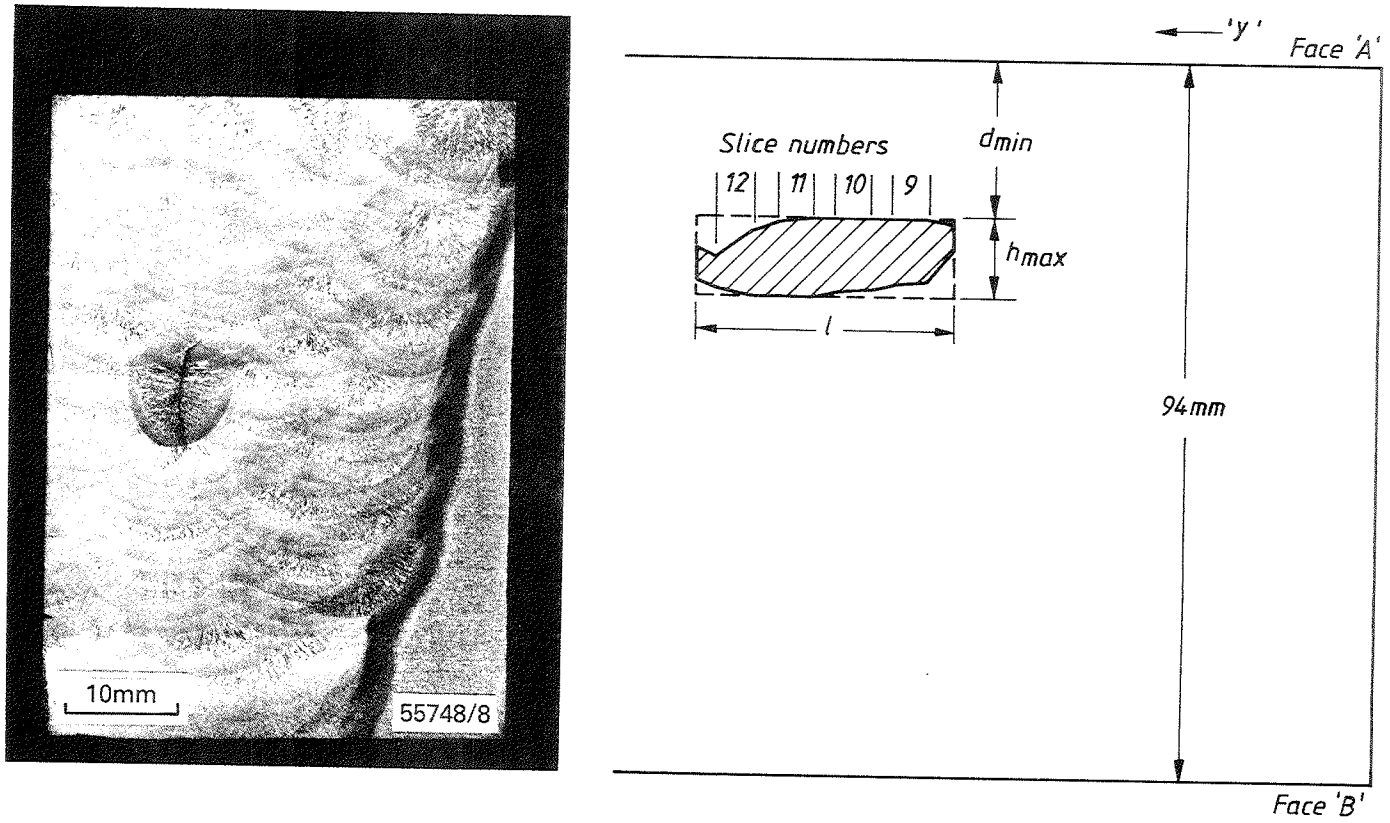

Fig.E2. Flaw profile determined by progressive sectioning, flaw 1 J301, solidification crack.

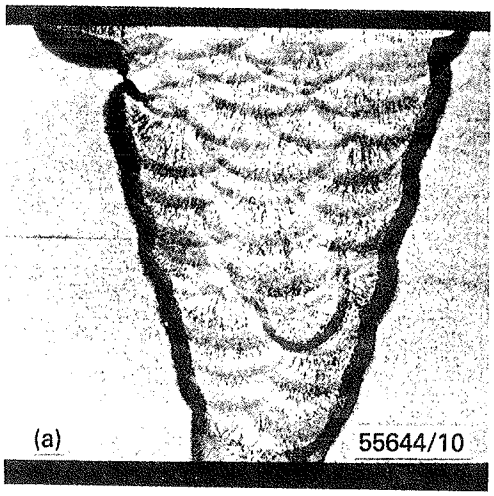

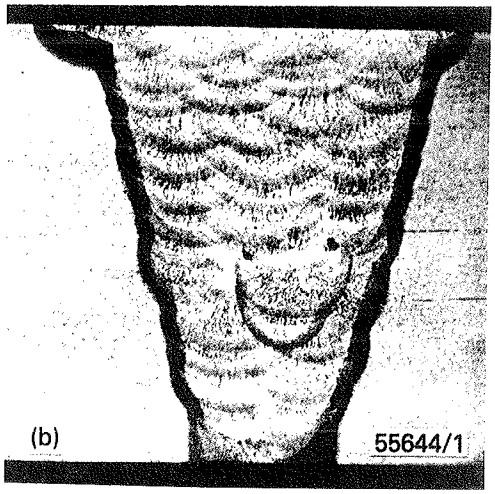

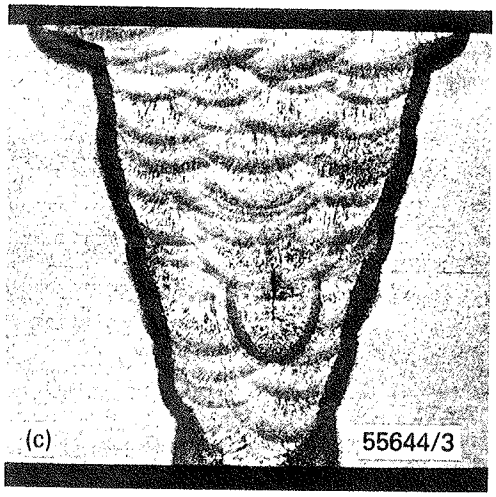

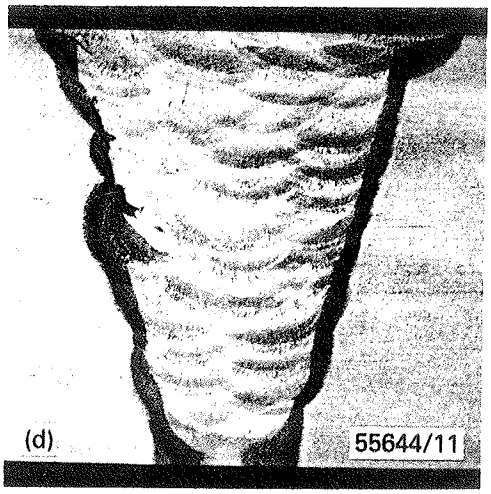

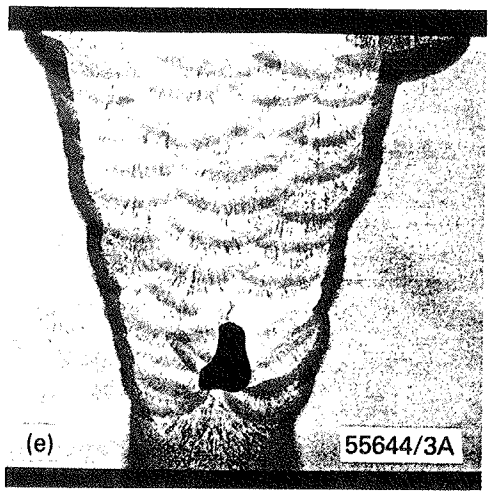

10mm

Fig.E3. Polished and etched sections through flaws in J307:

a) lack of sidewall fusion, flaw 25
b) unintentional flaws, slag entrapments and cracks in HAZ
c) solidification crack, flaw 26
d) lack of sidewall fusion, flaw 27
e) slag line with crack, flaw 28

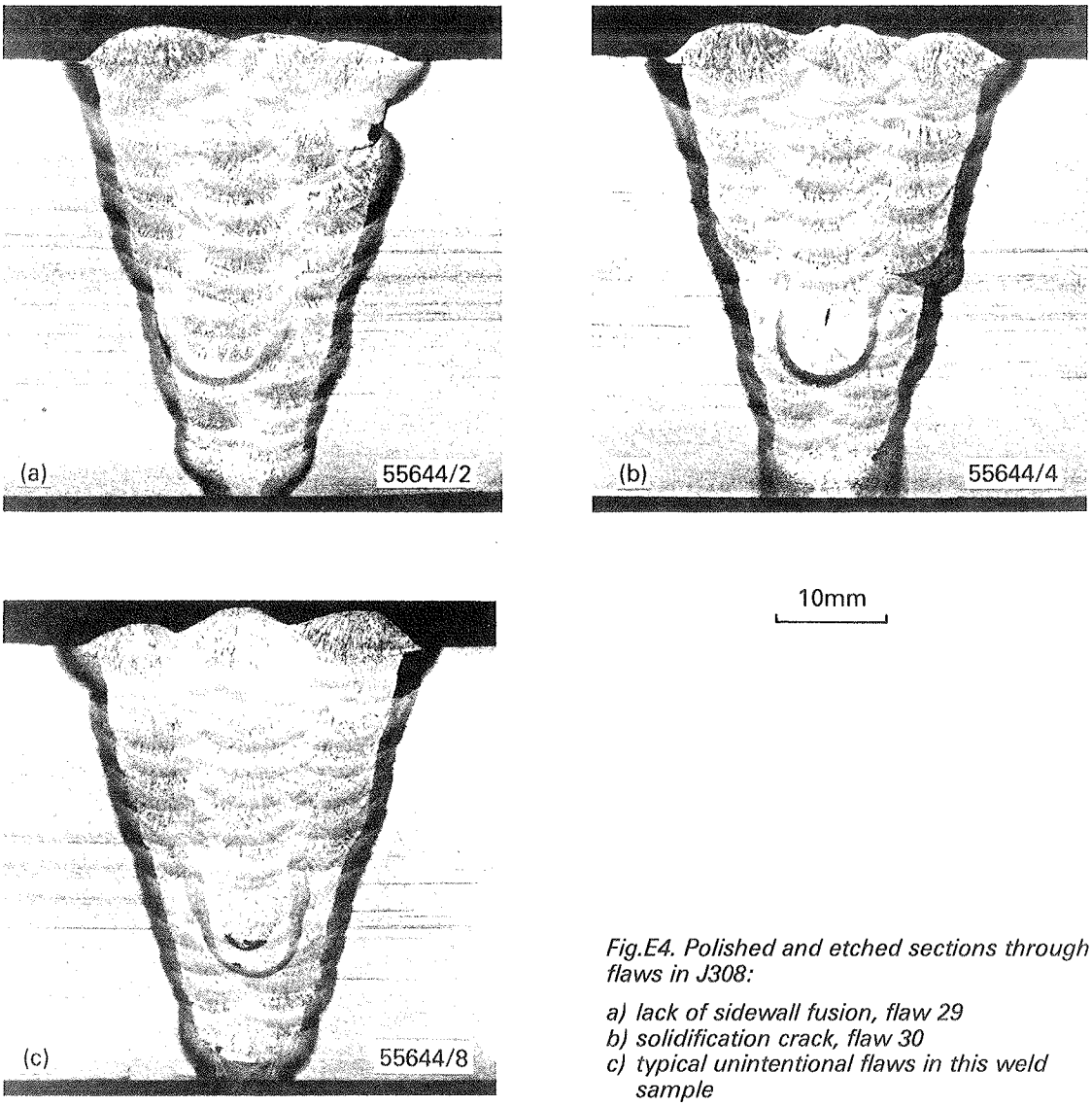

Fig.E4. Polished and etched sections through flaws in J308:

a) lack of sidewall fusion, flaw 29
b) solidification crack, flaw 30
c) typical unintentional flaws in this weld sample

APPENDIX F

TIME-OF-FLIGHT TEST PROCEDURES

As the time-of-flight technique for flaw location and sizing is a non-standard technique (i.e. it is still under development) and employs non-standard equipment, test procedures were not in existence at the outset of the project. As a result of trials prior to the commencement of the main testing activity and experience during the course of the program these have now been defined. The procedures are based on practical experience with the time-of-flight system developed for this project described in Appendix D. The procedures followed are given in the following document, F1.

The transducer centre separation for each weld geometry and plate thickness was determined initially by the requirement for a minimum of two scans from each scanning surface and values were found by overlaying a diagram of the spread of the ultrasonic beam on a sketch of the weld. A table of scan parameters required for each plate thickness and joint preparation are given in Table F1 and details of the scans actually carried out on each specimen are to be found in Table F2. As predicted, it proved difficult to interpret signals arising from flaws in the thinnest plate (10mm), therefore only a limited number of tests were performed on these - one from each test surface.

NDT/RP/5 PROCEDURE FOR TIME-OF-FLIGHT DATA ACQUISITION AND ANALYSIS USING Mk II SYSTEM JULY 1984

This procedure covers the use of the Mk II system for the collection, display and analysis of ultrasonic time-of-flight data. Use of the computer as a stand-alone unit is covered elsewhere.

Start-up procedures

i) Power-up: By use of an appropriate extension lead and multiway adapters all units are powered up together. On power-up the computer operating system boots itself (i.e. initiates operation) and some introductry text is displayed on the VDU screen. Should the system fail to boot, type:

173000G

ii) Set system date by typing e.g.

DATE 20-JUL-84 (return)

iii) To run the time-of-flight program type

RUN TOFT3 (return)

iv) The user is then asked to select the mode of operation

1. set up for test,
2. perform test,
3. analyse results.

Active commands may be listed at any time by typing **H.** The command **E** is used to exit from the program or to change the mode of operation.

Setting up for a test

Practical aspects;

i) Position scanner on test piece - such that the lead screw is over the weld centre line. Activate magnetic clamps to hold scanner firmly in position, level and adjust height to give adequate pressure on the transducers, once in place. It is important that the lead screw be parallel with the test surface otherwise, due to the mechanism for spring loading the transducers, the transducer separation will not be constant along the scan length.

ii) Choice of transducer angle - select polystyrene wedges to give 60° refracted angle in steel unless beam centres are required to intersect at depths in excess of 50mm in which case select 45°, or plate thickness is around 10mm in which case select 70°.

iii) Transducer centre separation - chosen on consideration of:-

a) depth of intersection of the beam centres (Fig. F1)

b) theoretical angular divergence of the ultrasonic beam (Fig. F2) overlaid on a scale drawing of the weld preparation (e.g. Fig. F3) to give a suitable depth zone.

This determines the number of scans that must be carried out from each surface to ensure coverage of the whole weld volume. It is recommended that a minimum of two scans are carried out from each test surface.

iv) Ensure that adequate couplant is used. Light machine oil has been found to be most suitable, but glycerin or a proprietary coupling gel (low viscocity) are possible alternatives. Industrial grease is not recommended due to its high viscocity.

Parameters required by the computer program

i) Transmit and receive channels i.e. time-of-flight or pulse echo are selected using the **Z** command. Fig. F4 shows the connections required on the side panel of the skypack container. Once selected, the A-Scan is displayed on the TV monitor.

ii) Set the number of averages 2^N using the **N** command. Normally N = 8.

iii) Generally the signals of interest do not occur within the first 512 sample (24.4 μs) time window and it is necessary to delay

the start of the trace. Delay (**D** command) may be calculated from the transducer centre separation and a knowledge of delay time in the polystyrene transducer wedges or by stepping through the A-Scan trace until the lateral wave, longitudinal backwall wave and if possible (depending on the specimen thickness) the half longitudinal/half shear backwall wave are visible on the monitor screen (Fig. F5).

iv) Attenuation (**A** command); in general for time-of-flight testing maximum sensitivity is required (i.e. 0dB attenuation), except for thinner specimens where some attenuation may be required (up to 6dB).

Performing a test

i) Position scanner at start using **M** command. Scan start is measured from datum to centre of transducer.

ii) Scan is started by typing **G.** The value of the scan increment (= 1mm) and the number of increments must be entered when requested by the computer program. Scanning will then start under computer control and the B-Scan picture is built up in real time on the TV monitor. The backwall and lateral waves should be observed closely as gross disturbances could be indicative of loss of coupling.

iii) Storing data. After 256 increments the scan will stop as the picture must be stored, using the **S** command, if data is not to be lost. The format for data-filename specification is

(Specimen identification) (Scan No.).**DAT**

Where: (Spec. id) is a field of 4 characters identifying the specimen

(Scan No.) is a field of 2 characters identifying the scan number

e.g. **J30701.DAT**

Header information is not stored until the whole scan is completed.

iv) Steps ii and iii are repeated until the scan is completed, with the exceptions that scan increment and number of increments are not repeatedly requested by **G** or file name by **S.**

v) Header information, to identify the scan, is stored when the final frame has been stored. The following information is requested:-

Date,

Name of sample,

Sample orientation,

Sample thickness,

Transducer centre separation,

Scan start position as mm from datum,

Scan finish position as mm from datum,

Any other remarks.

Analysis of results

Flaw detection

i) Recall the stored data (**F** - fetch command) and select display with markers for distance across the specimen every 50mm.

ii) Contrast enhance the picture as necessary (Tables 3 or 8 using the **C** command) for flaw detection.

iii) Summon up Y cursor and use it to identify the extremeties of any flaw, attempting to take into account beam spread effects. The cursor position as scan increments from the start of the present page is displayed on the VDU screen.

Measurement of flaw depth below the test surface and its height

i) The time data must be linearised to represent distance into the material but first the position of the lateral wave must be determined

EITHER- from a page of the B-Scan data (Fig. 7) above. An X cursor is used to identify the first white-to-black transition of the lateral wave, in terms of the number of picture points from the edge of the picture.

OR- A line of A-Scan from the picture (Fig. F5) may be plotted (**P** command) and the X cursor used to identify the first negative to positive zero crossing of the lateral wave.

ii) Linearise the data using the **L** command. To get a one to one depth ratio on a hard copy of the screen the maximum depth plotted is 190mm. A linearised plot, with distance markers if required, is then displayed on the TV monitor.

iii) In order to identify the picture the **A** command may be used to display alphanumeric characters on the TV monitor.

iv) Take a hard copy of each page of the linearised data and record on each the filename and page number and any other data required to identify it if not entered under (iii) above.

v) Flaw depth and height, where the signals from the top and bottom are resolvable, may then be measured directly from the hard copy output as long as the scale is 1:1, remembering to take phase changes into account.

TABLE F1. Scans required for each plate thickness and joint preparation.

Specimen thickness mm	(inch)	Joint preparation	angle	Test surface	Probe angle deg.	Probe separation 2S mm	(inch)
38	(1.5)	Single "V"	60° included angle	A	60	70	(2.76)
				A	60	100	(3.94)
				B	60	100	(3.94)
				B	60	70	(2.76)
				B	60	40	(1.57)
38	(1.5)	Single "U"	15° semi-angle	A	60	80	(3.15)
				A	60	65	(2.56)
				B	60	100	(3.94)
				B	60	70	(2.76)
				B	60	40	(1.57)
38	(1.5)	Double "V"	60° included angle	A	60	90	(3.54)
				A	60	70	(2.76)
				B	60	70	(2.76)
				B	60	95	(3.74)
95	(3.74)	SIngle "U"	15° semi-angle	A	60	100	(3.94)
				A	45	110	(4.33)
				B	45	100	(3.94)
				B	45	170	(6.70)
				B	60	80	(3.15)
10	(0.39)	-	-	A	70	45	(1.77)
				B	70	38	(1.50)

TABLE F2a. Time-of-flight scan data - 38mm specimens.

Specimen	Scan number	Test surface	Probe deg.	Probe separation mm	(inch)	Scan start mm	(inch)	Scan finish mm	(inch)
J302	1	A	60	70	(2.76)	10	(0.39)	292	(11.50)
	2	A	60	100	(3.94)	10	(0.39)	326	(12.83)
	3	A	60	38	(1.50)	10	(0.39)	326	(12.83)
	4	B	60	100	(3.94)	10	(0.39)	386	(15.20)
	5	B	60	70	(2.76)	9	(0.35)	385	(15.16)
	6	B	60	40	(1.57)	10	(0.39)	385	(15.16)
J307	1	A	60	80	(3.15)	0	(0)	435	(17.13)
	2	A	60	68	(2.68)	0	(0)	435	(17.13)
	3	B	60	100	(3.94)	7	(0.28)	435	(17.13)
	4	B	60	70	(2.76)	7	(0.28)	435	(17.13)
	5	B	60	40	(1.57)	7	(0.28)	435	(17.13)
J308	1	A	60	80	(3.15)	10	(0.39)	290	(11.42)
	2	A	60	62	(2.44)	10	(0.39)	290	(11.42)
	3	B	60	40	(1.57)	10	(0.39)	290	(11.42)
	4	B	60	70	(2.76)	10	(0.39)	290	(11.42)
	5	B	60	100	(3.94)	10	(0.39)	290	(11.42)
J309	1	A	60	80	(3.15)	10	(0.39)	290	(11.42)
	2	A	60	64	(2.52)	10	(0.39)	290	(11.42)
	3	B	60	40	(1.57)	10	(0.39)	290	(11.42)
	4	B	60	70	(2.76)	10	(0.39)	290	(11.42)
	5	B	60	100	(3.94)	10	(0.39)	290	(11.42)
J310	1	A	60	88	(3.46)	12	(0.47)	402	(15.83)
	2	A	60	72	(2.83)	12	(0.47)	402	(15.83)
	3	B	60	94	(3.70)	12	(0.47)	402	(15.83)
	4	B	60	66	(2.60)	12	(0.47)	402	(15.83)
J311	1	A	60	88	(3.46)	12	(0.47)	454	(17.87)
	2	A	60	72	(2.83)	12	(0.47)	448	(17.64)
	3	B	60	94	(3.70)	12	(0.47)	448	(17.64)
	4	B	60	68	(2.68)	12	(0.47)	448	(17.64)

TABLE F2b. Time-of-flight scan data - 95mm specimens.

Specimen	Scan number	Test surface	Probe angle deg.	Probe separation mm	(inch)	Scan start mm	(inch)	Scan finish mm	(inch)
J301	1	A	60	100	(3.94)	12	(0.47)	328	(12.91)
	2	A	45	110	(4.33)	12	(0.47)	328	(12.91)
	3	B	45	100	(3.94)	12	(0.47)	328	(12.91)
	4	B	45	170	(6.70)	12	(0.47)	328	(12.91)
	5	B	60	80	(3.15)	12	(0.47)	328	(12.91)
J303	1	A	45	110	(4.33)	12	(0.47)	407	(16.02)
	2	A	60	100	(3.94)	12	(0.47)	407	(16.02)
	3	B	60	80	(3.15)	12	(0.47)	292	(11.50)
	4	B	45	100	(3.94)	12	(0.47)	432	(17.01)
	5	B	45	170	(6.70)	12	(0.47)	432	(17.01)
	6	B	60	80	(3.15)	250	(9.84)	435	(17.13)
J304	1	A	60	100	(3.94)	13	(0.51)	405	(15.94)
	2	A	45	110	(4.33)	13	(0.51)	405	(15.94)
	3	B	60	80	(3.15)	8	(0.31)	438	(17.24)
	4	B	45	100	(3.94)	8	(0.31)	438	(17.24)
	5	B	45	170	(6.70)	8	(0.31)	438	(17.24)
J305	1	A	60	100	(3.94)	13	(0.51)	405	(15.94)
	2	A	45	110	(4.33)	13	(0.51)	405	(15.94)
	3	B	60	80	(3.15)	10	(0.39)	413	(16.26)
	4	B	45	100	(3.94)	9	(0.35)	412	(16.22)
	5	B	45	170	(6.70)	10	(0.39)	413	(16.26)
J306	1	A	45	110	(4.33)	12	(0.47)	392	(15.43)
	2	A	60	100	(3.94)	12	(0.47)	392	(15.43)
	3	B	45	170	(6.70)	10	(0.39)	293	(11.54)
	4	B	45	100	(3.94)	10	(0.39)	293	(11.54)
	5	B	60	80	(3.15)	10	(0.39)	390	(15.35)

TABLE F2c. Time-of-flight scan data 10mm specimens.

Specimen	Scan number	Test surface	Probe angle	Attenuation dB	Probe separation mm	(inch)	Scan start mm	(inch)	Scan finish mm	(inch)
J312	1	A	70	12	45	(1.77)	70	(2.76)	150	(5.91)
	2	B	70	6	38	(1.50)	70	(2.76)	150	(5.91)
J313	1	A	70	12	45	(1.77)	-3	(-0.12)	192	(7.56)
	2	B	70	6	38	(1.50)	-3	(-0.12)	197	(7.76)
J314	1	A	70	12	48	(1.89)	-2	(0.08)	194	(7.64)
	2	B	70	6	38	(1.50)	-2	(-0.08)	194	(7.64)
J315	1	A	70	6	47	(1.85)	3	(0.12)	126	(4.96)
	2	B	70	6	38	(1.50)	3	(0.12)	121	(4.76)
J316	1	A	70	6	45	(1.77)	3	(0.12)	133	(5.24)
	2	B	70	6	38	(1.50)	2	(0.08)	132	(5.20)
J317	1	A	70	6	45	(1.77)	3	(0.12)	134	(5.28)
	2	B	70	6	38	(1.50)	2	(0.08)	132	(5.20)
J318	1	A	70	6	45	(1.77)	9	(0.35)	139	(5.47)
	2	B	70	6	38	(1.50)	10	(0.39)	144	(5.67)
J319	1	A	70	6	45	(1.77)	9	(0.35)	141	(5.55)
	2	B	70	6	38	(1.50)	10	(0.39)	142	(5.59)

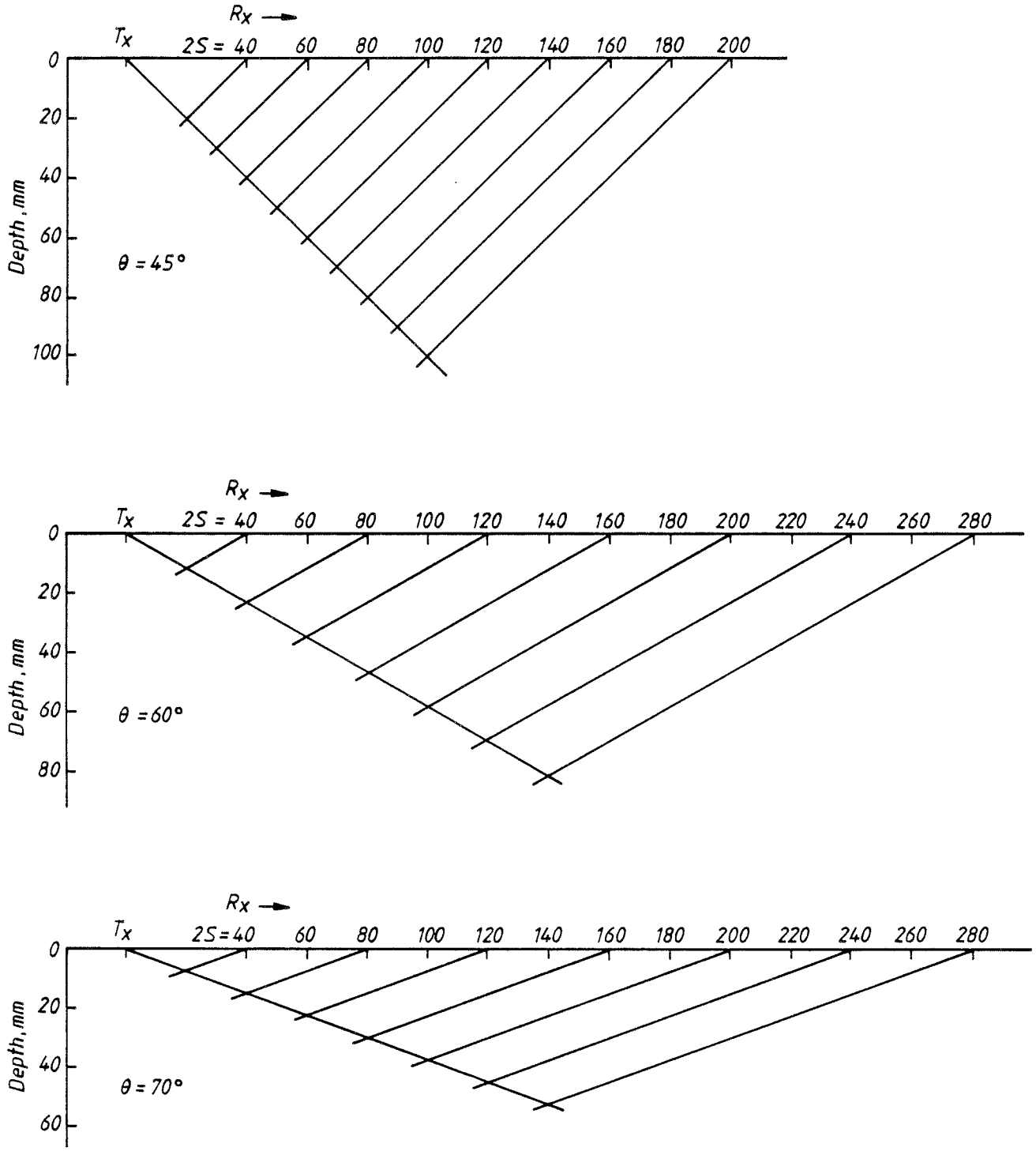

Fig.F1. Variation of depth of intersection of beam axes with probe separation (2S) for 45, 60 and 70° probes.

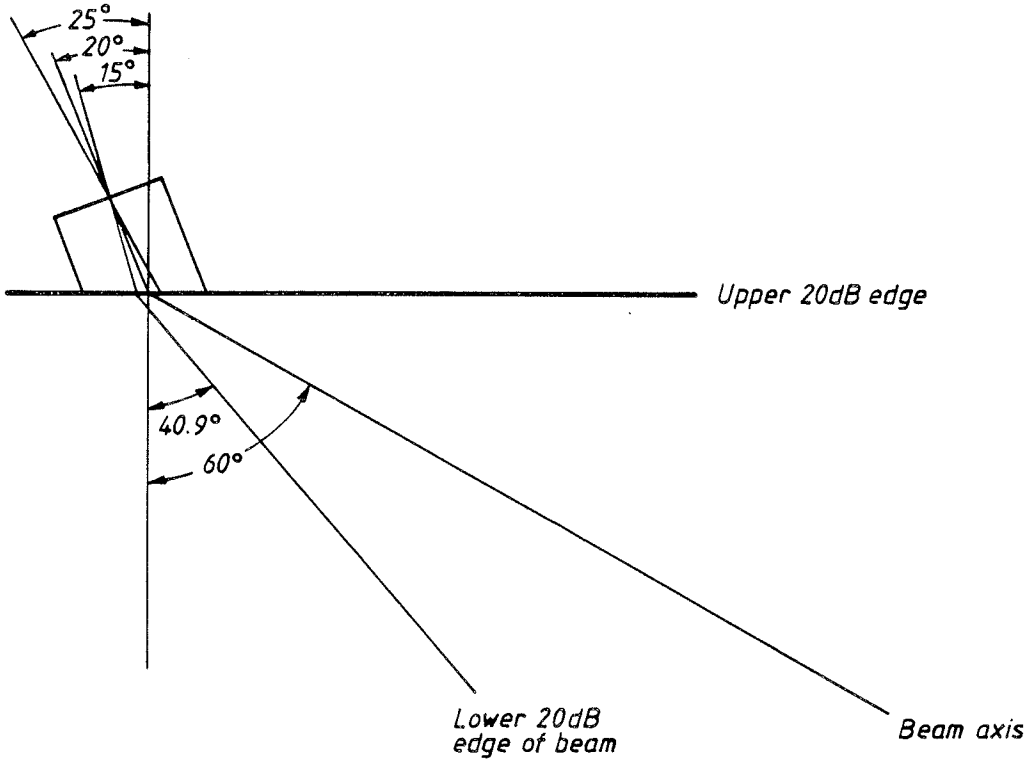

Fig.F2. Theoretical angular divergence of ultrasonic beam, 20dB edges, 60° refracted angle in steel.

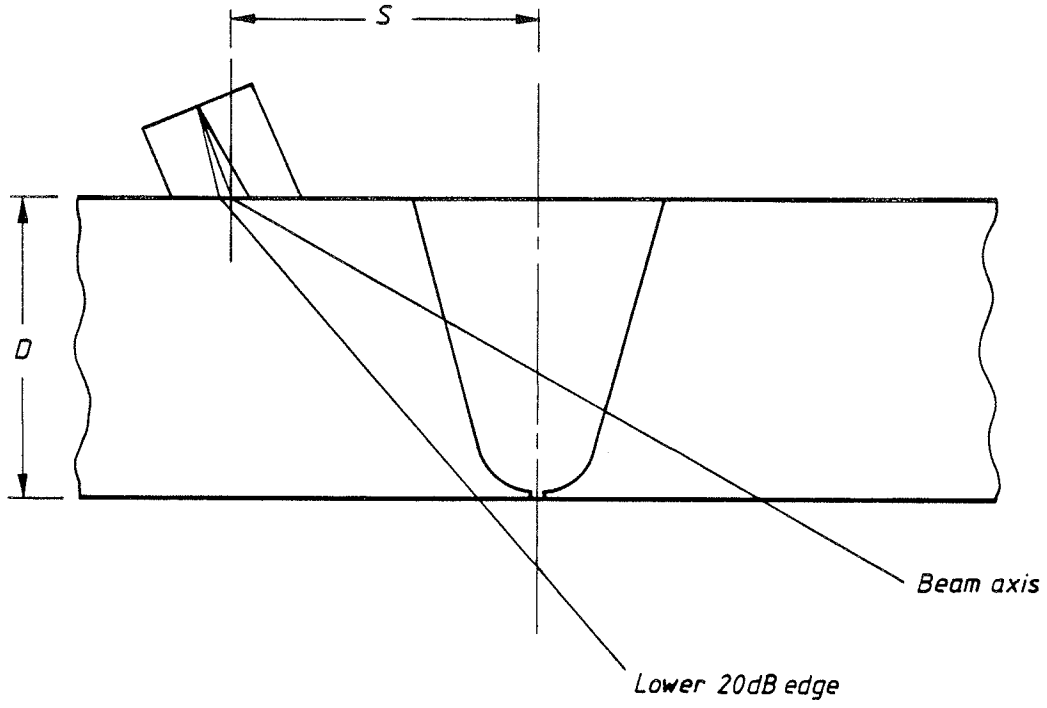

Fig.F3. Theoretical 20dB beam spread overlaid on sketch of weld preparation, showing coverage of whole weld volume. S = 40mm, D = 40mm.

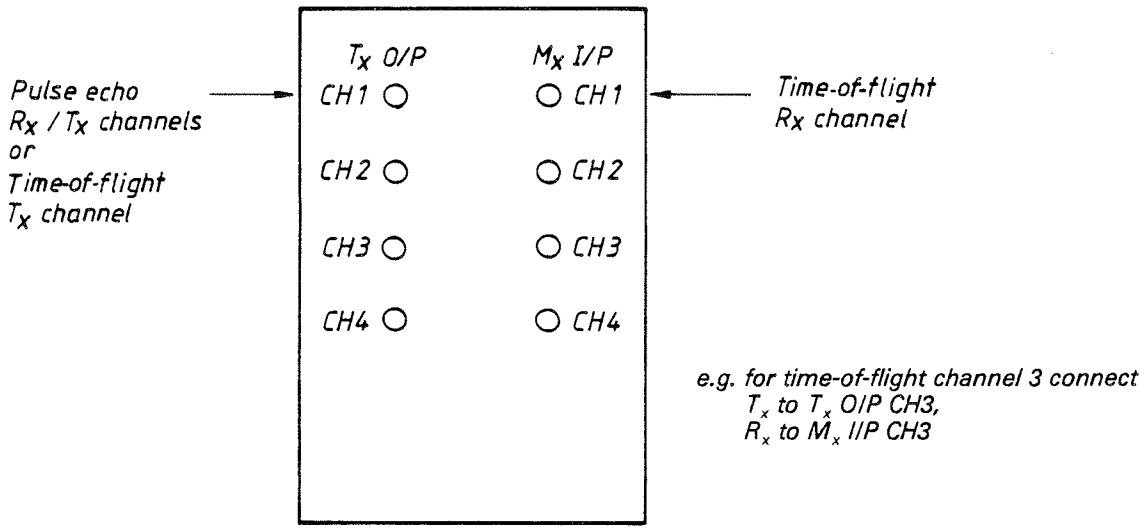

Fig.F4. Front top left hand terminal panel showing transmit/receive (T_x/R_x) connections for time-of-flight and pulse echo.

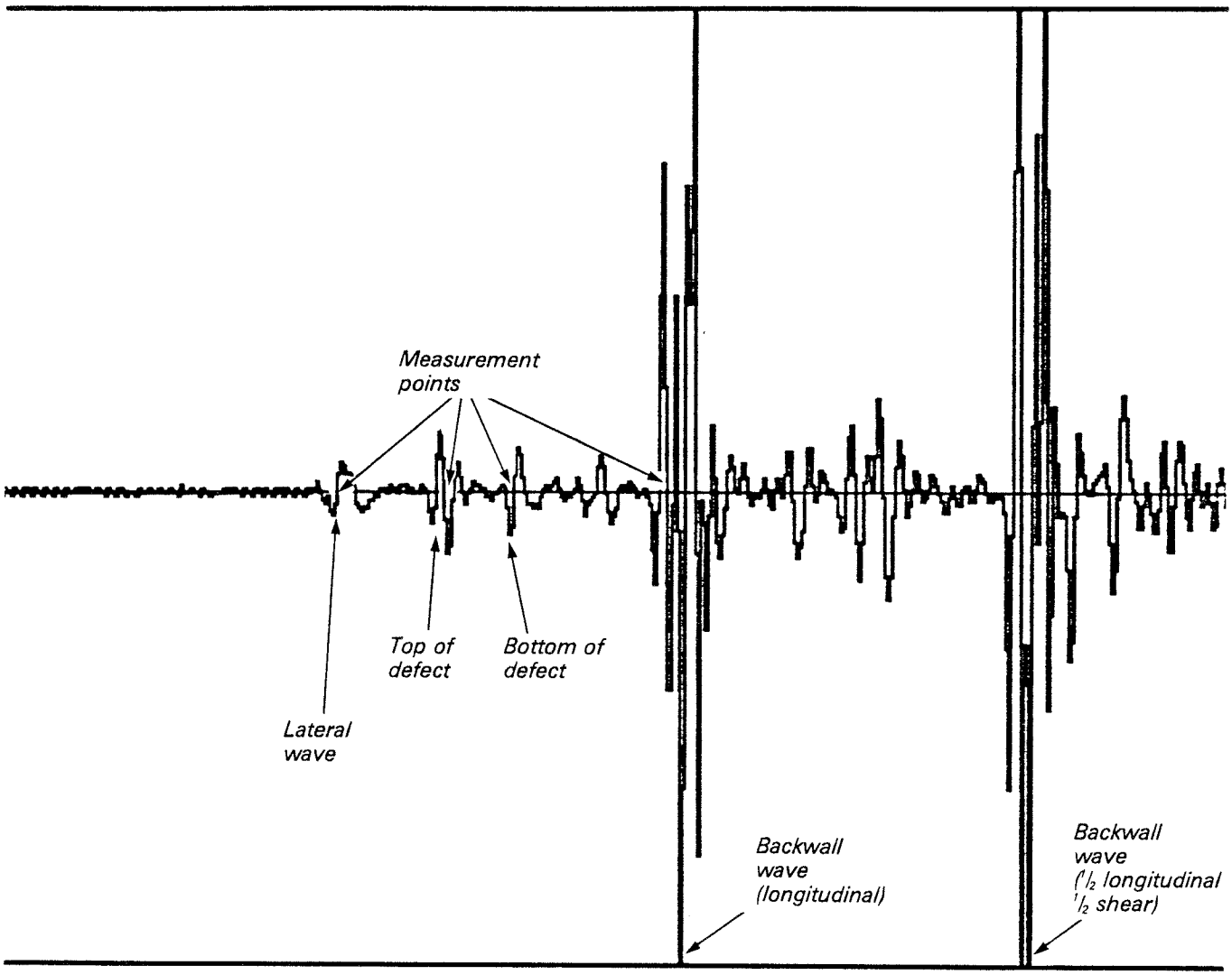

Fig.F5. A-scan measurement points.

APPENDIX G

RESULTS

In fracture mechanics analyses to determine the fitness-for-purpose of welded constructions the critical dimension of a flaw is its through thickness dimension (35). For butt welds in plate, where the applied stress is in the plane of the plate and perpendicular to the weld, this can be described as being the height (h_{max}) of the rectangle, parallel with the test-piece surface, which totally encloses the flaw (Fig. 1). Where possible time-of-flight test results have been analysed to yield this dimension and for correlation purposes this dimension was also made available from the destructive tests.

A few examples are also given of interpretation of some of the B-Scan images and limited results of processing by the SAFT algorithm are presented.

Interpretation of Selected B-Scan Images

J308, Flaws 29 and 30

A B-Scan of J308 (Scan 2, test surface "A", transducer separation = 62mm) is shown in Fig. G1. Signals beyond the longitudinal back wall wave have been ignored.

Between 30-80mm from "Y" there is evidence of a flaw (No. 29) buried in the lateral wave. However, the flaw (a lack of sidewall fusion, Fig. E4a) was easily identified and sized from scans from the opposite plate surface.

From the start of the scan to 175mm from "Y" there are a number of indications in addition to Flaw 29. These all have the characteristic phase of a signal from the top of a flaw. From this it may be inferred that the signals are all from flaws whose top and bottom tip signals cannot be resolved rather than from a larger single flaw. Their depths below the surface can be calculated and plotted (Fig. G2). Sectioning revealed a number of small unintentional flaws - lack of interrun fusion, linear porosity etc (e.g. Fig. E4c) of a size that would not be expected to be resolved (Fig. C7). When superimposed on the time-of-flight results good agreement between the two sets of results is again evident.

A flaw of measurable height is observable between 175 and 250mm from "Y" although towards the 250mm from "Y" end the tip signals become unresolvable. The profile of the flaw (a solidification crack, flaw 30) as determined from time-of-flight measurements is shown in Fig. G2 with the results from sectioning superimposed.

J301, Flaws 1 and 2

Part of a scan of a 95mm thick sample, J301 (Scan 1, test surface "A", transducer separation = 100mm) is shown in Fig. G3. Top and bottom signals of the two flaws (Nos. 1 and 2) present are distinguishable by the characteristic phase change. Although it is just possible to distinguish these flaws as two separate flaws from this scan, SAFT processing of the data (see below) allowed their identification quite readily. An alternative means of increasing confidence in the fact that these are two separate flaws would have been to carry out two transverse scans. This would have given different transverse positions for each flaw. Alternatively, the results of two longitudinal scans,

with different transducer separations could have been combined to enable the lateral positions to be calculated by eliminating X in Equation C8 in Appendix C. The time-of-flight profiles of the flaws with results from destructive tests superimposed are shown in Fig. G4.

J301, Flaws 3 and 4

Fig. G5 shows part of a B-Scan of Specimen J301 (Scan 3 surface "B", transducer separation = 100mm). A complex indication is observed between 200 and 320mm from "Y". Signals exhibiting phase reversal, indicative of their being from the top or bottom of a flaw are annotated "T" or "B" respectively. It was apparent that there were in fact two flaws of different through thickness dimensions at different transverse locations, and again the use of scans transverse to the weld would verify this to be the case. The time-of-flight profiles of the flaws (Nos. 3 and 4) with destructive results superimposed are shown in Fig. G6.

J307, Flaws 25-28

These are discussed in detail in Chapter 3 of the main text.

Time-of-Flight Results (Measurements of h_{max} and d_{min})

The stored B-Scan images from tests on all specimens were analysed in accordance with the procedures laid down in Document F1 of Appendix F. The lateral wave and diffracted signals from the top and bottom of each flaw, where the tip signals were resolvable, were located on the B-Scan display using the cursors and the time-to-depth linearisation was performed. Alternatively h_{max} and d_{min} were measured directly from a hard copy of each linearised B-Scan.

The results from specimens in each plate thickness are presented separately below.

38mm (1½ inch) thick specimens

An example of a non-linearised B-Scan image is shown in Fig. G1. The various features of these are indicated on each picture; including some unintentional flaws. As can be seen from Table G1a, all flaws were detected by scans from one surface of the specimen. However for near surface flaws it was necessary to consider results from the opposite test surface in order to estimate d_{min} and h_{max}. This is due to the minimum transducer separation being limited by the presence of the weld crown and to the depth/time non-linearities in the near surface region.

All scans were linearised and d_{min} and h_{max} estimated where possible. These results are summarised in Table G1. Example linearised scans are shown in Fig. G7.

95mm (3.75 inch) thick specimens

Transducer separations for tests on 95mm thick specimens were larger than for the other two specimen thicknesses. This was necessitated by the presence of the weld crown (face "A") and the requirements to detect flaws at greater depths. Due to the longer sound path lengths the amplitude of diffracted flaw tip signals was in general lower, as was that of the lateral wave. Typical non-linearised B-Scans from a 95mm thick specimen (J301) are shown in Figs. G1 and G5.

All intentional flaws in each specimen were detected by the combination of scans from both surfaces. Flaws were sized by linearising the time domain data and plots of the minimum rectangle enclosing the flaw

were drawn. The results are summarised in Table G1b. However, even after contrast enhancement of the B-Scan image, when each A-Scan had been averaged 256 times, it was not possible to estimate reliably the size of 3 of the 21 flaws in this plate thickness. Part of this problem can be attributed to insufficient amplifier gain in the analogue part of the system. Preliminary trials using a low noise pre-amplifier of 64dB gain indicated a substantial improvement to the quality of the results although a further increase in signal to noise ratio would be desirable.

10mm (0.4 inch) thick specimens

Consideration has already been given to the maximum time window between the lateral wave and the back wall wave available for the detection of flaws for 10mm thick specimens for a transducer separation of 38mm (i.e. S = 19mm). The path difference between the lateral wave and the back wall wave in this case is only 2.5mm (0.1 inch) which is equivalent to 0.84)s or 20 samples. This is illustrated in Fig. G8 (a) and (b) which show digitised A-Scan traces without and with a flaw present. The non-linearised B-Scan image of the region of the flaw in this specimen (J312) is shown in Fig. G9. Here, detection of the flaw is clearly demonstrated, as was the case for all 10mm specimens. Flaw length measurements correlated well with radiographic and manual ultrasonic results. Results from the single scan from each surface of these specimens are summarised in Table G1c.

In general the diffracted signal from the bottom tip of the flaw was detected and that from the top was buried in the lateral wave. An attempt has been made to define d_{min} and h_{max} by combining the results from scans from both test surfaces "A" and "B". The depth of the bot-

tom tip of the flaw was calculated from measurement of the arrival time of the diffracted wave. These time delays where measured to the appropriate white-to-black transition on the B-Scan image or the appropriate negative-to-positive zero crossing on the A-Scan. This was possible for three of the specimens tested. The specimens would have to be examined destructively in order to determine the accuracy of this approach. The most probable error in height measurement on consideration of the accuracy with which depth can be determined is 2.3mm. $\pm$ (using equations from Appendix C).

Possible areas of development of the time-of-flight technique for the sizing of flaws in thinner section have been discussed in the main text and in Appendix C.

Correlation of Time-of-Flight Results with Destructive Data

A total of six specimens in the 38mm and 95mm ($1\frac{1}{2}$ inch and 3.75 inch) thicknesses were examined destructively (Appendix E). Figs. G10 to G15 show interpretations of d_{min} and h_{max} from the time-of-flight results with the destructive results superimposed for each of the specimens sectioned. For each flaw, the time-of-flight measurement shown is the largest h_{max} measured from all scans carried out. A good correspondence is seen between measured flaw dimensions in the through wall direction and actual dimensions. Flaw length, from the time-of-flight results, was determined by a more conventional transducer movement technique. Improvements to length measurement could be achieved by applying the SAFT algorithm (see below).

The errors in measurement of flaw height and depth are summarised graphically in Figs. G16 and G17 respectively where the measured value has been plotted versus the actual value. Results are shown for those

measurements that yielded the maximum value of h_{max} for each flaw. The mean error and the standard deviation of the mean are given in Table G2 where the accuracies achieved may be compared with the results of previous work (2, 5). The comparison is favourable between the three sets of results for the measurement of h_{max}. They indicate a significant improvement in sizing accuracy over work carried out in Phase 1 of this programme (2) using simple equipment as was predicted and even a slight improvement over other reported results.

It is evident from the figures given that the error in flaw height measurement is significantly less than the error in depth measurement. This was predicted in Appendix C, and is a result of the fact that for flaw height measurements errors in the measurement of the transducer separation and the arrival times of the various pulses tend to cancel out. Another factor is the effect of the flaw not being on the centre line between the transducers. This results in an overestimation in flaw depth below the test surface (see Appendix C) and was the case for quite a few of the flaws. However, as can be seen from Fig. G16 and G17 the height measurements were not affected significantly.

SAFT Results

A few B-Scan images were processed at the NDT Centre, AERE Harwell using the linear SAFT algorithm (22). This was in order to evaluate the improvements to resolution along the length of the weld by synthetically focussing the ultrasonic beam and effectively eliminating beam spread effects. Two examples of scans processed in this way are given in Figs. G18 and G19. These are of Specimens J307 and J301 respectively and may be compared directly with the unprocessed data in Fig. G3 and Fig. G12. Table G3 compares the flaw lengths from destructive

tests with those determined from processed and unprocessed data. From the limited trials there appears to be an improvement to the ease with which flaw length can be measured but insufficient data exists to quantify improvements if any, to accuracy. However, the time penalties on processing the data even with a high speed LSI 11/73 processor were quite considerable - of the order of 10 minutes for 400 scan increments (around 16" of weld tested at the resolution employed in this work). This would not therefore be suitable for implementing on a slower processor for a dedicated site instrument but may be worthwhile considering for more detailed analysis.

Table G1a) Results of time-of-flight tests 38mm thick specimens

Specimen	Flaw Number	Scan No.	Test Surface	Y mm	(inches)	l mm	(inches)	d_{min} mm	(inches)	h_{max} mm	(inches)
J302	5	1	A	66	(2.60)	52	(2.05)	16.5	(0.65)	7.5	(0.30)
		2	A	71	(2.80)	45	(1.77)	16.0	(0.63)	7.5	(0.30)
		3	A^f	-[a]		-		-		-	
		4	B	46	(1.81)	70	(2.76)	14.0	(0.55)	7.5	(0.30)
		5	B	56	(2.20)	80	(3.15)	14.0	(0.55)	9.0	(0.35)
		6	B	-[6]		-		-		-	
J302	6	1	A	139	(5.47)	57	(2.24)	26.5	(1.04)	7.0	(0.28)
		2	A	137	(5.39)	58	(2.28)	26.5	(1.04)	7.0	(0.28)
		3	A^f	-[a]		-		-		-	
		4	B	140	(5.51)	44	(1.73)	25.0	(0.98)	-	
		5	B	140	(5.51)	43	(1.69)	25.0	(0.98)	8.0	(0.31)
		6	B	138	(5.43)	46	(1.81)	25.0	(0.98)	7.5	(0.30)
J302	7	1	A	198	(7.80)	59	(2.32)	55.0	(0.22)	7.5	(0.30)
		2	A	199	(7.83)	58	(2.28	-		-	
		3	A^f	-[a]		-		-		-	
		4	B	180	(7.09)	85	(3.35)	4.0	(0.16)	7.0	(0.28)
		5	B	179	(7.05)	83	(3.27)	2.5	(0.10)	8.0	(0.31)
		6	B	-[1]		-		-		-	

Table G1a) Results of time-of-flight test 38mm thick specimens, Continued

Specimen	Flaw Number	Scan No.	Test Surface	Y mm	(inches)	l mm	(inches)	d_{min} mm	(inches)	h_{max} mm	(inches)
J302	8	1	A	278	(10.94)	-[e]		5.5	(0.22)	7.5	(0.30)
		2	A	277	(10.91)	43	(1.69)	-[c]		-	
		3	A[f]	-[6]		-		-		-	
		4	B	275	(10.83)	49	(1.93)	2.0	(0.08)	8.0	(0.31)
		5	B	275	(10.83)	48	(1.89)	-		-	
		6	B	279	(10.98)	44	(1.73)	-		-	
J307	25	1	A	43	(1.69)	52	(2.05)	~ 6	(0.24)	-[c]	
		2	A	46	(1.81)	53	(2.09)	~8	(0.31)	-[c]	
		3	B	38	(1.50)	62	(2.44)	-		-	
		4	B	43	(1.69)	56	(2.20)	5.5	(0.22)	3.0	(0.12)
		5	B	43	(1.69)	43	(1.69)	-[f]		-	
J307	26	1	A	160	(6.30)	63	(2.48)	20.0	(0.79)	7.5	(0.30)
		2	A	161	(6.34)	61	(2.40)	21.0	(0.83)	7.0	(0.28)
		3	B	163	(6.42)	56	(2.20)	20.0	(0.79)	7.0	(0.28)
		4	B	150	(5.91)	73	(2.87)	20.0	(0.79)	7.0	(0.28)
		5	B	166	(6.54)	55	(2.17)	20.5	(0.81)	6.0	(0.24)
J307	27	1	A	255	(10.03)	60	(2.36)	8.0	(0.31)	12.5	(0.49)
		2	A	257	(10.12)	57	(2.24)	8.5	(0.33)	12.5	(0.49)
		3	B	260	(0.24)	54	(2.13)	6.5	(0.26)	14.0	(0.55)
		4	B	254	(10.00)	61	(2.40)	-[f]		-	
		5	B	257	(10.12)	60	(2.36)	-[f]		-	
J307	28	1	A	360	(14.17)	46	(1.81)	24.0	(0.94)	10.0	(0.39)
		2	A	354	(13.94)	54	(2.13)	24.0	(0.94)	10.0	(0.39)
		3	B	364	(14.33)	44	(1.73)	24.0	(0.94)	-[d]	
		4	B	363	(14.29)	44	(1.75)	22.5	(0.89)	-[d]	
		5	B	358	(14.09)	46	(1.81)	22.5	(0.89)	-[d]	

Table G1a) Results of time-of-flight tests 38mm thick specimens, Continued

Specimen	Flaw Number	Scan No.	Test Surface	Y mm	(inches)	l mm	(inches)	d_{min} mm	(inches)	h_{max} mm	(inches)
J308	29	1	A	27	(1.06)	57	(2.24)	< 8	(0.31)	–[c]	
		2	A	26	(1.02)	57	(2.24)	< 9	(0.35)	–[c]	
		3	B[f]	–		–		–		–	
		4	B	10	(0.39)	74	(2.91)	–[f]		–	
		5	B	10	(0.39)	75	(2.95)	2.0	(0.08)	6.0	(0.24)
J308	30	1	A	175	(6.89)	62	(2.44)	23.5	(0.93)	3.0	(0.12)
		2	A	173	(6.81)	67	(2.64)	23.0	(0.91)	3.5	(1.38)
		3	B[f]	–		–		–		–	
		4	B	177	(6.97)	60	(2.36)	22.5	(0.89)	3.0	(0.12)
		5	B	178	(7.01)	55	(2.17)	< 25	(0.98)	–[c]	
J309	31	1	A	97	(3.82)	64	(2.52)	10.0	(0.39)	7.5	(0.30)
		2	A	95	(3.74)	65	(2.56)	10.0	(0.39)	8.0	(0.31)
		3	B	94	(3.70)	56	(2.20)	–[c]		–	
		4	B	94	(3.70)	63	(2.48)	9.0	(0.35)	8.5	(0.33)
		5	B	102	(4.02)	48	(1.89)	10.0	(0.39)	8.0	(0.31)
J309	32	1	A	211	(8.31)	53	(2.09)	27.0	(1.06)	8.0	(0.31)
		2	A	207	(8.15)	57	(2.24)	27.0	(1.06)	7.5	(0.30)
		3	B	205	(8.07)	64	(2.52)	25.0	(0.98)	–[d]	
		4	B	209	(8.23)	54	(2.13)	26.0	(1.02)	–[d]	
		5	B	–[c]		–		–		–	
J310	33	1	A	67	(2.63)	60	(2.36)	–[f]		–	
		2	A	67	(2.63)	58	(2.28)	–[f]		–	
		3	B	68	(2.68)	55	(2.17)	–[c]		–	
		4	B	66	(2.60)	51	(2.01)	–[c]		–	
J310	34	1	A	209	(8.23)	26	(1.02)	–[c]		–	
		2	A	210	(8.27)	30	(1.18)	–c		–	

Table G1a) Results of time-of-flight test 38mm thick specimens, Continued.

Specimen	Flaw Number	Scan No.	Test Surface	Y mm	(inches)	l mm	(inches)	d_{min} mm	(inches)	h_{max} mm	(inches)
		3	B	199	(7.83)	79	(3.11)	-		-	
		4	B	-[e]		-		-		-	
J310	35	1	A	283	(11.14)	79	(3.11)	9.0	(0.35)	-[d]	
		2	A	282	(11.10)	82	(3.23)	9.5	(0.37)	-[d]	
		3	B	287	(11.30)	82	(3.23)	7.0	(0.28)	4.0	(0.16)
		4	B	285	(11.22)	80	(3.15)	6.0	(0.24)	4.0	(0.16)
J311	36	1	A	49	(1.93)	80	(3.15)	22.0	(0.87)	-[d]	
		2	A	50	(1.97)	80	(3.15)	23.0	(0.91)	-[d]	
		3	B	46	(1.81)	86	(3.39)	23.5	(0.93)	-[d]	
		4	B	47	(1.85)	86	(3.39)	22.5	(0.89)	-[d]	
J311	37	1	A	129	(5.08)	67	(2.64)	13.0	(0.51)	-[d]	
		2	A	132	(5.20)	64	(2.52)	12.5	(0.49)	-[d]	
		3	B	135	(5.31)	82	(3.23)	11.5	(0.45)	6.5	(0.26)
		4	B	143	(5.63)	71	(2.80)	11.0	(0.43)	6.0	(0.24)

Notes

a) Flaw not detected.

b) Flaw detected but measurements not possible.

c) Flaw partially or completed obscured by lateral wave.

d) Tip signals not resolvable.

e) Scan finished prematurely.

f) Difficult to interpret.

g) Flaws not resolvable from each other from B-Scan image.

Table G1b) Results of time-of-flight tests 95m thick specimen

Specimen	Flaw Number	Scan No.	Test Surface	Y mm	(inches)	l mm	(inches)	d_{min} mm	(inches)	h_{max} mm	(inches)
J301	1	1	A	47	(1.85)	42	(1.65)	21	(0.83)	10.5	(0.41)
		2	A	50	(1.97)	38	(1.50)	21.5	(0.85)	10.0	(0.39)
		3	B	–		–		–		–	
		4	B	51	(2.01)	40	(1.57)	21.5	(0.85)	10.0	(0.39)
		5	B	–[a]		–		–		–	
J301	1A	1	A	–[b]		–		–		–	
		2	A	24	(0.94)	32	(1.26)	40.5	(1.59)	11.0	(0.43)
		3	B	22	(0.87)	36	(1.42)	36.0	(1.42)	12.0	(0.47)
		4	B	23	(0.91)	31	(1.22)	38.0	(1.50)	12.0	(0.47)
		5	B	–		–		–		–	
J301	2	1	A	112	(4.41)	75	(2.95)	23	(0.91)	11.0	(0.43)
		2	A	116	(4.57)	63	(2.48)	23	(0.91)	11.0	(0.43)
		3	B	–[a]		–		–		–	
		4	B	–[b]		–		–		–	
		5	B	–[a]		–		–		–	
J301	3	1	A	221[g]	(8.70)	74	(2.91)	–		–	
		2	A	215[g]	(8.46)	85	(3.35)	–		–	
		3	B	210	(8.27)	55	(2.17)	47.5	(1.87)	2.5	(0.10)
		4	B	210[g]	(8.27)	98	(3.86)	–		–	
		5	B	–[b]		–		–		–	
J301	4	1	A	221[g]	(8.70)	74	(2.91)	48.5	(1.91)	–	
		2	A	215[g]	(8.46)	85	(3.35)	48.0	(1.89)	–	
		3	B	249	(9.80)	73	(2.87)	48.0	(1.89)	10.0	(0.39)
		4	B	210[g]	(8.27)	98	(3.86)	–		–	
		5	B	–		–		–		–	
J303	9	1	A	15	(0.59)	83	(3.27)	67.0	(2.64)	9.0	(0.35)

Table G1b) Results of time-of-flight test 95mm thick specimens, Continued

Specimen	Flaw Number	Scan No.	Test Surface	Y mm	(inches)	l mm	(inches)	d_{min} mm	(inches)	h_{max} mm	(inches)
		2	A	-[a]		-		-		-	
		3	A	43	(1.69)	49	(1.93)	66.0	(2.60)	8.5	(0.33)
		4	B	36	(1.42)	40	(1.57)	67.5	(2.66)	-[c]	
		5	B	35	(1.38)	58	(2.28)	71.0	(2.80)	-[c]	
J303	10	1	A	136	(5.35)	87	(3.43)	52.5	(2.07)	7.0	(0.28)
		2	A	135	(5.31)	86	(3.39)	55.0	(2.17)	5.5	(0.22)
		3	B	150	(5.90)	30	(1.97)	54.0	(2.13)	5.0	(0.20)
		4	B	117	(4.61)	105	(4.13)	51.0	(2.01)	7.5	(0.30)
		5	B	132	(5.20)	109	(4.29)	52.5	(2.07)	8.5	(0.33)
J303	11	1	A	268	(10.55)	49	(1.93)	33.5	(1.32)	9.0	(0.35)
		2	A	268	(10.55)	48	(1.89)	34.5	(1.36)	7.5	(0.30)
		3	B	-[a]		-		-		-	
		4	B	240	(9.45)	75	(2.95)	31.0	(1.22)	-[f]	
		5	B	240	(9.45)	70	(2.76)	33.0	(1.30)	7.0	(0.28)
J303	12	1	A	346	(13.62)			18.0	(0.71)	10.0	(0.39)
		2	A	351	(13.82)	53	(2.09)	18.5	(0.73)	10.0	(0.39)
		3	B	-[a]		-		-		-	
		4	B	-[a]		-		-		-	
		5	B	337	(13.27)	67	2.64	18.5	(0.73)	9.5	(0.37)
J304	13	1	A	-[a]		-		-		-	
		2	A	59	(2.32)	39	(1.54)	76.0	2.99)	-[f]	
		3	B	-[b]		-		-		-	
		4	B	-[b]		-		-		-	
		5	B	-[a]		-		-		-	
J304	14	1	A	-[a]		-		-		-	
		2	A	-[b]		-		56.5	(2.22)	-[f]	
		3	B	-[b]		-		-		-	

Table G1b) Results of time-of-flight tests 95mm thick specimen, Continued.

Specimen	Flaw Number	Scan No.	Test Surface	Y mm	(inches)	l mm	(inches)	d_{min} mm	(inches)	h_{max} mm	(inches)
		4	B	-[b]		-		-		-	
		5	B	-[a]		-		-		-	
J304	15	1	A	-[b]		-		-		-	
		2	A	220	(8.66)	87	(3.43)	33.5	(1.32)	11	(0.43)
		3	B	-[b]		-		-		-	
		4	B	-[b]		-		-		-	
		5	B	-[b]		-		-		-	
J304	16	1	A	-[b]		-		-		-	
		2	A	-[a]		-		-		-	
		3	B	-[b]		-		-		-	
		4	B	-[b]		-		-		-	
		5	B	362	(14.25)	21	(0.83)	-		-	
J305	17	1	A	28	(1.10)	35	(1.34)	74.5	(2.93)	8.0	(0.31)
		2	A	13	(0.51)	44	(1.73)	74.0	(2.91)	12.0	(0.47)
		3	B	10	(0.39)	66	(2.60)	72.5	(2.85)	13.0	(0.51)
		4	B	-[b]		-		-		-	
		5	B	-[a]		-		-		-	
J305	18	1	A	-[b]		-		-		-	
		2	A	142	(5.59)	46	(1.81)	55.0	(2.17)	-	
		3	B	147	(5.79)	60	(2.36)	53.0	(2.09)	12.0	(0.47)
		4	B	145	(5.71)	56	(2.20)	54.0	(2.13)	11.5	(0.45)
		5	B	-[a]		-		-		-	
J305	19	1	A	219	(8.62)	49	(1.93)	31.5	(1.24)	11.5	(0.45)
		2	A	222	(8.74)	38	(1.50)	31.0	(1.22)	12.0	(0.47)
		3	B	205	(8.07)	53	(2.09)	-[f]		-	
		4	B	202	(7.95)	73	(2.87)	-f		-	
		5	B					27.5	(1.08)	11.5	(0.45)

Table G1b) Results of time-of-flight tests 95mm thick specimen, Continued.

Specimen	Flaw Number	Scan No.	Test Surface	Y mm	(inches)	l mm	(inches)	d_{min} mm	(inches)	h_{max} mm	(inches)
J305	20	1	A	312	(12.28)	50	(1.97)	22.5	(0.89)	11.5	(0.45)
		2	A	314	(12.36)	43	(1.69)	20.0	(0.79)	13.0	(0.51)
		3	B	-[a]		-		-		-	
		4	B	-[a]		-		-		-	
		5	B	305	(12.01)	44	(1.73)	19.5	(0.79)	11.0	(0.43)
J306	21	1	A	44	(1.73)	51	(2.01)	77.5	(3.05)	6	(0.24)
		2	A	-[a]		-		-		-	
		3	B	-		-		-		-	
		4	B	46	(1.81)	37	(1.46)	-[c]		-	
		5	B	45	(1.77)	49	(1.92)	73.5	(2.90)	9.5	(0.37)
J306	22	1	A	102	(4.02)	48	(1.89)	34.5	(1.36)	9	(0.35)
		2	A	-[b]		-		-		-	
		3	B	104	(4.09)	45	(1.77)	-		-	
		4	B	102	(4.02)	48	(1.89)	-		-	
		5	B	107	(4.21)	40	(1.57)	-		-	
J306	23	1	A	265	(10.43)	46	(1.81)	-[f]		-	
		2	A	267	(10.51)	37	(1.46)	-		-	
		3	B	-[e]		-		-		-	
		4	B	265	(10.43)	-[e]		51.5	(2.03)	8.5	(3.35)
		5	B	265	(10.43)	41	(1.61)	-		-	
J306	24	1	A	325	(12.80)	46	(1.81)	26	(1.02)	10.5	(0.41)
		2	A	327	(12.87)	39	(1.54)	-		-	
		3	B	-[e]	-	-		-			
		4	B	-[e]		-		-		-	
		5	B	326	(12.83)	42	(1.65)	-	-	-	

Table G1c) Results of time-of-flight tests 10mm thick specimens

Specimen	Flaw Number	Scan No.	Test Surface	Y mm	(inches)	l mm	(inches)	d_{min} mm	(inches)	h_{max} mm	(inches)
J312	38	1	A	91	(3.58)	30	(1.18)	0.5	(0.02)	55	(0.22)
		2	B	89	(3.50)	34	(1.34)				
J313	39	1	A	119	(4.69)	23	(0.91)	3.5	(0.14)	3.0	(0.12)
		2	B	121	(4.76)	24	(0.94)				
J314	40	1	A	70	(2.76)	40	(1.57)	0.5	(0.02)	5.0	(0.20)
		2	B	65	(2.56)	50	(1.97)				
J315	41	1	A	51	(2.01)	32	(1.26)	-[f]		-	
		2	B	53	(2.09)	30	(1.18)	-[f]		-	
J316	42	1	A	71	(2.80)	46	(1.81)	-		-	
		2	B	-[c]		-		-		-	
J317	43	1	A	59	(2.32)	12	(0.47)	-		-	
		2	B	-[c]		-		-		-	
J318	44	1	A	-[f]		-		-		-	
		2	B	-[c]		-		-		-	
J319	45	1	A	-[f]		-		-		-	
		2	B	-[c]		-		-		-	

TABLE G2. Statistical data on accuracy of flaw through-wall size measurement for time-of-flight tests.

Test	Mean error $\bar{x}$ mm	(inches)	Standard deviation, σ mm	(inches)	95% probability limits 2σ mm	(inches)
h_{max} (maximum values)	-0.17	(-0.007)	1.00	(0.039)	2.00	(0.079)
d_{min} (from above maxima)	+0.55	(+0.022)	1.31	0.052	2.62	(0.103)
Results from previous Welding Institute program (2) with simple equipment (h_{max})	-1.03	(-0.041)	1.63	(0.064)	3.26	(0.128)
Results from previous Welding Institute program (5) with complex equipment (h_{max})	0.50	(0.020)	1.80	(0.071)	3.60	(0.142)

TABLE G3. Results of flaw length measurement from SAFT processed data.

Specimen	Flaw No.	Actual measurement				Measurement from TOF results before SAFT processing				SAFT processed TOF			
		Y mm	(inches)	l mm	(inches)	Y mm	(inches)	l mm	(inches)	Y mm	(inches)	l mm	(inches)
J301	1	56	(2.20)	34	(1.34)	47	(1.85)	42	(1.65)	42	(1.65)	38	(1.50)
Scan 1	2	115	(4.53)	65	(2.56)	112	(4.41)	75	(2.95)	117	(4.61)	64	(2.52)
J305	17	22	(0.87)	51	(2.01)	28	(1.10)	35	(1.38)	30	(1.18)	40	(1.57)
Scan 1	18	145	(5.71)	53.5	(2.11)	147	(5.79)	60	(2.36)	149	(5.87)	43	(1.69)
	19	220	(8.66)	50	(1.97)	219	(8.62)	49	(1.93)	223	(8.78)	49	(1.93)
	20	310	(12.20)	48	(1.89)	312	(12.28)	50	(1.97)	312	(12.28)	47	(1.85)
J307	25	40.0	(1.57)	52	(2.05)	43	(1.69)	52	(2.05)	46	(1.81)	49	(1.93)
Scan 1	26	169	(6.65)	50	(1.97)	160	(6.30)	63	(2.48)	165	(6.50)	58	(2.28)
	27	258.5	(10.18)	49	(1.93)	255	(10.04)	60	(2.36)	259	(10.20)	55	(2.17)
	28	357.5	(14.07)	52	(2.07)	360	(14.17)	46	(1.81)	362	(14.25)	44	(1.73)

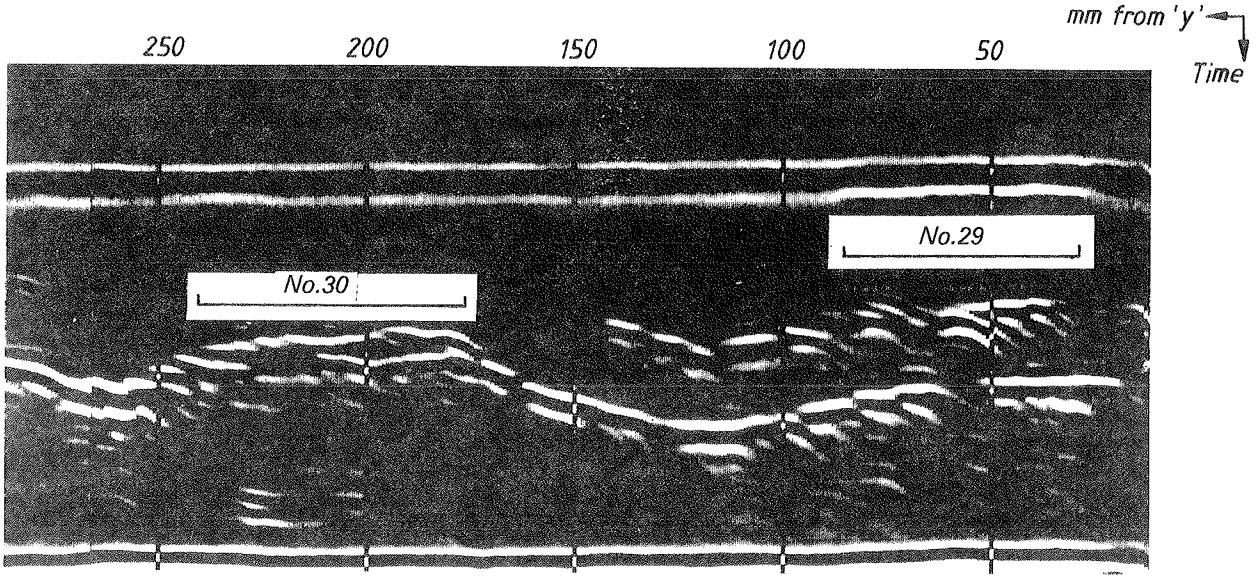

Fig.G1. B-scan image (not linearised) J308, scan 2.

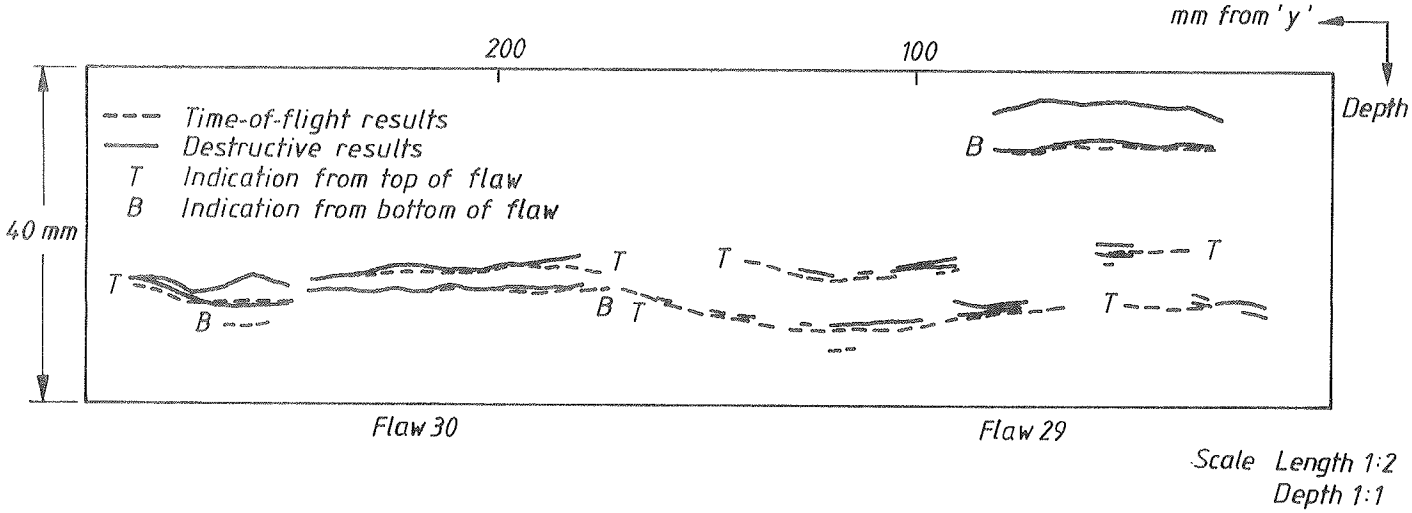

Fig.G2. Flaw profiles determined from time-of-flight results with destructive results superimposed, J308.

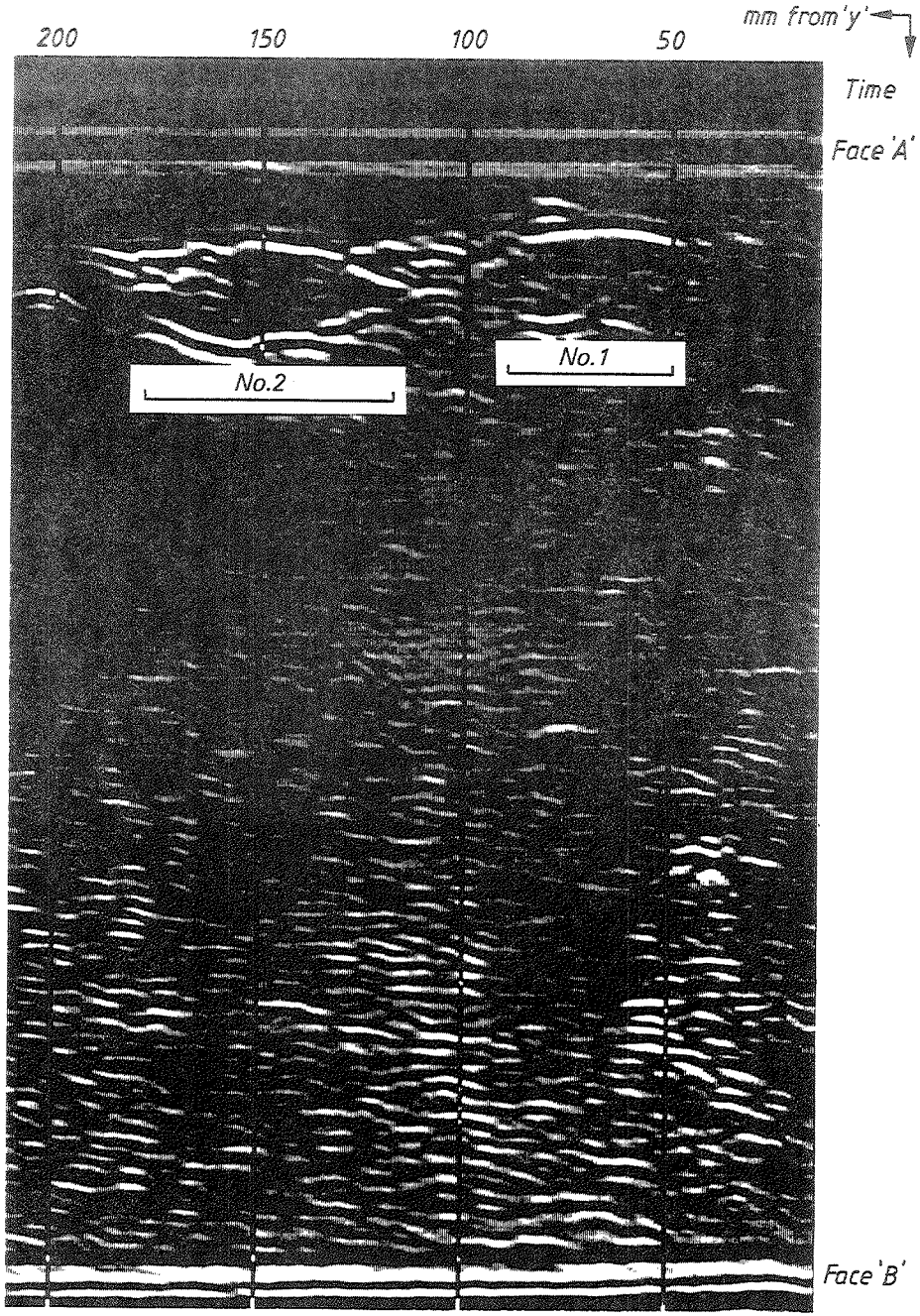

Fig.G3. B-scan image (not linearised) J301, flaws 1 and 2, scan 1.

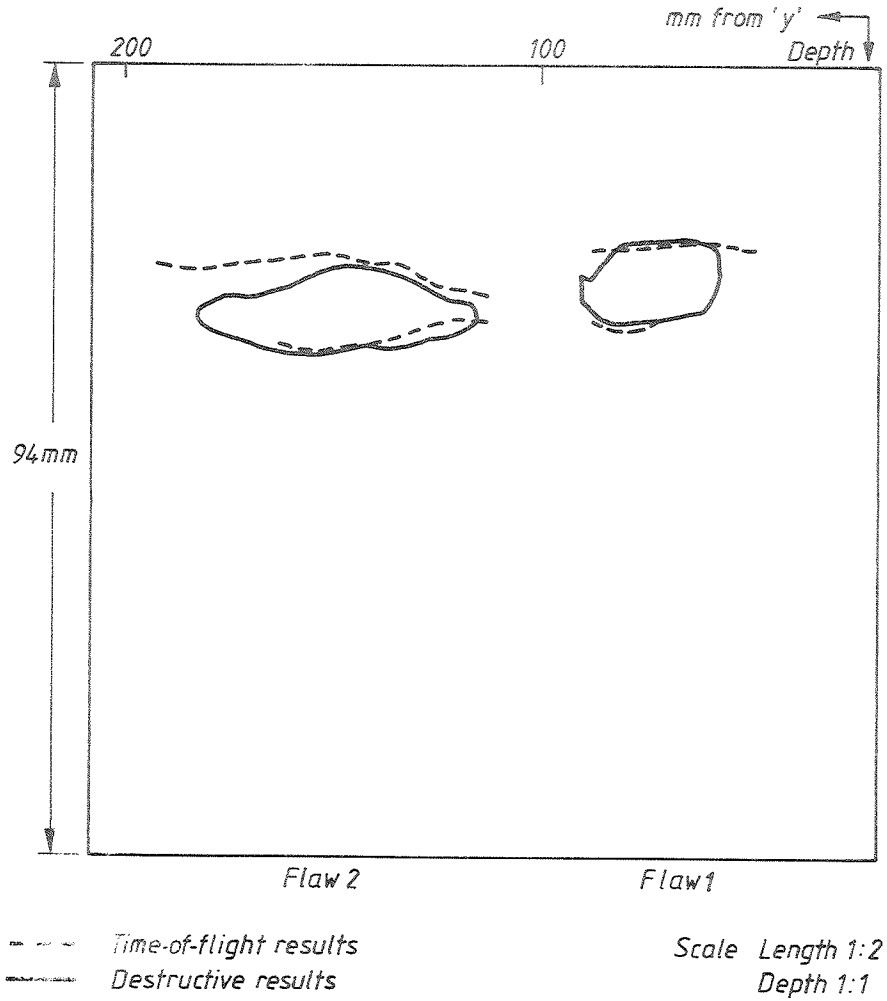

Fig.G4. Flaw profiles determined from time-of-flight results with destructive results superimposed, J301, flaws 1 and 2.

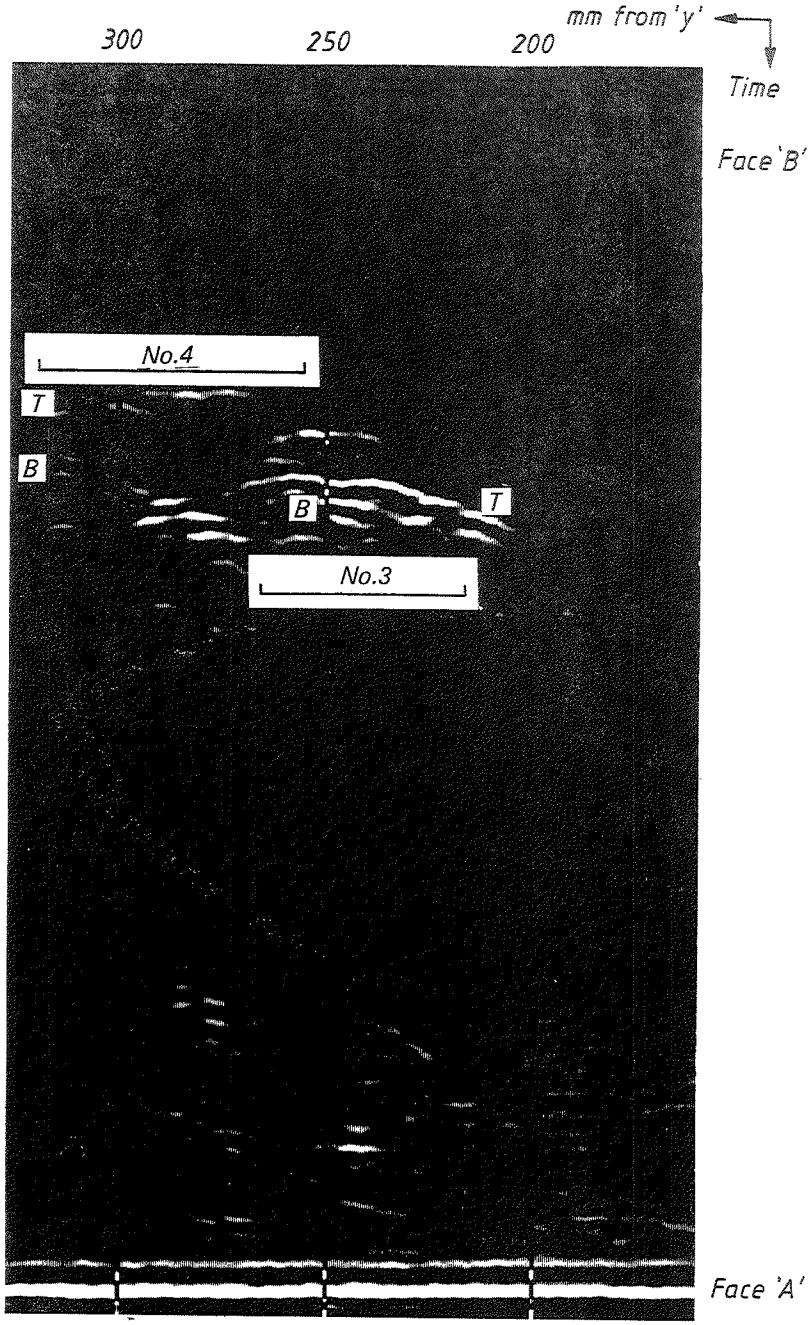

Fig.G5. B-scan image (not linearised) J301, flaws 3 and 4, scan 3.

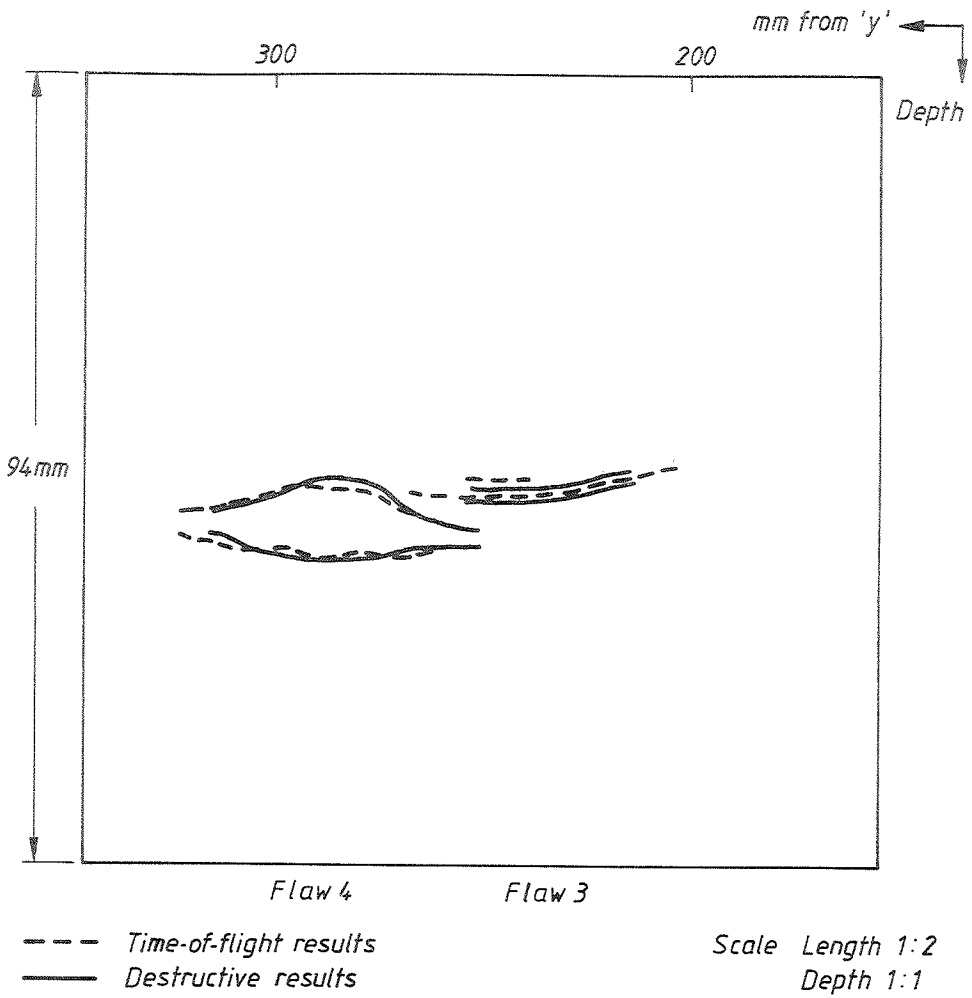

Fig.G6. Flaw profiles determined from time-of-flight results with destructive results superimposed, J301, flaws 3 and 4.

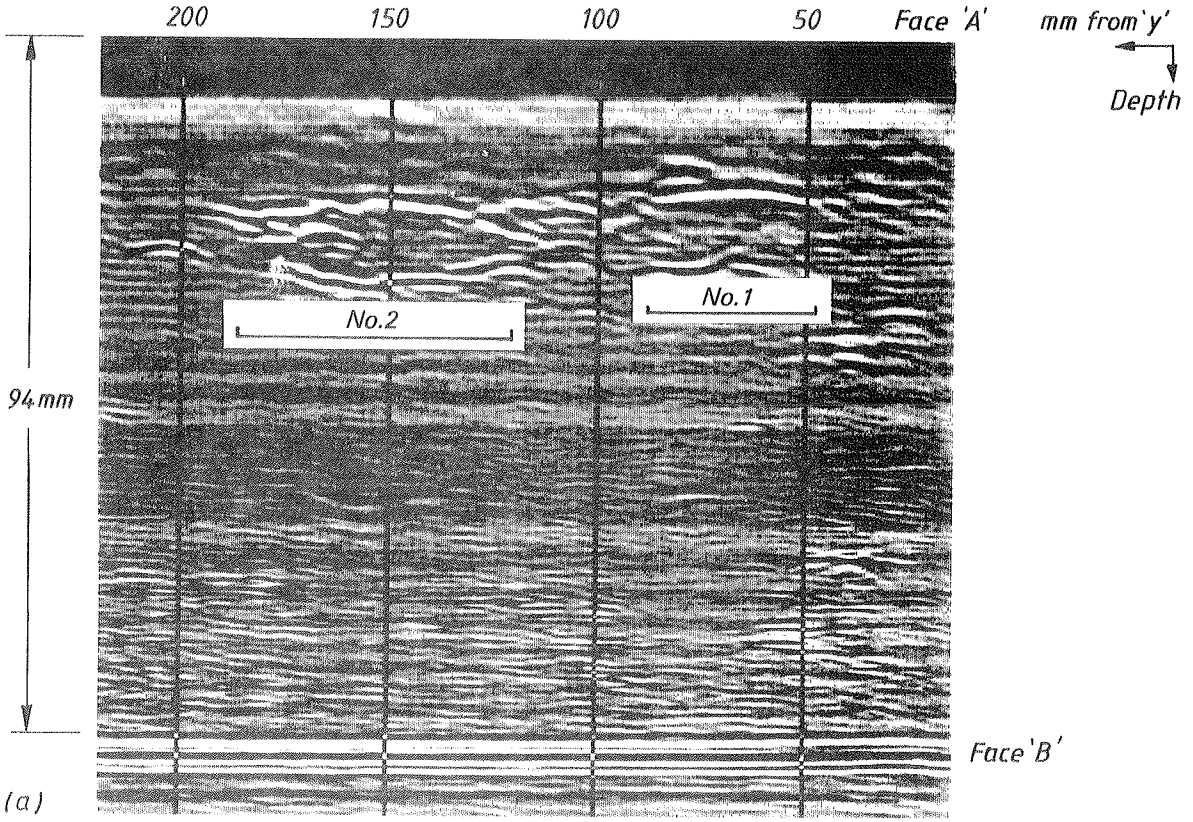

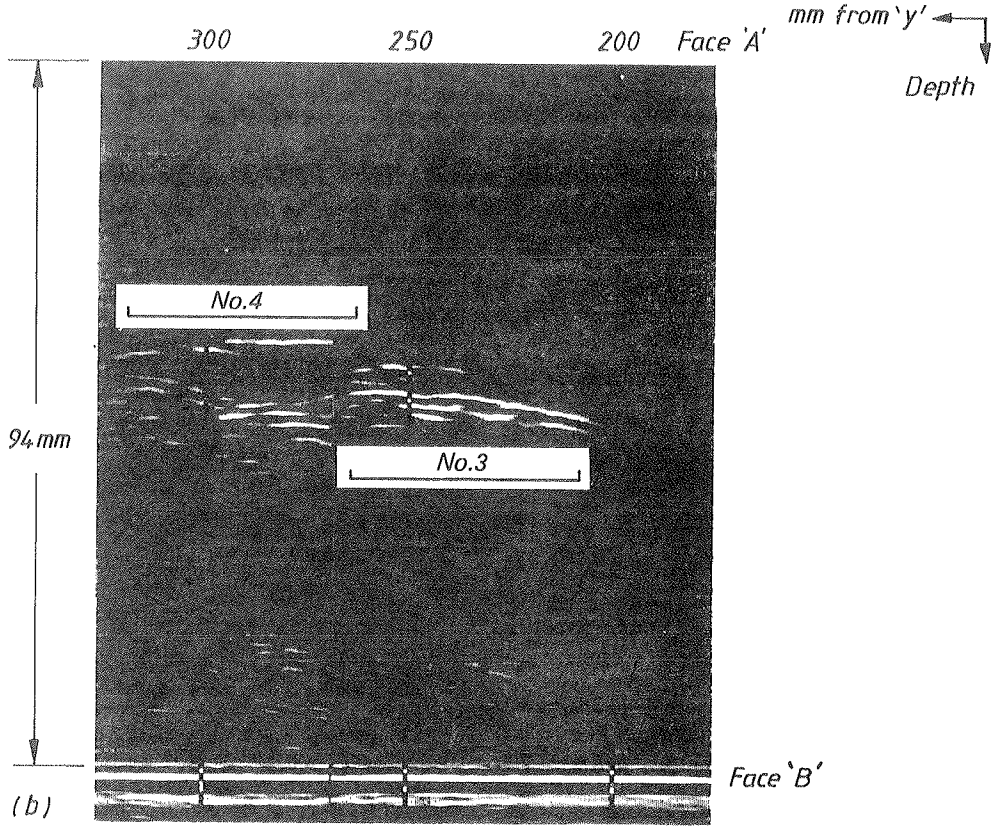

Fig.G7:

a) B-scan of J301, scan 1 (part) linearised
b) B-scan of J301, scan 3 (part) linearised

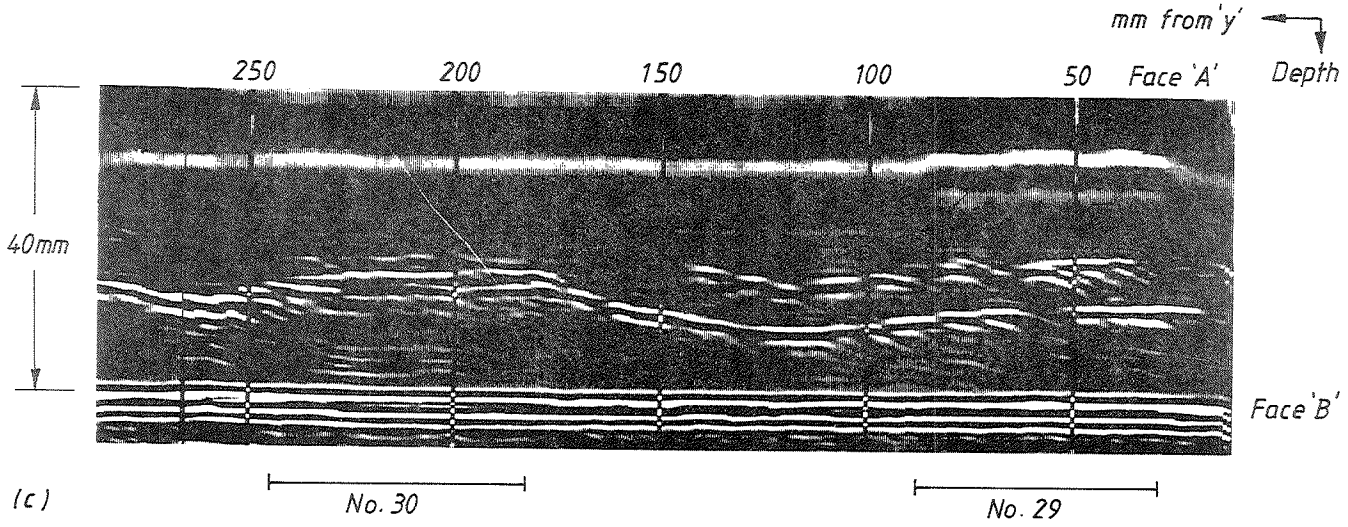

Fig.G7 contd:

c) B-scan of J308, scan 2, linearised

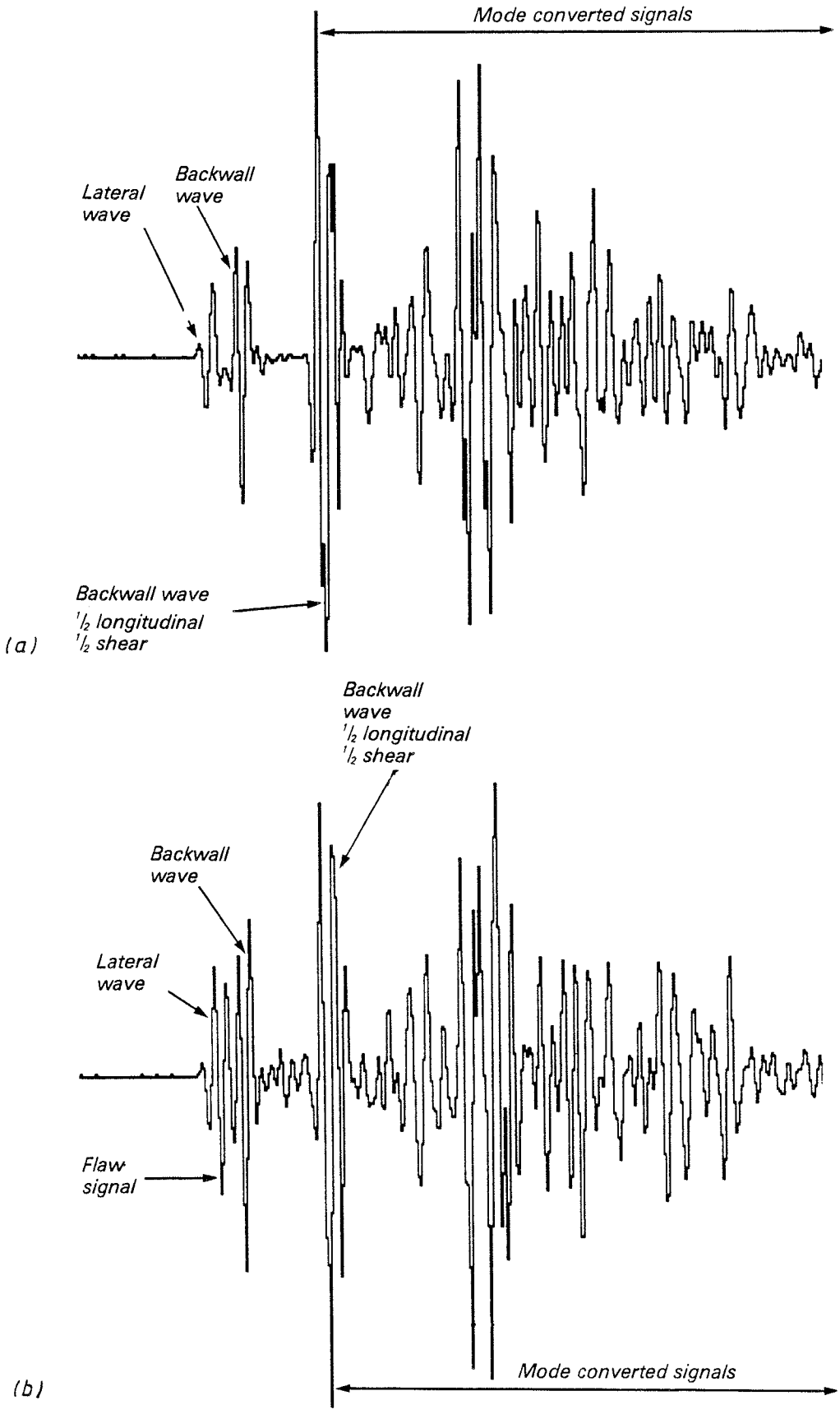

Fig.G8. A-scans from 10mm thick specimen J312:

a) flaw free region
b) in region of flaw

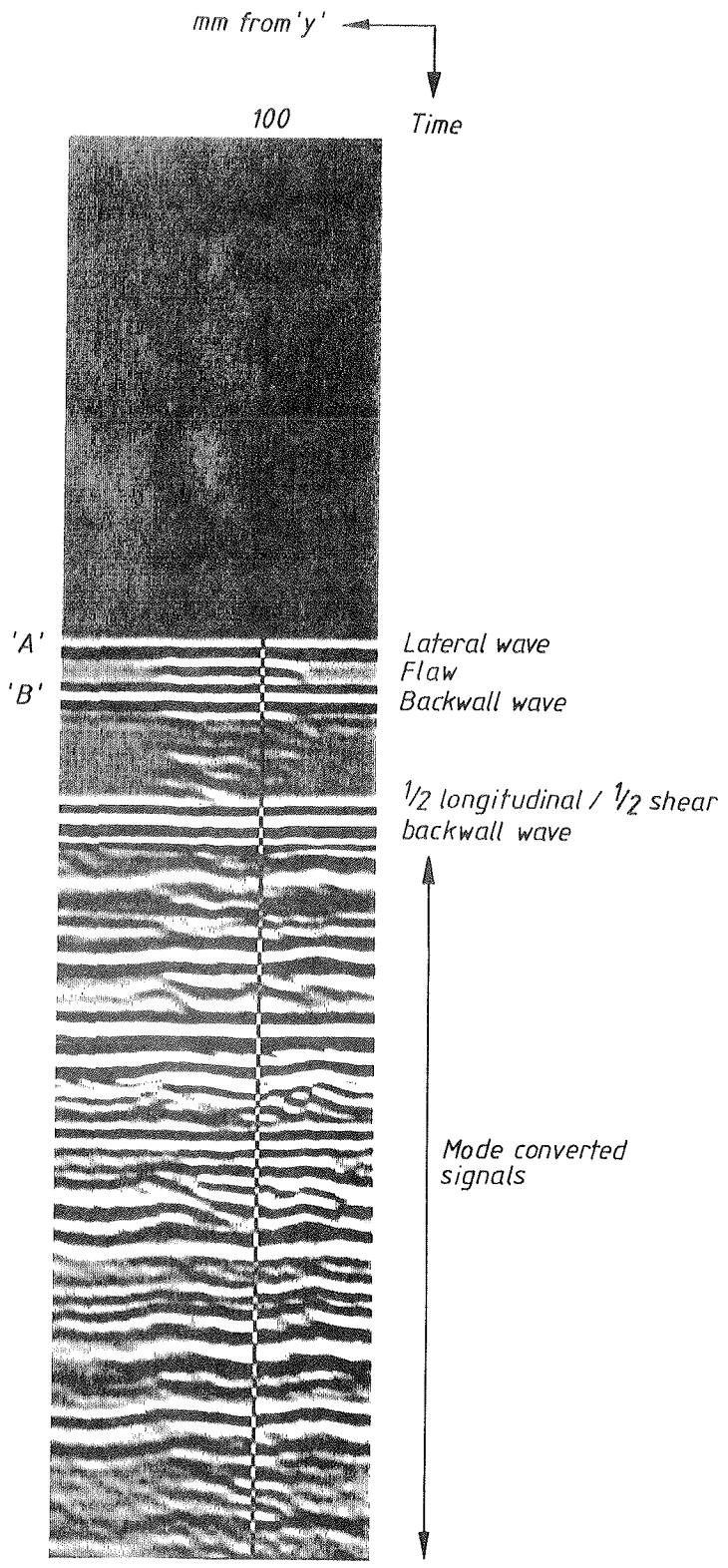

Fig.G9. B-scan image of J312.

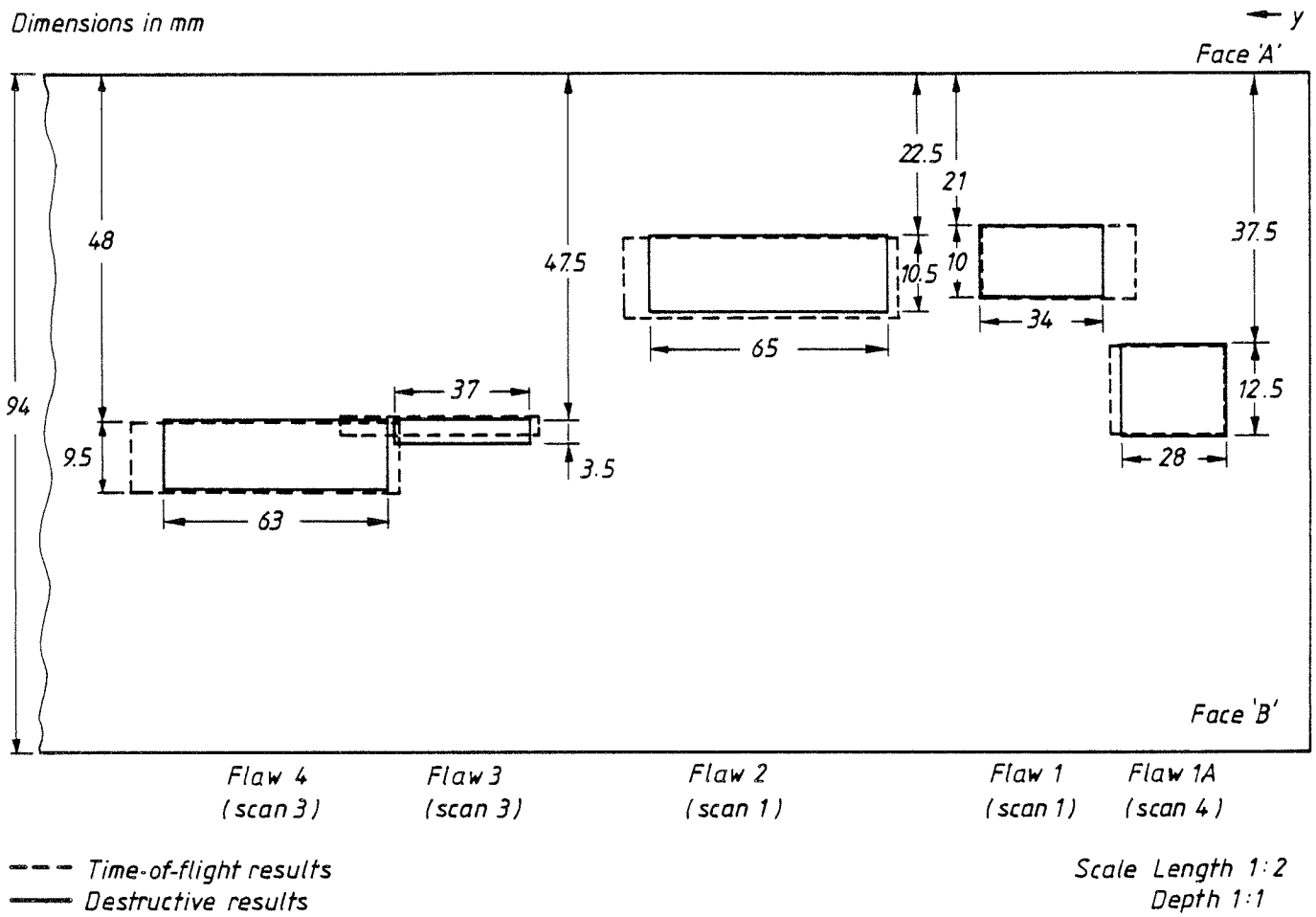

Fig.G10. Correlation of measured and actual flaw sizes J301.

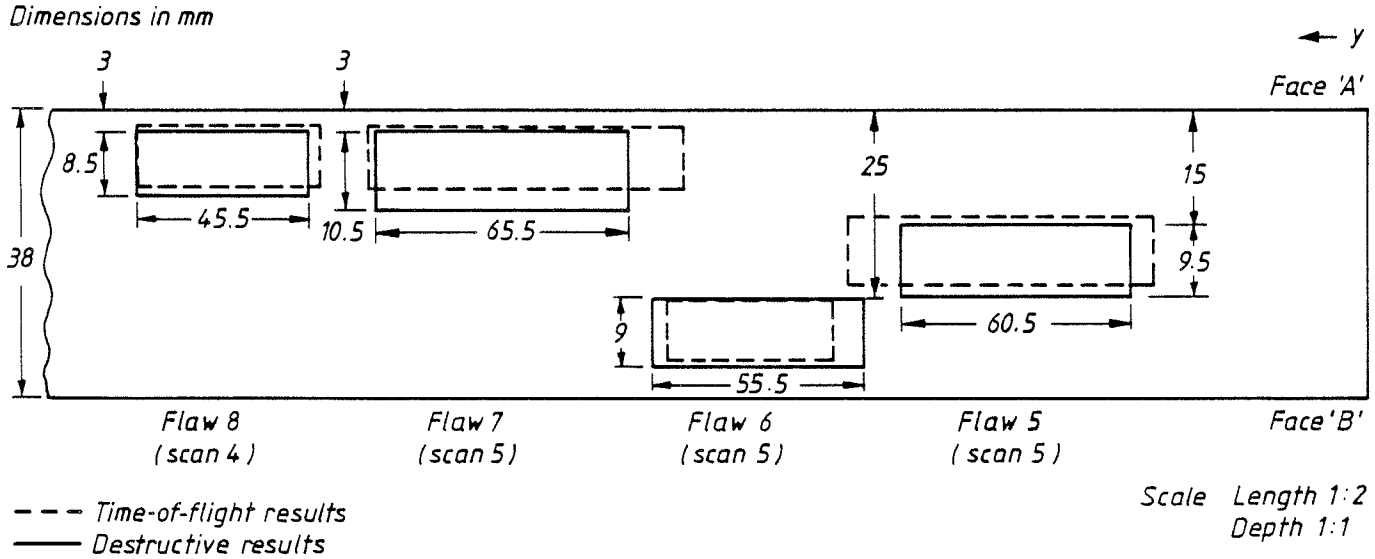

Fig.G11. Correlation of measured and actual flaw sizes J302.

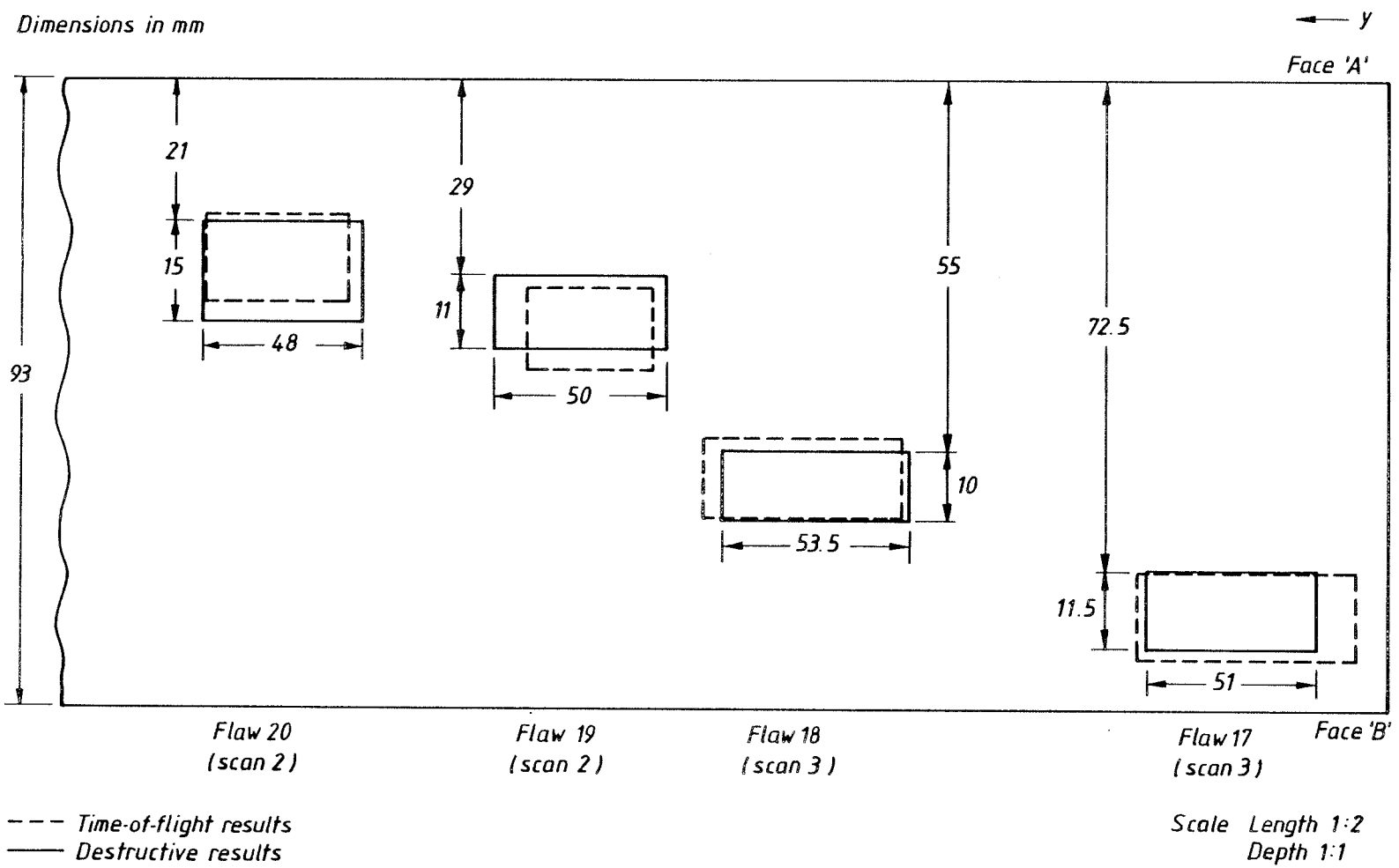

Fig.G12. Correlation of measured and actual flaw sizes J305.

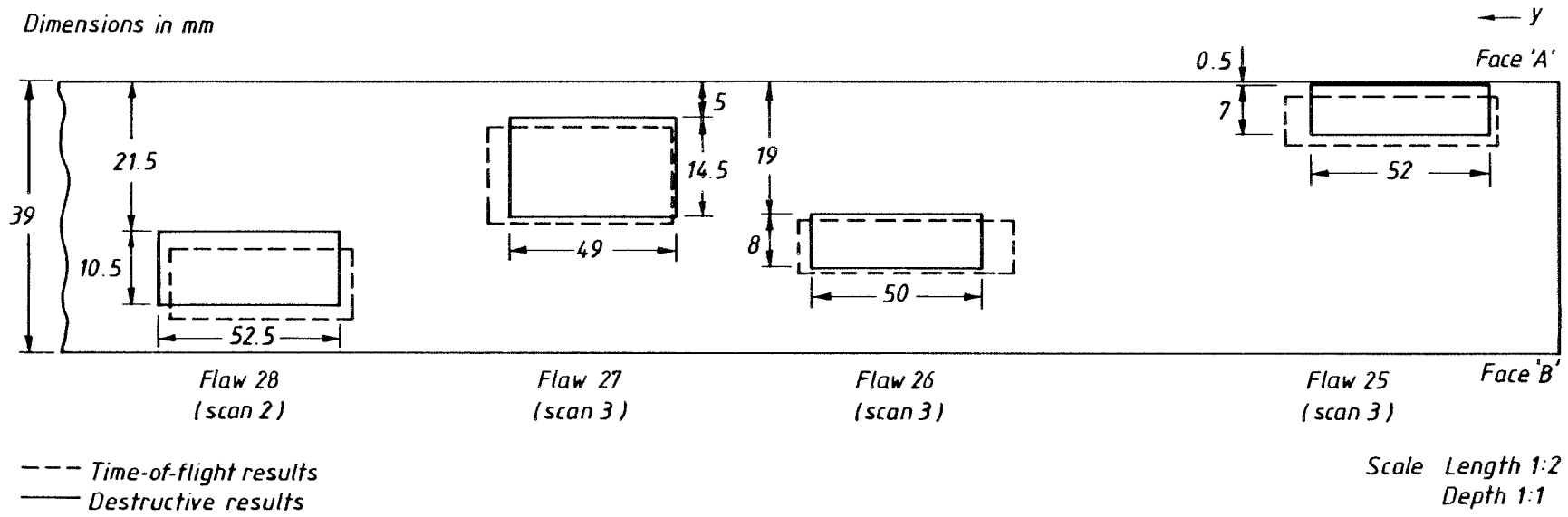

Fig.G13. Correlation of measured and actual flaw sizes J307.

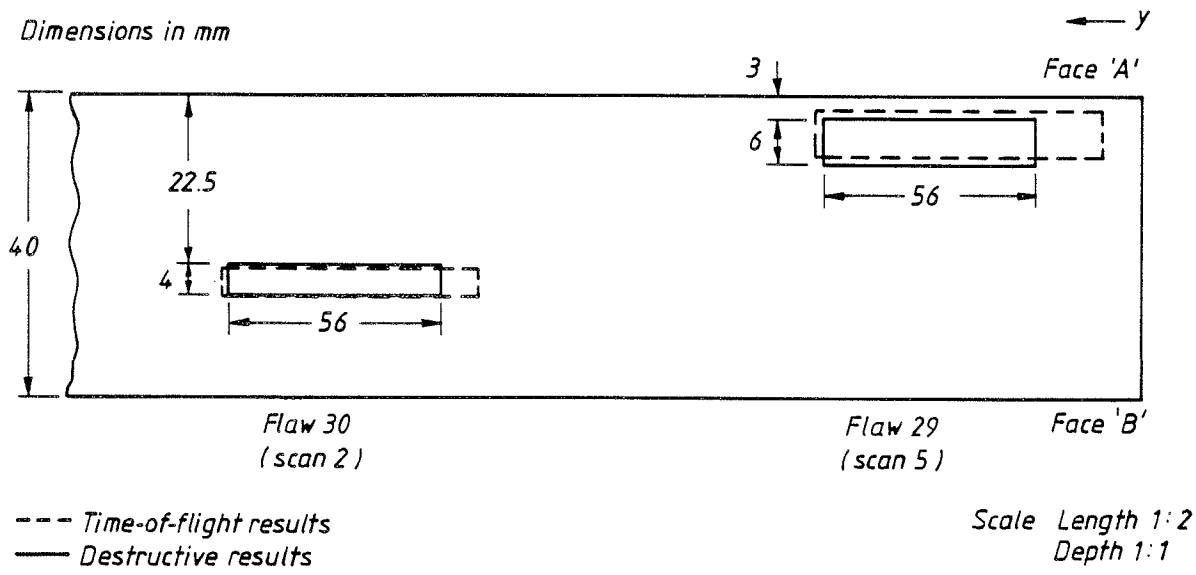

Fig.G14. Correlation of measured and actual flaw sizes J308.

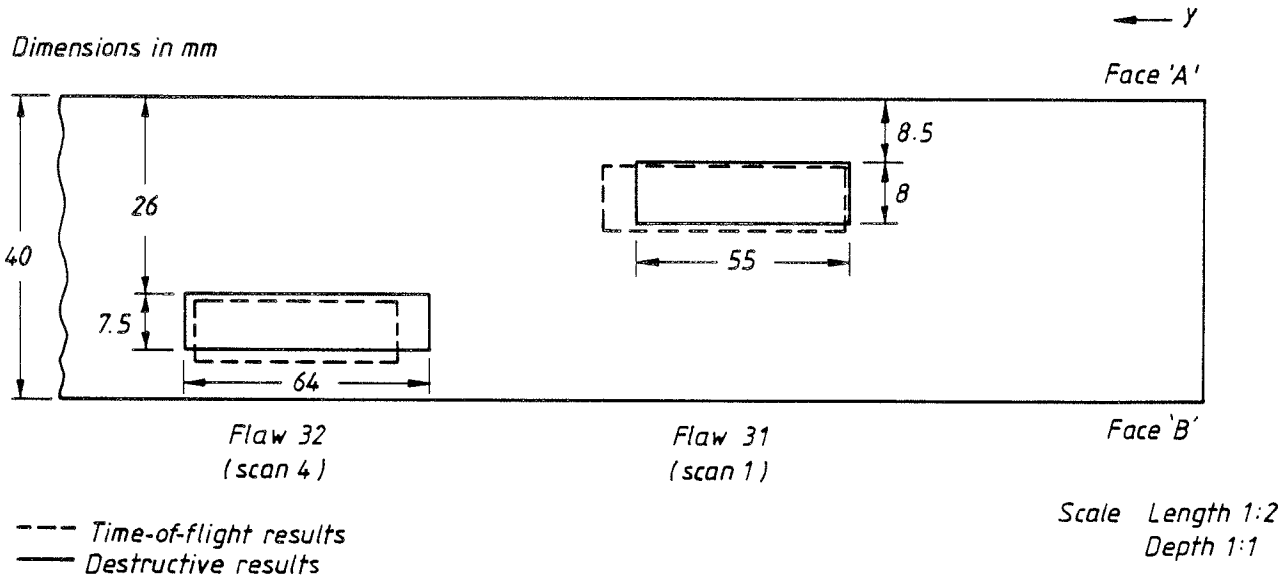

Fig.G15. Correlation of measured and actual flaw sizes J309.

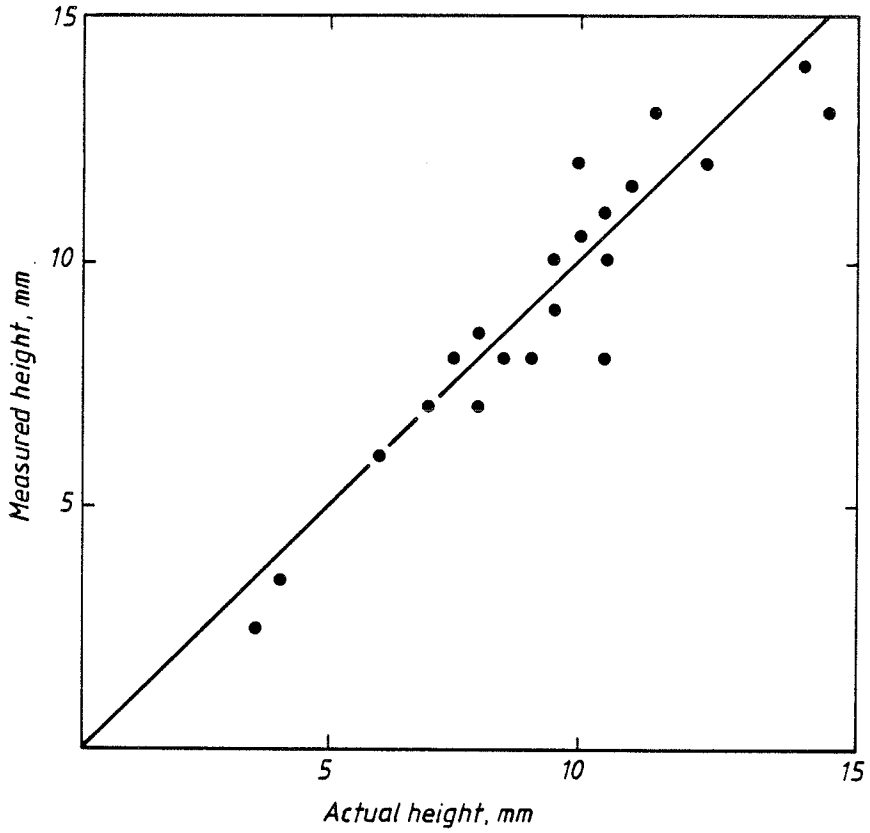

Fig.G16. Measured v. actual flaw through-thickness height (h_{max}) for time-of-flight tests for each flaw.

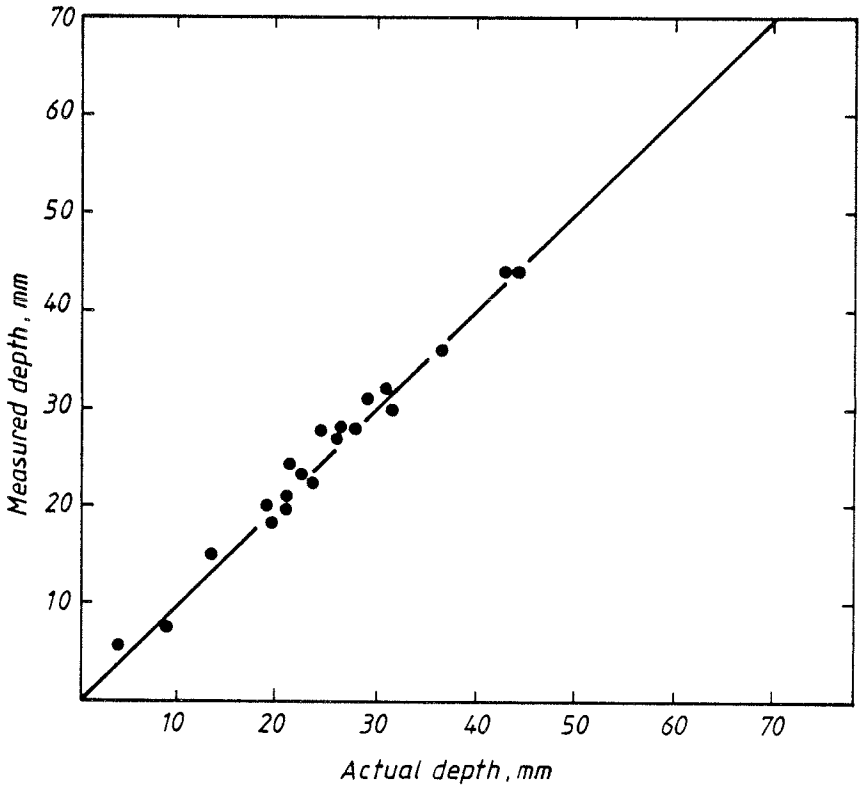

Fig.G17. Measured v. actual flaw depth below testing surface (d_{min}) for time-of-flight tests.

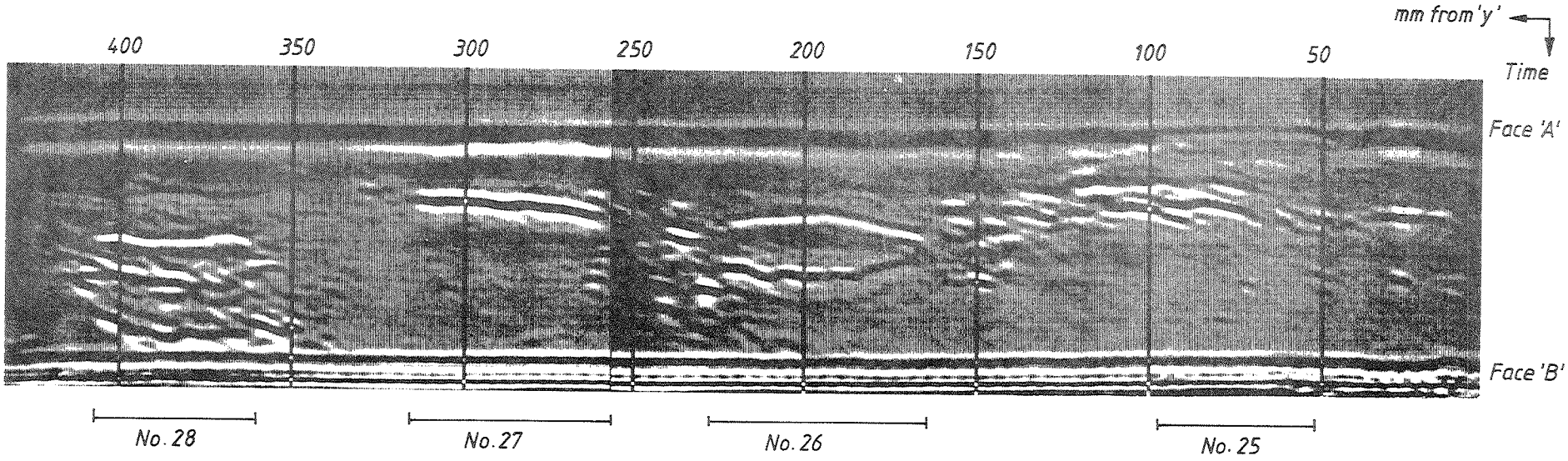

Fig.G18. B-scan image of J307, scan 1, SAFT processed (not linearised).

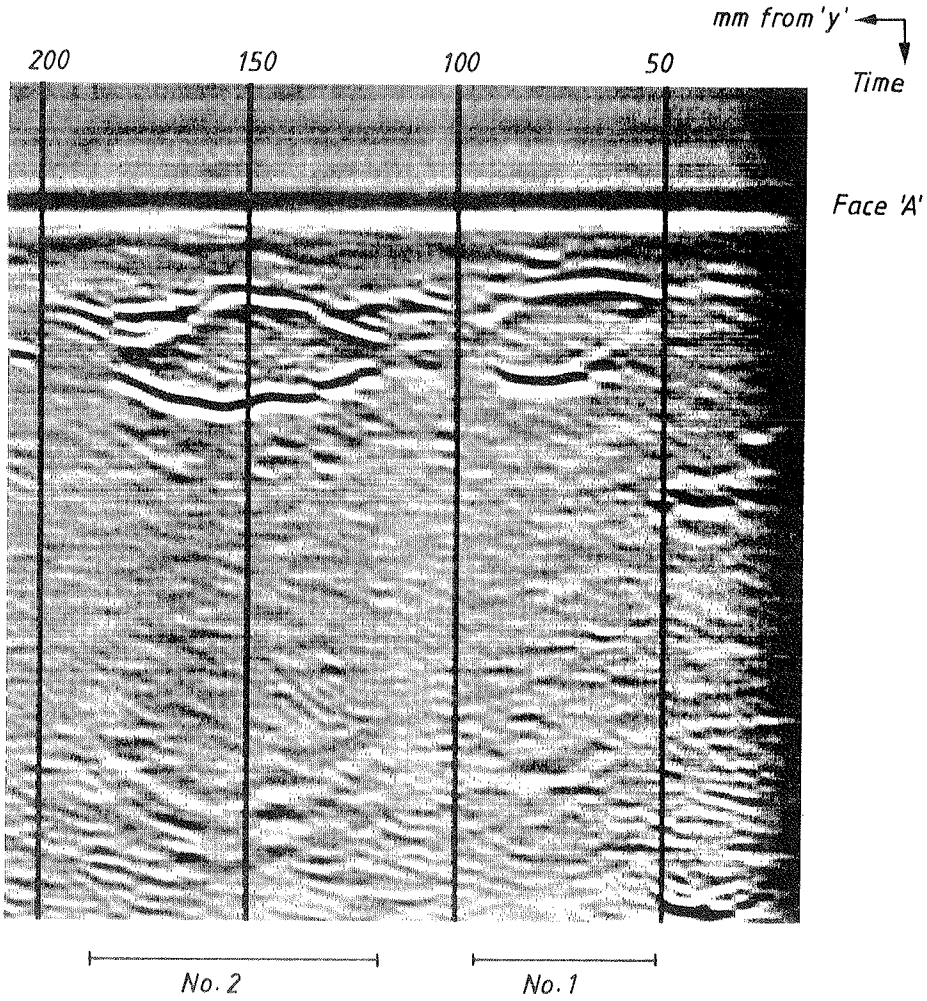

Fig.G19. B-scan image of part of J301, scan 1, SAFT processed, (not linearised).